The Role of the Meiotic Chromosome Axis in the Formation of Crossovers in *Brassicas*

By

Miguel Pachón Peñalba

A thesis submitted to

the University of Birmingham

for the degree of

DOCTOR OF PHILOSOPHY

School of Biosciences

College of Life and Environmental Sciences

University of Birmingham

March 2022

UNIVERSITY OF
BIRMINGHAM

University of Birmingham Research Archive

e-theses repository

This unpublished thesis/dissertation is copyright of the author and/or third parties. The intellectual property rights of the author or third parties in respect of this work are as defined by The Copyright Designs and Patents Act 1988 or as modified by any successor legislation.

Any use made of information contained in this thesis/dissertation must be in accordance with that legislation and must be properly acknowledged. Further distribution or reproduction in any format is prohibited without the permission of the copyright holder.

Abstract

Meiosis is a specialised cell division, which halves the chromosome number, giving rise to the formation of four haploid products, which in plants give rise to the formation of spores. Male meiosis results in the formation of four microspores, which after various rounds of cell division form pollen grains, the male gametophytes. Similarly, female meiosis results in the formation of four haploid products of which only one survives forming the megaspore that develops into the female gametophyte after several mitotic divisions. During meiosis, the homologous chromosomes undergo homologous recombination which leads to the formation of crossovers (COs). These COs can be visualised as chiasmata during metaphase I and they allow the correct segregation of the chromosomes in anaphase I. Moreover, as an outcome of meiotic recombination, new allelic combinations arise, being a major source of genetic variation for both: natural and artificial selection. In this way, CO formation constitutes a limiting factor in plant breeding programmes as CO formation is limited in terms of their number and distribution through the genome.

One of the key characteristics of meiotic chromosomes is the formation of the axial elements (AEs). These are proteinaceous structures assembled between the sister chromatids during the leptotene stage and are composed of cohesin and condensin complexes among other proteins. In plant meiosis, proteins such as ASY1, ASY3, and ASY4, are associated with these AEs. In addition, the AEs undergo a remodelling process, mainly directed by PCH2, concomitant with the polymerisation of the synaptonemal complex (SC). The meiotic chromosome axis and its remodelling is essential for synapsis and recombination between the homologous

chromosomes. In this way, *asy1/3/4* and *pch2* mutants show major defects in the polymerisation of the SC and CO formation, which lead to chromosome missegregation and reduced fertility.

This study aims to translate the knowledge of meiosis accumulated from the plant model species *Arabidopsis thaliana* to crops of the *Brassica* genus, focusing on the role of the coiled-coil domain protein ASY3 and the axis remodelling protein PCH2 in CO formation. In this way, by means of a reverse genetic approach the *ASY3* and *PCH2* orthologs of *B. rapa* and *B. oleracea* have been studied through the cytological analysis of meiosis in TILLING and CRISPR mutants. In a complementary way, the relation between the AEs and their remodelling with CO formation has been examined in *B. rapa*. This has been achieved through an analysis of double mutants combining backgrounds defective for the class II anti-recombinase FANCM and the class I pro-CO factor MSH4 with mutations for the axis-associated and axis remodelling proteins ASY1, ASY3 and PCH2.

Altogether the results obtained have allowed the identification of small divergences in the functions of ASY3 and PCH2 in *Brassica* compared to *A. thaliana* despite carrying out similar roles in meiosis. In addition, ASY1/3 and PCH2 have been revealed as critical factors for the formation of both classes of COs.

“Nothing in biology makes sense except in the light of evolution”.

-Theodosius Dobzhansky (1973). *American Biology Teacher*, 35 (3): 125–129.

For my friends & family

Acknowledgements

I want to thank my supervisor Dr Eugenio Sanchez-Moran for his guidance and support during the course of my PhD and for encouraging me to pursue my goals. I also want to give special thanks to my colleague and friend Dr Pablo Parra Núñez, who has been together with me since I was an undergrad, when he became my tutor in the lab. Thanks for training and supporting me during these years, for all the scientific and non-scientific discussions and for guiding me through this journey. I also want to thank Dr Kim Osman her guidance and advice during my PhD and to all the members and ex-members of the laboratory.

From outside the lab, I want to thank my former supervisors Dr Mónica Pradillo and Prof. Juan Luis Santos for their advice and assistance during my undergrad and postgraduate years. Without their guidance I would not have become the scientist I am today. In addition, I want to thank my friend and fellow PhD candidate Miguel Hernández for accompanying me through this journey, for the long discussions and the drinks we shared together. Also, thanks to the members and ex-members of the Gibbs and Coates labs for accompanying me during my PhD. As well, I want to express my gratitude to our collaborators from the IPK Gatersleben, Dr Stefan Heckmann and Dr María Cuacos, and to Dr Eric Jenczewsky for his advice on working with *Brassica* and for providing us with the seeds we required. I also want to thank the other fellow members of the MEICOM network for their support during my PhD.

Finally, I want to thank my friends and family for their support, thanks to mom and dad for encouraging to pursue my goals. In particular, I want to thank Hannah, my

partner, for sharing her life with me and for accompanying me through this journey. Without her kindness and support this thesis would not have been possible. Thanks for being there on the bad days and for making the good ones better.

This PhD was funded by the European Union: Marie Skłodowska-Curie Actions Innovative Training Networks (ITN) H2020-MSCA-ITN-2017 Horizon 2020; Grant agreement number 765212 MEICOM.

Table of Contents

Chapter 1. Introduction 1

1.1. Overview of the meiotic cell division 2

1.2. The cytological aspects of meiosis 2

1.3. Homologous recombination during meiosis 7

1.3.1. Formation of Double-Strand Breaks 10

1.3.1.1. SPO11 complex 10

1.3.1.2. SPO11 accessory proteins and the “tethered-loop axis” model 11

1.3.1.3. DSB hotspots 13

1.3.2. DSBs processing and Strand Invasion 15

1.3.3. CO formation 19

1.3.3.1. The role of the ZMM proteins in dHJ stabilisation and commitment to CO formation 19

1.3.3.2. Class I CO formation through dHJ resolution by MLH1/3 24

1.3.3.3. Class II CO formation 26

1.3.4. NCO formation 27

1.3.4.1. Synthesis-Dependant Strand-Annealing (SDSA) 28

1.3.4.2. dHJ dissolution 30

1.3.5. Positive interference 33

1.4. The dynamic structure of the chromosomes in meiosis 35

1.4.1. The Axial/Lateral Elements 35

1.4.1.1. Axial element components I: Cohesins 37

1.4.1.2. Axial element components I: Condensins 39

1.4.1.3. Axial element components II: Axis-associated proteins 40

1.4.1.4. Chromosome axis remodelling through prophase I: Post-translational modifications and the role of the AAA+ ATPase PCH2 50

1.4.2. The formation of the Synaptonemal Complex (SC).....55

1.5. The functional and physical relation between the chromosome axes, the SC, and the recombination complexes 58

1.6. The polyploid origin of *Brassica* species.....63

1.7. Food security and research in meiosis.....67

1.8. Project objectives 69

Chapter 2. Materials and methods.....71

2.1. Plant material.....72

2.1.1. *Brassica rapa* TILLING lines 72

2.1.2. *Brassica oleracea* PCH2 CRISPR/Cas9 mutagenized lines 75

2.1.3. Plant growth conditions.....76

2.1.4. *Brassica* crosses.....76

2.2. Mutant generation.....76

2.2.1. Generation of *B. rapa* mutant lines through TILLING.....76

2.2.2. Generation of *B. oleracea* PCH2 CRISPR/Cas9 mutant.....78

2.3. Genotyping.....79

2.3.1. DNA extraction from plant tissues.....79

2.3.2. Derived Cleaved Amplified Polymorphic Sequences (dCAPS) genotyping for *B. rapa* TILLING mutant lines 79

2.3.3. Identification of potential *B. oleracea* CRISPR/Cas9 mutants.....83

2.4. Cytological analysis of meiosis.....84

2.4.1. Spreading of Pollen Mother Cells (PMCs) 84

2.4.2. Immunolocalisation of meiotic proteins by *spreading* technique 86

2.4.3. Immunolocalisation of meiotic proteins by *spreading* technique for Structured Illumination Microscopy (SIM) 88

2.4.4. Microscopy and image analysis 89

2.5. Statistical analysis.....92

2.6. Bioinformatics and analysis of sequencing data 93

Chapter 3. Meiotic axis remodelling in *Brassica* crops: Analysis of the function of the AAA+ ATPase PCH2 in *B. rapa* and *B. oleracea* 94

3.1. Introduction 95

3.2. Results 97

3.2.1. Cytological analysis of meiosis in the *B. rapa braA.pch2-9* mutant line shows defects in the completion of synapsis, formation of univalents, and missegregation problems 97

3.2.2. Chiasma analysis in *braA.pch2-9* indicates defects in recombination and changes in CO frequency distribution 99

3.2.3. The analysis of bivalent shape and chiasma localisation reveals that in *braA.pch2-9* there is a shift towards rod bivalent formation despite no changes in chiasma localisation 102

3.2.4. The polymerisation of the synaptonemal complex is severely compromised in *braA.pch2-9* 104

3.2.5. Immunolocalisation of the class I CO protein HEI10 indicates a major deficiency in CO maturation in *braA.pch2-9* 105

3.2.6. The number of Class I COs does not seem to be related with the extension of the SC in *braA.pch2-9* 110

3.2.7. BraA.PCH2 requires BraA.ASY1 to carry out its function during meiosis 111

3.2.8. Obtention and identification of CRISPR/Cas9 PCH2 mutagenized plants in *B. oleracea* 114

3.2.9. Characterisation of the meiotic phenotype of the *boC.pch2-1* mutant line reveals a drastic abrogation of meiosis. 116

3.2.10. Analysis of chiasma formation in *boC.pch2-1* reveals severe defects in HR 121

3.2.11. Analysis of the bivalent configurations and chiasma localisation in *boC.pch2-1* 123

3.2.12. PCH2 is absent in *boC.pch2-1* leading to defects in the association of ASY1 with the AEs and in the polymerisation of the synaptonemal complex....125

3.2.13. The absence of functional PCH2 in *boC.pch2-1* leads to a severe defect in the establishment of synapsis between the homologs 129

3.2.14. The axis association of ASY1, its remodelling and the chromosome compaction during prophase I are abnormal in *boC.pch2-1* 132

3.2.15. BoC.PCH2 is required for the timely processing of DSBs.....135

3.2.16. Class I CO formation is severely compromised in *boC.pch2-1* 138

3.4. Discussion.....141

3.4.1. BraA.PCH2 and BoC.PCH2 constitute the orthologs of PCH2 in *B. rapa* and *B. oleracea*.....141

3.4.2. The defects in CO formation observed in *braA.pch2-9* and *boC.pch2-1* are due to a severe decrease in class I CO formation 142

3.4.3. SC polymerisation is greatly reduced in *braA.pch2-9* and *boC.pch2-1*, correlating with the CO levels observed.....143

3.4.4. AE remodelling and ASY1 axis-association are defective in *boC.pch2-1*145

3.4.5. DSB repair is delayed in the absence of functional PCH2 147

Chapter 4. Axis structure in *Brassica* crops: The role of the coiled-coil domain protein ASY3 in *B. rapa* 148

4.1. Introduction.....149

4.2. Results.....150

4.2.1. Identification of a possible ASY3 ortholog in *Brassica rapa* 150

4.2.2. Defects in BraA.ASY3 lead to complete sterility in *B. rapa* 153

4.2.3. Characterisation of the phenotype in meiosis of two different *BraA.ASY3* TILLING mutant lines shows defects in synapsis and bivalent formation. 157

4.2.4. Chiasma frequency analysis in the *braA.asy3* mutant lines reveals a strong defect in recombination.....161

4.2.5. The *braA.asy3* mutants shows a decrease in ring and rod bivalent formation despite no changes in the localisation of COs 163

4.2.6. The allelism test between *asy3-2* and *asy3-3* demonstrates that the *B.rapa* ortholog of ASY3 is essential for meiosis.....166

4.2.7. ASY3 is essential for the correct formation of the meiotic chromosome axis and the establishment of synapsis in *B. rapa*.....168

4.2.8. DSB processing is delayed in *braA.asy3* 176

4.2.9. Class I CO formation is severely impaired in *asy3-2*.....179

4.2.10. ASY1 and ASY3 contribute equally to CO formation in *B. rapa* 181

4.2.11. *braA.asy3* is epistatic with respect to *braA.pch2*.....183

4.3. Discussion.....186

4.3.1. BraA.ASY3 is essential for the maintenance of fertility as it participates in the segregation of the homologous chromosomes 186

4.3.2. BraA.ASY3 is necessary for the correct structure of the AEs (ASY1 loading) and the polymerisation of the SC 187

4.3.3. BraA.ASY3 is necessary for CO formation and contributes to the establishment of the *Inter-Homolog Bias* and DSB repair dynamics.....189

4.3.4. BraA.ASY1 stable localisation to the AEs mediated by BraA.ASY3 is essential for BraA.ASY1 to carry out its function. 190

Chapter 5. Relation between the meiotic axis structure, its remodelling and crossover formation in *B. rapa* 192

5.1. Introduction.....193

5.2. Results.....194

5.2.1. The combination of axis defective backgrounds with the loss of function of the class II anti-CO factor FANCM results in a decrease of CO formation.....199

5.2.2. The combination of axis defective backgrounds with the loss of function of the ZMM protein MSH4 results almost complete abrogation of CO formation ..208

5.3. Discussion.....216

5.2.1. The combination of a FANCM defective background with mutations disrupting the axis-associated proteins ASY1/3, and the AAA ATPase PCH2 results in further defects in CO formation.....216

5.2.2. MSH4-dependant class I COs account for the vast majority of COs in *asy1-14, asy3-2*, and *pch2-9* 218

Chapter 6. General Discussion 220

6.1. PCH2 is a key axis remodelling factor in plant meiosis 221

6.2. *B. rapa* ASY3 ortholog is essential for meiosis progression 227

6.3. The formation of both classes of COs is severely compromised in the context of deficient AEs 230

6.4. Future research 232

6.5. Conclusions.....234

References 235

Appendix 256

A.1. Cytological analysis of the *msh4-1 fancm-11* double mutant.....257

A.2. Scientific communications 257

A.2.1. Conferences 257

A.2.2. Seminars 258

A.2.3. Participation in outreach events 258

Table of Figures

Figure 1.1. Overview of the meiotic cell division.....6
Figure 1.2. Homologous recombination model 9
Figure 1.3. Schematic representation of the meiotic chromosome axis organisation.....48
Figure 1.4. Schematic representation of the ASY1 remodelling by PCH2 during early and mid-late prophase I.....54
Figure 1.5. Schematic representation of the relation between the different steps in the homologous recombination pathway and the changes in the chromosome structure associated with pairing and synapsis during prophase I. 62
Figure 1.6. Tringle of U (1935), showing the origin of the allopolyploid Brassicas. 64

Figure 2.1. Visual representation of the B. rapa genes studied. 73
Figure 2.2. Schematic illustration of the structure of the protein products of the genes, and mutant alleles studied. 74
Figure 2.3. Localisation of the different genes studied within the karyotype of *B. rapa* 75
Figure 2.4. Map of the pL2-Bo binary vector containing the CRISPR/Cas9 cassette.....78
Figure 2. 5. Example of the use of a dCAPS genotyping to detect the presence of the point mutation of the *braA.asy3-2* allele.....81
Figure 2.6. Summary of the procedure taken for the analysis of bivalent shapes for the analysis of chiasma frequency and localisation. 91

Figure 3.1. Meiosis in *B. rapa* WT (R-o-18) and the mutant line *braA.pch2-9*.....98
Figure 3.2. Chiasma frequency analysis of the different genotypes of the *braA.pch2-9* line. 100
Figure 3.3. Chiasma frequency distribution analysis in the different genotypes of the *braA.pch2-9* line.....102

Figure 3.4. Position of chiasmata within the chromosomes and bivalent shape analysis in WT and *braA.pch2-9* 103
Figure 3.5. Quantification of the total SC length per cell in WT and *braA.pch2-9* late pachytene PMCs 105
Figure 3.6. Double immunolocalisation of HEI10 and ZYP1 throughout different stages of the pachytene-diplotene transition in *B. rapa* WT R-o-18 plants.....107
Figure 3.7. HEI10 foci scoring in WT and *braA.pch2-9* 109
Figure 3.8. Synaptonemal complex measuring in braA.pch2-9 cells and correlation analysis of the SC extension and number of HEI10 foci in *braA.pch2-9* PMCs.....111
Figure 3.9. Chiasma frequency analysis in the *braA.asy1-14 braA.pch2-9* double mutant 113
Figure 3.10. *BoC.PCH2* sgRNA targets.....114
Figure 3.11. Comparison of the DNA sequences and protein products of BoPCH2 between the WT and the *boC.pch2-1* line. 115
Figure 3.12. Meiotic cell division in *B. oleracea* DH1012 117
Figure 3.13. Meiotic cell division in *boC.pch2-1* 120
Figure 3.14. Scatter plot of the chiasma frequency per cell in the plants of the *boC.pch2-1* line and the WT control. 121
Figure 3.15. Analysis of the chiasma frequency distribution in *boC.pch2-1*. ..123
Figure 3.16. Bivalent configuration and chiasma localisation analyses in *boC.pch2-1*.....124
Figure 3.17. Atlas of the dynamics of ASY1, ZYP1 and PCH2 during different stages of meiosis in *B. oleracea* DH1012.....126
Figure 3.18. Immunolocalisation of ASY1, ZYP1 and PCH2 in prophase I of WT and *boC.pch2-1* 128
Figure 3.19. Analysis through Structure Illumination Microscopy of the polycomplex structures formed in *boC.pch2-1* 129
Figure 3.20. Immunolocalisation of ASY1 and ZYP1 prophase I of WT and *boC.pch2-1*.....131
Figure 3.21. Analysis of the SC extension in *boC.pch2-1*.....132

Figure 3.22. Analysis of the intensity signal of ASY1 and SMC3 in the synapsed and non-synapsed areas of prophase I meiocytes of WT and *boC.pch2-1* 134
Figure 3.23. Immunolocalisation of γH2AX, SMC3, and ZYP1 in different stages of prophase I in WT and *boC.pch2-1* meiocytes 136
Figure 3.24. Analysis of DSB formation and processing in different stages of prophase I in WT and *boC.pch2-1* 137
Figure 3.25. Analysis of class I CO formation in WT and *boC.pch2-1* 139

Figure 4.1. Protein sequence alignment between AtASY3 and the putative *B. rapa* ortholog *BraA.ASY3* (Bra004486) 152
Figure 4.2. Analysis of seed production and silique length in *asy3-2* and *asy3-3* 155
Figure 4.3. Comparison of the silique length between the WT (R-o-18) plants and the different genotypes of the *asy3-2* and *asy3-3* mutant lines 156
Figure 4.4. Stages of meiosis in homozygous, heterozygous, and segregating WT plants of the *asy3-2* TILLING mutant line 159
Figure 4.5. Stages of meiosis in homozygous, heterozygous, and segregating WT plants of the *asy3-3* TILLING mutant line 160
Figure 4.6. Chiasma frequency analysis and chiasma frequency distribution analysis in the *B. rapa asy3* mutants 163
Figure 4.7. Bivalent shape and chiasma localisation analysis in *asy3-2* and *asy3-3* mutant lines 165
Figure 4.8. Meiotic cell division in the *asy3-2 x asy3-3* cross 166
Figure 4.9. Scatter plot of the chiasmata frequency analysis of *asy3-2 x asy3-3* 167
Figure 4.10. Triple immunolocalisation of ASY1 (magenta), ASY3 (cyan) and ZYP1 (yellow) through different stages of prophase I in WT (R-o-18) plants 169
Figure 4.11. ASY3 immunolocalisation (magenta) in prophase I meiocytes of the *asy3-2* line 171
Figure 4.12. Double immunolocalisation of ASY1 (magenta) and SMC3 (yellow) in prophase I PMCs of *asy3-2* and the WT (R-o-18) control 173

Figure 4.13. Immunolocalisation of SMC3 (magenta) and ZYP1 (yellow) in prophase I meiocytes of *asy3-2* and the WT control (R-o-18) 175
Figure 4.14. DSB formation and repair analysis in *braA.asy3*.....178
Figure 4.15. HEI10 foci analysis in *asy3-2* and the WT control (R-o-18).....180
Figure 4.16. Chiasma frequency analysis in the *asy1-14 asy3-2* double mutant 182
Figure 4.17. Chiasma frequency analysis in the *asy3-2 pch2-9* double mutant 184

Figure 5.1. Metaphase I chromosome spreads of PMCs of the double and single mutants analysed in the chapter.....196
Figure 5.2. Summary of the cytological analysis of metaphase I spreads carried out in the single and double mutants analysed in the chapter 5 197
Figure 5.3. HEI10 foci analysis in the *pch2-9 fancm-11* double mutant and the single mutant *pch2-9* 207

Figure 6.1. Proposed model of differential ASY1 loading in the *pch2* mutants of *A. thaliana, B. rapa, and B. oleracea*.....226

Figure A.1. Chiasma frequency analysis in the *msh4-1 fancm-11* double mutant 257

List of Tables

Table 1.1. Axis-associated proteins across the different taxa 49

Table 2.1. Sequence and target location of the different sgRNAs used in the CRISPR/Cas9 mutagenesis of *BoC.PCH2* 78
Table 2.2. Primers and restriction enzymes used in the dCAPS genotyping of the B. rapa mutants.....82
Table 2.3. PCR programme used for the genotyping of *B. rapa* TILLING lines..83
Table 2.4. Primers used for the sequencing and genotyping of the different *B. oleracea* CRISPR/Cas9 mutagenized lines; and for the detection of the CRISPR construct.....84
Table 2.5. Primary antibodies and dilutions used in immunolocalisation......87
Table 2.6. Secondary antibodies and dilutions used in immunolocalisation......87

Table 3.1. Summary of the cytological analysis of meiosis of *braA.pch2-9* and *boC.pch2-1*.....140

Table 5.1. Summary of the results of the cytological analysis of single and double mutants......198
Table 5.2. Outcomes of the Dunnet'sT3 test comparing the chiasma frequency per cell between the *asy1-14 fancm-11* double mutant, the single mutants, and the WT control. 199
Table 5.3. Results of the Games-Howell's test comparing the number of univalent pairs per cell between the *asy1-14 fancm-11* double and single mutants. 200
Table 5.4. Results of the Dunnet'sT3 test comparing the number of ring and rod bivalents per cell between the *asy1-14 fancm-11* double mutant, the single mutants and the WT control. 201
Table 5.5. Summary of the Dunnet'sT3 test outcome comparing the chiasma frequency per cell between the *asy3-2 fancm-11* double mutant, the single mutants, and the WT control. 202

Table 5.6. Results of the Games-Howell's test comparing the number of univalent pairs per cell between the *asy3-2 fancm-11* double mutant and the single mutants. 203
Table 5.7. Results of the Dunnet'sT3 test comparing the number of ring and rod bivalents per cell between the a*sy3-2 fancm-11* double mutant, the single mutants, and the WT control. 204
Table 5.8. Summary of the Dunnet'sT3 test comparing the chiasma frequency per cell between the *pch2-9 fancm-11* double mutant, the single mutants, and the WT control. 205
Table 5. 9. Results of the Games-Howell's test comparing the number of univalent pairs per cell between the *pch2-9 fancm-11* double and single mutants. 205
Table 5.10. Results of the Dunnet'sT3 test comparing the number of ring and rod bivalents per cell between the *pch2-9 fancm-11* double mutant, the single mutants and the WT control. 206
Table 5.11. Summary of the Dunnet'sT3 test outcome comparing the chiasma frequency per cell between the *asy1-14 msh4-1* double mutant, the single mutants, and the WT control. 208
Table 5.12. Results of the Games-Howell's test comparing the number of univalent pairs per cell between the *asy1-14 msh4-1* double mutant and the single mutants. 209
Table 5.13. Results of the Dunnet'sT3 test comparing the number of ring and rod bivalents per cell between the *asy1-14 msh4-1* double mutant, the single mutants, and the WT control. 210
Table 5.14. Summary of the Dunnet'sT3 test comparing the chiasma frequency per cell between the *asy3-2 msh4-1* double mutant, the single mutants, and the WT control. 211
Table 5.15. Results of the Games-Howell's test comparing the number of univalent pairs per cell between the *asy3-2 msh4-1* double and single mutants. 212

Table 5.16. Results of the Dunnet'sT3 test comparing the number of rod bivalents per cell between the *asy3-2 msh4-1* double mutant, the single mutants and the WT control. 212
Table 5.17. Summary of the Dunnet'sT3 test outcome comparing the chiasma frequency per cell between the *pch2-9 msh4-1* double mutant, the single mutants, and the WT control. 213
Table 5.18. Results of the Games-Howell's test comparing the number of univalent pairs per cell between the *pch2-9 msh4-1* double mutant and the single mutants. 214
Table 5.19. Results of the Dunnet'sT3 test comparing the number of ring and rod bivalents per cell between the *pch2-9 msh4-1* double mutant, the single mutants, and the WT control. 215

Table 6.1. Summary of the mutant phenotypes of different PCH2 orthologs described in plants 224

List of frequently used abbreviations

AEs Axial Elements

CO Crossover

CRISPR Clustered Regularly Interspaced Short Palindromic Repeats

dHJ Double Holliday Junction

DNA Deoxyribonucleic Acid

DSB Double-Strand Break

DSBR Double-Strand Break Repair

GC Gene-Conversion

HR Homologous Recombination

I Univalent

II Bivalent

IH Bias Inter-Homolog Bias

IHR Inter-Homologous Recombination

ISR Inter-Sister Recombination

IS Repair Inter-Sister Repair

JM Joint Molecules

LEs Lateral Elements

NCO Non-Crossover

PMCs Pollen Mother Cells

SC Synaptonemal Complex

SDSA Synthesis-Dependant Strand Annealing

SEI Single-End Invasion

SIM Structured Illumination Microscopy

SNP Single Nucleotide Polymorphism

TF Transverse Filaments

WT Wild-Type

Xta Chiasmata

Chapter 1. Introduction

1.1. Overview of the meiotic cell division

Meiosis is a specialized cell division, which halves the chromosome number, giving rise to the formation of four haploid products (Fig.1.1), which in plants give rise to the formation of spores. Male meiosis results in the formation of four microspores, which after various rounds of cell division form pollen grains, the male gametophytes. Similarly, female meiosis results in the formation of four haploid products of which only one survives forming the megaspore that develops into the female gametophyte after several mitotic divisions. Meiosis consists of a single round of replication followed by two consecutive rounds of cell division: the first meiotic division, which is reductional as it separates homologous chromosomes; and the second meiotic division, which is equational as it separates the sister chromatids, resembling a mitotic division. Thus, the four resulting haploid products are non-identical (due to the process of meiotic recombination; see section 1.3). The first meiotic division is characterised by an extended prophase I which itself is divided into five substages: Leptotene, zygotene, pachytene, diplotene, and diakinesis (Fig.1.1).

The biological significance of meiosis was firstly hypothesised by Boveri (1893) and Sutton (1902, 1903), after demonstrating that meiosis reduces by half the number of chromosomes so the original chromosome number can be restored after fertilisation. Moreover, this hypothesis about the separation of paternal and maternal chromosomes in the first meiotic division concurred with the independent assortment of characters described by Mendel (Mendel, 1865).

1.2. The cytological aspects of meiosis

The onset of meiosis is characterised by the condensation of the chromosomes, forming visible thin threads of chromatin which give name to this stage, leptonema or

leptotene stage (from Greek “thin threads”). This condensation is due to the organisation of the chromatin as a linear array of loops with their bases held by the Axial Elements (AEs) (Moens and Pearlman, 1988; Zickler and Kleckner, 1999; Kleckner, 2006; Sanchez-Moran *et al.*, 2008). The AEs are proteinaceous structures that form during the leptotene stage of meiosis, and are composed of cohesins, condensins and other meiosis-specific axis-associated proteins (see section 1.4.1). Next, the meiocytes advance towards zygonema or zygotene stage (paired threads) as the homologs recognise each other in a process of pairing characterised by the alignment of the homologs at distances 400-300 nm, and the appearance of inter-axis bridges composed of DNA, axis proteins, and recombination proteins (see section 1.5) (Albini and Jones, 1987; Moens *et al.*, 2007; Dubois *et al.*, 2019). In most organisms, during leptotene and zygotene the chromosomes adopt a bouquet configuration, consisting of the clustering of the telomeres in a region of the nucleus after their association with the nuclear envelope. In plants, bouquet formation and its subsequent effect in the polarisation of events during meiosis and crossover (CO) formation have been studied in great detail in hexaploid wheat (Martínez-pérez *et al.*, 1999; Osman *et al.*, 2021). It has been suggested that the telomere clustering facilitates the recognition between the homologs (Hamant, Ma and Cande, 2006), although in some species as *Arabidopsis thaliana* this clustering is only transient, not forming a stable bouquet (Armstrong, Franklin and Jones, 2001). Also, during the zygotene stage, the homologs come into close juxtaposition with the formation of the Synaptonemal Complex (SC) between them (see section 1.4.2). The SC comprises a tripartite proteinaceous structure as it was initially described by Fawcett (1956) and Moses (1956) by means of electron microscopy. The structure of the SC consists of

two Lateral Elements (LEs), which derivate from the AEs and a central region composed of Transverse Filaments (TFs) (reviewed in: Zickler and Kleckner, 1999). Interestingly the width of the SC seems to be conserved across species, having a constant distance between the LEs of 100 nm (Denise Zickler and Kleckner, 1999). Once the formation of the SC is complete and the homologous chromosomes show synapsis in all their length, the cell enters pachynema or pachytene stage (thick threads). All the processes involved in homologous recombination take place during these early stages of prophase I (see section 1.3); from the formation of programmed Double Strand Breaks (DSBs) during the leptotene stage, to their repair as genetic COs or non-crossovers (NCOs), throughout the stages of zygotene and pachytene. After pachytene, the SC starts to disassemble and the chromosomes keep increasing their condensation, entering the diplotene stage or diplonema (two threads), in some organisms the pairs of homologs (bivalents) start to become noticeable. The condensation continues increasing until the bivalents are fully visible, the cell then moves into diakinesis, the last stage of prophase I. During this stage, the nuclear envelope disassembles and chiasmata (from the Greek “cross”), the cytological manifestation of COs, begin to appear (e.g. Watson and Callan, 1963). After prophase I the cell enters metaphase I, during which the bivalents align in the equatorial plate (Fig.1.1), with the homologs bioriented to opposite poles due to the counter action of the pulling forces of the spindle and chiasmata (reviewed in: Carpenter, 1994; Hunter, 2015; Mercier *et al.*, 2015;), which are fully visible as the chromosomes reach their maximum condensation. In this way, there must be at least one chiasmata/CO per chromosome pair to ensure their segregation, this is known as the “obligatory chiasma”. The homologous chromosomes are separated to

opposite poles in anaphase I and decondense during telophase I. The second meiotic division is similar to a mitotic division. It is worth to mention that in male meiosis of dicot plants, such as *Brassica spp.*, the two products of the first meiotic division remain together in the same cytoplasm, and the nuclei are separated by an organelle barrier (Fig.1.1). By contrast, in monocots the two daughter cells formed after the first meiotic division are separated upon the formation of the callose wall between them (Furness and Rudall, 1999). The chromosomes start to condense again during prophase II. Then, in metaphase II the chromosomes align in the equatorial plate, and subsequently, the sister chromatids separate in anaphase II. Finally, the chromosomes decondense again in telophase II and the four haploid products are seen forming a tetrad (Fig.1.1).

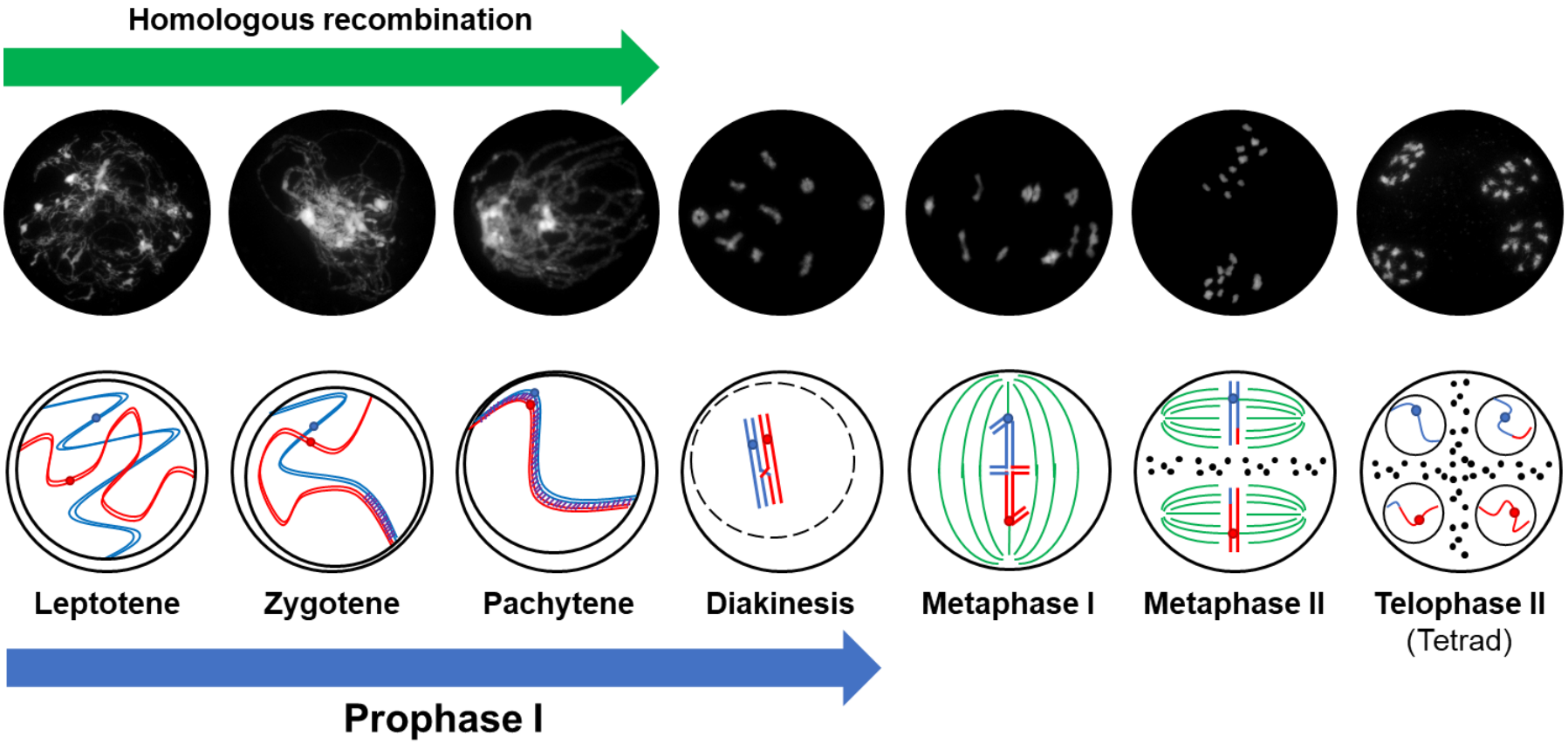


Figure 1.1. Overview of the meiotic cell division. DAPI spreads of *Brassica rapa* (n=10). The diagrams depict the configuration of the chromosomes and other subcellular processes that occur during the different stages of meiosis.

It is worth to mention that the timing of meiosis has been studied in great detail in plants, showing great variability between species (Bennett, 1977). In this way, in the plant model organism *A. thaliana* it has been observed that meiosis takes around 32-34 hours from pre-meiotic G2 to telophase II, although with slight changes depending on the technique used (Armstrong, Franklin and Jones, 2003; Sanchez-Moran *et al.*, 2007; Prusicki *et al.*, 2019). By contrast, the last reports from wheat showed that meiosis takes a total of 43 hours in this organism (Osman *et al.*, 2021). Nevertheless, regardless of the total time of meiosis, in all organisms the duration of prophase I vastly exceeds that of the other phases (Bennett, 1977), lasting around 20 hours in *A. thaliana* (taken as a reference), of which zygotene and pachytene constitute the longest stages, taking 6 and 9.5 hours, respectively (Prusicki *et al.*, 2021).

1.3. Homologous recombination during meiosis

The process of Homologous Recombination (HR), also called Inter-Homologous Recombination (IHR), or Meiotic Recombination, occurs concomitant with the first stages of the meiotic division. The current model for HR during meiosis is the Double-Strand Break Repair (DSBR) model, initially proposed by Szostak *et al.* (1983). This process begins with the formation of programmed Double-Strand Breaks (DSBs), which will be repaired as: i) COs, reciprocal exchanges of genetic information between the homologs; ii) NCOs, which are non-reciprocal exchanges of genetic information between the homologous chromosomes; iii) inter-sister recombination events (ISR) (reviewed in: Haber, 2007; Hunter, 2015; Mercier *et al.*, 2015; Gray and Cohen, 2016; Lambing, Franklin and Wang, 2017).

The establishment of COs between the homologs through HR will ultimately lead to the appearance of chiasmata, thus being essential for the correct segregation of the

homologous chromosomes in the first meiotic division. Moreover, as a secondary outcome, meiotic recombination is the greatest source of variability upon which natural selection can act due to the generation of new combinations of alleles due to CO formation.

It is worth to mention that the relation between genetic COs and the cytological chiasmata was first hypothesised by Janssens (1909) in his **"Theory of the Chiasmatype"** (Originally: "La Theorie de la Chiasmatypie"), and later, a more detailed interpretation of chiasmata and their relation with COs was proposed by Wilson and Morgan (1920). Finally, the demonstration came from Creighton and McClintock (1931, 1935) through the analysis of the inheritance of traits linked to observable chromosome features (heterochromatic knobs) in maize.

The Fig.1.2 is a schematic representation of the consensus model for meiotic recombination.

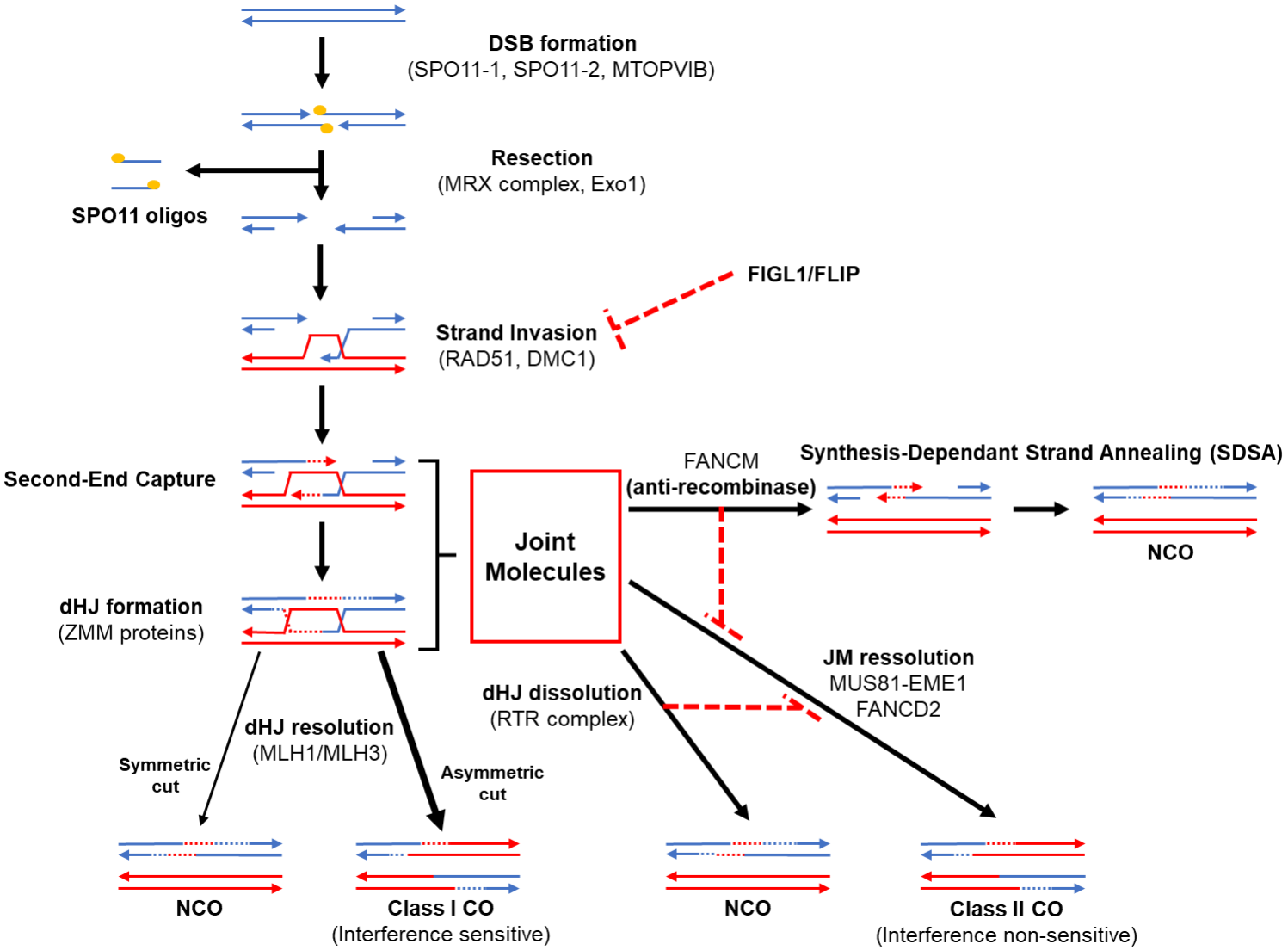


Figure 1.2. Homologous recombination model. Based on: Pradillo *et al.*, 2014**;** Mercier *et al.*, 2015**;** Gray and Cohen, 2016**.**

1.3.1. Formation of Double-Strand Breaks

1.3.1.1. SPO11 complex

The formation of programmed DSBs is the first step in the IHR process (Fig.1.2), it takes place during the leptotene stage along with the polymerisation of the AEs. The formation of DSBs is catalysed by the highly conserved topoisomerase SPO11 (SPORULATION 11), whose essential role in meiosis was originally identified in the budding yeast *Saccharomyces cerevisiae* (Atcheson *et al.*, 1987). However, its function in DSB formation and recombination initiation in budding yeast was lately proposed by Cao, Alani and Kleckner (1990), and finally confirmed by Keeney, Giroux and Kleckner (1997). SPO11 shares great homology to an archaeal type II topoisomerase, the topoisomerase VI (Bergerat *et al.*, 1997). This kind of topoisomerases participate in resolving DNA catenation by introducing DSBs in the DNA, allowing the other DNA molecule to go through the break and eventually catalysing the re-ligation of both DNA molecules. In the case of the archaeal topoisomerase VI, this forms heterotetrameric complexes of two A and two B subunits (Bergerat *et al.*, 1997). SPO11 has been found to share homology with the A subunit of this topoisomerase and is thought to form a dimeric complex to play its role in DSB formation. In most of the model organisms used to study meiosis (e.g.: budding yeast, worm, fruit fly), SPO11 is encoded by a single gene. However, in other lineages, such as in plants, there are several SPO11 paralogs. For instance, *A. thaliana* has three SPO11 copies: SPO11-1, SPO11-2, and SPO11-3. Nevertheless, only the SPO11-1 and SPO11-2 homologs participate in meiotic recombination, likely by forming an heterodimeric complex, whereas SPO11-3 does not seem to be essential in meiosis (Grelon *et al.*, 2001; Stacey *et al.*, 2006; Hartung *et al.*, 2007).

Moreover, a homolog of the B subunit of the archaeal topoisomerase VI has also recently been identified in *Arabidopsis,* the MTOPVIB protein (Meiotic Topoisomerase VIB–like), which seems to be involved in DSB formation by mediating the formation of the SPO11-1/SPO11-2 heterodimer (Vrielynck *et al.*, 2016). A similar situation has also been found in mice with the TOPVIBL topoisomerase (Robert *et al.*, 2016). Regarding the catalysis of the formation of DSBs by the SPO11 complex, it is known that two monomers are required for the formation of a single DSB. Each one catalyses the breaking one strand of DNA, leaving a 2 bp 5' overhang in each of the strands at the DSB site to avoid the re-ligation of the products. Moreover, the SPO11 protein monomers remain covalently attached to the 5' DNA ends at the break point (Liu, Wu and Lichten, 1995) until they are removed during the DSB processing (Neale, Pan and Keeney, 2005).

1.3.1.2. SPO11 accessory proteins and the "tethered-loop axis" model

Nevertheless, SPO11 requires of several other accessory proteins in order to carry out its function in DSB formation (de Massy, 2013; Gray and Cohen, 2016). In this way, in *S. cerevisiae*, at least 9 proteins have been identified to interact directly or indirectly with the SPO11 complex, being required for DSB formation: Ski8, Rec102, Rec104, Rec114, Mei4, Mer2, Mre11, Rad50, Xrs2. Only some of these accessory proteins are conserved between lineages, and others are specific (de Massy, 2013). For instance, in the plant organism *Arabidopsis thaliana*, several SPO11 accessory proteins have been found: PRD1, PRD2, PRD3, and DFO (De Muyt *et al.*, 2009). Of these, PRD2 shares homology with yeast and mouse Mei4, and PRD1 is a possible homolog of mouse Mei1. On the other hand, PRD3 and DFO are plant specific, and the MRX complex (MRE11, RAD50, XRS2/NBS1; section 1.3.2) participates only in

resection, not in DSB formation (De Muyt *et al.*, 2009; Lambing, Franklin and Wang, 2017). Moreover, recent studies have shed some light on the interaction between these accessory proteins, the core complex formed by SPO11-1, SPO11-2, MTOPVIB, and the AEs (Vrielynck *et al.*, 2021). In this way, Vrielynck *et al.* (2021) showed that MTOPVIB and PRD1 interact with the rest of the accessory proteins with the exception of PRD3, which only does it with PRD1. Thus, MTOPVIB would be a bridge between the SPO11 complex and the accessory proteins, whereas PRD1 would act as a platform for them. Moreover, this study also revealed a strong interaction between MTOPVIB and the accessory protein PRD2 with the axis-associated proteins ASY1/3/4; and between ASY1 and PRD3, being ASY1 also necessary for its correct loading to the AEs.

In addition, *A. thaliana* SWI1 (SWITCH1) is required to enter meiosis, “switching” from a mitotic to a meiotic programme (Mercier *et al.*, 2001; Boateng *et al.*, 2008).

Data from budding yeast, fission yeast and mouse has led to the proposition of a model for DSB formation in which DSBs occur in the context of the meiotic chromosome axis, this model has been called “*tethered-loop axis model*” (Blat *et al.*, 2002; Borde and de Massy, 2013; de Massy, 2013). This model suggests that as the chromatin in meiosis is organised as a linear array of loops with their base held by the AEs, the DSBs would occur and be processed in the context of the axis, as the SPO11 accessory proteins have been found to localise in the axis in several organisms, for instance in fission yeast (Panizza *et al.*, 2011). In this way, the SPO11 complex would be recruited to the chromatin loops in sites of open chromatin. Next, the DSB site would be tethered to the chromosome axis where the SPO11 accessory proteins required for DSB formation are located. Finally, the SPO11 complex would

catalyse the formation of DSBs upon its activation by its accessory proteins (Borde and de Massy, 2013).

1.3.1.3. DSB hotspots

Regarding the number and localisation of the DSBs through the genome, it is known that the number of DSBs in the majority of the organisms studied greatly exceeds the number of CO products (Serrentino and Borde, 2012). For instance, in *S. cerevisiae* there are 140-170 DSBs per meiosis vs. ~90 COs, in mouse 230-400 DSBs *vs.* ~26 COs, in *A. thaliana* 150-200 DSBs *vs.* ~10 COs, and the exception would be *C. elegans* that shows only ~10 DSBs *vs.* ~5 COs (de Massy, 2013). The DSBs, are not randomly distributed, they tend to localise in DSB hotspots, creating non-random distributions of DSBs and COs. In this way, hotspots are permissive regions of the genome with high probability of being cleaved by SPO11 (Cooper, Garcia and Neale, 2016; Tock and Henderson, 2018). However, the current data points out that there is no single key factor that determines a region in the genome to become a hotspot. Instead, it seems that the co-occurrence of several different factors organised in layers of regulation is what creates a favourable environment for DSBs to occur (Cooper, Garcia and Neale, 2016). In this way, it is worth to mention that, in *A. thaliana* DSB formation appears to be depleted in regions of the genome with highly repetitive sequences and nucleosome dense such as the pericentromeric heterochromatin and the centromeres (Choi *et al.*, 2018). Interestingly, DSB hotspots in *A. thaliana* seem to be associated with regions containing DNA transposons such as the *Helitron* family, whereas DSB coldspots appear associated with RNA transposons as the *Gypsy* family (Choi *et al.*, 2018). In addition, the regions containing rDNA in *A. thaliana* present a reduction in the formation of meiosis-

specific DSBs as a consequence of forming part of the nucleolus during meiosis, and the DNA lesions formed in these regions are repaired though NHEJ (Sims, Copenhaver and Schlögelhofer, 2019). The rationale for this is to avoid any possible non-allelic or ectopic recombination between highly repetitive regions, as it can lead to genome instability (Tock and Henderson, 2018). By contrast, in maize DSB formation occurs homogeneously through all chromosome regions, including pericentric heterochromatin and centromeric regions. In addition, in maize most DSBs seem to form in repetitive sequences, predominantly corresponding with retrotransposons of the *Gypsy* family, suggesting different regulatory mechanisms to the ones described in *A. thaliana*. However, most COs form in regions adjacent to genes (He *et al.*, 2017). A second layer of regulation has been observed in yeast and plant species, such as budding yeast, the plant model organism *A. thaliana* and maize. In these species DSBs maps reveal that hotspots frequently appear in Nucleosome-Depleted Regions (NDRs), and thus, it seems that the chromatin accessibility plays a role in allowing meiotic DSB formation (Choi and Henderson, 2015; Cooper, Garcia and Neale, 2016; Tock and Henderson, 2018). It is worth to mention that the meiotic chromosome structure plays a significant role in defining the position of the hotspots as according to the *tethered-loop model*, these are located within the chromatin loops and not at their bases. In this way, it has been observed in *A. thaliana* that regions enriched for the meiosis-specific cohesion REC8 correspond with DSB cold spots (Lambing *et al.*, 2020). Also, it has been observed in *Arabidopsis* that promoter and terminator regions, concurring with the open chromatin conformation adopted in gene rich euchromatic regions, correspond with DSB and recombination hotspots (Tock and Henderson, 2018). Moreover, a common

feature between *S. cerevisiae*, plants and mammals is the deposition of histone modifications in DSB hotspots, mainly the trimethylation of the lysine 4 of the histone 3 (H3K4me3) (Choi and Henderson, 2015; Cooper, Garcia and Neale, 2016). Studies in budding yeast (Borde *et al.*, 2009; Acquaviva *et al.*, 2013; Sommermeyer *et al.*, 2013) have demonstrated the link between the H3K4me3 modification and the initiation of meiotic recombination. In this way, the SET domain protein Spp1 was discovered to interact with both the H3K4me3 histone modification in the chromatin and the SPO11 accessory protein Mer2, which is located in the chromosome axis. Thus, the function of Spp1 correlates with the *tethered-loop axis model* and effectively links the potential hotspots to the recombination machinery. However, no such protein has yet been identified in plants (Tock and Henderson, 2018).

By contrast with budding yeast and plants, mice and human DSB hotspots seem to be located in intergenic regions and their position determined by the histone-lysine trimethyl-transferase protein PRDM9. This protein is able to recognise 12-bp motifs in the DNA by its zinc-finger array, and designates them as DSB hotspots by labelling the loci with the H3K4me3 histone modification (Baudat *et al.*, 2010).

1.3.2. DSBs processing and Strand Invasion

After the formation of DSBs by the topoisomerase SPO11, these breaks are processed to generate 3’ overhangs by the action of several nucleases (Sun, Treco and Szostak, 1991). This DSB processing is carried out by the MRX complex (MRE11, RAD50, XRS2/NBS1) together with COM1, which cleave the DNA strand downstream of the end where SPO11 remains covalently attached (Prinz, Amon and Klein, 1997; Daoudal-Cotterell, Gallego and White, 2002; Bleuyard *et al.*, 2004; Waterworth *et al.*, 2007). This, allows the release of the SPO11-DNA molecule, also

called SPO11-oligo (Neale, Pan and Keeney, 2005). These oligos vary in length from 12 to 23 bp and are used for DSB hotspot mapping (Choi and Henderson, 2015). After the cleavage by the MRX complex, the 5' ends suffers a further resection by the 5'-3' exonuclease activity of the enzyme Exo1 (of around 550 nucleotides in budding yeast; Zakharyevich *et al.*, 2010), extending the 3' free ssDNA ends. After the resection the ssDNA ends are coated by the RPA protein (REPLICATION PROTEIN A), whose function is to protect the fragile ssDNA strands and to facilitate the assembly of the RAD51-DMC1 nucleoprotein filament (see below) (Soustelle *et al.*, 2002; Sung *et al.*, 2003). However, whereas in yeast RPA is required for the early steps of meiotic recombination to prevent further 5' resection and the accumulation of intermediates that cannot progress (Soustelle *et al.*, 2002); in plants, it has been shown in *A. thaliana* that RPA1a is necessary for CO formation but not for the early steps of recombination (Osman *et al.*, 2009). Interestingly RPA competes with RAD51 and DMC1 for its binding to DNA, and must be displaced by them to form the nucleoprotein filament required for the following steps of meiotic recombination (Sung *et al.*, 2003).

Once the DSB resection has taken place, two RecA homologs, the recombinases RAD51 and DMC1 bind to these 3' ends forming a nucleoprotein filament (Li *et al.*, 2004, Pradillo *et al.,* 2014) which seeks for homology in the homologous chromatid, ultimately leading to the displacement of the complementary strand in a process called *Single End Invasion* (SEI) (Hunter and Kleckner, 2001). Following the SEI, the 3' end acts as a primer for the polymerisation of DNA, generating a D-loop structure that grows displacing the homologous DNA strand. It is worth to mention that the DSBR model predicts the formation of an heteroduplex DNA (hDNA) molecule (a

DNA duplex formed by two complementary strands from different sources; in this case, two homologous chromosomes) as a consequence of the SEI (Szostak *et al.*, 1983). The occurrence of hDNA in HR was later proven in budding yeast by Allers and Lichten (2001), corroborating the DSBR model for meiotic recombination.

Regarding the functions of the RecA homologs, yeast RAD51 is needed for DNA repair during mitosis and meiosis, as mutants for this gene accumulate externally induced DSBs during mitosis and SPO11-dependent DSBs during meiosis (Shinohara, Ogawa and Ogawa, 1992). On the other hand, *S. cerevisiae* DMC1 seems to be meiosis specific and required to direct recombination towards the homologous chromosome and for completion of synapsis (Bishop *et al.*, 1992). Studies on the role of RAD51 and DMC1 in the plant model organism *A. thaliana* have given further information about the functions and interplay of these proteins. In this way, *atrad51* mutants, show synapsis defects and chromosome fragmentation during segregation in anaphase I (Li *et al.*, 2004). Similarly to yeast Dmc1, AtDMC1 seems to be required only for recombination with the homologous chromosome as synapsis is incomplete in this mutant, although instead of chromosome fragmentation, 10 univalents are observed in metaphase I, showing absence of CO formation with the homologous chromosome (Couteau *et al.*, 1999). Other study conducted by Pradillo *et al.* (2012) about the relation between both proteins in meiotic recombination showed: i) that RAD51 is indeed required for DNA repair through HR in somatic cells as previously described in yeast; ii) DMC1 seems to be necessary to direct the recombination towards the homologous chromosome; iii) RAD51 appears to be essential for strand invasion and DNA repair, directing homology search towards the sister chromatid or the homologous chromosome.

Moreover**,** in plants and vertebrates, in addition to RAD51 and DMC1 there are 5 paralogs (XRCC2, XRCC3, RAD51B, RAD51C and RAD51D) (reviewed in Pradillo et al., 2014). Of these only RAD51C and XRCC3 are essential for meiotic recombination, leading to chromosome fragmentation in their absence, whereas the rest participate only in somatic DNA repair (Bleuyard and White, 2004; Abe *et al.*, 2005; Bleuyard *et al.*, 2005; Li *et al.*, 2005; reviewed in Pradillo *et al.*, 2014). Also, it has recently been reported by Hernandez Sanchez-Rebato *et al.* (2021) that RAD54, a cofactor of RAD51 is essential for DNA repair in meiosis in the absence of DMC1.

It is worth to mention that in a diploid cell, after DNA replication, there are 3 other possible molecules that can be taken as a template for DNA repair via HR: two corresponding to the chromatids of the homologous chromosome, and one to the sister chromatid. Therefore for a DSB to be repaired with the homologous chromosome to form a CO, there must exist a bias towards using the homologous chromatid as a template instead of the sister chromatid, this is called *Inter-Homolog Bias* (IH Bias) (Schwacha and Kleckner, 1997).

Interestingly, the number of SEI intermediates is limited by the action of the AAA+ ATPase FIDGETIN-LIKE 1 (FIGL1) and its partner protein FLIP1 (FIDGETIN-LIKE INTERACTING PARTER 1). It has been proposed that these factors disassemble RAD51/DMC1 coated nucleofilaments, thus preventing the formation or the extension of the D-loop, preventing abnormal invasions or the accumulation of locked intermediates. In the absence of the FIGL/FLIP complex these aberrant intermediates would be resolved by the class II CO pathway (see section 1.3.3.3) (Girard *et al.*, 2015; Fernandes *et al.*, 2018).

After the SEI and the extension of the D-loop, a subset of these early recombination intermediates can be disrupted, disengaging from the homolog, and being repaired through *Synthesis-Dependant Strand-Annealing* (SDSA). The result of the SDSA repair is the formation of NCOs (see section 1.3.4.1).

1.3.3. CO formation

Following the DSBR model of meiotic recombination (Szostak *et al.*, 1983), after the SEI and the extension of the D-Loop, the capture of the opposite homologous strand of the DSB can occur (*Second End Capture*). Consequently, a second region of heteroduplex DNA will appear (Fig.1.2; Allers and Lichten, 2001). This will lead to the formation of late recombination intermediates called *double Holliday Junctions* (dHJs). However, despite dHJs were incorporated to the DSBR model by Szostak *et al.* (1983), single Holliday Junctions (HJs) had been previously described in previous models for meiotic recombination and gene conversion in fungi (Holliday, 1964, 1974). These late recombination intermediates can be resolved as class I COs, sensitive to positive interference (the reduction of the probability of forming another CO in the proximities of a pre-existing one; section 1.3.5) (Sturtevant, 1913).

1.3.3.1. The role of the ZMM proteins in dHJ stabilisation and commitment to CO formation

A group of proteins called ZMMs, initially identified in *S. cerevisiae* are involved in the stabilisation of these late recombination intermediates (dHJs) and their commitment to be resolved as class I COs, and particularly in yeast, all of them are required for synapsis initiation and their mutants suffer arrest at pachytene (Lynn, Soucek and Börner, 2007). The acronym ZMM stands for: Zip1, Zip2 (SHOC1), Zip3 (HEI10), Mer3, Msh4, Msh5; the name of the yeast proteins involved in this process. These

proteins can be classified according to their molecular function as it has been proposed by Lynn, Soucek and Börner (2007). In this way, there are proteins that: i) interact directly with the DNA such as Mer3, Msh4, and Msh5; ii) participate in protein-protein interactions and SUMOylation as Zip2, Zip3, and Spo22/Zip4; iii) participate in SC formation such as the TF protein Zip1. Starting with the first group, Mer3 is a DNA helicase necessary for the stabilisation recombination intermediates, being involved in heteroduplex extension during the SEI, and is also essential for the formation of class I COs in yeast. Consequently, mutants for this protein show: hyper-resection of the DSBs; defects in the transition from early to late recombination intermediates; reduction in CO frequencies with the remaining COs randomly distributed and non-disjunction of chromosomes in the first meiotic division (Nakagawa and Ogawa, 1999; Nakagawa and Kolodner, 2002; Mazina *et al.*, 2004). The Msh4 and Msh5 proteins are homologous to the bacterial MutS mismatch repair protein (MutS HOMOLOG 4 and 5). These proteins and their meiotic role was initially discovered in budding yeast (Ross-Macdonald and Roeder, 1994; Hollingsworth, Ponte and Halsey, 1995). Both participate in CO formation during meiosis despite having no role in mismatch repair. Moreover, these proteins seem to work together in an heterodimer that binds to DNA duplexes at the sites of strand invasion and in dHJ (proposed by Zalevsky *et al.* (1999) in *C. elegans*), being essential for the formation of class I COs and synapsis extension in yeast (Pochart, Woltering and Hollingsworth, 1997; Novak, Ross-Macdonald and Shirleen Roeder, 2001). Regarding the second group of ZMM proteins, Zip2 was identified by Chua and Roeder (1998), they observed that this protein was localised in the early recombination nodules, and through the analysis of mutants, its essential roles in CO

formation and synapsis initiation. However, no clear putative molecular functions have been identified although it seems to share some homology with the *Arabidopsis* XPF-endonuclease SHOC1 (Macaisne *et al.*, 2008). Other protein of this second group of ZMMs is Zip3, that seems to have an E3 ubiquitin ligase putative function due to its RING domain (Perry, Kleckner and Börner, 2005). The meiotic role of this protein was previously described by Agarwal and Roeder (2000), who observed that Zip3 is required for normal levels of synapsis and CO formation since its mutants show incomplete synapsis, reduced recombination and missegregation of chromosomes. Moreover, Zip3 was also shown to interact with: i) early recombination factors as Mre11 and Rad51; ii) the TF protein Zip1 (See below); iii) Zip2 at the synapsis initiation sites, being required for its recruitment since overexpression of Zip2 in a *zip3* mutant background recovered synapsis. The last one of this second group of ZMMs is Zip4, a tetratricopeptide domain protein, that like the rest of the ZMM proteins is essential for CO formation and synapsis in yeast, despite having no role in NCO formation (Perry, Kleckner and Börner, 2005). Also, it forms a complex with Zip2, working separately from Zip3 as they depend on each other and on Zip3 for their localisation in the chromosomes, but Zip3 does not depend on them to localise in the axis. Moreover, Zip4 seems to be part together with the other ZMMs of the *Synapsis Initiation Complex* in yeast, as it shows colocalization with Zip2 and Zip3, and appears as foci over the SC (Tsubouchi, Zhao and Roeder, 2006). The only difference between them is that whereas Zip2 and Zip4 are required for synapsis initiation, Zip3 is required for the extension of the SC. Finally, from the last group of ZMMs, Zip1 is a coiled-coil domain protein with a globular domain on each end, which forms the TFs of the central region of the SC in yeast. In this way, Zip1 is

required to achieve synapsis despite not being required for pairing or early recombination as the *zip1* mutants show commitment of the recombination intermediates to CO formation although they do not progress further due to the pachytene arrest, not being able to complete reciprocal recombination between the homologs (Sym, Engebrecht and Roeder, 1993). Regarding its function in the formation of the SC (further explained in section 1.4.3), Zip1 seems to form dimers that polymerise during synapsis in a head-to-head manner with their N-terminal domains located in the central region of the SC and the C-terminals located in the LEs, giving rise to the characteristic ladder-like structure between the homologs (Tung and Roeder, 1998; Dong and Roeder, 2000).

Several orthologs of the yeast ZMMs have been found in plants, mainly in the model organism *Arabidopsis thaliana:* ZYP1, SHOC1 (ZIP2), HEI10 (ZIP3), ZIP4, MSH4, MSH5, MER3 (Higgins *et al.*, 2004; Higgins *et al.*, 2005; Mercier *et al.*, 2005; Osman *et al.*, 2006; Chelysheva *et al.*, 2007; Higgins *et al.*, 2008; Macaisne *et al.*, 2008; Chelysheva *et al.*, 2012). The exception would be the plant specific ZMM protein PTD (PARTING DANCERS) as it shares no homology with any of the yeast ZMMs (Asela *et al.*, 2006). However, there are several key differences between the yeast and plant ZMMs: i) plants defective for these proteins do not show meiotic arrest at pachytene since plants lack such a strong meiotic checkpoint; ii) these proteins, with the exception of ZYP1, are not required for the formation of the SC; iii) ZYP1 in *A. thaliana* is required for the formation of the SC, to ensure recombination between the homologous chromosomes (See section 1.4.3) as RNAi knock down mutants show multivalent formation together with a slight decrease in COs, and also plays a key role in the establishment of interference between the class I COs (Higgins *et al.*,

2005; Capilla-Pérez *et al.*, 2021; France *et al.*, 2021). Moreover, specific differences have been found when studying these proteins in different plant species. For instance, in wheat there are four copies of ZIP4, three located on each of chromosomes of the group 3 (3A, 3B and 3D) , and a fourth copy present in the chromosome 5B, which duplicated and diverged from the 3B copy (Griffiths *et al.*, 2006; Rey *et al.*, 2017). The ZIP4 diverged copy of chromosome 5B is required to ensure synapsis and recombination between the homologous chromosomes, being responsible of the phenotype observed in meiosis when the *Ph1* locus is deleted, resulting in early synapsis and CO formation between homoeologous chromosomes (Martín *et al.*, 2017; Rey *et al.*, 2017; Martín, Alabdullah and Moore, 2021). Other example is the barley ortholog of ZYP1, which is essential for synapsis and CO formation, contrasting with the hyper-recombinant phenotype observed in the *zyp1* mutant of *A. thaliana* previously mentioned (Barakate *et al.*, 2014). In the case of wheat MSH4 and MSH5, even though the different copies present redundancy, they are essential for CO formation (Desjardins *et al.*, 2020). Similarly, in *B. napus* both MSH4 copies present redundancy as even only one dose of the least expressed copy is able to restore CO formation, although interestingly, a dosage effect on CO formation between homoeologous chromosomes was observed in allohaploids (Gonzalo *et al.*, 2018). By contrast, the phenotypes observed for the *ZEP1, MER3, ZIP4,* and *HEI10* mutants of rice are similar to those reported for their *Arabidopsis* orthologs (Wang *et al.*, 2009, 2010, 2012; Shen *et al.*, 2012).

Despite these differences, plant ZMMs are required for the stabilisation of the late recombination intermediates and their resolution as COs, as plants defective for these proteins show: i) reduction in fertility due to non-disjunction of chromosomes in

anaphase I; ii) reduction in chiasma/CO formation to a 15%, except for *mer3* mutants that show a 25% reduction; iii) complete synapsis during pachytene.

Interestingly, it has been observed that CO levels are highly sensitive to the HEI10 dosage, as transforming *A. thaliana* with supplemental copies of the gene encoding this protein is enough to double the number of COs per meiocyte. Thus, providing an insight about how recombination levels can be altered by regulating the number of functional copies of *HEI10* (Ziolkowski *et al.*, 2017). Moreover, it has recently been reported that a coarsening model for HEI10 in which this protein undergoes a transition from localising throughout the SC to coalesce in small regions observed as foci could explain CO pattering in *A. thaliana* (Morgan *et al.*, 2021).

1.3.3.2. Class I CO formation through dHJ resolution by MLH1/3

Finally, the last step of the class I CO pathway is the resolution of the dHj intermediates. This step is conducted by the homologs of the bacterial mismatch repair protein MutL, the MLH1 and MLH3 proteins. These proteins work in a heterocomplex that catalyses the resolution of the dHJs towards the formation of COs due to their nuclease activity (Gray and Cohen, 2016). MHL1 was primarily identified in mouse as a mismatch repair protein involved in meiosis. In this manner, MLH1 deficient mice showed infertility due to the absence of CO formation despite showing complete synapsis, and moreover, MLH1 seemed to be localised in the late recombination nodules (Baker *et al.*, 1996). Later, its roles in CO formation in yeast and the formation of an heterocomplex with MLH3 were identified (Hunter and Borts, 1997; Wang, Kleckner and Hunter, 1999). However, regarding the resolution of dHJs by MLH1/3, it is worth to mention that dHJ processing can occur in two different ways, which generate either COs or NCOs. In this way, if the cut of the dHjs is

symmetric, the outcome will be a NCO; and conversely, if MLH1/3 produces an asymmetric cut, the resulting outcome will be a CO. Nevertheless, there is a bias towards the asymmetric processing of the dHJs, yielding mostly COs (Gray and Cohen, 2016; Manhart and Alani, 2016). In plants, MLH1 has been studied in *A. thaliana* and rice. In *A. thaliana* MLH1 plays a key role in CO formation and in mitotic recombination. In this way, the *mlh1* mutants present decreased levels of CO formation during meiosis as observed by Chelysheva *et al.* (2012) and in somatic cells, it seems to be necessary for DNA repair by homologous recombination and to prevent recombination between homoeologous sequences as shown by (Dion *et al.*, 2007). In addition, in rice MLH1 has also been observed to be necessary for CO formation as its depletion leads to a decrease in chiasma formation and missegregation problems (Mao *et al.*, 2021). Similarly, a homolog of MLH3 has been identified in *A. thaliana* by Jackson *et al.* (2006), where it was shown that MLH3 colocalised with MLH1 in the recombination nodules at the end of prophase I. Also, the plants defective for MLH3 displayed a decrease in the CO number despite showing no effects in the number or localisation of MSH4 foci (associated with dHJs), and complete synapsis in pachytene.

Recently, a class I CO anti-recombinase factor has been identified, the PROTEIN PHOSPHATASE X1 (PPX1), which seems to limit the formation of class I COs and in a much more reduced extent, class II CO formation (Nageswaran *et al.*, 2021). In this way, PPX1 seems to physically interact with MLH1 and several ZMM proteins, and it has been hypothesised that it might counteract the phosphorylation signals carried out by the kinases CDKA;1, DDK, and ATM/ATR.

1.3.3.3. Class II CO formation

Not all COs belong to the interference-sensitive Class I as in some organisms such as in budding yeast and *A. thaliana* it has been demonstrated the presence of a second class (Class II) of COs that are dHJ independent and non-sensitive to interference (De los Santos *et al.*, 2003; Hollingsworth and Brill, 2004). In the vast majority of organisms these only represent a subset of the total number of COs. Such is the case in plants and budding yeast, in which class II COs seem to correspond to a 10-15% of the total number of COs (De los Santos *et al.*, 2003; Higgins *et al.*, 2008). However, in other organisms as the fission yeast *S. pombe* class II COs account for all the CO events (Hollingsworth and Brill, 2004). Class II COs were first identified in budding yeast as the remaining COs in mutant strains of the MSH4/5 ZMM proteins that represented a small subset of the total, were randomly distributed, and did not affect the NCO outcome (De los Santos *et al.*, 2003). In budding yeast, fission yeast, and plants, the formation of class II COs is catalysed by the action of the MUS81 structure-specific endonuclease which forms a complex with the MMS4 protein or its ortholog in plants and fission yeast EME1 (De los Santos *et al.*, 2003). Class II COs are formed through the processing of early recombination intermediates (Joint Molecules, JMs) directly to a CO by the endonuclease activity of the MUS81-EME1/MMS4 complex (De los Santos *et al.*, 2003; Hollingsworth and Brill, 2004; Berchowitz *et al.*, 2007; Higgins, *et al.*, 2008; Geuting *et al.*, 2009). Interestingly, these proteins are involved in somatic DNA repair as their yeast and plant mutants are sensitive to DNA damaging agents such as methyl-methane sulfonate (MMS) and γ-irradiation (Hollingsworth and Brill, 2004; Hartung *et al.*, 2006; Berchowitz *et al.*, 2007). However, in plants, the formation of MUS81-EME1 dependent class II

COs is limited by the action of the FANCM helicase which acts as an anti-recombinase factor (see section 3.2.4). Moreover, it has been recently discovered that there could be an alternative route of Class II CO formation via the action of the FANCD2 protein, involved in DNA repair (Kurzbauer *et al.*, 2018).

1.3.4. NCO formation

As briefly mentioned in the previous sections, NCOs constitute non-reciprocal exchanges of genetic information between the homologous chromosomes in meiosis. NCOs are associated with the phenomenon of Gene Conversion (GC) if they are associated with the conversion of a heterozygous marker (e.g.: Single Nucleotide Polymorphisms, SNPs) (Szostak *et al.*, 1983; Hunter, 2015). GC was first described in *Ascomycetes* fungi such as *Sordaria spp.* as the formation of asci after meiosis allowed the study of the four resulting haploid products of meiosis, and particularly the analysis of the eight-spored asci of *Sordaria spp.* allowed the tracing of the eight strands of DNA (one duplex per chromatid, two chromatids per homologous chromosome) and their genetic content throughout meiosis (Szostak *et al.*, 1983). In this way, instead of the expected Mendelian 4:4 segregation of heterozygous markers after meiosis, in a lower proportion of the asci 6:2 and 2:6 aberrant segregations were present. These events mirrored the transference of genetic information from a DNA duplex to its homolog in a non-reciprocal manner (Szostak *et al.*, 1983). Moreover, these kinds of aberrant segregations were not the only ones observed, sometimes 5:3 segregations were spotted. These are the result of post-meiotic segregation of markers due to the presence of mismatches in the hDNA that originates during recombination (see section 1.3.2, above) which have not been repaired (Szostak *et al.*, 1983; Hunter, 2015).

The current model for HR during meiosis establishes that there are mainly two routes for NCO formation: SDSA and dHJ resolution.

1.3.4.1. Synthesis-Dependant Strand-Annealing (SDSA)

The SDSA model for DSB repair through NCO formation was initially proposed by Resnick (1976), as a way for repairing mitotic DSBs without CO formation. It was later on when the work of Nassif *et al.* (1994) in the GC events induced by the P-element transposon of *Drosophila melanogaster* proposed its current nomenclature. The SDSA model illustrates that the repair of a DSB occurs after the invasion of the intact homologous DNA molecule by a 3' overhang generated after the resection of the DSB (SEI during meiosis). Then, DNA synthesis takes place using the homologous chromatid as a template, extending the 3' overhang past the DSB site. Next, by contrast with somatic DNA replication the resulting JM is disrupted and the 3' extended overhang can re-anneal with its partner strand of the DSB and after further DNA synthesis the re-annealed product can re-ligate. Next, the mismatch repair machinery repairs any heteroduplex resulting from this process, which sometimes can lead to GC if there is conversion of an heterozygous marker from the donor intact homolog to the duplex where the DSB was originated (Resnick, 1976; Nassif *et al.*, 1994; McMahill, Sham and Bishop, 2007; reviewed in: Pâques and Haber, 1999 and Haber, 2007). A consequence of this model is that meiotic DSBs repair through SDSA is independent from dHJ formation, and thus, it involves an "early decision" for a DSB to be repaired as CO or NCO, which would then occur at the moment of the SEI or soon after (Allers and Lichten, 2001a). Moreover, McMahill, Sham and Bishop (2007) gave specific proof that most of the NCOs formed in yeast

meiosis were originated from the SDSA pathway and not from dHJ resolution by symmetrical cut.

In plants, the FANCM helicase is the main regulator of the SDSA pathway, acting as an anti-recombinase factor by limiting the formation of MUS81-EME1 dependent class II COs and directing the recombination intermediates towards their repair by the SDSA pathway, resulting in their resolution as NCOs (Fig.1.2) (Crismani *et al.*, 2012; Knoll *et al.*, 2012; Blary *et al.*, 2018). Thus, FANCM is essential for the repair of recombination intermediates as double mutant plants for FANCM and MUS81 show chromosome fragmentation in meiosis (Crismani *et al.*, 2012b). Moreover, it seems that in *A. thaliana*, *B. rapa,* and the allopolyploid *B. napus,* the disruption of FANCM in combination with different ZMM mutants is able to increase recombination and fertility to levels similar to those of the WT plants by promoting class II CO formation (Knoll *et al.*, 2012; Crismani *et al.*, 2012; Blary *et al.*, 2018). It is worth to mention that FANCM stands for Fanconi Anaemia Complementation group M, as in mammals mutations in the genes encoding for this group of proteins are responsible of the Fanconi Anaemia Syndrome (Gari *et al.*, 2008; Knoll *et al.*, 2012). In this way, FANCM is needed for DNA repair in somatic cells, having great affinity for branched structures of DNA such as stalled replication forks and HJs (Gari *et al.*, 2008). The yeast FANCM ortholog MPH1 appears to have as well a role in DNA repair in somatic cells as the *mph1* mutants seem to be sensitive for chemical DNA damaging agents such as MMS and EMS (Scheller *et al.*, 2000). Moreover, it seems that the DNA repair role of yeast MPH1 is related to the somatic HR pathway as *mph1* mutation in combination with other HR repair proteins of the RecQ family increases heteroallelic mitotic recombination (Schürer *et al.*, 2004). Thus, by contrast with plants, yeast, and

mammal FANCM orthologs do not seem to play a role in meiotic recombination. Interestingly, in plants the FANCM mediated SDSA repair of somatic and meiotic DSBs requires of another factor, the MHF1 protein (Dangel, Knoll and Puchta, 2014).

1.3.4.2. dHJ dissolution

Nevertheless, not all the dHJs are repaired as COs, they can be processed to form NCOs if they are dissolved by the anti-recombinases of the RTR complex (RECQ4A/B, TOP3α, RMI/BLAP75) (Yin *et al.*, 2005, White, 2008, Hartung *et al.*, 2007). This complex is well known in animals, budding yeast and plants not only for its role in NCO formation during meiosis but for its activity in maintaining genome stability in somatic cells by participating in DSB repair, dissolving dHJs, and thus, avoiding CO formation in mitotic cells (Knoll, Schröpfer and Puchta, 2014).

The first component of the RTR complex is the helicase RECQ4, which in the plant model organism *A. thaliana* is encoded by two paralogs: *RECQ4A* and *RECQ4B.* Both copies have redundant anti-recombinase roles during meiosis as only the disruption of both paralogs can increase recombination and recover CO formation in a *msh4* mutant background (Séguéla-Arnaud *et al.*, 2015). Nevertheless, *RECQ4A* copy seems to have an important role in somatic DNA repair through its interaction with MUS81 and TOP3α, whereas *RECQ4B* does not (Frank Hartung, Suer and Puchta, 2007). In this way, the lethal phenotype of the *top3α* null mutants can be partially rescued in combination with the depletion of *RECQ4A*, despite chromosome fragmentation is present during meiosis in the double mutant *top3α recq4a*. And, in addition, the double mutant *recq4a mus81* is inviable (Hartung *et al.*, 2006; F. Hartung, Suer and Puchta, 2007; Séguéla-Arnaud *et al.*, 2015). By contrast, the depletion of *RECQ4B* in *top3α* mutant background is not able to rescue its lethality

(explained below), and neither the *recq4b mus81* plants are inviable (Frank Hartung, Suer and Puchta, 2007). This suggests that the intermediates produced by RECQ4A are genotoxic if TOP3α does not repair them (F. Hartung, Suer and Puchta, 2007). Sgs1, the yeast RECQ4 homolog seems to play similar roles as the plant RECQ4A helicase. In this way, it was identified as a suppressor of the *top3* slow growth phenotype in *S. cerevisiae*, where Sgs1 seems to create recombination intermediates that unless repaired by Top3 produce genotoxic stress (Gangloff *et al.*, 1994). Later studies showed that Sgs1 is necessary to suppress mitotic recombination and to maintain genome stability during the somatic development (Watt *et al.*, 1996). Concerning the meiotic role of Sgs1, it shows anti-CO activity as despite the *sgs1* mutation shows no effect in terms of CO or NCO formation, when combined with mutations of ZMM proteins it is able to increase recombination and to partially rescue synapsis (Jessop *et al.*, 2006). Moreover, *SGS1* also seems to have a genetic interaction with MUS81-EME1 as the combination of *sgs1* and *mus81/mms4* mutations is synthetically lethal due to the accumulation of unresolved JM (Jessop and Lichten, 2008). A homolog of this RecQ helicase can be found in mice and humans, the BLM (Bloom Syndrome's Mutated) helicase, its name refers to the genetic diseases caused by mutations in this protein. The Bloom Syndrome is an autosomal recessive mutation characterised by sterility, growth delay and predisposition to cancer. The meiotic phenotype of the mutation has been studied in conditional KO mutants in mice, showing that the absence of BLM causes defects in pairing and synapsis, together with increased CO levels and multichromatid events (Holloway *et al.*, 2010).

Regarding next component of the RTR complex, TOP3α is the *Arabidopsis* ortholog of the yeast type IA topoisomerase TOP3. The role of this topoisomerase has been extensively characterised in yeast, where *top3* mutants display somatic hyper-recombination, sporulation defects, and chromosome instability (Gangloff *et al.*, 1994). In *A. thaliana top3α* null mutations are lethal, and hypomorphic mutants display increased sensitivity to genotoxic agents as MMS and cisplatin as well as increased somatic HR. The meiotic phenotype of these mutants consists of extensive chromosome fragmentation in anaphase I that is dependent on SPO11 programmed DSBs and epistatic to the *rad51* mutation (Hartung *et al.*, 2008).

The last component of the RTR complex is the RMI/BLAP75 protein. Within the complex, RMI seems to have a more structural role by physically interacting and bringing together RECQ4A and TOP3α. *Arabidopsis* RMI null-mutant plants show increased sensitivity to genotoxic agents and in meiosis display 5 bivalent-like structures that result in chromosome fragmentation in anaphase I (Chelysheva *et al.*, 2008; Hartung *et al.*, 2008).

It is worth to mention that, due to the hyper-recombinant phenotype of the plants defective for these proteins (as the RTR complex has anti-CO activity), these mutants (particularly *recq4A*) have been used in combination with other mutant alleles of different anti-CO factors that limit class II CO formation to generate plants with increased CO formation (Fernandes *et al.*, 2017; Mieulet *et al.*, 2018). In this way, if the limitations on the translation of this knowledge to crops can be overcome (i.e.: mutant generation), this could constitute a powerful tool to be included in breeding programs as combinations of alleles of linked traits could be achieved more

efficiently, boosting the generation of new crop varieties (Blary and Jenczewski, 2019).

Interestingly**,** a recent publication has pointed out the role of the class II CO recombinase FANCD2 and the class II anti-recombinases FANCM, FIGL1 and RMI1 in the regulation of the distribution of class I COs. In this way, mutants for the genes named above show shorter inter-CO distances despite not changing the overall CO levels, indicating changes in the strength of the interference signal (Li *et al.*, 2021b). Moreover, similar results were obtained in the analysis of *fancm* mutants in lettuce, which presented problems in the formation of the obligatory CO despite showing similar levels of class I CO formation (Li *et al.*, 2021a).

1.3.5. Positive interference

In most organisms, COs tend to occur evenly spaced along the chromosomes rather than clustered together. This peculiar patterning of CO events is due to the phenomenon of positive interference, which was initially described more than a century ago by Sturtevant in the context of his studies on genetic linkage in the fruit fly *Drosophila melanogaster* (Sturtevant, 1913, 1915). In this way, he observed that the number of double COs within two adjacent genetic intervals was lower than the number expected if CO events occurred by random, as if the formation of a CO in one interval "interfered" with the formation of another CO in the contiguous interval. Therefore, "*positive interference"* can be defined as the reduction in the probabilities of the formation of a CO nearby a pre-existing one (Zickler and Kleckner, 2016). It is worth to mention that as explained by Zickler and Kleckner (2016): "*the metric of interference is physical distance along the chromosomes*"; even though we can measure its effect over recombination in genetic distance between markers (cM) and

genomic distances expressed in Mb. Moreover, the strength of the interference signal tends to be maximal at short inter-CO distances and progressively decrease with the distance from a CO event, thus involving some sort of communication along the chromosome (Kleckner, 2006). Remarkably, whereas several different models have been proposed to explain the mechanical basis of interference, the particular interactors mediating this phenomenon are still unknown.

The current model that sets a mechanical basis to explain how the interference signal is generated and spread along the chromosomes is the "*Beam-Film model*" (Kleckner *et al.*, 2004; Kleckner, 2006; Zhang *et al.*, 2014; Zickler and Kleckner, 2016). This model proposes that the interference signal arises and is propagated along the chromosome as a mechanical stress. Thus, it creates a mechanical system in which communication occurs automatically through the redistribution of the stress. In this way, the mechanical stress would appear as a compression force over the meiotic chromosome axis as a result of the expansion of the chromatin that takes place during the first stages of meiosis. On the other hand, the interactions between homologous chromosomes that occur in the inter-axis bridges would be the CO precursors, once a precursor is designated to form a CO the interference signal would appear as a result of the stress relief due to the formation of the CO, extending into the vicinity of the CO event (Kleckner *et al.*, 2004; Kleckner, 2006; Zickler and Kleckner, 2016). Therefore, as explained in (Zickler and Kleckner, 2016) the "*Beam-Film model*" implies that: i) The interference signal spreads to both sides from a CO-designation site, reducing its intensity with distance, and disfavouring the formation of another CO nearby; ii) CO designation occurs sequentially, with further CO designation sites occurring away from the previous ones in a "fill in the holes"

manner, resulting in an even spacing of the COs; iii) the process of CO-designation is very strong, ensuing the “obligatory CO” and the occurrence of further CO-designations until they are limited by the interference signal.

Despite that the biochemical mechanisms underlying the spreading of the interference signal have yet to be uncovered, recent studies have pointed out that several factors might be involved. In this way, Capilla-Pérez *et al.* (2021) and France *et al.* (2021) have shown that in the model organism *A. thaliana* the SC component ZYP1 might have a critical role in the establishment of interference between the class I COs. On the other hand, studies about the diploidisation process in *A. arenosa* have pointed out that the AEs might also have a role in the transference of the interference signal as the tetraploid alleles of the axis associated proteins ASY1 and ASY3 seem to play a role in reducing the formation of multivalents by regulating the CO pattering (Morgan *et al.*, 2020; Morgan *et al.*, 2021).

1.4. The dynamic structure of the chromosomes in meiosis

1.4.1. The Axial/Lateral Elements

The AEs are proteinaceous structures formed between the sister chromatids at the onset of meiosis and are part of the Synaptonemal Complex (SC) at pachytene, comprising the LEs. Within the AEs the chromatin is organised as a linear array of loops with their base held at the chromosome core (axis). The AEs are formed during leptotene between both sister chromatids, that have their loops opposed to each other. However, this configuration changes after the formation of the SC, when the sister chromatids are co-oriented with the loops extruding outwards from the LEs of the SC (Denise Zickler and Kleckner, 1999; Kleckner, 2006). Interestingly the loop length varies among different species but remains relatively constant between

individuals of the same species (Moens and Pearlman, 1988; Zickler and Kleckner, 1999). Moreover, the number of loops per µm of the pachytene LEs is conserved across species, being ~20 loops per µm (Zickler and Kleckner, 1999; Kleckner, 2006). In this way, it has been proposed the existence of a "*loop base module*" of conserved dimensions across taxa, and therefore, the differences in genome size are accommodated within these modules by different loop sizes. Also, the modules are "*dual loop modules*" as the AEs accommodate both sister chromatids (Kleckner, 2006). For instance, *S. cerevisiae* shows 0.5 µm loops accommodating a relatively small genome, whereas in mouse the loops are about 3 µm, accommodating a much larger genome (Moens and Pearlman, 1988).

The AEs are composed of cohesins, condensins, and meiosis-specific axis-associated proteins. Cohesins and condensins are responsible for the generation and maintenance of a higher-order chromosome structure as they are essential for the individualisation of the chromosomes, keeping both sister chromatids together and mediating the changes in the compaction levels from G2 to metaphase I. Without the maintenance of the chromosome structure during meiosis, pairing, synapsis, and recombination between the homologous chromosomes is severely compromised as well as the conservation of sister chromatid cohesion (Mainiero and Pawlowski, 2014). The meiosis-specific axis-associated proteins are not essential for the maintenance of the chromosome structure during meiosis but are necessary for pairing, the establishment of the SC, and recombination between the homologs. A schematic representation if the meiotic chromosome axis is provided in Figure 1.3.

1.4.1.1. Axial element components I: Cohesins

Cohesins are essential components of the chromosomes in eukaryotic organisms, being essential for maintaining chromosome structure, and for the correct segregation of the sister chromatids during mitosis and the homologous chromosomes during meiosis. Cohesins are ring shaped complexes that hold the sister chromatids together by catching them within their structure, thus maintaining Sister Chromatid Cohesion (SCC) throughout the cell cycle, from their loading during the S-phase to their cleavage in anaphase (reviewed in Mainiero and Pawlowski, 2014; Bolaños-Villegas *et al.*, 2017).

The cohesin complexes comprise 4 different structural proteins (Mainiero and Pawlowski, 2014; Bolaños-Villegas *et al.*, 2017): i) two Structure Maintenance of Chromosome proteins (SMC1, SMC3); composed by a N-terminal ATP binding domain, two antiparallel coiled-coil domains separated by a hinge region, and a C-terminal DA box; ii) one α-kleisin Sister Chromatid Cohesion protein 1 (SCC1) that maintains the ring closed by interacting with the SMC N-terminal ATP binding domain; iii) one SCC3 subunit that interacts with SCC1.

The mitotic and meiotic cohesin complexes differ in their composition, particularly in the α-kleisin subunit that closes the ring. Whereas in mitosis this role corresponds to SCC1, during meiosis SCC1 is substituted by the RECOMBINATION 8 protein REC8, first identified in budding yeast (Klein *et al.*, 1999; reviewed in Mainiero and Pawlowski, 2014; Bolaños-Villegas *et al.*, 2017). In plants REC8/SYN1 has been widely studied in maize (ADF1) (Golubovskaya *et al.*, 2006), and particularly in *A. thaliana* (REC8/SYN1/DIF1) (Bhatt *et al.*, 1999; Dong, Cai and Makaroff, 2001; Cai *et al.*, 2003; Chelysheva *et al.*, 2005; Lambing *et al.*, 2020). During meiosis,

REC8/SYN1 is associated with the chromatin independently of SPO11-mediated DSBs, it appears between the sister chromatids of the homologs from the pre-meiotic S-phase, labelling the AEs and the LEs in zygotene and pachytene, until metaphase I, when it remains only in the centromeres (Cai *et al.*, 2003; Chelysheva *et al.*, 2005). REC8/SYN1 mutant plants show disorganised chromatin during the first stages of meiosis, defects in pairing and synapsis, univalents and chromosome fragmentation in metaphase I, and missegregation at the end of meiosis (Bhatt *et al.*, 1999; Cai *et al.*, 2003). Interestingly, the defects on pairing and synapsis are due to defects in the formation of the meiotic axis and the localisation of the ASY1 and ASY3 meiosis-specific axis-associated proteins, which seem to be forming polycomplex-like structures, often associated with recombination nodules (which would explain the formation of chiasmata often observed) (Chelysheva *et al.*, 2005; Zhao *et al.*, 2006; Lambing *et al.*, 2020). In this way, in *Arabidopsis*, directly or indirectly, REC8/SYN1 is required for: i) establishing sister chromatid cohesion during meiosis; ii) pairing and synapsis by favouring the axis localisation of the axis of the axis-associated proteins ASY1 and ASY3; iii) meiotic recombination; iv) DSB repair ; v) the recruitment of SCC3, the fourth component of the cohesin ring.

The cohesin complex interacts with several proteins involved in regulating its dynamics through the cell cycle (Mainiero and Pawlowski, 2014; Bolaños-Villegas *et al.*, 2017): i) the SCC2 and SCC4 proteins are involved in the loading of the cohesin complexes during the S-phase (Sebastian *et al.*, 2009); ii) the Eco1/Ctf7 protein is involved in the establishment of cohesion during the S-phase after the loading of the cohesins to the chromatin, to achieve this Eco1 acetylates 2 conserved lysine residues of SMC3 as it has been observed in yeast and humans (Skibbens *et al.*,

1999; Zhang *et al.*, 2008; Bolaños-Villegas *et al.*, 2013) ; iii) The WAPL1/2 proteins participate in the timely release of the cohesion by disassembling the cohesin ring, being essential for segregation in anaphase I (Kueng *et al.*, 2006; De *et al.*, 2014), its action is counteracted by the SMC3 acetylation by Ctf7 (Zhang *et al.*, 2008); iv) the PDS5 protein also intervenes in SCM3 acetylation (Chan *et al.*, 2013), which antagonizes WAPL (Vaur *et al.*, 2012). Interestingly, whereas in Arabidopsis *pds5* mutants only have mild defects in meiosis consisting in anaphase I bridges, somatic development is severely affected (Pradillo *et al.*, 2015).

1.4.1.2. Axial element components I: Condensins

Another important component of the chromosome axis in mitosis and meiosis are the condensin complexes, which regulate changes in the compaction of the chromatin across the cell cycle (Reviewed in: Nasmyth and Haering, 2005; Hirano, 2012; Mainiero and Pawlowski, 2014). Condensins are V-shaped pentameric complexes similar to cohesins, their components determine the formation of two different types of condensin complexes with different roles in condensation. Type I condensins are involved in lateral compaction of the chromosomes whereas the type II participate in axis shortening (Nasmyth and Haering, 2005; Hirano, 2012; Mainiero and Pawlowski, 2014). Both types of condensins have SMC2 and SMC4 proteins with a N-terminal ATP binding “head” domain and a “hinge” domain. However, the rest of the components are different between the two types of condensins (Nasmyth and Haering, 2005; Hirano, 2012; Mainiero and Pawlowski, 2014): i) Type I condensins have a CAP-H kleisin and the accessory proteins CAP-D2 and CAP-G; ii) Type II condensins have a CAP-H2 kleisin and the accessory proteins CAP-D3 and CAP-G2.

The role of the condesin complexes in chromosome compaction has been widely studied in mitosis, in both plants and animals. However, few studies have enlightened the key task that these protein complexes carry out during the meiotic division. Smith, Osman and Franklin (2014), characterised the meiotic role of both types of condensins through the analysis of T-DNA and RNAi mutants of SMC4, CAP-D2 (Type I), and CAP-D3 (Type II). In this manner, SMC4 was observed to be essential for maintaining chromosome compaction, particularly at the centromeres during metaphase I and anaphase I despite having no role in pairing and synapsis and finding only a modest decrease in CO formation in the RNAi line. A similar role was deducted for the type I condensin since the *cap-d2* RNAi line showed an undistinguishable phenotype from the *smc4* mutant. On the other hand, the type II condensin was shown to play a different role concomitant with its participation in axis shortening, since no defects in centromeric compaction were observed in the *cap-d3* mutants, but mild chromosome fragmentation and interconnections between the chromosomes arose in metaphase I.

1.4.1.3. Axial element components II: Axis-associated proteins

Together with the condensins and cohesins that form the chromosome cores, during meiosis, a group of proteins specific of this cell division characterise the formation of the AEs. These are not required for maintaining the structure of the chromosome axis but are associated with it and are required for synapsis and recombination. These proteins can be grouped into two different categories: HORMA domain proteins and coiled-coil domain proteins. The presence of homologs of these proteins identified in different taxa has been summarised in the Table 1.1.

The HORMA domain proteins take their name from the chromatin interaction domain present in their amino acid sequences. The name of this domain derivates from three unrelated proteins from budding yeast: HOP1, REV7 and MAD2 (Rosenberg and Corbett, 2015). The general structure of the HORMAD proteins consist of a HORMA domain located in the N-terminal, which itself contains the core of the domain and a safety-belt region that interacts with the HORMA domain creating open and closed conformations. The HORMAD proteins usually bind a closure motif in their C-terminal to mediate their self-assembly and oligomerisation (Kim *et al.*, 2014; Rosenberg and Corbett, 2015). Remarkably, the closure motif in the meiotic HORMADs is part of their own protein sequence and it is located in their disordered C-terminal region and allows their own self-assembly by directly interacting with the HORMA domain (Kim *et al.*, 2014; Gu, Desai and Corbett, 2022).

Regarding the plant meiotic HORMADs, the most studied one is the *Arabidopsis thaliana* Hop1 ortholog ASY1 (ASYNAPTIC 1), even though a putative paralog (ASY2) has also been identified despite it remains to be characterised. *ASY1* was primarily identified in a screen of T-DNA mutants with defects in fertility, and later on, its homology with the yeast meiotic HORMAD HOP1 was found (Ross *et al.*, 1997; Caryl *et al.*, 2000). Plants defective for ASY1 show defects in synapsis, even though pairing is only mildly reduced as it becomes more unstable (due to the absence of synapsis) and reduced levels of CO formation which lead to missegregation and fertility problems (Ross *et al.*, 1997; Armstrong, Franklin and Jones, 2001; Sanchez-Moran *et al.*, 2001). Moreover, *asy1* mutant plants seem to mainly form distal chiasmata close to the telomeric regions, an effect also observed in plants heterozygous for the mutation of *asy1* (Moran *et al.*, 2001; Lambing, *et al.*, 2020).

This phenomenon, seems likely to be a consequence of the remaining telomeric pairing and short SC stretches (Pradillo *et al.*, 2007). In *Wild-Type* (WT) plants ASY1 associates to the AEs during the early stages of prophase I, having a more linear appearance, and after the establishment of the SC it is depleted form the LEs by the action of the AAA+ ATPase PCH2, remaining attached to the chromatin associated with the LEs (Armstrong *et al.*, 2002; Lambing *et al.*, 2015). Remarkably, ASY1 and its association with the chromosome axis seems to be conserved across the flowering plants (Sanchez-Moran *et al.*, 2008). In this way, orthologs of ASY1 have been identified, and in some cases thoroughly characterised, in other plant organisms as: *A. arenosa* and *A. lyrata*, both members of the *Arabidopsis* genus; other plants of the Brassicaceae family as *B. rapa* and *B. oleracea;* and in cereals such as barley, wheat, rice (named PAIR2), and maize (Armstrong *et al.*, 2002; Nonomura *et al.*, 2004; Boden *et al.*, 2007; Lee *et al.*, 2015; Colas *et al.*, 2017; Morgan *et al.*, 2020a; Seear *et al.*, 2020; Cuacos *et al.*, 2021). Regarding its role in HR, despite having no role in DSB formation in plants, ASY1 seems to participate in the stabilisation of DMC1 (see section 1.3.2) during the homologous strand invasion process (Sanchez-Moran *et al.*, 2007, 2008). According with the complexity of the meiotic cell division ASY1 is subject to a tight regulation during meiosis based on post-translational modifications such as phosphorylation by the cyclin dependant kinase CDKA1 (Yang *et al.*, 2019; Chao Yang *et al.*, 2020), which has been observed in *Arabidopsis* and *Brassica* (Osman *et al.*, 2018a), and its depletion from the AEs to the LE associated chromatin in synapsed regions by PCH2 as previously mentioned (Lambing *et al.*, 2015). This interplay between both processes constitutes the best-known part of the meiotic axis remodelling and is explained in more detail in the

section 1.4.1.4 (below). Axis-associated meiotic HORMA domain proteins have also been studied in great detail in animals such as in mouse, where two of these proteins (HORMAD1 & HORMAD2) have been found to have similar roles on synapsis and DSB repair as the ones described for plants and yeast, and also these are depleted from the LEs after synapsis by the PCH2 ortholog TRIP13 (Wojtasz *et al.*, 2009; Roig *et al.*, 2010; Kim *et al.*, 2017; Fujiwara *et al.*, 2020). Interestingly, it has also been suggested that the cohesin REC8 participates in their recruitment to the axis, which is stabilised by the coiled coil domain protein SYCP2 (Fujiwara *et al.*, 2020). Moreover, the nematode worm *C. elegans* possess 4 different meiosis specific HORMA domain proteins (HIM-3, HTP-1, HTP-2, and HTP-3), with similar yet separate roles during meiosis (Kim *et al.*, 2014). In this way, HTP-3 is necessary for the axis localisation of the other three, pairing, synapsis, DSB formation and sister chromatid cohesion; HIM-3 is required for pairing and synapsis, also participating in the IH Bias*;* and HTP-1/2 have similar roles, HTP-1 is necessary to prevent non-homologous synapsis, and despite HTP-2 mutants do not seem to have a clear phenotype the double mutant shows a more severe disruption of the meiotic programme (Martinez-Perez and Villeneuve, 2005; Kim *et al.*, 2014).

The other two key axis-associated proteins in plants are the coiled-coil domain proteins ASY3 and ASY4. In the first place, ASY3 is the *Arabidopsis* ortholog of the yeast RED1 (Rockmill and Roeder, 1988; Smith and Roeder, 1997; Ferdous *et al.*, 2012), and mouse SYCP2 (Yang *et al.*, 2006; West *et al.*, 2019); whereas, ASY4 seems to be the *Arabidopsis* ortholog of mouse SYCP3 (Chambon *et al.*, 2018; Osman *et al.*, 2018; West *et al.*, 2019). *A. thaliana* ASY3 associates with the chromosome axis from the onset of meiosis to pachytene, remaining as part of the

LEs after the formation of the SC by contrast with ASY1, which is depleted of from the axis after synapsis (Ferdous *et al.*, 2012). Moreover, the correct association of ASY3 with the chromosome axis requires the presence of the REC8 cohesin (Ferdous *et al.*, 2012; Lambing, Tock, *et al.*, 2020). During meiosis, ASY3 is required for the formation of the SC and COs between the homologous chromosomes, being essential for the correct axis localisation of ASY1, to which it physically interacts through the association between its N-terminal closure-motif and the HORMA domain of ASY1 (Ferdous *et al.*, 2012; West *et al.*, 2019). In addition to its role in ASY1 recruitment, ASY3 is required to maintain WT levels of: DSBs, early and late recombination intermediates; as the number of γH2AX, RAD51, DMC1, MSH4, and MLH1 foci are significantly reduced in the *asy3* mutants, consequently with the reduction in chiasma formation (Ferdous *et al.*, 2012; West *et al.*, 2019). Further ASY3 orthologs have been found to play similar roles in in other plant organisms as PAIR3 in rice and DSY2 in maize (Yuan *et al.*, 2009; Wang *et al.*, 2011; Lee *et al.*, 2015). The functions of these coiled-coiled domain proteins seem to be evolutionary conserved across kingdoms as RED1, the yeast ortholog of ASY3 has comparable functions in meiosis (Rockmill and Roeder, 1988a, 1990; Smith and Roeder, 1997). In this way, RED1 is as well associated with the chromosomes axis during prophase I, remaining in the AEs during pachytene; and is also required for: i) the chromosomal association of HOP1; ii) the formation of the synaptonemal complex, iii) maintaining WT levels of reciprocal recombination between the homologs; iv) the proper segregation of the chromosomes during meiosis. However, by contrast with ASY3, RED1 is not required for WT levels of DSBs. Moreover, mouse ASY3/RED1 ortholog SYCP2 seems to play a similar role as it is necessary for the formation of

the SC and the stabilisation of the ASY1 ortholog HORMAD1 in the AEs after its recruitment by the cohesins REC8 and RAD21L (Yang *et al.*, 2006; Fujiwara *et al.*, 2020).

In plants and mice, together with the coiled-coil domain axis-associated proteins ASY3 and SYCP2 (Yang *et al.*, 2006; Ferdous *et al.*, 2012), other meiosis-specific small coiled-coil domain proteins have been found to be involved in the formation of the meiotic chromosome axis. These proteins are ASY4 in *A. thaliana* and SYCP3 in mouse, which share moderate homology with their counterparts (Yuan *et al.*, 2000; Chambon *et al.*, 2018; Osman *et al.*, 2018a). In plants, in the same manner as ASY1 and ASY3, ASY4 is essential for synapsis and CO formation as plants defective for ASY4 show an asynaptic phenotype and reduced CO formation. Nevertheless, the meiotic defects of the *asy4* mutant are milder than the ones found in *asy1* and *asy3* mutant lines, displaying higher levels of COs and synapsis between the homologs (Chambon *et al.*, 2018). ASY4 localises to the chromosome axis in a similar way as ASY3, remaining associated to the LEs after synapsis, and physically interacts with ASY1, ASY3 and itself (Chambon *et al.*, 2018; West *et al.*, 2019). Similar functions have been found for SYCP3, the murine ortholog of ASY4 (Yuan *et al.*, 2000).

Recent studies have shed some light over the contributions of the coiled coil domain proteins to the chromosome axis morphogenesis and their physical relations within this structure (West *et al.*, 2019). In this way, it has been proposed that SYCP2 and SYCP3 associate 2 by 2 forming antiparallel heterotetrameric complexes, that polymerise into filamentous structures by their end to end association and associate to the HORMA domain proteins through their N-terminal closure motif (West *et al.*, 2019). This way of organisation has been suggested to be conserved for ASY3 and

ASY4 in plants, whereas in budding yeast RED1 would associate forming homotetramers due to the absence of a SYCP3/ASY4 ortholog (West *et al.*, 2019). Interestingly, the coiled-coil domain proteins associated to the AEs are absent in the organisms with alternative modes of meiosis such as *C. elegans* or *D. melanogaster*, where recombination is dependent on synapsis, and ciliates as *T. thermophila* where the SC is absent, and the nuclei elongate to favour the recognition between the homologs (West *et al.*, 2019; Chi *et al.*, 2014). In addition, no HORMA domain proteins have been identified in *D. melanogaster* and *T. termophila* (Chi *et al.*, 2014).

It is worth exploring into more detail the particular role of the axis-associated proteins in favouring IHR during meiosis. In this manner, thanks to the great resolution of the molecular techniques used in *S. cerevisiae* to observe the different recombination intermediates generated, HOP1 and RED1 have been shown to be essential for the establishment of the IH Bias. In this manner, IHR (COs and NCOs) is greatly reduced in favour of ISR in the mutants for HOP1 and RED1 (Hollingsworth and Byers, 1989; Rockmill and Roeder, 1990; Kim *et al.*, 2010). Moreover, it has been proposed that the tandem HOP1-RED1 would counteract the action of the meiosis-specific cohesin subunit REC8, which at the early steps of recombination favours *Inter-Sister Single-End Invasion* and repair by keeping both sister chromatids in close proximity (Kim *et al.*, 2010). This concurs with the enrichment of REC8 in CO depleted regions observed in *A. thaliana* by Lambing *et al.* (2020).These observations agree with the phenotypes present in the *asy1* and *asy3* mutants of *A. thaliana,* in which recombination with the homologous chromosome is greatly reduced while no chromosome fragmentation is observed, indicating that the DSBs produced by

SPO11 must be repaired with the sister chromatid (Armstrong *et al.*, 2002; Sanchez-Moran *et al.*, 2007, 2008; Ferdous *et al.*, 2012).

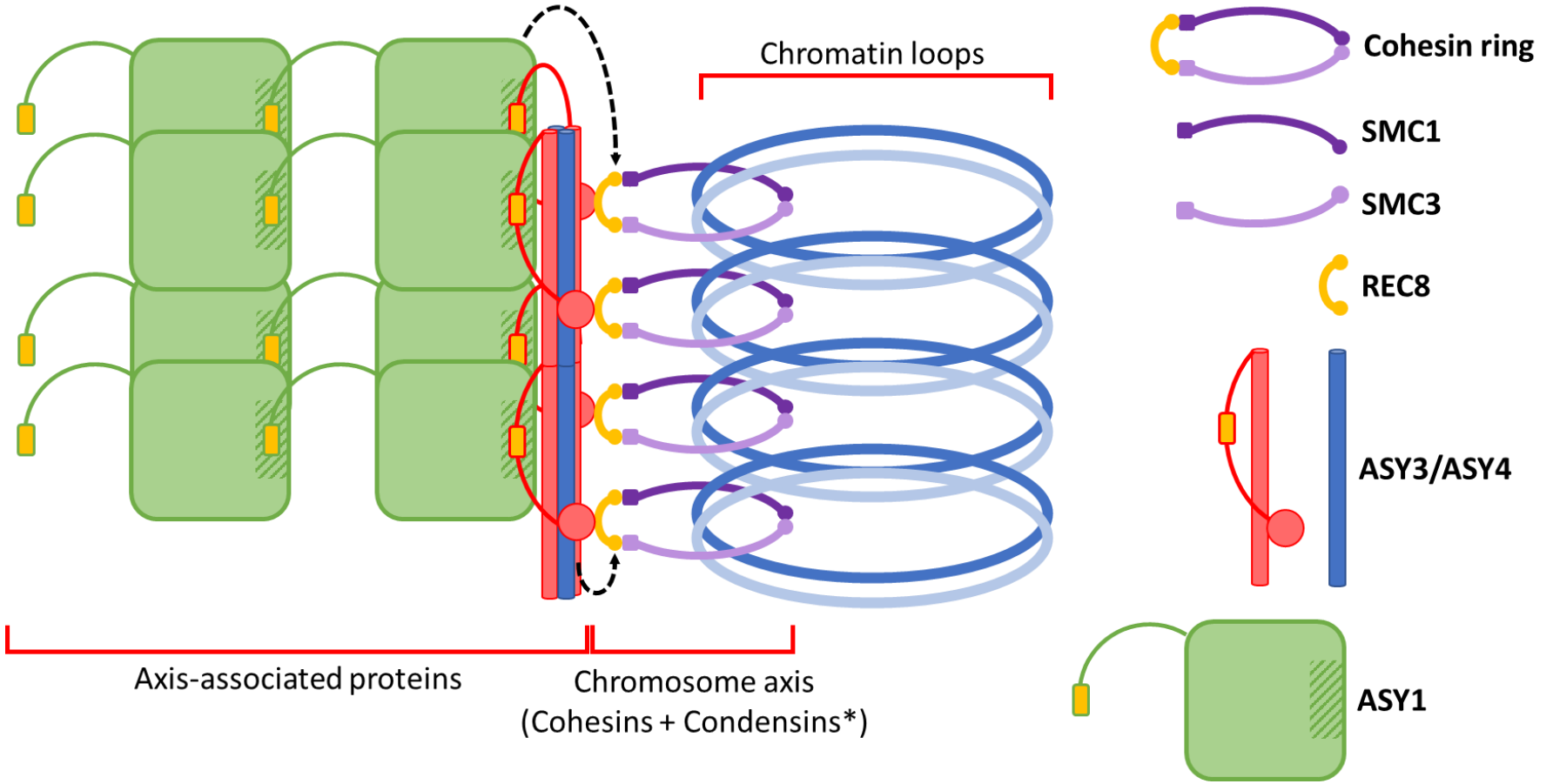


**Figure 1.3. Schematic representation of the meiotic chromosome axis organisation. ***For the sake of simplicity condensins are not represented in this scheme. The black arrows represent interactions that have been suggested in different organisms but are still to be confirmed (Kim *et al.*, 2014; West, Komives and Corbett, 2018; West *et al.*, 2019; Fujiwara *et al.*, 2020; Lambing *et al.*, 2020). The yellow boxes represent the C-terminal closure domains of ASY1 and ASY3. The dark green diagonal pattern indicates the HORMA domain of ASY1.

Table 1.1. Axis-associated proteins across the different taxa

Organism	HORMA domain proteins	Coiled-coil domain proteins (aa)		References
		Large	Small	
B. rapa	ASY1	ASY3 (769)	-	(Cuacos et al., 2021)
A. thaliana	ASY1 / ASY2	ASY3 (793)	ASY4 (212)	(Caryl *et al.*, 2000; Armstrong *et al.*, 2002; Ferdous *et al.*, 2012; Chambon *et al.*, 2018)
A. arenosa	ASY1	ASY3 (792-818)	-	(Morgan *et al.*, 2020)
A. lyrata	ASY1	ASY3 (789)	-	(Seear *et al.*, 2020)
H. vulgare	ASY1	-	-	(Colas *et al.*, 2017)
T. aestivum	ASY1	-	-	(Boden *et al.*, 2007)
O. sativa	PAIR2	PAIR3 (844)	-	(Yuan *et al.*, 2009; K. Wang *et al.*, 2011)
Z. mays	ASY1	DSY2 (758)	-	(Lee *et al.*, 2015)
M. musculus	HORMAD1 / HORMAD2	SYCP2 (1500)	SYCP3 (254)	(Yang *et al.*, 2006)
S. cerevisiae	HOP1	RED1 (827)	-	(Rockmill and Roeder, 1988b; Hollingsworth and Ponte, 1997; Smith and Roeder, 1997)
S. pombe	HOP1	REC10 (791)	-	(Lorenz *et al.*, 2004; Latypov *et al.*, 2010)
C. elegans	HIM-3 / HTP-1 / HTP-2 / HTP-3	-	-	(Kim *et al.*, 2014)
D. melanogaster	-	-	-	(West *et al.*, 2019)
T. thermophila	-	-	-	(Chi *et al.*, 2014)

The number in parenthesis indicate the number of amino acid residues.
- Indicates that the corresponding ortholog is absent or it has not been identified yet.

1.4.1.4. Chromosome axis remodelling through prophase I: Post-translational modifications and the role of the AAA+ ATPase PCH2

As briefly mentioned in section 1.4.1.3, one of the main parts of the meiotic axis remodelling in plants is the interplay between: i) the phosphorylation of ASY1 by CDKA;1; ii) the state changes of ASY1 through the interaction with PCH2; iii) the depletion of ASY1 from the synapsed regions by PCH2.

For the sake of simplicity, although chronologically the role of each interactor has been characterised in different publications in recent years, we will describe the functions of each protein separately and then the whole model of ASY1 regulation as proposed by (Yang *et al.*, 2020). In the first place we will talk about the role of the AAA+ ATPase PCH2 (PACHYTENE CHECKPOINT 2) in the depletion of ASY1 from the AEs to the chromatin associated with the axis and its importance in mediating the state changes of ASY1 during prophase I. PCH2 is the *A. thaliana* ortholog of the yeast Pch2 (Borner, Barot and Kleckner, 2008), and mouse TRIP13 (Roig *et al.*, 2010). PCH2 is necessary for the completion of synapsis and the maintenance of normal levels of CO formation between the homologs in *Arabidopsis*. In this way, the *pch2* mutant plants display a reduction in SC extension of a 68%, and a decrease in CO levels of a 30% likely due to defects in CO maturation as only late recombination intermediates such as HEI10 or MLH1 seem to be affected in *pch2* (Lambing *et al.*, 2015). Moreover, super-resolution analysis of *pch2* late prophase I meiocytes showed that ASY1 remained associated with the LEs of the SC, demonstrating that PCH2 is required for the rearrangement of ASY1 from the LEs to the chromatin (in the WT, ASY1 in the synapsed regions appears as a hazy signal in the chromatin) (Lambing *et al.*, 2015). This role in the control of HORMA domain protein distribution

and recombination has also been observed in other organisms. For instance, in budding yeast Pch2 regulates the localisation of Hop1 in hyper-abundant domains that alternate with Zip1, and the pachytene checkpoint, being able to rescue the pachytene arrest observed in *zip1* (Borner, Barot and Kleckner, 2008; Joshi *et al.*, 2009; Chen *et al.*, 2013; Vader, 2015). Similarly, mice TRIP13 participates in the depletion of the ASY1 orthologs HORMAD1/2 from the synapsed regions, being essential for completion of synapsis, regulating early recombination events and CO formation (Wojtasz *et al.*, 2009; Roig *et al.*, 2010).

Regarding the second role of PCH2 regulating the state changes of ASY1 in plant meiosis (Fig. 1.4), two recent findings have shed light in this process. In the first place, it was recently found that the HORMA domain of ASY1 is able to interact with its own C-terminal closure motif, thus allowing ASY1 to adopt two conformations, open and closed (O-ASY1 and C-ASY1, respectively); and to self-polymerise (West *et al.*, 2019). Secondly, Yang *et al.* (2020) found that PCH2 is essential for the nuclear localisation of ASY1 by changing its conformation from a closed to an open state by disengaging the interaction between the HORMA and closure motifs of ASY1. Moreover, the change to an opened stage is needed for the nuclear import and chromosome loading of ASY1 during early prophase, and the interaction of PCH2 with the closure motif is necessary for its correct depletion from synapsed regions in late prophase I (Chao Yang *et al.*, 2020). It is worth to mention that in order for PCH2 to interact with ASY1 it needs the cofactor protein COMET/p31^{COMET} which acts as a bridge between both (Balboni *et al.*, 2020).

In a complementary way, together with the changes between open and closed states mediated by PCH2, ASY1 is subject to extensive phosphorylation during prophase I

(Osman *et al.*, 2018a). This phosphorylation is mainly carried out by the cyclin-dependant kinase CDKA;1 which is an essential regulator of cell cycle during mitosis and meiosis as different hypomorphic alleles show: defects in somatic development, premature meiosis exit, reduced CO formation, and disruption of synapsis (Dissmeyer *et al.*, 2007; Wijnker *et al.*, 2019; Yang *et al.*, 2019). A more detailed analysis of the role of CDKA;1 in the axis morphogenesis by Yang *et al.* (2019) showed that ASY1 phosphorylation by CDKA;1 is essential for the axis association of ASY1 by enhancing its affinity to ASY3 and promoting its self-assembly. Moreover, ASY1 phosphorylation during prophase I counteracts its axis dissociation by PCH2, which at the same time seems to be necessary for its nuclear localisation. Interestingly, this study also revealed the colocalization of ASY1 and CDKA;1 in the non-synapsed regions, and the partner cyclins of CDKA;1 in ASY1 phosphorylation: SDS and TAM.

The models for CDKA;1 phosphorylation and PCH2 mediated state change of ASY1 proposed by Yang *et al.* (2019, 2020) can be combined in a single model of ASY1 remodelling through prophase I. In this way, during early prophase I PCH2 promotes the change of ASY1 to an open conformation in the cytoplasm by disrupting the association of the HORMA domain to the closure motif, thus, facilitating its nuclear import. Inside the nucleus PCH2 ensures the presence of a pool of ASY1 in its open conformation, which then, promoted by the phosphorylation by CDKA;1, associates with the chromosome axis through the interaction with the closure motif of ASY3. According to (Chao Yang *et al.*, 2020) PCH2 during early prophase I would also act as a quality control by disassembling incorrectly bound ASY1. At the same time, the phosphorylation by CDKA;1 would inhibit the disassociation of ASY1 from the meiotic

axis by counteracting PCH2. During late prophase PCH2 is recruited to the SC and promotes ASY1 depletion from the LEs (ASY1 would remain attached to the chromatin) in the synapsed regions by promoting its open/unlocked configuration. Nevertheless, as explained by Yang *et al.* (2019) this model does not account for a mechanism to explain how PCH2 is able to disassemble the phosphorylated ASY1 in the synapsed regions during late prophase I.

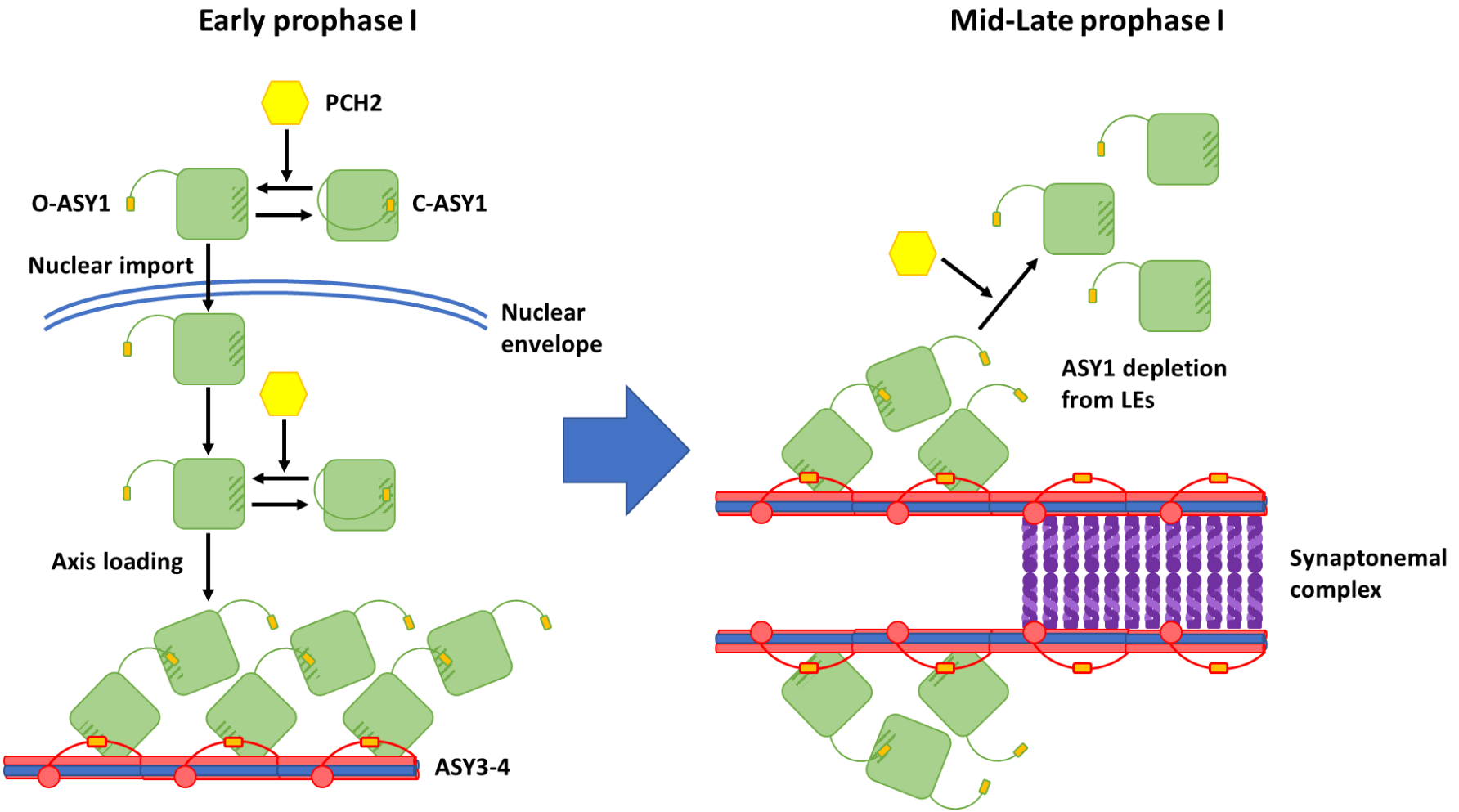


Figure 1.4. Schematic representation of the ASY1 remodelling by PCH2 during early and mid-late prophase I. Modified from Yang *et al.* (2020).

1.4.2. The formation of the Synaptonemal Complex (SC)

The Synaptonemal Complex is a tripartite ladder-like proteinaceous structure formed between the homologous chromosomes during prophase I. It starts to be assembled during the zygotene stage following the pairing and coalignment of the homologs. During pachytene the formation of the SC is completed, and the homologous chromosomes show synapsis in all their length, remaining in close juxtaposition. Finally, as prophase I advances the SC is disassembled during the diplotene stage. The SC is composed by two LEs and a Central Region (CR) formed by the TFs and a linear structure that runs parallel to the LEs called the Central Element (CE), where the TFs interdigitate (Solari and Moses, 1973; Zickler and Kleckner, 1999). The first descriptions of the SC were produced by Moses (1956) and Fawcett (1956) through the study of the meiotic chromosome ultrastructure of crayfish and vertebrate spermatocytes using electron microscopy. Interestingly, the width of the Central Region is evolutionary conserved across taxa, having an overall width of 100 nm (Zickler and Kleckner, 1999).

Interestingly, despite of being an evolutionary conserved structure, little homology is found between the components of the SC from different organisms, in terms of their number and the sequence similarity between functionally related elements (Heyting, 1996; Osman *et al.*, 2006).

In previous sections we have already described the proteins that compose the LEs of the SC (axis associated proteins, cohesins, and condensins). Thus, in this section we will focus mainly on the components of the TFs as their polymerisation between the homologous chromosomes characterises the formation of the SC. The molecular structure of the TFs proteins consists of a N-terminal globular domain followed by a

central coiled coil domain and a C-terminal globular domain (Tung and Roeder, 1998; Dong and Roeder, 2000; Higgins *et al.*, 2005). The TF proteins associate in parallel to form dimers, which in the SC are oriented with their C-terminal located within the LEs and their N-terminal globular domain oriented towards the CE. The TF dimers interact through their N-terminal domains in a head-to-head association, interdigitating and giving rise to the CE, this association spans the total width of the Central Region (Tung and Roeder, 1998; Dong and Roeder, 2000). In plants, the only component of the TFs that has been characterised so far is the *A. thaliana* ZYP1 protein and its corresponding rice and barley orthologs (Higgins *et al.*, 2005; Osman *et al.*, 2006; Wang *et al.*, 2010; Barakate *et al.*, 2014; Capilla-Pérez *et al.*, 2021; France *et al.*, 2021). In *A. thaliana*, ZYP1 is encoded by 2 copies (*ZYP1a* and *ZYP1b*), located close to each other, which seem to have been originated after a gene duplication event. Both copies are redundant as neither single mutant presents a meiotic phenotype, which only appears when both copies are silenced or disrupted (Higgins *et al.,* 2005; Capilla-Pérez *et al.*, 2021; France *et al.*, 2021). The study of RNAi *zyp1* KD mutants in *A. thaliana* by Higgins *et al.* (2005) revealed that ZYP1, and therefore the SC, is not essential for CO formation as the mutant shows only a mild decrease in chiasma formation. Interestingly, despite the total absence of SC in the *zyp1* RNAi lines, chromosome alignment over large regions could be observed in a small proportion of prophase I nuclei. However, ZYP1 is required for normal progression of meiosis and to avoid non-homologous recombination, as in its absence prophase I suffers a 20h delay and multivalents between non-homologous chromosomes are formed at a great frequency (Higgins *et al.*, 2005). However, more recent studies of the role of AtZYP1 in meiosis by Capilla-Pérez *et al.* (2021) and

France *et al.* (2021) through the use of CRISPR/Cas9 generated double mutants have offered more information about the functions of this protein during meiosis. In this way, ZYP1 appears to be necessary for the establishment of the obligatory CO and interference between the class I COs. Consequently, the *zyp1* double mutants present an increase in recombination due to higher levels of class I CO together with the appearance of a small number of univalents in metaphase I. Moreover, although ZYP1 is essential for the formation of the SC, it is dispensable for pairing as in its absence the homologs are extensively coaligned. Moreover, as shown by France *et al.* (2021) the increase of CO formation observed in in the *zyp1* double mutants is absolutely dependant on: the axis associated proteins ASY1 and ASY3, the axis remodelling ATPase PCH2, and the class I recombinases MSH5 and MLH3. Interestingly, the polymerisation of ZYP1 and the subsequent formation of the SC requires of early recombination events such as DSB formation and SEI to occur as neither the *spo11* nor the *dmc1* mutants present synapsis, and pairing is also greatly reduced in both (Grelon *et al.*, 2001; da Ines *et al.*, 2012). Remarkably, the study of barley and rice mutant plants for their respective ZYP1 orthologs (ZYP1 and ZEP1) showed slightly different phenotypes and possible functions of the SC (Wang *et al.*, 2010; Barakate *et al.*, 2014). In this way, as shown by Wang *et al.* (2010) rice *zep1* mutants display: i) complete pairing between the homologs despite absence of SC; ii) increased CO formation; iii) increased foci number of the ZMM protein MER3, which is depleted less efficiently than in WT; iv) no depletion of the ASY1 ortholog PAIR2 from the axis, which normally occurs after synapsis. Thus, it seems that in rice the SC plays a role in limiting CO formation despite being dispensable for pairing, concurring with the findings of *A. thaliana*. On the other hand, in barley, ZYP1 seems

to be essential for CO formation and timely progression of meiosis (Barakate *et al.*, 2014). Analysis of *zyp1* KD mutants showed a lack of bivalent formation in metaphase I, together with a reduction in MLH1 foci; and a delay in prophase I progression.

In *S. cerevisiae*, the role in SC formation, recombination and meiosis progression of the Zip1 protein, the yeast ortholog of ZYP1, has been extensively studied (Sym, Engebrecht and Roeder, 1993; Heyting, 1996; Tung and Roeder, 1998; Dong and Roeder, 2000). In this manner, yeast Zip1 is essential for the formation of the SC between the homologous chromosomes, being part of the TFs, although in its absence these remain paired at distances between 100-400 nm, showing close interactions in certain points. Moreover, Zip1 defines a meiotic checkpoint in yeast, as *zip1* mutants present arrest at pachytene, which can be overcome in combination with the mutation of Pch2. Also, although Zip1 is not required for the formation and CO commitment of recombination intermediates, it´s needed for their resolution as CO formation is abolished in *zip1*.

1.5. The functional and physical relation between the chromosome axes, the SC, and the recombination complexes

In plants, as in other organisms such as yeast and mammals, the processes of pairing and synapsis depend upon recombination, at least on its early steps of DSB formation and SEI. In this way, it has been observed that in mutants of genes involved in DSB formation, DSB processing or SEI (e.g.: SPO11, MRX complex, RAD51/DMC1), pairing and the formation of the SC between the homologs is abolished (Grelon et al., 2001; Storlazzi *et al.*, 2003; Da Ines *et al.*, 2012; reviewed in: Zickler and Kleckner, 1999; Zickler and Kleckner, 2015). It is worth to mention

that, in other organisms such as *C. elegans* and *D. melanogaster* pairing and synapsis precede the initiation of recombination (Colaiácovo, 2006; Lui and Colaiácovo, 2013; Zickler and Kleckner, 2015; Zickler and Kleckner, 2016).

The group of organisms that rely on recombination for pairing and synapsis is characterised for having a number of DSBs that greatly exceeds the number of COs (e.g.: the DSB-CO ratio in *A. thaliana* is 15-30:1, and in mice is 10:1), although the exception would be *S. cerevisiae* with a 2:1 ratio due to the great number of COs per meiosis (de Massy, 2013). On the opposite, in the organisms in which synapsis is independent of recombination the ratio DSBs:COs tends to be very low (e.g.: 2 DSBs per CO in *C. elegans* and *D. melanogaster*) (de Massy, 2013). Thus, focusing in the first group, many of the recombination intermediates that are not resolved as reciprocal exchanges between the homologs are processed NCOs and Inter-Sister exchanges (Jones, 1971; Schwacha and Kleckner, 1997; Zickler and Kleckner, 2015). However, it has been proposed that the rest of the DSBs, which are the vast majority and do not intervene in CO formation, are necessary for the recognition of the homologs and to bring them together during the pairing process (Zickler and Kleckner, 2015). In this way, after the formation and processing of the DSBs, which occur in the context of the chromosome axis according to the “tethered-loop” model (section 1.2.1.2), the nucleoprotein filament formed by RecA orthologs RAD51/DMC1 would act as a “tentacle” that seeks for homology on the other chromosomes until it finds its partner (Kim *et al.*, 2010). Then, during the SEI (section 1.2.2) both homologs are brought together leading to their pairing and coalignment in which they remain at distances of 300-400 nm (Zickler and Kleckner, 2015).

Interestingly, the process of paring comes together with the formation of characteristic structures associated with the AEs and related to the recombination steps (Fig.1.5). In this way**,** during the early stages of prophase I some ellipsoid shaped nodules (called Zygotene Nodules/ZNs or Early Recombination Nodules) appear associated with the AEs as soon as the homologs begin their pairing. The ZNs are numerous and come into view associated: i) with one of the AEs; ii) in between two AEs; iii) as rod-shaped structures bridging both axes, forming part of structures called inter-axis bridges; iv) associated with stretches of the SC (Albini and Jones, 1987). Immunocytological and molecular studies of the ZNs and the inter-axis bridges, have observed that they are composed of: proteins associated with early recombination such as RPA, RAD51, DMC1, MER3, ZIP2, ZIP4 and MSH4; structural proteins like cohesins; and DNA (Tarsounas *et al.*, 1999; Moens *et al.*, 2002; Moens *et al.*, 2007; Dubois *et al.*, 2019). However, as prophase I progresses towards pachytene, the number of ZNs suffers a dramatic decrease, and these are substituted by Late Nodules (LNs), spherical electrodense structures of bigger size than the ZNs that appear associated with the Central Elements of the SC (Carpenter, 1975a; Carpenter, 1975b). This LNs are related in number to the COs/chiasmata and are associated with recombination and DNA synthesis (they were initially named Recombination Nodules/RNs) (Moens, 1978; Carpenter, 1981; Stack, Anderson and Sherman, 1989). Immunocytological studies showed the association of these LNs with proteins associated with late recombination such as MLH1 and HEI10 (Moens *et al.*, 2002; Anderson *et al.*, 2014; Dubois *et al.*, 2019). Remarkably, the observation that some of the ZNs which eventually become late RNs associated with SC polymerisation has led to the conclusion that the recombination intermediates (ZNs

associated with inter-axis bridges) designated to form COs become sites of SC nucleation. Nevertheless, the reverse is not true as not all the sites of SC nucleation are CO sites (Albini and Jones, 1987; Kleckner, 2006).

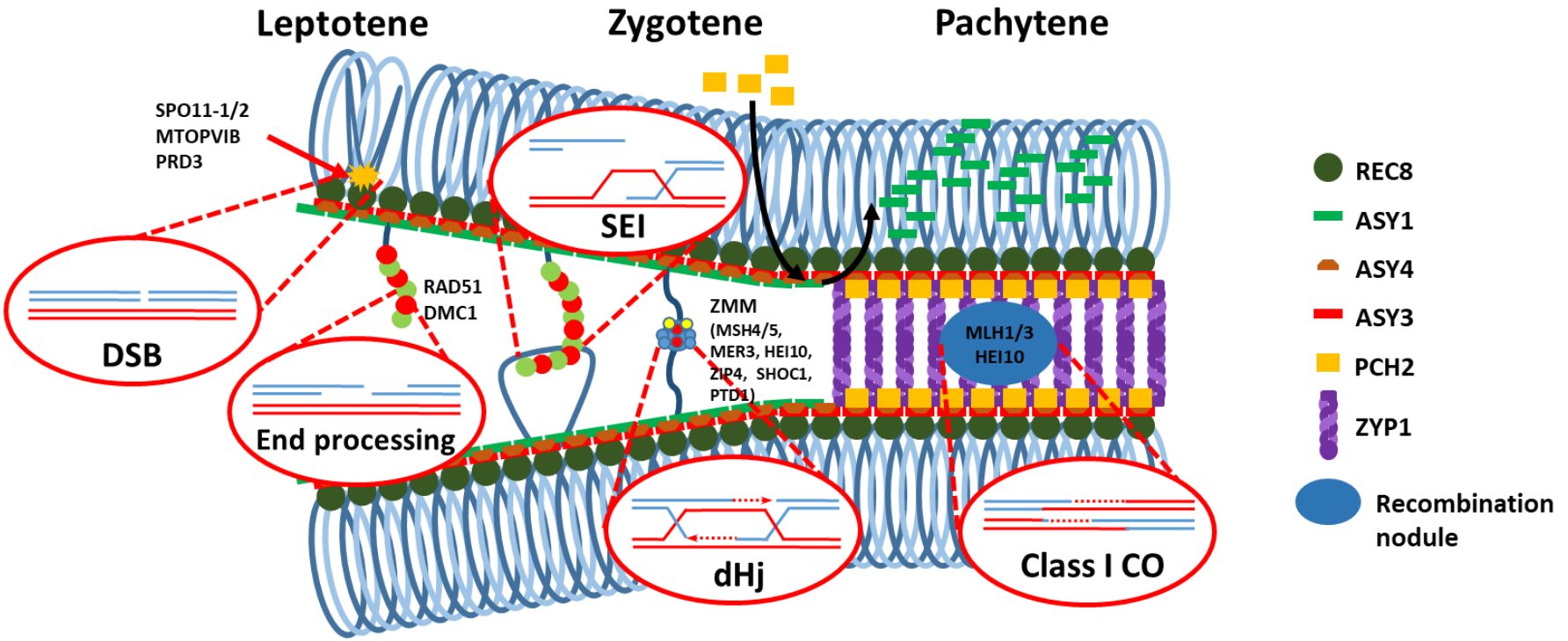


Figure 1.5. Schematic representation of the relation between the different steps in the homologous recombination pathway and the changes in the chromosome structure associated with pairing and synapsis during prophase I.

1.6. The polyploid origin of *Brassica* species

Because the plant model organisms in which this thesis project is focused are *Brassica rapa*, and *Brassica oleracea*, both belonging to the Brassicaceae family, it is of great importance to bear in mind the genetic context of this taxa, a context of polyploidy.

In the first place, we must make a distinction between both classes of polyploids: autopolyploid and allopolyploid. Autopolyploids arise as a result of Whole Genome Duplication (WGD) of a diploid parental and the resulting tetraploid bears four identical copies of each chromosome (four homologs). On the other hand, an allopolyploid is formed in two steps: a first step of hybridisation between two closely related parental species followed by WGD. This results in a tetraploid hybrid bearing two chromosome copies of each parental genome which are closely related, although not identical, and that receive the name of "*homoeologous chromosomes*" (Grandont, Jenczewski and Lloidl, 2013).

In the case of the *Brassica* species, they have suffered 4 to 5 rounds of polyploidisation during their whole evolutionary history (Jenczewski, Chèvre and Alix, 2013). The first three rounds (α, β, and γ) are shared between all the species of the Brassicaceae family. Being the γ-event, the most ancient one and common to all eudicots, whereas the α, and β are specific for the Brassicaceae family**.** One of the last events of polyploidisation occurred at the origin of the *Brassica* species, being an event of Whole Genome Triplication which constituted the separation of the *Brassica* genus from the *Arabidopsis* lineage (Lysak et al., 2005; Jenczewski, Chèvre and Alix, 2013; Cheng *et al.*, 2014). Therefore, all the Brassica species seem to descend from a paleohexaploid ancestor. Finally, the last polyploidisation event has occurred in the

recent history of this taxa (<10.000 years ago). This event was originated when the diploid ancestors of the actual *B. rapa* (A genome, n=10), *B. nigra* (B genome, n=8), and *B. oleracea* (C genome, n=9) inter-hybridized to originate three allopolyploid hybrids (Fig.1.6): *B. napus* (AACC, n=19), *B. carinata* (BBCC, n=17), and *B. juncea* (AABB, n=18); as described by U, (1935). Moreover, as the genomes of *B. rapa, B. oleracea* and *B. nigra* still present remnants of their ancestral paleohexaploid genome these are considered as mesopolyploid species (Mandáková *et al.*, 2010; X. Wang *et al.*, 2011; Jenczewski, Chèvre and Alix, 2013; Cheng *et al.*, 2014).

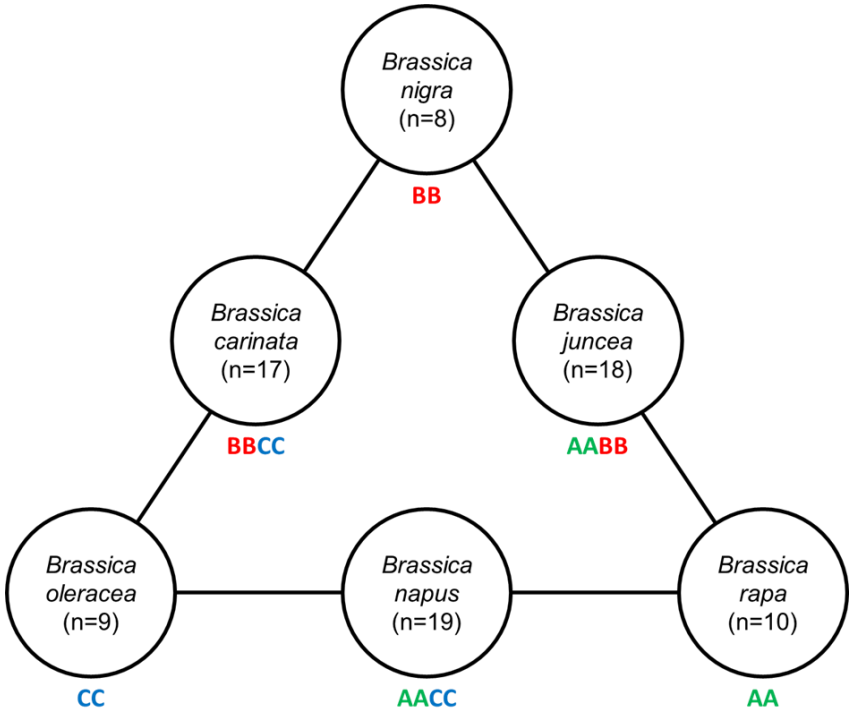


Figure 1.6. Tringle of U (1935), showing the origin of the allopolyploid Brassicas.

Regarding the consequences of polyploidy (in both allo- and autopolyploids), they involve genetic and cytogenetic challenges as new gene copies are acquired (gene duplication) and four chromosome sets instead of two have to be managed during meiosis (Jenczewski & Alix, 2004; Grandont, Jenczewski and Lloidl, 2013).

In the first place, the genetic consequences of polyploidy are based on the appearance of gene duplication as at least two copies for each gene are found. This situation usually leads to the loss of one copy through fractionation, the divergence of one of the copies (gaining new functions), or sometimes to the maintenance of both copies (Lloyd *et al.*, 2014; Lloyd *et al.*, 2018). However, this situation in allopolyploids is slightly more complex as the copies differ as they come from different genomes, for instance in *B. napus* homoeologous copies tend to be lost due to Homoeologous Exchanges (see below). Interestingly, although usually there is no preference for retaining a particular copy, a tendency has been observed to retain the copies from the A genome in *B. napus* (Lloyd *et al.*, 2018). In particular, meiotic genes tend to return to a single copy faster than the rest of the genome. Nevertheless, this seems to be achieved in a passive manner as the presence of duplicates for these genes does not seem to be actively counter-selected (Lloyd *et al.*, 2014). One of the most extreme examples is the gene encoding the ZMM protein MSH4, which appears as a single copy in most organisms except for those who have undergone very recent WGD (Gonzalo *et al.*, 2019).

The cytogenetic consequences of a polyploidy event arise during meiosis due to the formation of multivalents instead of bivalents, which can have deleterious effects as sometimes are associated with missegregation and chromosome rearrangements (in allopolyploids) specially during the first generations after the polyploidy events (Zielinski and Mittelsten Scheid, 2012; Sybenga, 1996; Gaeta & Pires, 2010). The formation of multivalents in polyploids is related to the formation of structures called “Synaptic Partner Switches” (SPSs) during the pachytene stage. The SPSs are produced when homologous chromosomes interact with more than one partner

during the pachytene stage and depending on how recombination occurs can lead to multivalent formation (Zielinski and Mittelsten Scheid, 2012; Sybenga, 1996). Whereas in autopolyploids multivalent formation is likely to happen as the four copies of a chromosome share complete homology, in allopolyploids SPSs arise due to regions of great homology between homoeologous chromosomes as they come from closely related parental species (Sybenga, 1969; Zielinski and Mittelsten Scheid, 2012). As previously mentioned, it has been observed in *B. napus* that the Homoeologous Exchanges (exchanges of chromosomal segments resulting from CO formation between the homoeologous chromosomes that arise as a consequence of multivalent formation) are responsible for the variations in copy number, copy retention and loss, and expression changes of duplicate genes (from the A or C genome) (Lloyd *et al.*, 2018). It is also worth to mention that allopolyploid species such as wheat and *B. napus* have developed mechanisms to prevent recombination between the homoeologous chromosomes. These are known as pairing loci such as the *Ph1* locus from wheat and the *PrBn* locus in *B. napus* (Riley and Chapman, 1958*;* Jenczewski *et al.*, 2003; reviewed in: Jenczewski and Alix, 2004).

Regarding the two *Brassica* species studied in this thesis, *B. rapa* and *B. oleracea*, their genomes with their respective annotations have been made available (Wang *et al.*, 2011 and Liu *et al.*, 2014; respectively) allowing their comparative analysis, which has revealed some interesting information. In this way, the most obvious difference between both genomes is relative to their size, which is larger in *B. oleracea* (~630 Mb) than in *B. rapa* (~389.2 Mb according to the last re-sequencing project by Cai *et al.* (2017)). This also appears to be related to a higher amount of Transposable Elements (TEs) in *B. oleracea* than in *B. rapa*, which in the former seems to have

accumulated since the divergence of both species ~4 MY ago, whereas in *B. rapa* has occurred only in the las 1 MY (Liu *et al.*, 2014).

1.7. Food security and research in meiosis

The World Food Summit (1996) defined food security as: “Food security exists when all people, at all times, have physical and economic access to sufficient, safe and nutritious food that meets their dietary needs and food preferences for an active and healthy life”. However, as pointed out by the most recent reports, the goal of ensuring food security is far from being achieved as the number of undernourished people has been increasing since 2014, reaching 821 million people in 2018 according to the most recent State of Food Security and Nutrition in the World report (FAO *et al.*, 2018). This problem is set to become even more difficult to overcome in the coming decades as the world’s population is predicted to reach 9.73 billion by 2050 and 11 billion by 2100 at the same time that the world will have to face the challenges that climate change is posing ahead (FAO, 2017). Moreover, this increase is going to take place mainly in Africa and Asia, in low- and middle-income countries. In this way, this report raises the question about whether agriculture will be able to meet the future needs of global food supply and if this could be achieved in a sustainable manner that will not impose further damage to the already eroded ecosystems. Regarding the impacts of climate change in food security, as pointed out by the Intergovernmental Panel on Climate Change report of 2014, climate change is already negatively affecting crop production through the increase of the frequency of extreme climate events (also named climate shocks), particularly droughts (IPCC, 2014). Moreover, despite there has been an steady growth of crop productivity since the last century this seems insufficient for ensuring food security in the upcoming decades, even

without considering the occasional losses generated by extreme climate events (Alexandratos and Bruinsma, 2012). In this way, one of the key areas of improvement pointed by the IPCC report of 2019 is the use of natural genetic resources as well as breeding programmes to facilitate the adaptation of the crop production to the challenges imposed by climate change and population growth (IPCC, 2019).

Plant breeding is essential for the generation of new crop varieties with improved traits, this is achieved by crossing parental crop varieties with different traits of interest and selecting the individuals with the combination of those traits within the progeny. From the genetic point of view, this involves the generation of new allele combinations of genes of interest which relies on the recombination events that take place during meiosis (Blary and Jenczewski, 2019). However, this is a very long process which expands several generations, taking long periods of time, which renders classic plant breeding as an inefficient technique to achieve the aforementioned goals of harnessing the vast amount of available genetic resources to improve the characteristics of our crops. Thus, the implementation of more modern molecular techniques to plant breeding is essential to speed up the generation of new crop varieties with the potential to overcome the future challenges of food security (Moose and Mumm, 2008; Li *et al.*, 2018). As previously mentioned, the success of plant breeding programmes depends on the generation of new allele combinations through the recombination process that takes place during meiosis. Nevertheless, this is greatly limited as CO formation is usually constrained to small portions of the genome, and CO numbers rarely exceed 2-3 COs per chromosome (reviewed in: Blary and Jenczewski, 2019; Taagen, Bogdanove and Sorrells, 2020).

One of the best examples is the chromosome 3B of wheat, where 80% of COs are located in distal regions which account only for around 20% of the total genome (Saintenac *et al.*, 2009; reviewed in Blary and Jenczewski, 2019). In this manner, the analysis of meiosis in model organisms to understand the mechanisms that govern CO formation and the translation of this knowledge to the crop species used in agriculture is essential for the success of future breeding programs that aim to generate a wide range of novel crop varieties to tackle the challenges that climate change and population growth will impose in ensuring food security (reviewed in: Blary and Jenczewski, 2019; Taagen, Bogdanove and Sorrells, 2020).

Thus, international research projects involving a wide range of laboratories with different backgrounds as the MEICOM-ITN Network are essential to develop new techniques to manipulate meiotic recombination and to translate this knowledge to crops so it can be effectively applied in plant breeding programs.

1.8. Project objectives

The main objective of our project is to study the dynamic organisation of the axis and its remodelling during prophase I, to comprehend how these processes influence the formation of both classes of COs in two diploid species of *Brassica*: *B. oleracea*, and *B. rapa*. This translation of knowledge of meiosis from the classic plant model species *A. thaliana* to *Brassica* crops aims to set a strong basis to understand the mechanisms that underlie CO formation in these species. Therefore, the results of this project may eventually contribute to the success of future breeding programmes in *Brassica*.

For this purpose, we focus on the role of the AAA+ ATPase PCH2 and the axis-associated protein ASY3 within these processes by conducting a reverse genetic analysis of the *Brassica* orthologs of these genes. This is based in the completion of the following secondary objectives:

- Use the CRISPR/Cas9 system to produce PCH2 defective mutants in *B. oleracea* and identification of null mutants of the *B. rapa ASY3* ortholog produced by TILLING mutagenesis.
- Cytological characterisation of the *pch2* and *asy3* mutants of *B. oleracea*, and *B. rapa* through the analysis of chromosome spreads and the immunodetection of SC and axis-associated components, together with recombination proteins.
- Cytological analysis of CO formation in double mutant lines defective for axis remodelling (*pch2*) and axis associated components (*asy1 and asy3*) in combination with null mutations of the class I CO factor MSH4 and the anti-recombinase FANCM1, to understand the relation between the axis morphogenesis, its remodelling, and CO formation in *B. rapa*.

Chapter 2. Materials and methods

2.1. Plant material

2.1.1. *Brassica rapa* TILLING lines

Plants of *B. rapa* R-o-18 inbred line (n=10) were used as WT controls in this study (Rusholme *et al.*, 2007). TILLING (Targeting Induced Local Lesions in Genomes) mutant lines for the genes *BraA.PCH2* (Bra013827), *BraA.ASY1* (Bra004222), *BraA.ASY3* (Bra004486), *BraA.MSH4* (Bra02105) and *BraA.FANCM* (Bra034416) were produced by EMS (ethyl-methane sulfonate) mutagenesis at the JIC (John Innes Centre, Norwich, UK; see section 2.2.1). The seeds of the *braA.msh4-1* line, previously used by Blary *et al.* (2018) were donated to us by Dr Eric Jenczewski (Institut Jean-Pierre Bourgin, INRA Versailles, Versailles, France). All the *B. rapa* mutant lines consist of point mutations (Fig.2.1) which create premature stop codons in the coding sequences, producing truncated versions of the proteins (Fig.2.2). It is worth to mention that the *braA.msh4-1* line, which bears a SNP that eliminates an splicing acceptor site of the 19th exon (position 4545 G>A), also results in the formation of a premature stop codon shortly after (Blary *et al.*, 2018). In *braA.pch2-9* the SNP is located in the position 662 (G>A); in the case of *braA.ASY3* all three lines bear point mutations all located at the first exon: *braA.asy3-1* (position 508, C>T); *braA.asy3-2* (position 1159, C>T); and *braA.asy3-3* (position 802, C>T); in the *braA.asy1-14* mutant, the SNP is located in the position 819 (G>A); and in the *braA.fancm-11* mutant line the point mutation is located in the position 682 (C>T). The position of the genes analysed within the *B. rapa* karyotype is indicated in Fig. 2.3.

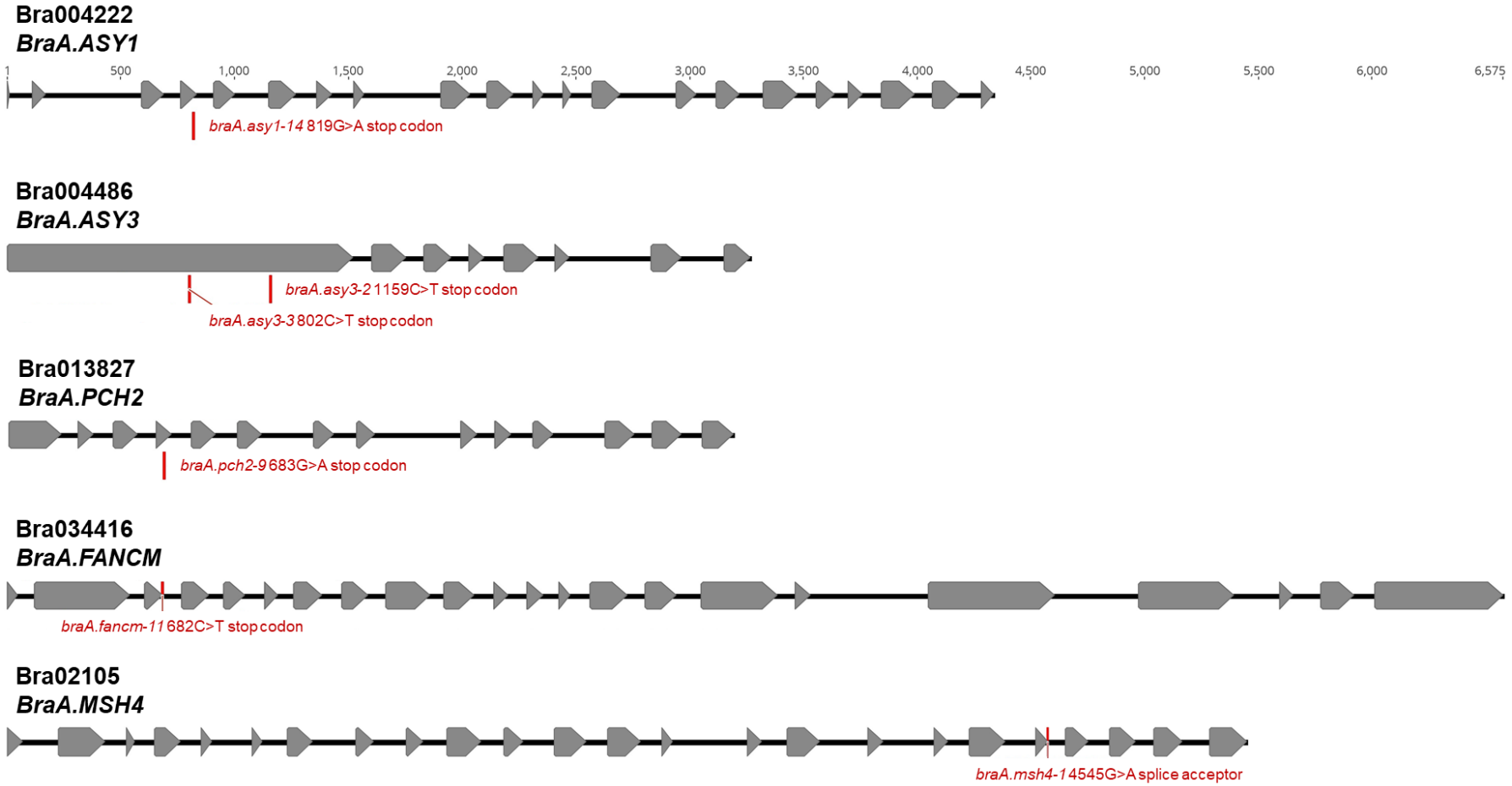


Figure 2.1. Visual representation of the *B. rapa* genes studied. The grey arrow boxes represent the exons, and the black lines the introns. The red lines show the positions of the point mutations and the label specifies the allele and position in bp within the sequence. the scale at the top indicates the length in bp. The *braA.asy3-1* line is not represented as no mutant plants were identified.

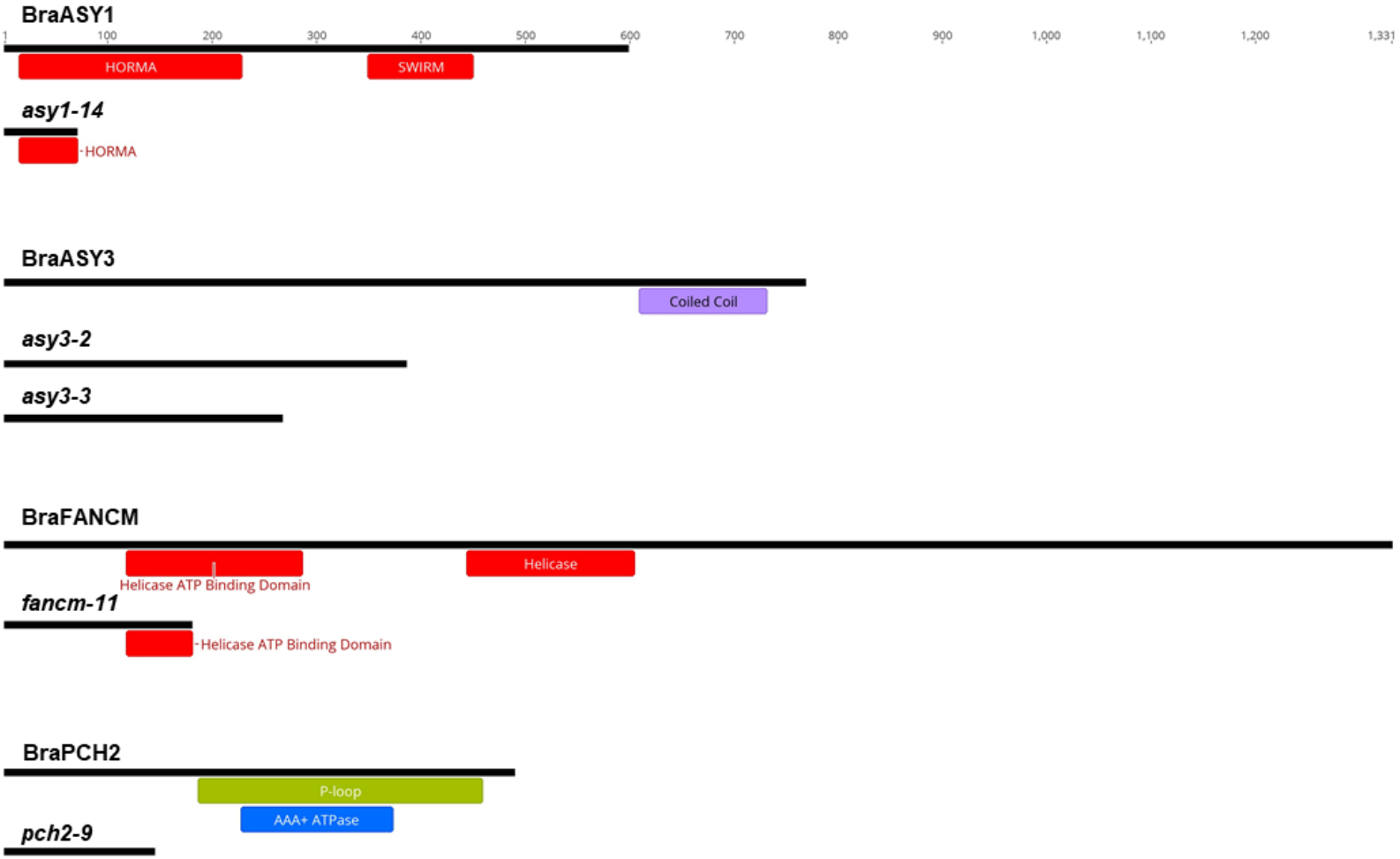


Figure 2.2. Schematic illustration of the structure of the protein products of the genes, and mutant alleles studied. The coloured boxes represent the different putative domains of each protein. The upper scale represents the length in amino acids. The protein products of BraA.MSH4 and its corresponding mutant line *braA.msh4-1* are not represented since the total length of the predicted amino acid product cannot be accurately estimated.

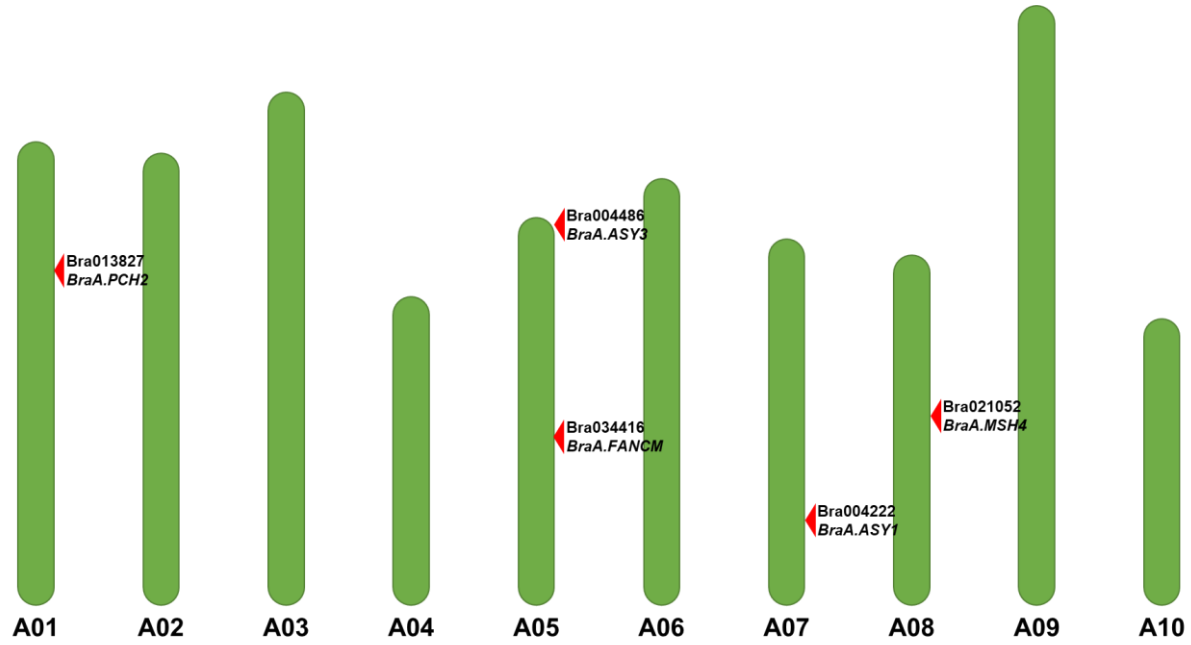


Figure 2.3. Localisation of the different genes studied within the karyotype of *B. rapa*.

The seeds of the *asy1-4 x pch2-9, asy1-14* x *fancm-11* and *pch2-9* x *fancm-11* crosses were kindly provided by Dr María Cuacos (Dr Stefan Heckmann's group, IPK Research Centre, Gatersleben, Germany).

2.1.2. *Brassica oleracea* PCH2 CRISPR/Cas9 mutagenized lines

Plants of the *B. oleracea* DH1012 (n=9) doubled haploid line (Bohuon *et al.*, 1996) were used as the WT controls in this study, the seeds of this line were provided by Dr Graham Teakle (University of Warwick, Warwick, UK). The seeds of the T1 transformant plants of *B. oleracea* DH1012 plants transformed with a CRISPR/Cas9 construct targeting the PCH2 ortholog (Bo1g039250) were donated to us by Dr. James Higgins (University of Leicester, Leicester, UK). The sgRNAs were designed, the constructs were produced, and the plants were transformed by the BRACT service at the John Innes Centre (Norwich, UK). Information about the generation of the CRISPR/Cas9 mutagenized lines can be found in section 2.2.2.

2.1.3. Plant growth conditions

Brassica seeds were sown directly in soil-based compost (4 parts M3 compost, 2 parts vermiculite, 1-part Silvaperl soil), and kept at 20 ºC with a light cycle of 16 h of light and 8 h of darkness.

2.1.4. *Brassica* crosses

Adult flowering plants (6-8 weeks) were selected to act either as pollen or egg donors. If the plats were selected to act as egg donors all the open flowers were removed together with all the flower buds except for those of bigger size close to opening. These larger buds were then dissected and emasculated by removing the sepals, the petals, and the anthers, only leaving the gynoecium. On the other hand, if the plant was used as a pollen donor, open flowers were taken and the anthers rubbed against the stigma of the previously dissected egg donor buds, making sure that these were covered in pollen. This procedure was repeated for three consecutive days.

2.2. Mutant generation

2.2.1. Generation of *B. rapa* mutant lines through TILLING

The *B. rapa* mutant lines used in this study were generated by the RevGenUK service at the John Innes Centre (Norwich, UK) using the R-o-18 inbred line through a reverse genetics process known as TILLING (Targeted Induced Local Lesions IN Genomes)(Stephenson *et al.*, 2010). This technique was developed by McCallum and collaborators (McCallum *et al.*, 2000a; McCallum *et al.*, 2000b) and is based on a first round of chemical mutagenesis, followed by the identification of point mutations in the target locus by a high throughput screening.

The round of chemical mutagenesis is carried out by applying EMS (Ethyl Methane Sulfonate), an alkylating agent that usually causes G/C to A/T changes, to the plant seeds (*B. rapa* R-o-18). The seeds are then grown, giving rise to the chimeric M1 generation that is allowed to self-fertilise in order to produce the M2 generation. The objective of the self-pollination is to produce non-chimeric individuals. Subsequently, DNA samples of the M2 generation individuals are taken and pooled in an 8-fold fashion. The 8x pooled DNA libraries are amplified with fluorescence-labelled primers (the forward and reverse primers bear different fluorescent tags) specific of the target locus (Colbert *et al.*, 2001). After the amplification, the resulting products are heated and cooled down so that in the presence of a point mutation, mismatched heteroduplex will form in the DNA. These samples are then digested with the CEL1 enzyme (Oleykowski *et al.*, 1998) that cleaves the mismatches and the digestion products are resolved in a slab gel. The wells containing a CEL1 cleaved product are identified as containing a potential mutant allele in the DNA pool. Once a potential mutant allele is detected, the 8 individuals of the DNA library are sequenced to identify the plant carrying the mutation.

However, one of the biggest disadvantages of this technique is that apart from the mutation in the target locus, a great number of background mutations are produced as well. Thus, two measures can be taken to overcome this problem; i) backcrossing with WT individuals for several generations; ii) if more than one mutant allele for the locus has been found, cross both individuals and analyse the phenotype of the heteroallelic progeny. In this way, the phenotype observed in the heteroallelic individuals can only be due to the non-complementing mutations of the target locus; and the background mutations will remain in heterozygosity, not expressing any phenotype (McCallum *et al.*, 2000b). Both strategies have been used in this study.

2.2.2. Generation of *B. oleracea* PCH2 CRISPR/Cas9 mutant

Four different sgRNAs were designed targeting different exons of the *BoC.PCH2* gene in order to maximise the chances of generating a mutation. Table 2.1 shows the sequence and target location of the sgRNAs used.

Table 2.1. Sequence and target location of the different sgRNAs used in the CRISPR/Cas9 mutagenesis of *BoC.PCH2*.

sgRNA	Sequence	Target location (bp)
sgRNA 1a	CCACTCGCTGCAACCGATCCTCC	Exon 1 (144-167)
sgRNA 1b	GGTTTAGGATGCTGGAAAATAGG	Exon 3 (427-450)
sgRNA 2a	GAGACCAAGTTCCTCGTATCTGG	Exon 1 (204-227)
sgRNA 2b	GGAAGGACCATGTGAGGAACTGG	Exon 5 (826-849)

The sgRNAs sequences were cloned grouped 2 by 2 (1a-1b; and 2a-2b) into the CRISPR constructs containing the Cas9. A diagram of the binary vector pLB-Bo containing the CRISPR construct is shown in Fig.2.4 (below).

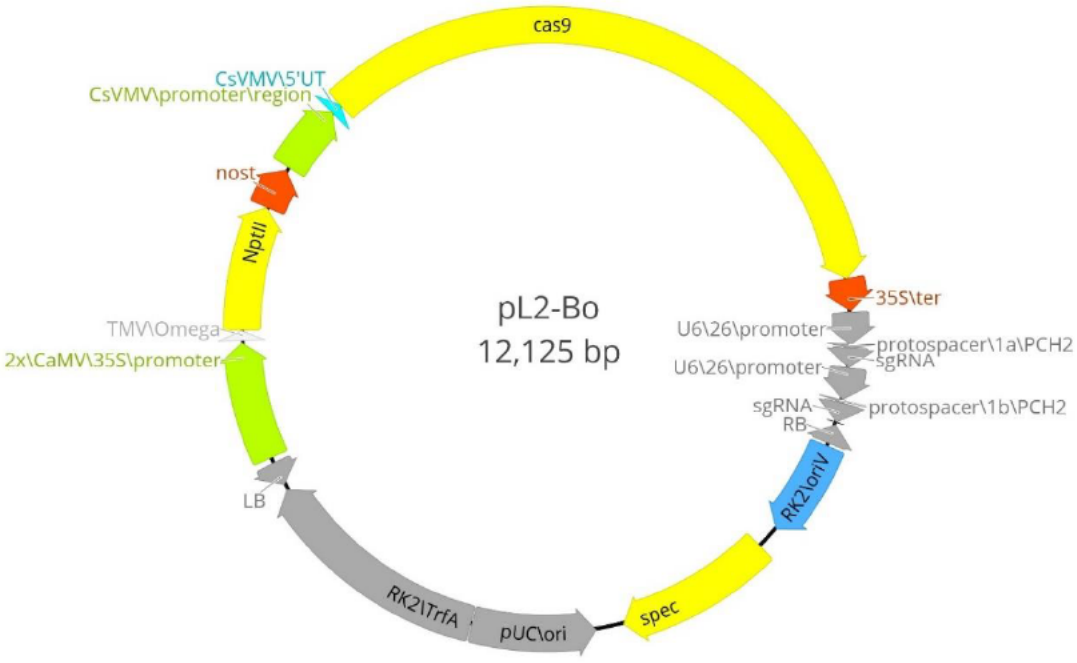


Figure 2.4. Map of the pL2-Bo binary vector containing the CRISPR/Cas9 cassette. This visual representation has been generated with Geneious (https://www.geneious.com).

As stated before, the transformation and callus regeneration were carried out at the facilities of the John Innes Centre (Norwich, UK) by the BRACT service (https://www.jic.ac.uk/research-impact/technology-research-platforms/crop-transformation/). The transformation protocol is available on-line (https://www.jic.ac.uk/research-impact/technology-platforms/genomic-services/crop-transformation/).

2.3. Genotyping

2.3.1. DNA extraction from plant tissues

Around 0.5 cm^2 of plant tissue was taken for every sample. The plant tissue was then homogenised in 50 µl of extraction buffer (250 mM KCl, 10 mM EDTA, and 100 mM TRIS-HCl at pH 9.5), and incubated at 95 ºC for 10 min, after which, the samples were kept in ice for 5 min. Finally, 50 µl of dilution buffer (3% Bovine Serum Albumin (BSA)) was added to each tube and the samples centrifuged for 2 min at 13.200 rpm. The samples were kept frozen at -20 ºC until used.

2.3.2. Derived Cleaved Amplified Polymorphic Sequences (dCAPS) genotyping for *B. rapa* TILLING mutant lines

Given that the *B. rapa* mutants used are all based on Single Nucleotide Polymorphisms (SNPs) generated through chemical mutagenesis, we decided to use the dCAPS genotyping technique as a quick and reliable method for the identification of plants carrying the mutations studied in this work.

This technique, as indicated by its name, uses a derivate from the CAPS markers (Cleaved Amplified Polymorphic Sequence; Konieczy and Ausubel, 1993), which at the same time are a PCR-based variant of the classic RFLP (Restriction Fragment Length Polymorphism; Botstein *et al.*, 1980). These methods are characterised by

the generation or loss of unique restriction enzyme sites by the presence of an SNP. However, in the majority of cases, the presence of a SNP does not generate a restriction site (Michaels and Amasino, 1998). Thus, the dCAPS genotyping was developed as a PCR-based technique able to generate unique restriction sites associated with the SNP of interest (Haliassos *et al.*, 1989; Michaels and Amasino, 1998; Neff *et al.*, 1998). This is achieved through the amplification of the region containing the base change with primers bearing one or two mismatches. Thus, the resulting amplification product contains those base changes, that together with the SNP generate a restriction site in one of the alleles. This allows differentiating between both after resolving the digestion products by electrophoresis in an agarose gel. An example using the dCAPS in the *braA.asy3-2* mutant is depicted in Fig.2.5 (below).

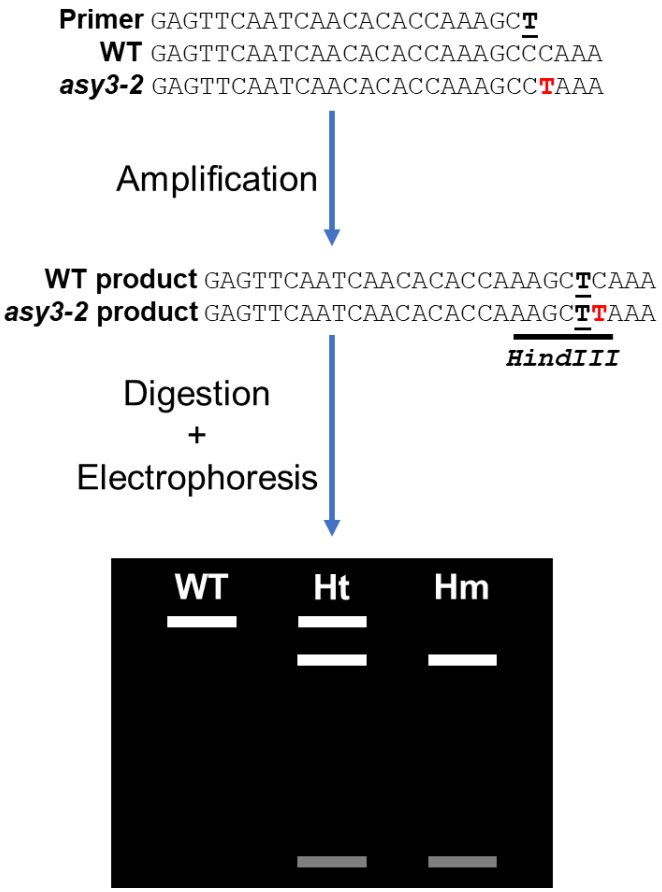


Figure 2. 5. Example of the use of a dCAPS genotyping to detect the presence of the point mutation of the *braA.asy3-2* allele. The red letter indicates the point mutation in *braA.asy3-2*. The underlined bold letter represents the mismatch in the primer, that is introduced in the amplification product, generating a HindIII restriction site in the *braA.asy3-2* allele amplicon. The three possible genotypes are shown: Wild Type (**WT**), Heterozygous (**Ht**), and Homozygous (**Hm**). When resolved in an agarose gel the WT allele shows one higher band (~250 bp; white) and the mutant allele shows two lower bands: one of very small size (~30 bp) usually imperceptible (depicted in grey); and another (represented in white) of bigger size (~220 bp).

The dCAPS primers containing the mismatches were designed using the dCAPS Finder 2.0 web-based tool (http://helix.wustl.edu/dcaps/; Neff *et al*., 2002). The second primer for each reaction was designed so that the resulting amplifying product has a size between 250-300 bp. Because the primers containing the mismatches have a length of 24-30 bp, this will be the difference in size between both alleles as the restriction site is always generated in the 3' end of the dCAPS primers (Fig.2.5). However, this small fragment of 24-30 bp is not usually observed in the electrophoresis gel.

The PCR mix is as follows: 6.25 µl DreamTaq polymerase (Thermo Fisher Scientific); 4.5 µl H_2O MilliQ; 0.7 µl primers (10 mM); 0.5 µl DNA extraction. The PCR programme used is as described in Table 2.3. The primers used for each allele are in Table 2.2. The amplification products were digested with the corresponding restriction enzymes (See Table 2.2). The digestion mix used was: 1.5 µl CutSmart (New England BioLabs); 8.3 µl H_2O MilliQ; 0.2 µl restriction enzyme; 5 µl amplification product. The samples were incubated at 37ºC for at least 2h. The digested and undigested PCR products were resolved via electrophoresis in a 2.5-3% agarose gel (w/v) together with 100 bp DNA Ladder (New England BioLabs).

Table 2. 2. Primers and restriction enzymes used in the dCAPS genotyping of the *B. rapa* mutants

Mutant line	Position		Primer sequence	T_a (°C)	Enzyme
braA.asy1-14	819 G>A	F	CGGTTCCTGCTCTAGgtaacaagc	60	EcoRI
		R	gctaaaATCATTAGAATACAAAAAACCTTTCT**GA**AT		
braA.fancm-11	682 C>T	F	CTCATAGCTGCAGTTGTAATGTATA**A**TT	55	NdeI
		R	GAAGAGAATCAAATCAAATGACATACAT		
braA.asy3-1	508 C>T	F	TTTGCAAGCAAACGTCTACC	55	HpaI
		R	CTTCTCTTCTCTCTGTGACGCAACC**G**TT**A**		
braA.asy3-2	1159 C>T	F	GAGTTCAATCAACACACCAAAGC**T**	55	HindIII
		R	AGGAGAAAGACAGGGGGAAG		
braA.asy3-3	802 C>T	F	GAGATCGAAACTGTGGGAAATATTGGGGAAA	63.5	BsrGI
		R	AATACCTCTGGCTCCCACCCTCCT**G**T		
braA.pch2-9	662 G>A	F	TGTAGATGGCCTTGTTCTCATACCTC	61	XbaI
		R	GGCATGGACAACAGGCTTAACTT**T**C		
braA.msh4-1	4545 G>A	F	ATGCAGAATGTCTCGAAC**C**G	57.5	HpaII
		R	GCTTTGAGCGATAACAGATGC		

The underlined bold letters indicate the position of the mismatches. (T^a). Annealing temperature.

Table 2.3. PCR programme used for the genotyping of *B. rapa* TILLING lines

Step	Number of cycles	Temperature	Duration
1	1	98	10 min
2	35	98	30 s
		Primer T_a	30 s
		72	2 min
3	1	72	10 min

2.3.3. Identification of potential *B. oleracea* CRISPR/Cas9 mutants

After regenerating from calluses, the T0 primary transformants were analysed to identify potential mutations in the targeted regions, which were sequenced (see sequencing primers in Table 2.2) in the T0 plants. The sequencing of the T0 plants was carried out by Dr. James Higgins (University of Leicester, Leicester, UK). Once identified, the plants bearing mutations in the targeted regions were allowed to set seed. Subsequently, the seeds of the T1 generation were sown in soil and the young seedlings genotyped for the presence of the previously identified mutations in *BoC.PCH2*. In this way, we sequenced the target regions with possible mutations in the T1 generation to confirm their pressence. In the first place, DNA was extracted from leaf tissue as described in section 2.3.1, and a PCR with primers designed for the region comprising the target was performed following the same protocol as in section 2.3.2 (the primers used to amplify and sequence the different target regions are show in Table 2.4). After the amplification the products were resolved in a 0.8% (w/v) agarose gel, the bands for each individual were cut and the amplification product was extracted from the gel using the QIAquick Gel Extraction Kit (Qiagen), following the instructions of the manufacturer. Finally, the samples were prepared for sequencing using the Mix2Seq Kit (Eurofins Genomics) as described by the manufacturer and sent for sequencing. The primers used for sequencing were the

same as the ones used in the amplification as the length of the reads was enough to cover the majority of the target regions. To test for the presence of the Cas9 construct in the T1 plants we conducted a PCR (as described in section 2.3.2) with primers designed to amplify the NTPII gene (Neomycin Phosphotransferase II), used as a selection marker, and present in the T-DNA containing the CRISPR construct (Fig.2.4). After the PCR, the amplification products were resolved in a 0.8% (w/v) agarose gel. The primers used are described in Table 2.4.

As the mutation of the *boC.pch2-1* line consisted of a 23 bp deletion, a second set of primers was designed to quickly identify through PCR the plants carrying the deletion in the sequence of *BoC.PCH2.* The pair of primers used was the BoPCH2-1 FP1 and RP1 (Table 2.4), which produced an amplicon of 255 bp in the WT sequence and of 232 bp in the mutant. The PCR programme and the mix were the same as described in section 2.3.2, and the PCR products were resolved in a 2.5% (w/v) agarose gel.

Table 2. 4. Primers used for the sequencing and genotyping of the different *B. oleracea* CRISPR/Cas9 mutagenized lines; and for the detection of the CRISPR construct.

Target	Primers	Sequence (5'-3')
sgRNA 1a, sgRNA 1b, sgRNA 2a	BoPCH2 F2	CGTGTTTCTCCAGAACACG
	BoPCH2Seqb	CTCCTTAGCAGGTAGAATCC
sgRNA 2b	BoPCH2 F3	TCCACGAGACCAAGTTCCTC
	BoPCH2 R3	TTCACGCAGAAGGGTGTTAA
	BoPCH2-1 FP1	TGTTCTCTTGTTCTGGCAAGTT
	BoPCH2-1 RP1	CATACTCCCGGACACACCTT
NTPII gene	NTPII F	GAGGCTATTCGGCTATGACTGG
	NTPII R	ATCGGGAGCGGCGATACCGTA

2.4. Cytological analysis of meiosis

2.4.1. Spreading of Pollen Mother Cells (PMCs)

The protocol for fixation of the plant material and the spreads of PMCs is an adaptation of the protocol first developed for tomato PMC spreads (Zhong *et al.,*

1996), and later adapted for *Arabidopsis thaliana* (Ross *et al.,* 1996). For *Brassica rapa* flower buds were fixed in 3:1 (ethanol : acetic acid) solution for 24h after which the fixative solution was removed and substituted for fresh one. The flower buds were stored at room temperature. By contrast, in the case of *Brassica oleracea*, the stage of meiosis was checked for every bud prior to the fixation to facilitate the analysis. In this way, the flower buds were dissected in a petri dish with a damp filter paper, separating the anthers from the rest of the tissues. Then, one anther per bud was taken and squashed in a glass slide with lacto-propionic orcein (1:1 diluted with water) and observed under a light microscope to verify the stage of meiosis. The rest of the anthers were fixed in 3:1 solution at room temperature and used after 24h.

Once the flower buds/anthers were fixed, we proceeded with the enzymatic digestion prior to the slide preparation. Consequently, they were placed in a watch glass and washed in citrate buffer (10 mM sodium citrate, pH 4.5) 3 times for 2 min to remove the fixative. Next, if using flower buds of *B. rapa*, these were incubated for 3h in enzyme mix (0.3 % pectolyase and 0.3 % cellulase in 10 mM citrate buffer) at 37ºC, after which the digestion was stopped by adding chilled (4 ºC) citrate buffer. In the case of *B. oleracea* anthers, the incubation time was reduced to 2h.

Following the pre-treatment of the flower buds/anthers, we continued with the preparation of the slides. In this way, one flower bud (5 anthers for *B. oleracea*) was placed in the centre of the slide with a small drop of citrate buffer and macerated with a mounted needle. Subsequently, 2x20 µl drops of 70% acetic acid were added to the mix and the slide placed in a hotplate at 42 ºC for 2 min, carefully stirring the drop, and adding more acetic acid if needed. Finally, 200µl of 3:1 fixative was added, first surrounding the acetic acid drop, and the slide was tilted to both sides in order to ensure that all the surface of the slide was covered. The slides were left to dry at

room temperature. After drying completely, the slides were mounted in 20 µl of Vectashield mounting medium (Vector Laboratories) containing 10 µg/ml DAPI (4',6-diamidino-2-phenylindole), and using 24x50 mm coverslips.

2.4.2. Immunolocalisation of meiotic proteins in PMCs by *spreading* technique

The immunolocalisation of meiotic proteins was conducted as described in Armstrong *et al.* (2002), with some modifications. *Brassica* flower buds were dissected in a petri dish containing a damp filter paper. One anther per flower bud was placed in a glass slide and squashed with lacto-propionic orcein; after which, it was observed under a light microscope to determine the stage of meiosis.

After staging the flower buds, the 5 remaining anthers were placed in a caveated slide with 10 µl of enzyme mix (1.5% sucrose, 0.4% cytohelicase, 1% polyvinylpyrrolidone), and incubated for 4 min at 37ºC in a moist chamber. Once the first incubation is completed the anthers were macerated in the enzyme mix with the help of a brass rod in order to extrude the meiocytes from the anthers. The rest of the anther tissue was removed with forceps and the resulting digestion mix incubated at 37ºC for 8 min.

To prepare the slides 25µl of 2% lipsol was placed on a polylysine slide and the digestion mix was subsequently added. The mixture was then stirred with a mounted needle for 2 min and left to rest at RT for another 6 min. Finally, the meiocytes were fixed by adding 30 µl of 4% paraformaldehyde (pH 8.0), the mixture was stirred again, and the slides were left to dry in a fume hood.

Once the slides were dry, they were washed 3x5 min in 1X PBST (Phosphate Buffered Saline 1X, 0.1% Triton X-100). After washing, 50 µl of blocking reagent (1X PBST-3% BSA) was added to a piece of parafilm (Sigma-Aldrich) which was then

placed over the slides. The slides were incubated with the blocking reagent for 45 min at 37ºC in a moist chamber. The primary antibodies were diluted in 1X PBST-3% BSA (Table 2.5), and, in the same fashion, added to a piece of parafilm (50 µl per slide) that was then settled over the slide. The slides with the primary antibodies were kept at 4 ºC overnight. Subsequently, the slides were soaked 5x5 min in 1X PBST, after which the secondary antibodies were added (50 µl per slide; Table 2.6). The slides were covered with a piece of parafilm and incubated at room temperature for 1h. Finally, the slides were washed again 5x5 min in 1X PBST, lightly dried removing the excess buffer, and stained with 20µl of 10 µg/ml DAPI diluted in Vectashield mounting medium (Vector Laboratories).

Table 2.5. Primary antibodies and dilutions used in immunolocalisation.

Antibody	Animal	Dilution	References/Manufacturer
α-ZYP1	Rat	1:500	Higgins *et al.*, 2005
α-ZYP1	Ginea pig	1:500	Osman *et al.*, 2018
α-ASY1	Ginea pig	1:500	Armstrong *et al.*, 2002
α-ASY1	Rabbit	1:500	Armstrong *et al.*, 2002
α-ASY3	Rabbit	1:500	Ferdous *et al.*, 2012
α-PCH2	Rabbit	1:200	Lambing *et al.*, 2015
α-SMC3	Rat	1:300	Ferdous *et al.*, 2012
α-γH2AX	Mouse	1:500	Millipore (Sigma-Aldrich)
α-HEI10	Rabbit	1:200	Desjardins *et al.*, 2020

Table 2. 6. Secondary antibodies and dilutions used in immunolocalisation.

Antibody	Fluorophore	Dilution	Manufacturer
α-Rat	Alexa 488	1:250	Invitrogen (Thermo Fisher Scientific)
α-Rat	Alexa 594	1:500	Invitrogen (Thermo Fisher Scientific)
α-Rabbit	Alexa 594	1:500	Invitrogen (Thermo Fisher Scientific)
α-Rabbit	Alexa 488	1:250	Invitrogen (Thermo Fisher Scientific)
α-Ginea pig	Alexa 594	1:500	Invitrogen (Thermo Fisher Scientific)
α-Ginea pig	AMCA	1:50	Jackson ImmunoResearch
α-Mouse	Alexa 594	1:500	Invitrogen (Thermo Fisher Scientific)

2.4.3. Immunolocalisation of meiotic proteins by *spreading* technique for Structured Illumination Microscopy (SIM)

The *spreading* technique used for SIM is a variation of the previously described method for immunolocalisation of meiotic proteins in an epifluorescence microscope. The difference resides in that for SIM the sample must be as close as possible to the objective, which is achieved by preparing the sample in the coverslip rather than the glass slide. This prevents the appearance of artifacts as *ghosting* during the image acquisition as the light does not have to travel for great distances between mediums with different diffraction indexes (Demmerle *et al.*, 2017).

In this way, the anther digestion mix was placed on a high precision coverslip (24x24 mm) together with 25 µl of 2% lipsol, stirred for 2 minutes and left to rest for another 6 min. Then a 30 µl drop of 4% paraformaldehyde (pH 8.0) was added to the mix, after which, the coverslips were left to dry in a fume hood. To facilitate the manipulation of the coverslips these were placed on a glass slide during this process.

Once dried, the protocol continues as described in section 2.4.2. However, it is worth to mention that the coverslips were placed in a Petri dish, where the subsequent washes of 1X PBST were conducted, avoiding disturbing the coverslips when changing the washing solutions. For the application of the blocking reagent and the antibodies the coverslips were mounted again on a glass slide with the samples facing upwards.

If DNA was stained, 50 µL of 1 µg/mL DAPI was added to the coverslip, covering it with parafilm and incubating it for 10 min at room temperature, after which the coverslips were washed 3x5 min with PBST. Finally, the coverslips were mounted on a clean glass slide using 10 µl Vectashield mounting medium (Vector laboratories).

2.4.4. Microscopy and image analysis

The microscopy analysis was performed using a Nikon 90i Epifluorescence microscope controlled with the NIS-Elements software of Nikon. The DAPI spread images were captured as a single stack; and the immunofluorescence images were taken using the "Multichannel acquisition tool", capturing as many stacks as needed (0.2 µm between stacks). The slides for SIM were imaged in a ZEISS Elyra 7 Lattice SIM^2 at the Birmingham Advanced Light Microscopy (BALM) facilities of the University of Birmingham. Further image analysis and editing was conducted with the FIJI (ImageJ) and Adobe Photoshop CC 2019 software.

Deconvolution was implemented for the epifluorescence microscope images of immuno-*spreading* as this reduces the noise signal improving the contrast of the images. This was achieved through the "Richardson-Lucy Total Variation" (RLTV) algorithm of the DeconvolutionLab2 plugin of ImageJ. The theoretical PSFs (Point Spread Functions) for each fluorophore were generated using the PSF Generator plugin of ImageJ with the appropriate parameters.

To minimise the bias when scoring foci, a "*blind"* analysis was performed whenever possible by pooling the images of the control and mutant plants.

Synaptonemal complex lengths were measured using the "Simple Neurite Tracer" plugin included in the ImageJ software.

The intensity analysis of the fluorescent signals was performed as follows:

1. The intensity of the signal in synapsed, non-synapsed and background regions was measured using the NIS-Elements software of Nikon. Five different points for each of the corresponding areas were taken in every cell

analysed. The saturated pixels and cells were avoided, and the points were spread as much as possible through the nucleus.

2. The data was exported to an Excel file where the 5-point average for the synapsed, non-synapsed, and background regions was calculated for every cell.
3. The average background signal was subtracted to the average signal intensities of the synapsed and non-synapsed regions.
4. The ratio “v” of intensity between the synapsed and non-synapsed regions was calculated for every cell by dividing the intensity of the synapsed areas by the intensity of the non-synapsed ones after the previous step.

The process to obtain “v” can be summarised with the following formula:

$$\nu = \frac{(\bar{x}_{synapsed} - \bar{x}_{background})}{(\bar{x}_{non-synapsed} - \bar{x}_{background})}$$

The estimation of the chiasma frequency per cell, was performed in metaphase I spreads of PMCs by analysing bivalents shapes as described by Sanchez-Moran *et al.* (2001) and Sybenga (1975). Fig.2.6 provides an insight about how bivalent shapes were interpreted to score the number of chiasmata per bivalent (Fig.2.6.A), how the chromosome arms were divided in two intervals (ID and IP) to elucidate the position of chiasmata within them (Fig.2.6.B), and how bivalent shapes are conditioned by the number and position of those chiasmata (Fig.2.6.C).

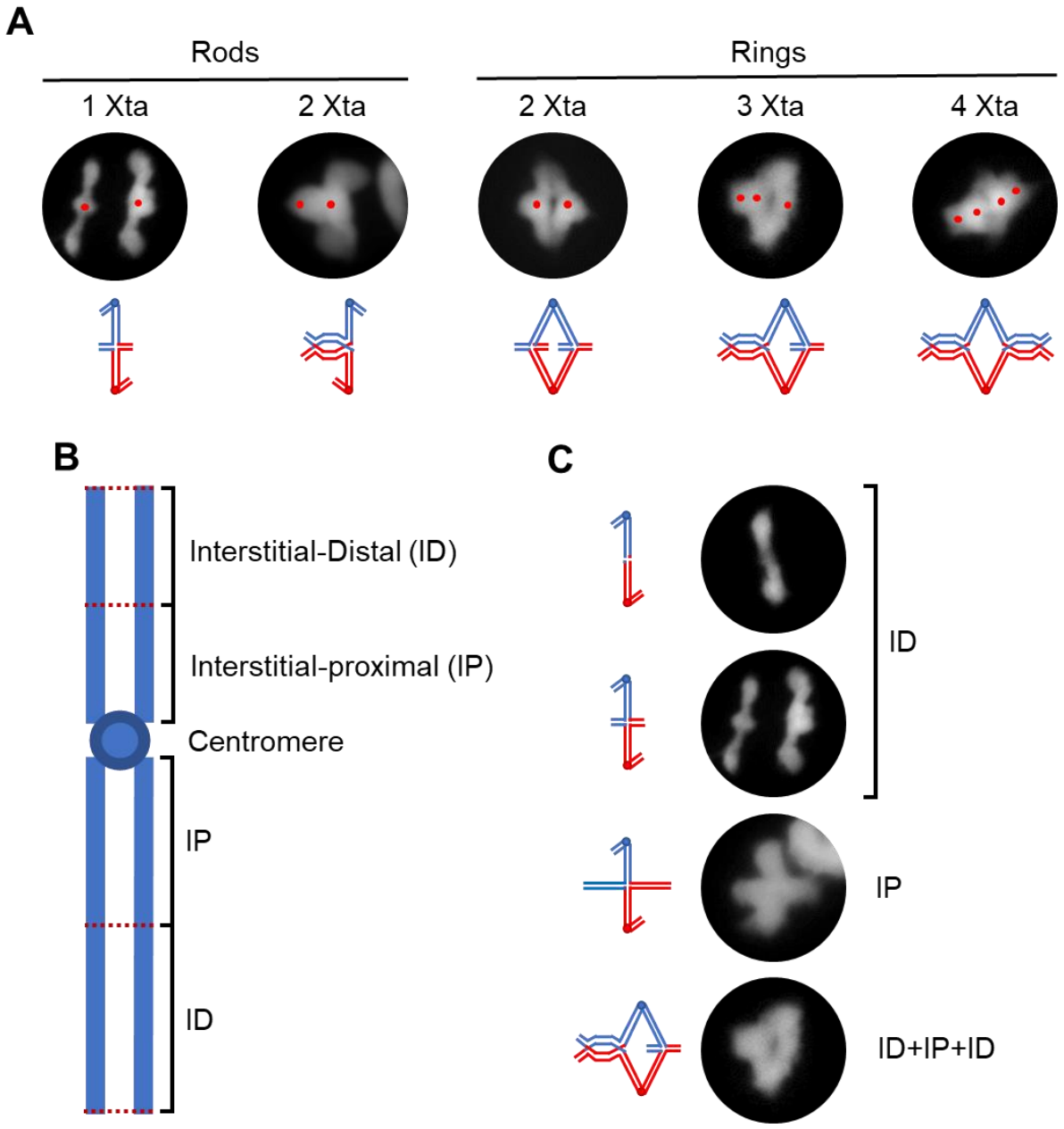


Figure 2.6. Summary of the procedure taken for the analysis of bivalent shapes for the analysis of chiasma frequency and localisation. (A) Ring and rod bivalent configurations with their corresponding number of chiasmata. The red dots indicate the position of chiasmata. **(B)** Scheme representing the division of the chromosome arms in two intervals (ID and IP) of equal distance, based on the position of the chiasmata with respect to the centromeres, telomeres, and centre of the chromosome arm. **(C)** Examples of bivalent shapes observed, with their schematic interpretation and localisation of the chiasmata observed.

2.5. Statistical analysis

All the statistical analyses were carried out using the GraphPad Prism 6 software, using the appropriate tests after checking that the different datasets met the conditions required for each analysis as explained below.

Normality was tested for each dataset using the D'Agostino-Pearson test. Non-parametric tests were used when the conditions of non-normality and low number of samples ($n<30$) were met. In these situations, if comparing two groups the Mann-Whitney U-test was performed. For the rest of the analyses, parametric tests were carried out. In this way, if comparing two groups the Welch's Test was conducted. For the comparisons between more than two datasets the Welch's One-Way ANOVA was used to seek for differences among them, this was followed by pairwise comparisons among the groups by means of a *post hoc* test. The *post-hoc* multiple comparisons tests used were the Dunnet's T3 test when $n<50$ and the Games-Howell's test if $n>50$. The Welch's variations of the classical Student's T-test and ANOVA were used to compensate for the differences in the standard deviation (SD) among the datasets analysed as this correction does not assume equal SDs (homoscedasticity). The Kolmogorov-Smirnov test of cumulative distributions was conducted when analysing the good of fitness of the frequency distribution of a dataset with respect to a predicted Poisson distribution. The Fisher's Exact test was conducted in the cases were changes in the proportions of categorical data were studied such as in the analysis of the proportion between distal and interstitial chiasmata as the sample number in the later tends to be low.

2.6. Bioinformatics and analysis of sequencing data

The sequencing data analysis and the alignments were carried out with the Geneious 11.1.5 software (Biomatters Ltd.). The nucleic acid and protein data was obtained from the EnsemblPlants database (https://plants.ensembl.org/index.html).

Chapter 3. Meiotic axis remodelling in *Brassica* crops: Analysis of the function of the AAA+ ATPase PCH2 in *B. rapa* and *B. oleracea*

3.1. Introduction

The AAA+ ATPase PCH2 was first identified as a pachytene checkpoint regulator in budding yeast and has also been studied in mice (TRIP13), *C. elegans*, and fruit fly, being essential for CO formation in mice and worm (San-Segundo and Shirleen Roeder, 1999; Bhalla and Dernburg, 2005; Joyce and Mckim, 2009; Wojtasz *et al.*, 2009; Roig *et al.*, 2010). In these organisms, except for mice, PCH2 is necessary for the establishment of a checkpoint during pachynema that leads to meiotic arrest in this stage in case that defects in synapsis are present (San-Segundo and Shirleen Roeder, 1999; Bhalla and Dernburg, 2005; Joyce and Mckim, 2009). Moreover, it also plays a role in the remodelling of the AEs by regulating the distribution of the HORMA domain protein Hop1 in yeast and by depleting HORMAD1/2 from the synapsed regions in mouse (Borner *et al.*, 2008; Wojtasz *et al.*, 2009; Roig *et al.*, 2010; Chen *et al.*, 2013). Regarding their plant counterparts, so far two orthologs of PCH2 have been characterised: PCH2 in *A. thaliana* and CRC1 in rice, which despite carrying out similar roles, present some important differences between them (Miao *et al.*, 2013; Lambing *et al.*, 2015; Yang *et al.*, 2020). In this way, AtPCH2 is required for the completion of synapsis between the homologs, the depletion of ASY1 from the synapsed regions, the formation of COs, and the correct association of ASY1 to the AEs by facilitating an open conformation (Lambing *et al.*, 2015; Chao Yang *et al.*, 2020). By contrast, OsCRC1 is required for DSB formation and plays a more important role in the axis loading of the ASY1 ortholog PAIR2, being also essential for the establishment of synapsis and COs between the homologs (Miao *et al.*, 2013). It is worth to mention that, contrasting with their orthologs in yeast, *C. elegans,* and *D. melanogaster*, the plant PCH2 orthologs are not required for the establishment of a pachytene checkpoint in plants. Thus, given the differences observed in the roles of

PCH2/CRC1 in plant meiosis it is of great importance to further study the functions of this protein during meiosis to fully understand the relation between the formation and remodelling of the AEs and HR. In this manner, the role of the AAA+ ATPase PCH2 has been investigated in two crop wild relative species from the Brassicaceae family, *B. rapa* and *B. oleracea*, which are closely related to the plant model organism *A. thaliana*. This study was conducted by means of a reverse genetic approach in which the meiotic phenotype was analysed in TILLING and CRISPR generated mutant lines of the PCH2 orthologs of *B. rapa* and *B. oleracea* (respectively). The results obtained suggest that even though BraA.PCH2 and BoC.PCH2 present conserved roles in meiosis similar to the ones previously described for AtPCH2, some differences are present between them.

It is worth to mention that, because in this chapter we are working with two different species: *B. rapa*, and *B. oleracea*, we have followed the nomenclature developed by Østergaard and King (2008) to refer to the genes and mutant lines analysed of each species. A simplified version of this nomenclature has been used in the chapters 4 and 5 as only *B. rapa* lines were used in them.

Our work in the characterisation of the role of *BraA.PCH2* was done in collaboration with Dr Maria Cuacos and Dr Stefan Heckmann (IPK Gatersleben, Germany), which led to the publication of the results in Cuacos *et al.* (2021), attached at the end of the thesis. The figures presenting data in this chapter are different from the ones published in the article, with the exception of Fig.3.5 and some images of Fig.3.6 (Mid-Pachytene and diplotene), which were obtained by me for the publication, and therefore, are used in the chapter. Similarly, the description of *BoC.PCH2* was conducted in collaboration with Dr James Higgins (University of Leicester, UK) who participated in the generation and identification of the *BoC.PCH2* CRISPR

mutagenized lines and donated the seeds to our laboratory to continue with the analysis. The results shown in this chapter are the result of my own work unless otherwise stated.

3.2. Results

3.2.1. Cytological analysis of meiosis in the *B. rapa braA.pch2-9* mutant line shows defects in the completion of synapsis, formation of univalents, and missegregation problems

To analyse the phenotype in meiosis of the *braA.pch2-9* mutant line we conducted DAPI spread preparations of PMCs as described in Section 2.4.1, using the R-o-18 line of *B. rapa* as the WT control (Fig.3.1.A-G).

B. rapa (n=10) follows a canonical meiotic division as described in detail in section 1.2 (Fig.3.1.A-G). In the case of the mutant (Fig.3.1.H-O) no obvious defects were seen during the leptotene and zygotene stages (Fig.3.1.H,I), which resemble those of the WT control (Fig.3.1.A,B). On the other hand, the meiotic phenotype of the *braA.pch2-9* line became evident from pachytene onwards. In this way, whereas pachytenes with complete synapsis appear in the WT (Fig.3.1.C), no full synapsis at pachytene was observed in *braA.pch2-9* as the formation of the SC seems incomplete in this mutant (analysed in detail in section 3.2.4), not progressing further than a late zygotene/pachytene-like stage (Fig.3.1.J), where a synapsed and non-synapsed areas can be observed (Fig.3.1.K, white and red arrowheads). Also, instead of the characteristic 10 bivalents observed in WT (Fig.3.1.D,E), a mixture of bivalents and univalents appeared at the diakinesis and metaphase I stages (Fig.3.1.L,M), indicating defects in recombination and CO formation. In this way, a 91.7% of the metaphase I cells of *braA.pch2-9* (n=108) showed univalents (Fig.3.1.M, red asterisks). The average of univalent pairs per cell found in this mutant

is 3.98±0.26 (mean±S.E.M.), and conversely, the average number of bivalents per cell is 6.02±0.26. These defects in bivalent formation led to non-disjunction problems observed in metaphase II (Fig.3.1.N); and to the formation of unbalanced nuclei and polyads at the end of meiosis (Fig.3.1.O), rather than the balanced segregations observed in these stages of the WT control (Fig.3.1.F,G).

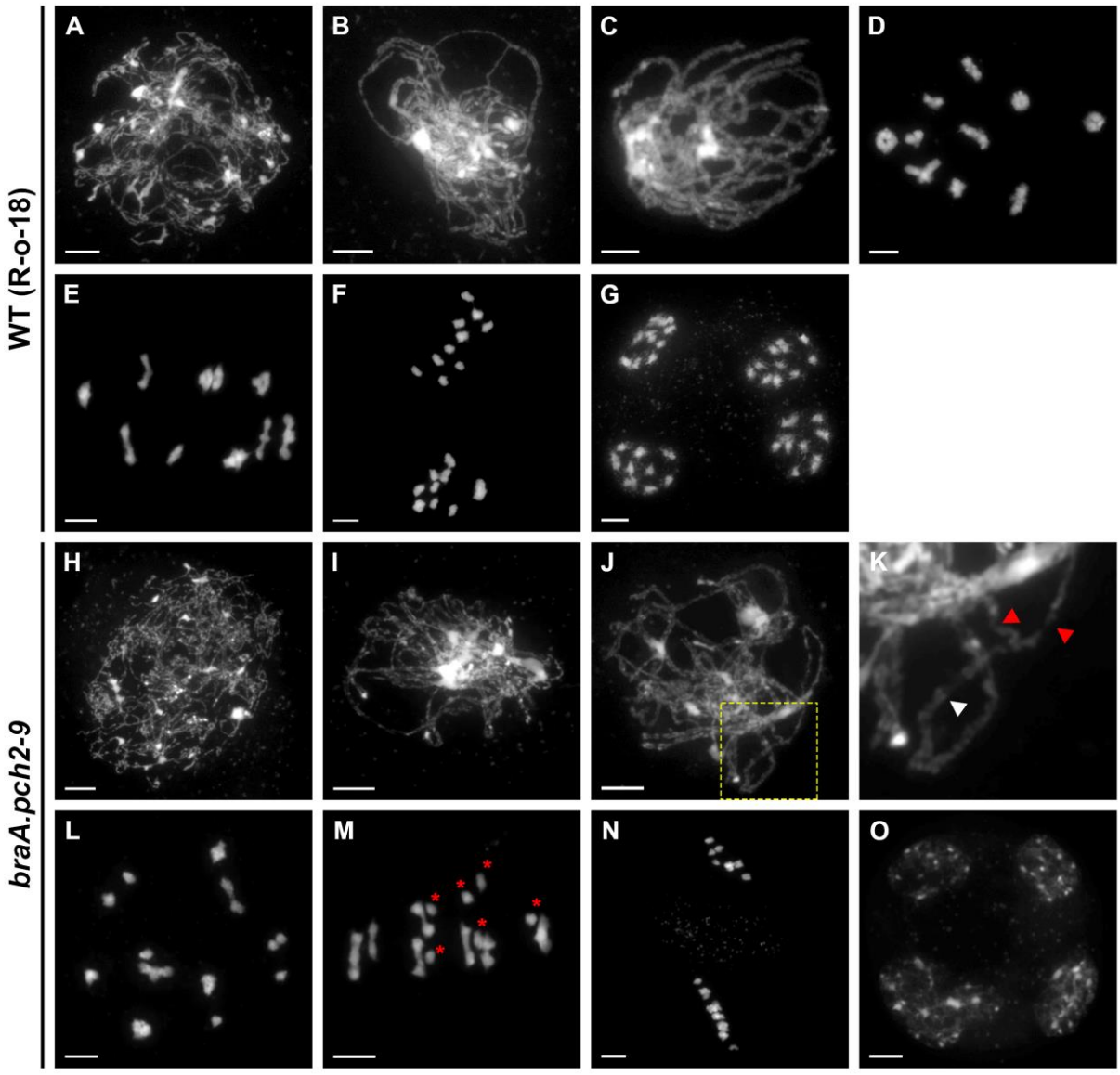


Figure 3.1. Meiosis in *B. rapa* WT (R-o-18) and the mutant line *braA.pch2-9*. (A,H) Leptotene. **(B,I)** Zygotene. **(C)** Full pachytene in WT. **(J)** Incomplete pachytene in *braA.pch2-9*. The yellow square indicates the magnified area in **(K)**. The white arrowhead indicates synapsed areas. The red arrowheads indicate non-synapsed regions. **(D,L)** Diakinesis. **(E,M)** Metaphase I. **(F,N)** Metaphase II. **(G)** WT tetrad. **(O)** Polyad due to missegregation in *braA.pch2-9*. The univalents are labelled with red asterisks. 5 µm bars.

3.2.2. Chiasma analysis in *braA.pch2-9* indicates defects in recombination and changes in CO frequency distribution

In order to assess how the disruption of *BraA.PCH2* was affecting recombination the chiasma frequency per cell was analysed in metaphase I cells as chiasmata constitute a direct indicator of recombination events (section 1.3). This analysis was conducted in plants: homozygous for the mutation (*braA.pch2-9*$^{-/-}$), heterozygous (*braA.pch2-9*$^{+/-}$), segregating WT (*braA.pch2-9*$^{+/+}$), and WT control (R-o-18) (Fig.3.2).

The outcome of the statistical analysis revealed that significant differences were present among the genotypes analysed (Welch's ANOVA test; W=131.0 [3.000, 109.4]; p<0.0001). This was followed by pairwise comparisons between these genotypes using the Dunnet's T3 *post hoc* test. This analysis showed that the chiasma frequency per cell in the homozygous plants was significantly lower (8.13±0.4, n=108; p<0.0001) in comparison with the WT control (15.79±0.27, n=34), the heterozygous plants (16.37±0.12; n=93), and the segregating WT plants (15.96±0.03; n=49). Moreover, no significant differences were spotted between the heterozygous and the segregating WT plants when compared among themselves (p=0.51) and with respect to the WT control (p=0.30 and p>0.99, respectively). Therefore, in agreement with Mendel's laws this confirms that the phenotype of *braA.pch2-9* is a monogenic trait consisting of a point mutation in the sequence of *BraA.PCH2*, which also constitutes a recessive allele since its phenotype is only expressed in the plants homozygous for this variant.

Remarkably, we observed a great range of variation in the number of chiasmata per cell in *braA.pch2-9*$^{-/-}$ (Fig.3.2), from cells with 0 to 17 chiasmata. Also, the mean chiasmata frequency per cell is 8.13±0.4, lower than the minimum number of chiasmata to ensure the obligatory CO (a minimum of 10 chiasmata per cell as *B.*

rapa has 10 pairs of bivalents). Thus, the percentage of cells with univalents and more than 10 chiasmata per cell was analysed, reporting that 21.3 % of cells show univalents despite having a number of COs that would be sufficient to ensure the obligatory CO.

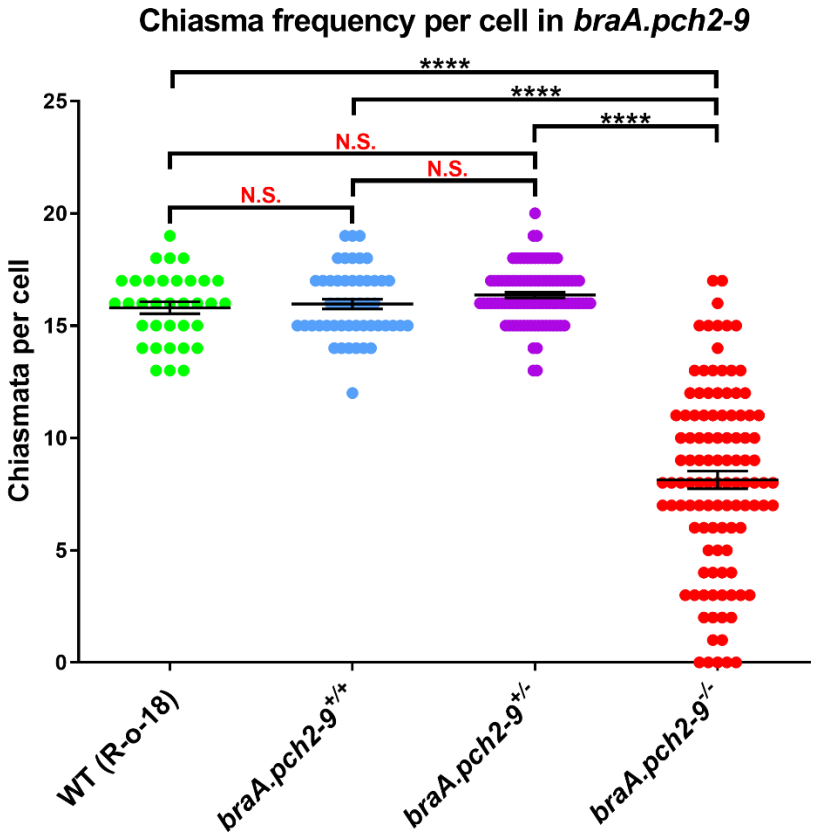


Figure 3. 2. Chiasma frequency analysis of the different genotypes of the *braA.pch2-9* line. Scatter plot of the chiasma frequency per cell data. The bars represent the mean and S.E.M. **N.S.** Non-significant. ********p<0.0001.

In a complementary way, to evaluate the nature of the remaining COs in *braA.pch2-9*, we analysed the distribution of the chiasma frequency per cell (Fig.3.3). Class I COs show positive interference between them, this means that the formation of a Class I CO in a certain place reduces the probability of forming another in the proximity, and therefore, their distribution is not random (section 1.2.5). On the other hand, Class II COs are non-sensitive to interference, and thus, they are independent from each other, being randomly distributed through the genome. In this way, if there

is a high proportion of Class II COs over Class I COs, the chiasma frequency should follow a Poisson distribution and vice versa. Therefore, to evaluate in an indirect way whether the remaining COs in *braA.pch2-9* belong to the Class II, the chiasma frequency distribution was compared to a predicted Poisson distribution generated with the observed data. In the case of the plants homozygous for the *braA.pch2-9* mutation (Fig.3.3.A), the distribution of the chiasma frequency was not significantly different from a Poisson distribution (Kolmogorov-Smirnov test; D=0.1538; p=0.9180). On the other hand, both, the heterozygous, segregating WT, and WT control plants (Fig.3.3.C,D) showed significant differences, and their frequency distribution did not fit a Poisson distribution (D=0.6571, D=0.6471, and D=0.6000, respectively; Kolmogorov-Smirnov test; $p<0.0001$). However, we must point out that the fact that the chiasma frequency distribution of the *braA.pch2-9* homozygous plants does not differ from a Poisson distribution only means that chiasma formation has a high random component. This could be due to a higher proportion of Class II COs as it has been pointed out in previous studies (Higgins *et al.*, 2004; Jackson *et al.*, 2006), or it could also be a result of other conditioning factors such as defects in CO maturation (see sections 3.2.4 to 3.2.6).

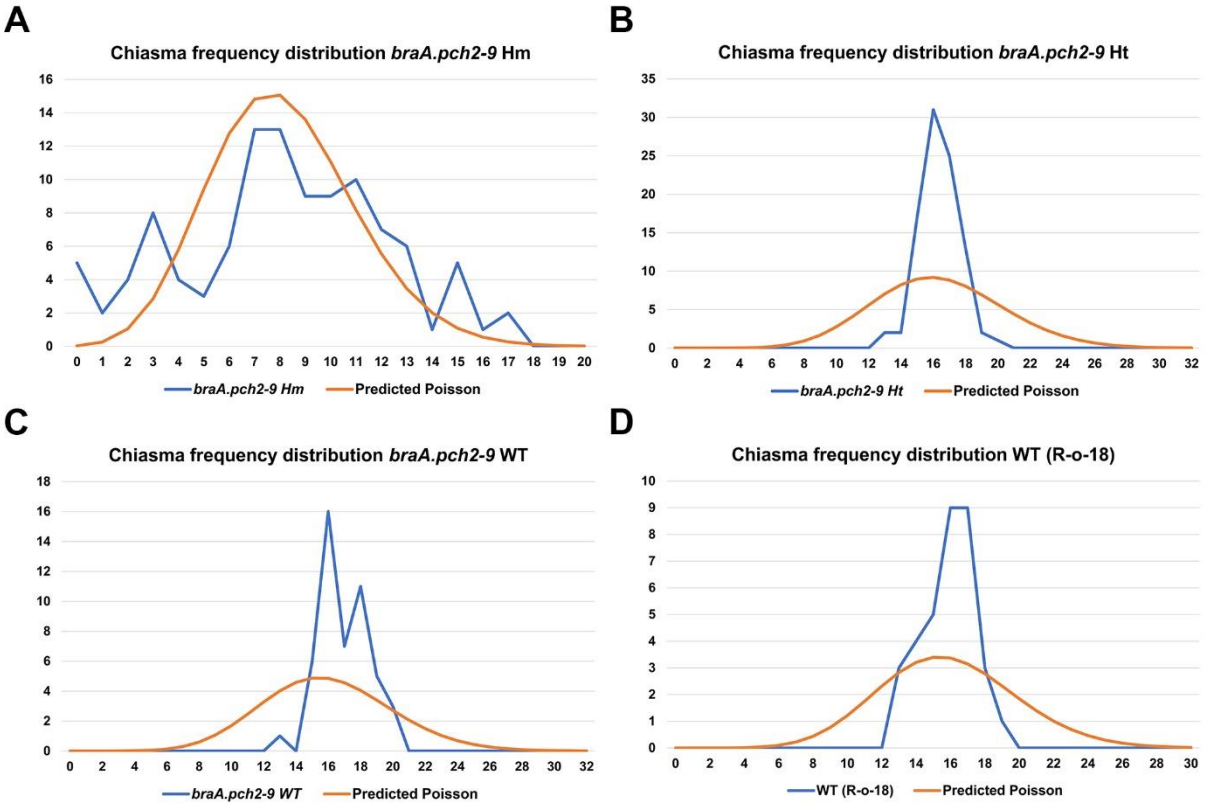


Figure 3.3. Chiasma frequency distribution analysis in the different genotypes of the *braA.pch2-9* line. Graphs showing the chiasma frequency distribution and the predicted Poisson distribution for different genotypes of *braA.pch2-9*. **(A)** Homozygous. **(B)** Heterozygous. **(C)** Segregating WT. **(D)** WT control.

3.2.3. The analysis of bivalent shape and chiasma localisation reveals that in *braA.pch2-9* there is a shift towards rod bivalent formation despite no changes in chiasma localisation

In a complementary way, bivalent shapes were studied in the metaphase I spreads of *braA.pch2-9* as means to assess how the decrease in recombination observed in this mutant was affecting at the chromosome level. Thus, rod and ring bivalents were scored in both the WT control and mutant plants (Fig.3.4.A). Rod bivalents are characterised by having at least one chiasmata or CO in only one of the chromosome arms, whereas ring bivalents have at least one CO event on each chromosome arm. In this way, a significant decrease in the number of ring bivalents per cell was found in the *braA.pch2-9* line in comparison with the WT plants (1.87±0.16 and 5.44±0.22,

respectively; Welch's T-test, t=13.23, df=69.21, p<0.0001). By contrast, no change in the number of rod bivalents per cell was detected between the *braA.pch2-9* mutants and the WT plants (4.15±0.21 and 4.56±0.22, respectively; Welch's T-test, t=1.36, df=94.23, p=0.1771).

The proportion between distal (ID) and interstitial (IP) chiasmata was also studied in the *braA.pch2-9* mutant line (Fig.3.4.B). In this manner, the disruption of *BraA.PCH2* did not seem to cause any significant changes in the localisation of chiasmata despite the defects in CO formation (Fisher´s Exact test, p>0.9999). Thus, the proportion in *braA.pch2-9* remained as a 10% of interstitial chiasmata vs a 90% of distally localised COs, which was close to the 9 % IP vs. a 91% ID of the WT R-o-18 plants.

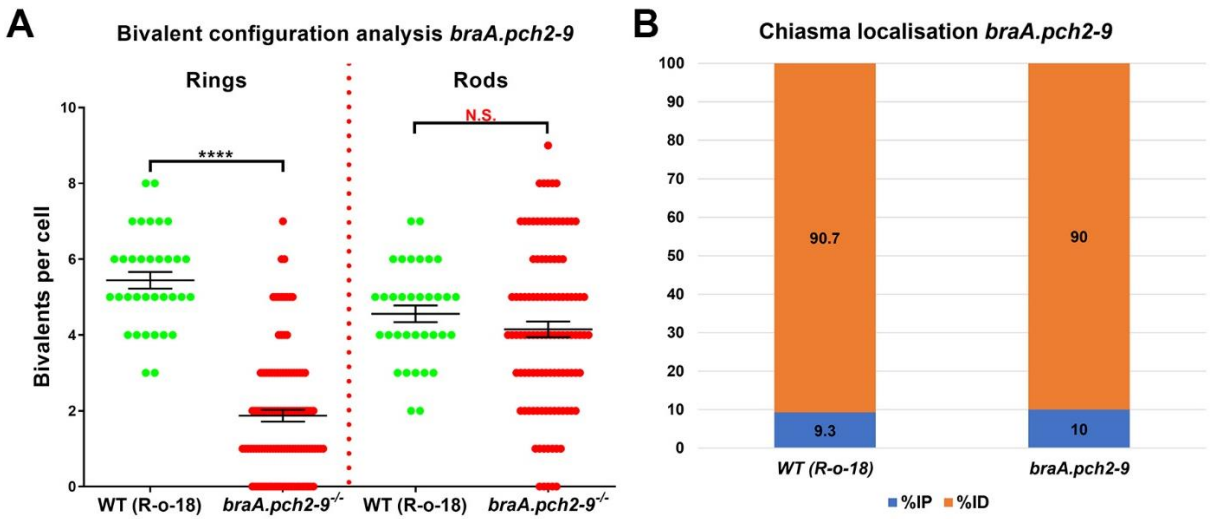


Figure 3.4. Position of chiasmata within the chromosomes and bivalent shape analysis in WT and *braA.pch2-9.* (A). Graph representing the proportions of interstitial vs distal chiasmata in WT and *braA.pch2-9.* The numbers represent the proportion of distal chiasmata**. (B & C).** Scatter plot of the number of ring **(B)** and rod **(C)** bivalents per cell in WT and *braA.pch2-9*. The bars represent the mean and the S.E.M. ********p<0.0001. **N.S.** Non-Significant

3.2.4. The polymerisation of the synaptonemal complex is severely compromised in *braA.pch2-9*

As seen in the DAPI spreads of PMCs of *braA.pch2-9*, synapsis between the homologous chromosomes was severely compromised in this mutant as no full pachytenes were observed (see section 3.2.1). Thus, in order to measure how the formation of the SC was affected by the absence of functional BraA.PCH2 an immunolocalisation of the SC component ZYP1 in PMCs of the WT and *braA.pch2-9* plants was conducted (Fig.3.5.A). Subsequently, the total length of the SC per cell was measured (section 2.4.4) and compared between both genotypes (Fig.3.5.B). It is worth to mention that the quantification of synapsis in *braA.pch2-9* was conducted in the same PMCs of used in section 3.2.5 to score HEI10 foci to be sure that the measures were done in cells that had reached the pachytene stage.

The statistical analysis reported a significant decrease in the total length of the SC per cell in *braA.pch2-9* in comparison with the WT control (Mann-Whitney U-test, $U=3$, $p<0.0001$; Fig.3.5.B). In this way, the WT plants show an average extension of the SC per cell of 367.3±11.43 µm (n=13), ranging from 279 to 432 µm. On the other hand, in *braA.pch2-9* PMCs the average length of the total SC per cell was 140.2±15.22 µm (n=31), with a minimum of 24 µm and a maximum of 329 µm (Fig.3.5.B). The reduction in the SC length observed in *braA.pch2-9* accounts for a 61.85% decrease, thus, PCH2 seems to be essential for the polymerisation of the SC in *B. rapa*.

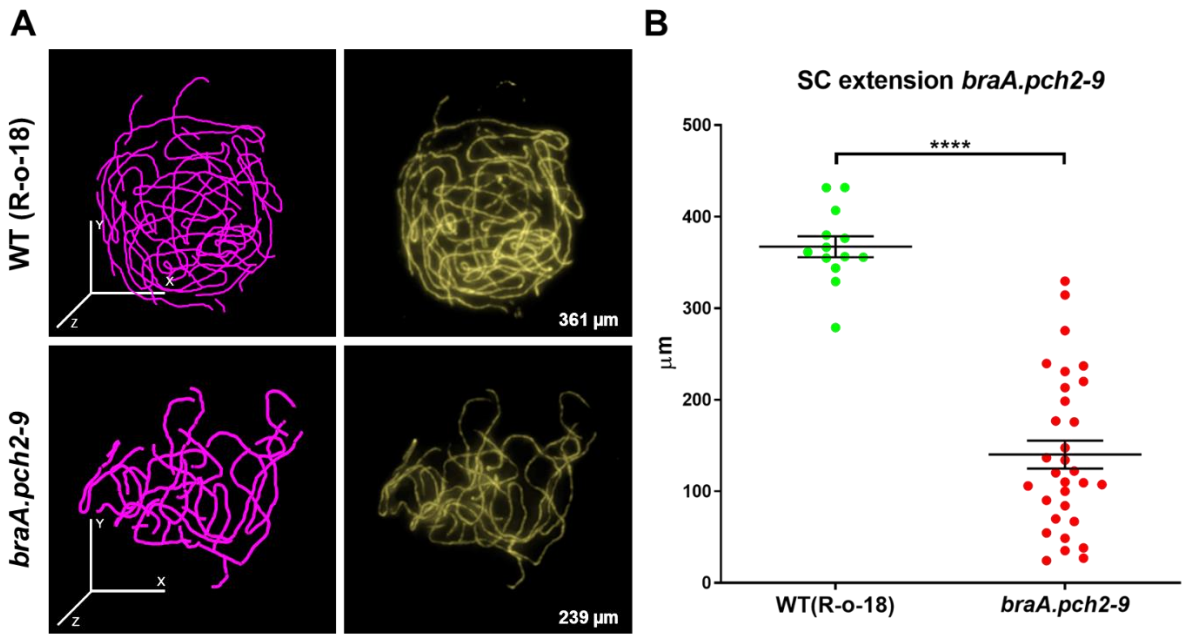


Figure 3.5. Quantification of the total SC length per cell in WT and *braA.pch2-9* late pachytene PMCs. (A). 3D reconstruction and tracing of the SC in late pachytene PMCs of WT and *braA.pch2-9* plants. Image obtained with Simple Neurite Tracer (ImageJ). The number on the lower right corner represents the total extension of the SC in that cell. **(B).** Graph of the total SC length per cell (µm) in WT and *braA.pch2-9* meiocytes. The bars represent the average and the S.D. ********p<0.0001. Modified from Cuacos *et al.* (2021).

3.2.5. Immunolocalisation of the class I CO protein HEI10 indicates a major deficiency in CO maturation in *braA.pch2-9*

To analyse whether the late recombination events were affected in *braA.pch2-9* a double immunolocalisation of the proteins HEI10 and ZYP1 was conducted in the WT control and mutant plants (Figs.3.6 and 3.7.A,B). ZYP1 is used as a marker of synapsis (see section 3.2.4) whereas HEI10 is one of the ZMM proteins involved in Class I CO formation (see section 1.2.3.1), and thus is widely used as a marker of these recombination events.

In the first place, since the timing of the localisation of HEI10 throughout prophase I has not yet been determined in *Brassica*, an analysis of the dynamics of this process was performed in WT plants, prior to the analysis of HEI10 foci in the *braA.pch2-9* mutant (Fig.3.6). In this way, we found that in mid pachytene, when the signal of

ZYP1 is more continuous, HEI10 seems to perfectly follow the signal of ZYP1, indicating that HEI10 is present along the SC during this stage. In late pachytene, when the signal of ZYP1 starts to lose its continuity and gain a dottier appearance, the signal of HEI10 associated with the SC starts to lose intensity and some brighter foci start to appear. In the pachytene-diplotene transition we observed that together with a very dotty ZYP1 signal the foci of HEI10 became brighter the more this stage advanced. Therefore, it is during this stage when the foci scoring took place. Finally, the HEI10 foci are still visible in what we identified as the diplotene stage, characterised by the almost complete depletion of ZYP1. These dynamics concur with recent findings in the plant model organism *A. thaliana* (Morgan, Fozard, *et al.*, 2021).

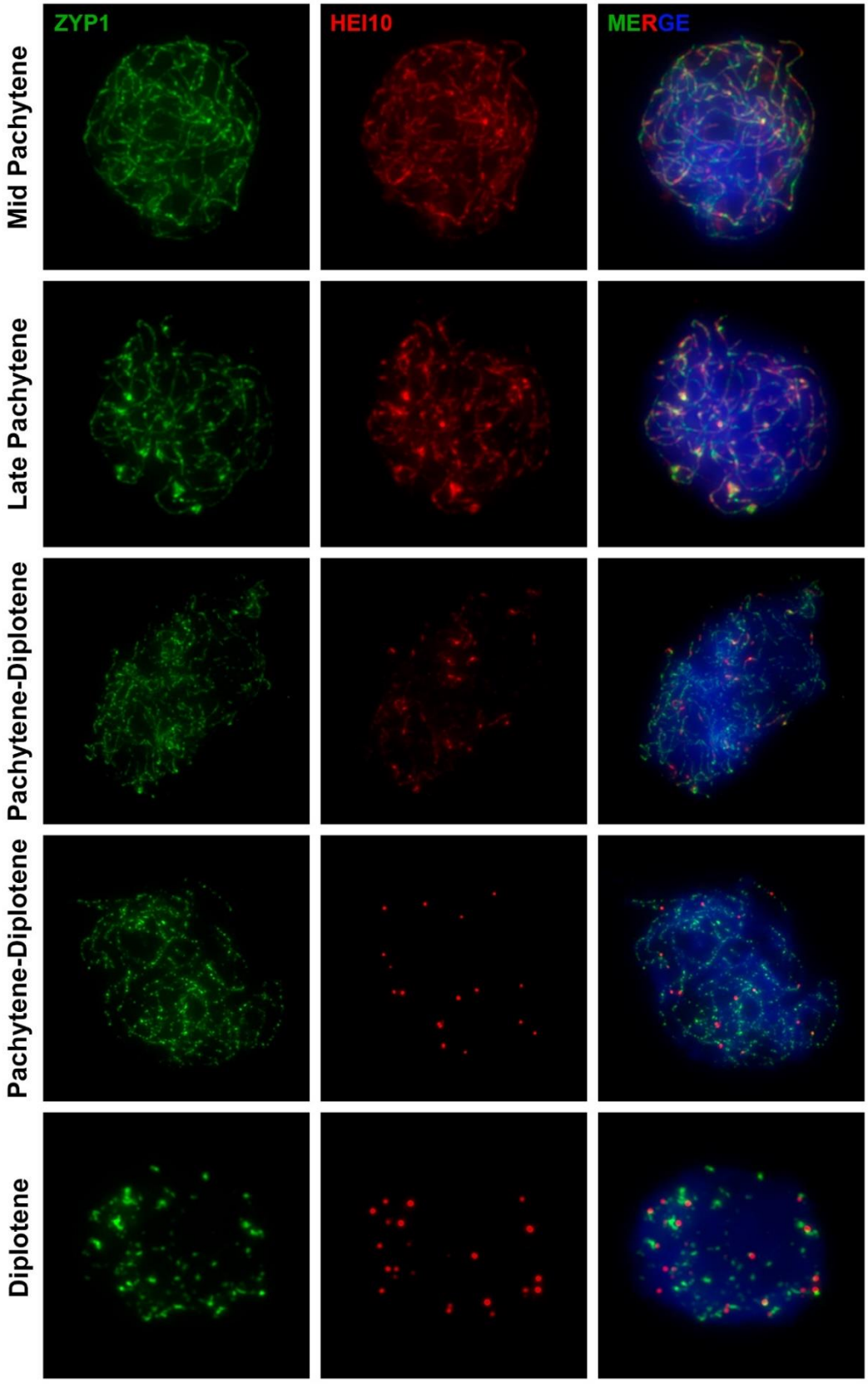


Figure 3.6. Double immunolocalisation of HEI10 and ZYP1 throughout different stages of the pachytene-diplotene transition in *B. rapa* WT R-o-18 plants. Modified from Cuacos *et al.* (2021).

Regarding the scoring of HEI10 foci per cell in *braA.pch2-9*, a significant decrease in the number of foci per cell was revealed in the *braA.pch2*-9 mutant with respect to the WT control (*braA.pch2*-9: 7.46±0.55, n=61; WT: 14.92±0.21, n=83; Welch's T-test, t=12.71, df=78.12, p<0.0001; Fig.3.7.B). This result concurs with the reduction of the chiasma frequency per cell seen in this mutant (section 3.2.2), pointing out that the late recombination events and Class I CO formation are affected in *braA.pch2-9*, resulting in the lack of chiasmata and bivalents observed in metaphase I. Moreover, in the WT a difference of approximately one CO between the chiasmata scoring and the HEI10 foci counts was observed. This difference is due to the fact that chiasmata scoring does not differentiate between class I and class II COs, whereas the HEI10 immunolocalisation does. Therefore, the extra CO observed in the chiasmata counts must correspond with class II COs, that seem to account for a 5% of the total number of COs in *B. rapa*. This estimate contrast with the higher chiasmata number observed in the *braA.msh4* mutant, as explained by Blary *et al.*, (2018) this could be due to closely located chiasmata indistinguishable in the WT.

Additionally, the HEI10 foci scoring in *braA.pch2-9* indicates that most of the remaining COs are Class I COs. This result is in conflict with the hypothesis that the remaining COs in *braA.pch2-9* could belong to the Class II due to their random behaviour (section 3.2.2). Consequently, we can deduce that the behaviour of the chiasma frequency per cell in this mutant must be conditioned by other causes such as problems in CO maturation and difficulties in establishing the IH Bias (discussed in more detail in section 3.3).

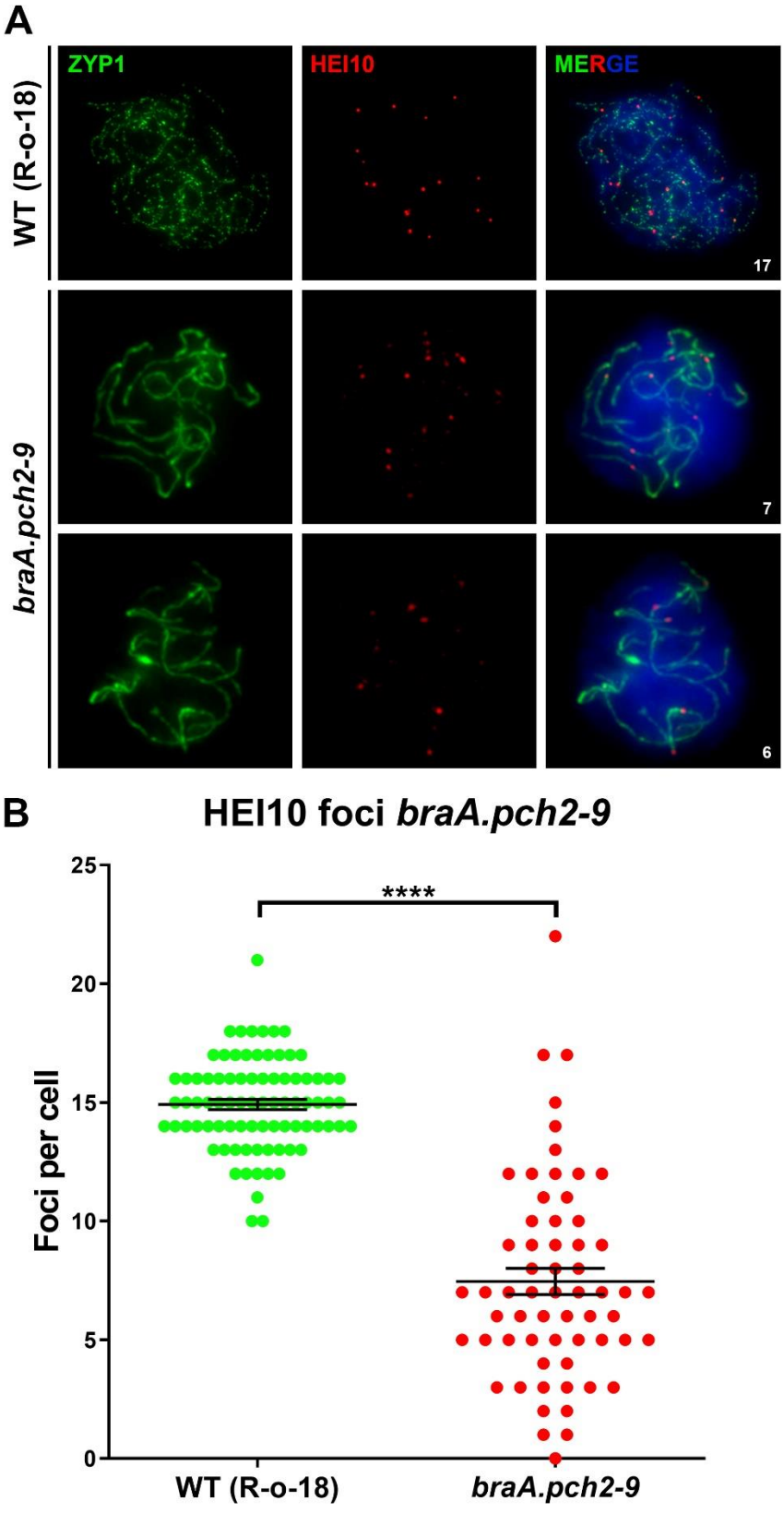


Figure 3.7. HEI10 foci scoring in WT and *braA.pch2-9*. (A) Comparison between WT and *braA.pch2-9* meiocytes, showing two mutant meiocytes with similar HEI10 foci counts but different levels of synapsis. **(B)** Scatter plot showing the foci counts per cell in WT and *braA.pch2-9*. The bars represent the mean and S.D. ********P<0.0001.

3.2.6. The number of Class I COs does not seem to be related with the extension of the SC in *braA.pch2-9*

As shown in Fig.3.7.B the HEI10 foci data of *braA.pch2-9* shows a great variability, which is also present in the extension of synapsis in found in these cells (section 3.2.4) and concurs with the variability found in the chiasmata counts (Fig.3.2). Thus, the possibility that there was any relation between the number of HEI10 foci present in a meiocyte and the extension of the SC was explored. In this way, the SC was traced, and its length measured in the *braA.pch2-9* meiocytes used in the HEI10 foci scoring (Fig.3.8.A,B). Consequently, a correlation analysis was performed between both variables (Fig.3.8.C). The results of the analysis showed that in *braA.pch2-9* there is no significant correlation between the number of HEI10 foci and the total synaptonemal complex length per cell, observing a very low correlation coefficient between both variables ($r=0.0702$; $p=0.7023$; $n=31$; Fig.3.8.C). Hence, in *braA.pch2-9* the number of HEI10 foci in a given meiocyte does not seem to be related with the extension of the SC.

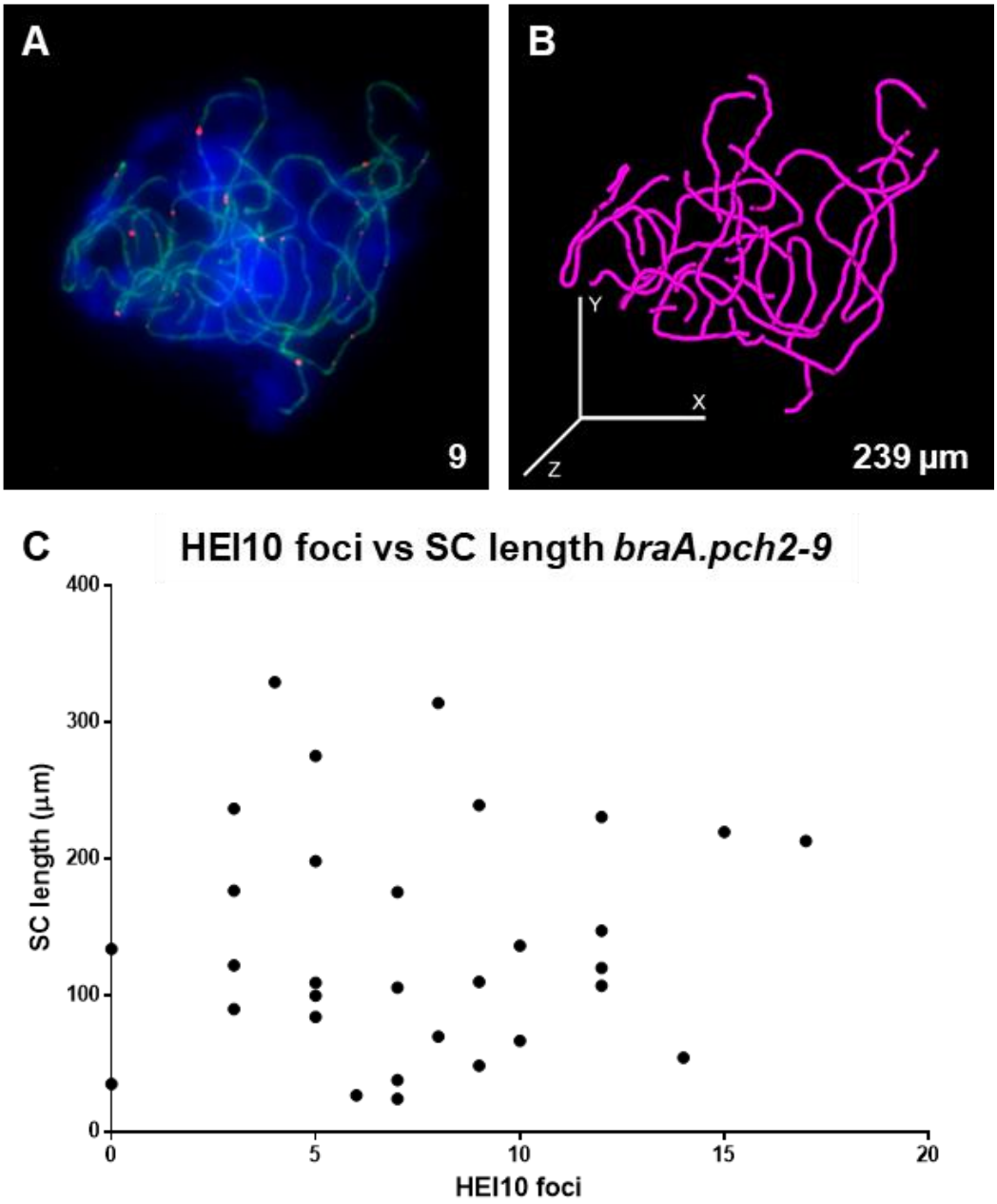


Figure 3.8. Synaptonemal complex measuring in *braA.pch2-9* cells and correlation analysis of the SC extension and number of HEI10 foci in *braA.pch2-9* PMCs. (A,B) 3D reconstruction of the SC of one of the cells used in the HEI10 foci counts, the number of foci and the SC length are shown in the lower right corner. Image obtained with Simple Neurite Tracer (ImageJ). **(C)** Plot of the SC length vs HEI10 foci in *braA.pch2-9* meiocytes.

3.2.7. BraA.PCH2 requires BraA.ASY1 to carry out its function during meiosis

As explained in detail in section 1.3.1.4, PCH2 has double role during meiosis participating in the loading of the axis-associated protein ASY1 to the AEs at the onset of meiosis and, later on, in its depletion from the synapsed areas (Lambing *et*

al., 2015; Yang *et al.*, 2020; Cuacos *et al.*, 2021). In this way, to study in more detail the functional relation between ASY1 and PCH2 in *B. rapa* a *braA.asy1-14 braA.pch2-9* double mutant was obtained and the chiasma frequency per cell was analysed in metaphase I spreads of PMCs, comparing it to that of the single mutants (Fig.3.9.A,B). The statistical analysis revealed that significant changes were present among the genotypes analysed (Welch's ANOVA test, W= 752.5 [3.000, 119.4], $p<0.0001$). Subsequently, a pairwise comparison test (Dunnet's T3 test) was conducted to compare the double mutant with respect to the single mutants and the WT control. The results of the *post-hoc* test showed that there was a significant decrease of the chiasma frequency per cell in the *braA.asy1-14 braA.pch2-9* double mutant (1.83±0.15) with respect to the WT control and the *braA.pch2-9* single mutant (n=80, n=34, and n=108, respectively; $p<0.0001$). By contrast, no differences were found between the double mutant and the single mutant *braA.asy1-14* (2.31±0.22, n=58, p=0.1947). Altogether, these results confirm the epistatic relation between *BraA.ASY1* and *BraA.PCH2* as the phenotype of the *braA.asy1-14* mutant predominates over the one of *braA.pch2-9*, indicating that, as expected, PCH2 depends on ASY1 to carry out its function.

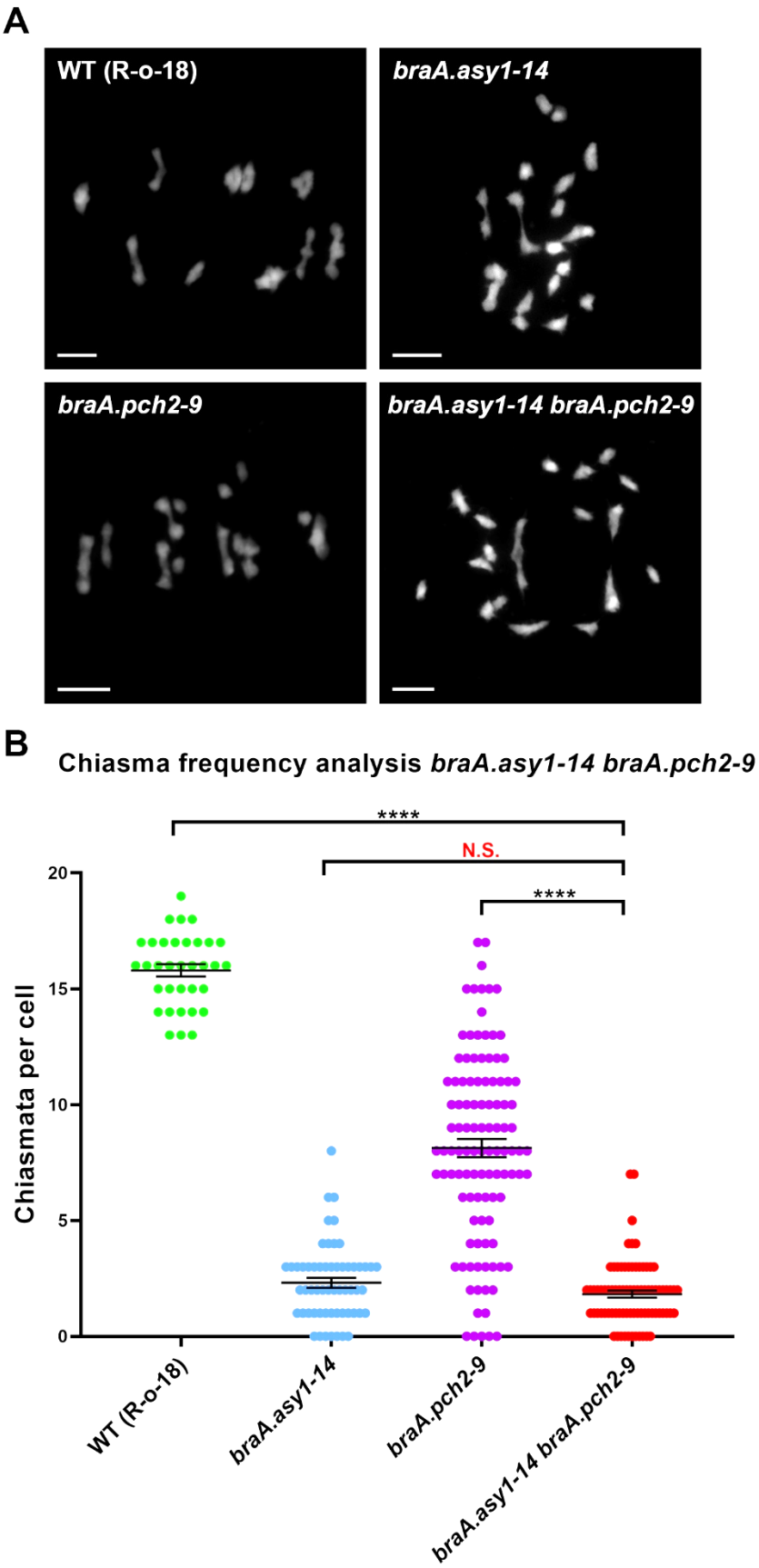


Figure 3.9. Chiasma frequency analysis in the *braA.asy1-14 braA.pch2-9* double mutant. A. Metaphase I meiocytes of the single mutants *braA.asy1-14* and *braA.pch2-9,* the double mutant *braA.asy1-14* and *braA.pch2-9,* and the WT control. **B.** Scatter plot of the mean chiasma frequency per cell in the previously mentioned genotypes. ****p<0.0001. **N.S.** Non-Significant.

3.2.8. Obtention and identification of CRISPR/Cas9 PCH2 mutagenized plants in *B. oleracea*

A total number of 26 T0 primary transformant plants were generated after the *Agrobacterium* mediated transformation of the CRISPR construct followed by callus regeneration by the BRACT service of the John Innes Centre (Norwich, UK; https://www.jic.ac.uk/research-impact/technology-research-platforms/crop-transformation/). Of these, 10 were transformed with the CRISPR construct containing the sgRNAs 1a and 1b, targeting the exons 1 and 3; and 16 were transformed with the construct containing the sgRNAs 2a and 2b, targeting the exons 1 (different region to 1a) and 5 (Fig.3.10).

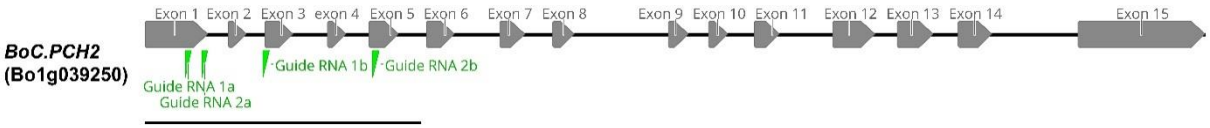


Figure 3.10. *BoC.PCH2* sgRNA targets. Grey arrow boxes indicate exons. Black lines indicate introns. Green triangles indicate the position and direction of the sgRNAs used in the CRISPR mutagenesis. 1kb bar.

The T0 plans were sequenced by Dr James Higgins (University of Leicester) at the JIC for both: presence and number of copies of the CRISPR construct and screening of mutations in the CRISPR targets. Only one T0 plant (B2460-2.03a) presented a change in the DNA sequence, and 2 insertions of the CRISPR construct, and thus it was selected to stablish a mutant line of the *BoC.PCH2* ortholog of *B. oleracea*. The induced mutation consisted of a 23 bp deletion (Fig.3.11.A) which creates a shift in the reading frame, generating a stop codon downstream from its location, therefore, a truncated version of the protein is expected in the B2460-2.03a line (Figure 3.11.B). This was also confirmed by us as we sequenced the target region in the T1 plants (explained below). The seeds of the T1 generation were sent to us by the Higgins lab

(University of Leicester) to continue with the characterisation on of these mutant lines.

In a complementary way, an attempt to find alternative mutant lines was performed in the T1 plants of 8 different transformant lines, given that the CRISPR construct could still be active and produce novel mutant alleles. The transformant lines were selected based on the criteria that they should have only one insertion of the CRISPR construct. Thus, the target regions of 5 T1 plants of each transformant line were sequenced to seek for possible mutations. Unfortunately, none presented any alterations with respect to the WT sequence. Therefore, the B2460-2.03a line (named *boC.pch2-1* from here onwards) was selected for further analysis as it was the only one in which the CRISPR construct successfully induced a change in the sequence of the *BoC.PCH2* gene.

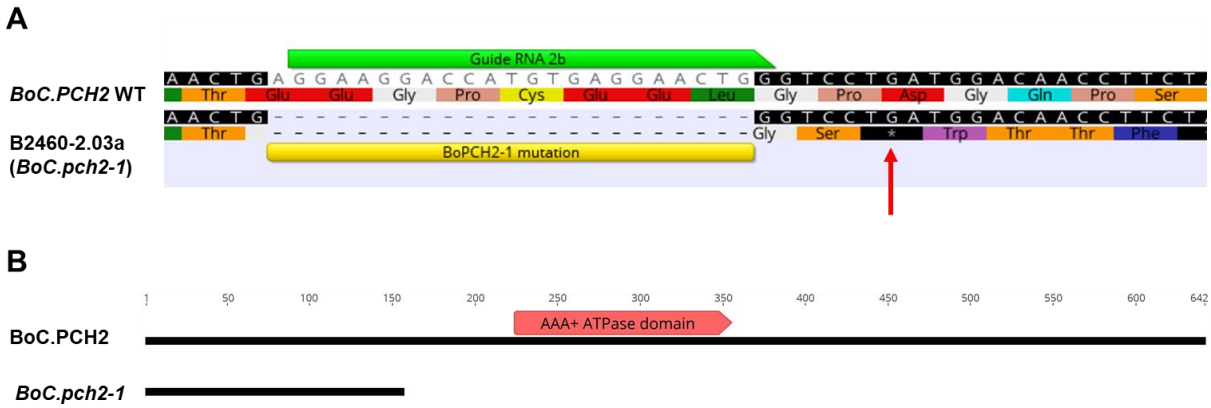


Figure 3.11. Comparison of the DNA sequences and protein products of BoC.PCH2 between the WT and the *boC.pch2-1* line (A) Alignment of the BoC.PCH2 and mutant sequences obtained from the sequencing of the T1 plants of the B2460-2.03a line (*boC.pch2-1*)**.** The deletion is labelled with a yellow box. The red arrow points the position of the stop codon generated by the mutation. **(B)** Comparison between the protein products of *BoC.PCH2* and the expected truncated version of *boC.pch2-1*.

Regarding our work with the *boC.pch2-1* line, 33 T1 plants were obtained from the seeds of the T0 plants. These were genotyped by PCR to check for the presence of

the CRISPR construct and the sgRNA2b target region was sequenced to confirm the presence of the mutation and that this was homogeneous among the progeny of the T1 plants (primers in section 2.3.3). The objective was to identify plants heterozygous for the mutation that did not bear the CRISPR construct due to its loss by segregation. In this way, we were able to identify two plants in the T1 generation that had lost the construct but were heterozygous for the mutation, these were allowed to set seed and meiosis was analysed in the following generations. The plants of the T2 generation were backcrossed with the parental WT (DH1012) line used for transformation to confirm that the phenotype observed was only due to the disruption of *BoC.PCH2* and not to any possible off-target mutations.

3.2.9. Characterisation of the meiotic phenotype of the *boC.pch2-1* mutant line reveals a drastic abrogation of meiosis.

To seek for any disruption of the meiotic programme, male meiosis was analysed in a first instance through DAPI spreads of PMCs, in all the possible genotypes of the *boC.pch2-1* line: homozygous (*boC.pch2-1*$^{-/-}$), heterozygous (*boC.pch2-1*$^{+/-}$) and segregating WT (*boC.pch2-1*$^{+/+}$); using the WT control (DH1012) as a reference (Figs.3.12 and 3.13). It is worth to mention that *B. oleracea* presents 9 pairs of homologous chromosomes (n=9), and thus 9 bivalents are observed in metaphase I.

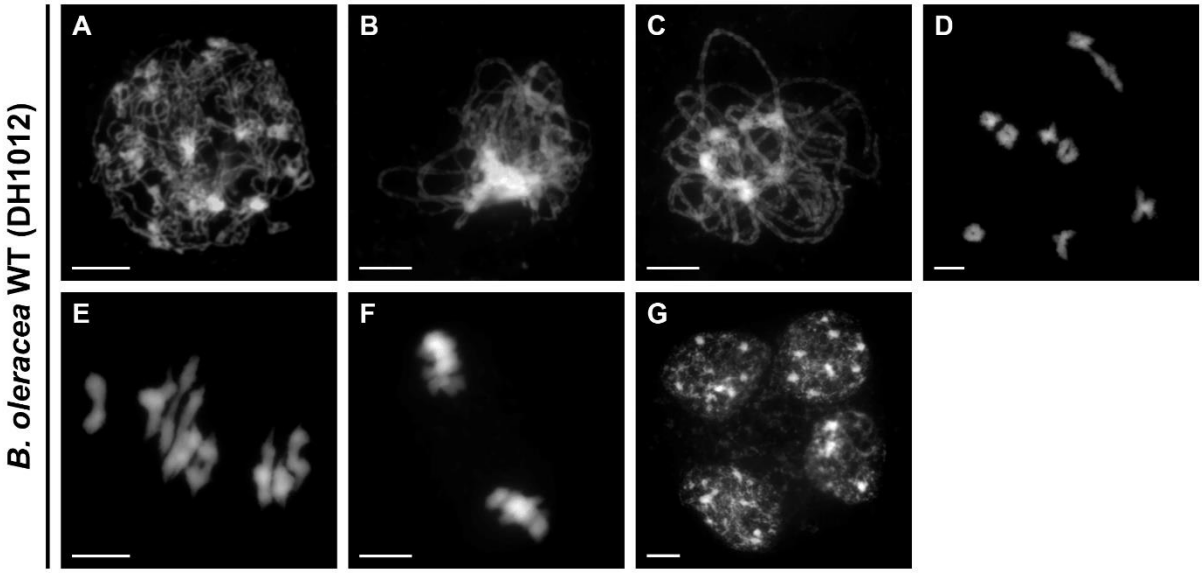


Figure 3.12. Meiotic cell division in *B. oleracea* DH1012. (A) Leptotene. **(B)** Zygotene. **(C)** Pachytene. **(D)** Diakinesis. **(E)** Metaphase I. **(F)** Metaphase II. **(G)** Telophase II/Tetrad. 5µm bars.

This analysis showed that the plants homozygous for the *boC.pch2-1* mutant allele (Fig.3.13. A-H) presented a severe disruption of the meiotic programme. On the other hand, the heterozygous and segregating WT plants were indistinguishable from the WT control (Fig.3.13. I-O and P-V). In this way, despite the *boC.pch2-1*$^{-/-}$ plants did not present any obvious differences in the leptotene and zygotene stages with respect to the WT control (Fig.3.13.A,B), an absence of meiocytes in the pachytene stage was found. Instead, and similarly to the *pch2* mutants in *B. rapa* (section 3.2.1), the meiocytes reached a late-zygotene/pachytene-like stage (Fig.3.13.C), which presented a combination of synapsed and non-synapsed regions (Fig.3.13.D) suggesting that synapsis was defective in *boC.pch2-1.* Moreover, in agreement with the meiotic phenotype of the *pch2* mutants characterised in *A. thaliana* and *B. rapa* (Lambing *et al.*, 2015; Cuacos *et al.*, 2021), a severe disruption of bivalent formation was observed in diakinesis and metaphase I as a high incidence of univalents was present in all the *boC.pch2-1*$^{-/-}$ metaphase I cells analysed (n=92) (Fig.3.13.E,F).

Interestingly, the WT control, segregating WT and heterozygous plants also showed a certain incidence of metaphase I cells with univalents (WT control: 16.67%, n=66; *boC.pch2-1*$^{+/+}$: 23%, n=73; *boC.pch2-1*$^{+/-}$: 25%, n=101), which did not seem to be translated into a decrease in chiasma formation (section 3.2.9). The statistical analysis of the number of univalents per cell showed that significant differences were present among the genotypes studied (Welch's One-Way ANOVA; W= 850.1 [3.000, 175.7]; p<0.0001). Successively, the Games-Howell's multiple comparisons test was used to perform pairwise comparisons between the groups. In this way, it reported that the plants homozygous for the *boC.pch2-1* allele presented significantly higher numbers of univalents per cell in comparison with the WT control, the segregating WT and the heterozygous plants (7.56±0.15, 0.17±0.05, 0.26±0.06, 0.27±0.05, respectively; p<0.0001). By contrast, no significant differences were found between the segregating WT and the heterozygous plants when compared to the WT control, and neither between themselves (p=0.59, p=0.49, and p=0.99, respectively). Thus, it seems that the presence of univalents in the WT control, the segregating WT and the heterozygous plants is most likely due to the fact that the DH1012 line is a doubled haploid, which could already present some background mutations fixed within the population. On the other hand, the great defect in bivalent formation observed in the *boC.pch2-1* homozygous plants suggests that it is due to the loss of function of BoC.PCH2. Moreover, this led to the non-disjunction of the chromosomes in anaphase II in *boC.pch2-1*$^{-/-}$, generating unequal sets of chromosomes observable in metaphase II and the formation of polyads with unbalanced nuclei at the end of meiosis (Fig.3.13.G,H).

To summarise, the analysis of DAPI spreads of PMCs revealed that, as expected, the loss of function of BoC.PCH2 in *B.* oleracea leads to problems in the formation of COs between the homologs, as these do not appear associated through chiasmata forming bivalents. Nevertheless, no obvious defects in the meiotic programme were observed in the segregating WT and heterozygous plants (Fig.3.13.I-O and P-V, respectively), as only a small decrease in bivalent formation was found in the later, which was also present in the WT control. Therefore, this indicates that the defects observed in meiosis in this line are associated with the disruption of the *BoC.PCH2* gene that occurs in the *boC.pch2-1* recessive mutant allele.

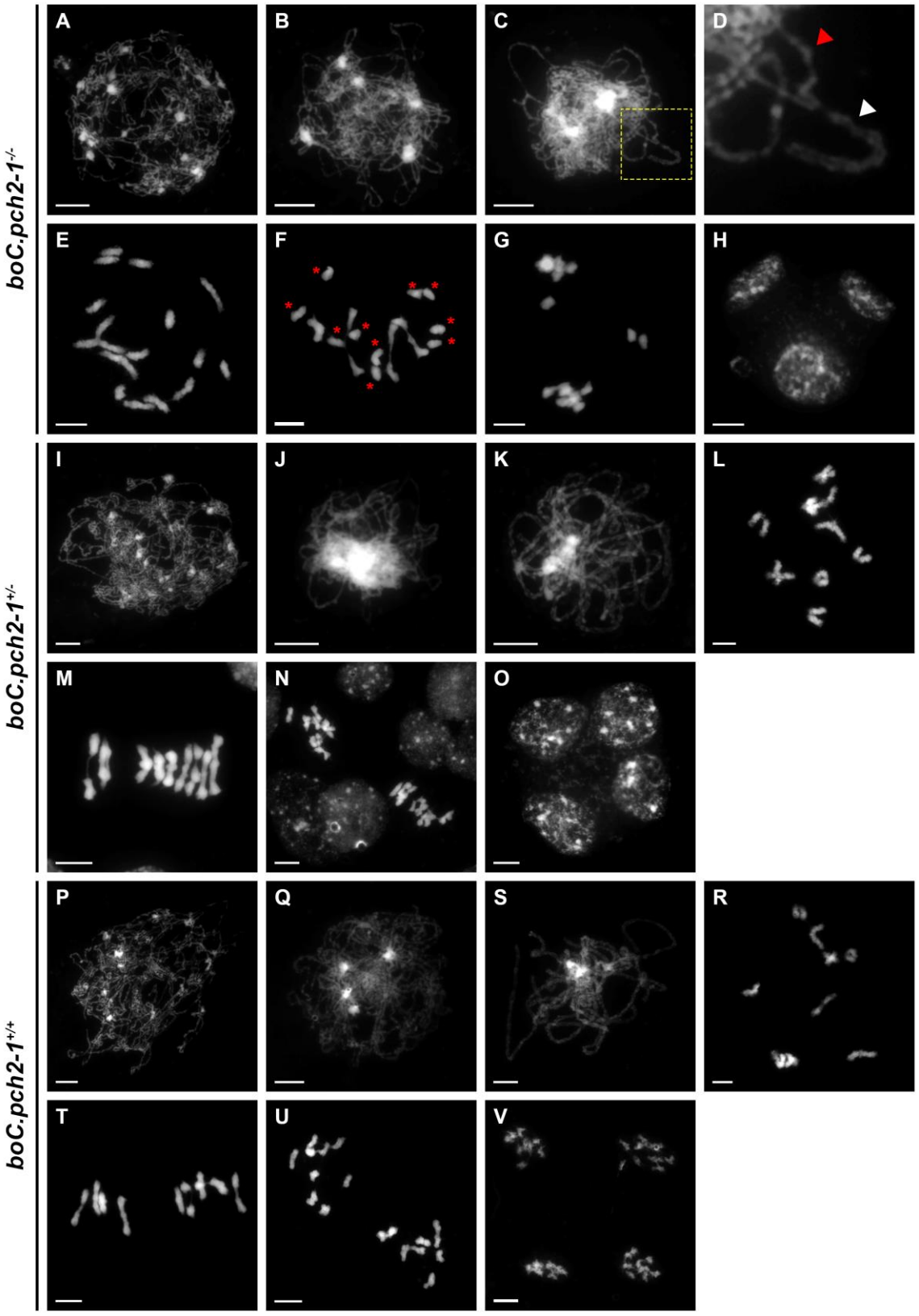


Figure 3.13. Meiotic cell division in *boC.pch2-1* homozygous (A-H), heterozygous (I-O), and segregating WT plants (P-V). (A, I, P) Leptotene. **(B, J, Q)** Zygotene. **(C)** Pachytene-like**. (D)** Close-up of synapsed, white arrowheads, and non-synapsed regions, red arrowheads. **(K, S)** Pachytene. **(E, L, R)** Diakinesis. **(F, M, T)** Metaphase I, the red asterisks indicate the presence of univalents. **(G, N, U)** Metaphase II. **(H, O, V)** Telophase II/Tetrad. 5µm bars.

3.2.10. Analysis of chiasma formation in *boC.pch2-1* reveals severe defects in HR

As the severe reduction in bivalent formation observed in the *boC.pch2-1*$^{-/-}$ plants suggested a major defect in CO formation, an analysis of the chiasma frequency per cell was conducted in all the genotypes of the *boC.pch2-1* line (Fig.3.14). Since chiasmata are the cytological expression of COs, these provide a reliable insight of the effect on HR of the *boC.pch2-1* induced mutation.

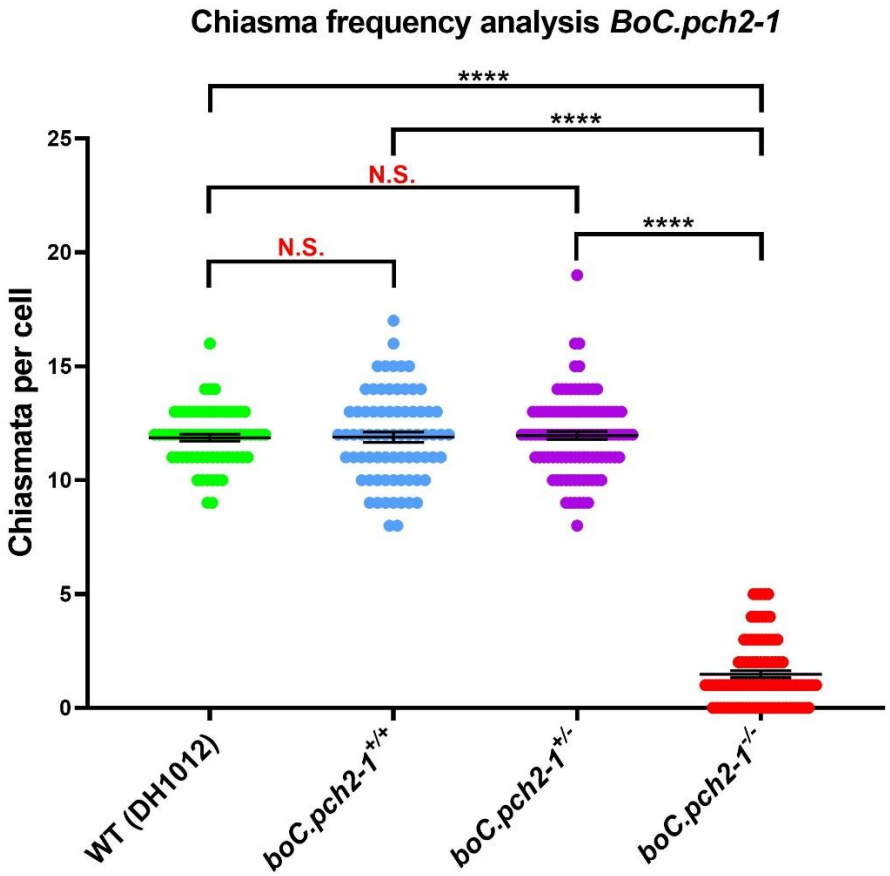


Figure 3.14. Scatter plot of the chiasma frequency per cell in the plants of the *boC.pch2-1* line and the WT control. The bars represent the mean±S.E.M. **N.S.** Non-Significant. ********p<0.0001.

The statistical analysis of the chiasma frequency per cell showed that significant differences were present among the genotypes analysed (Welch's One-Way ANOVA, W= 1075 [3.000, 174.6]; p<0.0001). Subsequently, the pairwise comparison between them (Games-Howell's *post hoc* test) revealed that the plants homozygous

for the mutation presented a great and significant reduction of the mean chiasma frequency per cell in comparison with the WT control, the segregating WT and the heterozygous plants (1.48±0.15, 11.86±0.15, 11.89±0.23, 11.96±0.17, respectively; $p<0.0001$). By contrast, no differences were found between the segregating WT and the heterozygous plants when compared among themselves and to the WT control ($p>0.99$, $p=0.99$, and $p=0.97$, respectively).

These results show that the absence of a functional PCH2 results in a severe reduction of CO formation (88%) in *B. oleracea*, even greater that the one observed in *B. rapa* (49%; Cuacos *et al.*, 2021; section 3.2.2) and *A. thaliana* (30%; Lambing *et al.*, 2015).

In the same manner as in the *braA.pch2-9* mutant, the distribution of the chiasma frequency was studied in the *boC.pch2-1* homozygous plants by comparing it to a predicted Poisson distribution (Fig.3.15). The statistical analysis showed that no differences were present between both distributions in the *boC.pch2-1*$^{-/-}$ plants (Kolmogorov-Smirnov test of cumulative distributions; $D=0.2941$; $p=0.45$; Fig.3.15.A). On the other hand, as expected, the distributions of the chiasma frequency per cell in the heterozygous, segregating WT and WT control plants were significantly different from a Poisson distribution (Kolmogorov-Smirnov test of cumulative distributions, $D=0.5484$, $p<0.001$; $D=0.5333$, $p<0.001$; $D=0.6333$, $p<0.0001$; Fig.3.15.B,C,D). Thus, these results suggest that the chiasma frequency per cell in *boC.pch2-1*$^{-/-}$ has a high random component, concurring with difficulties in the formation of class I COs.

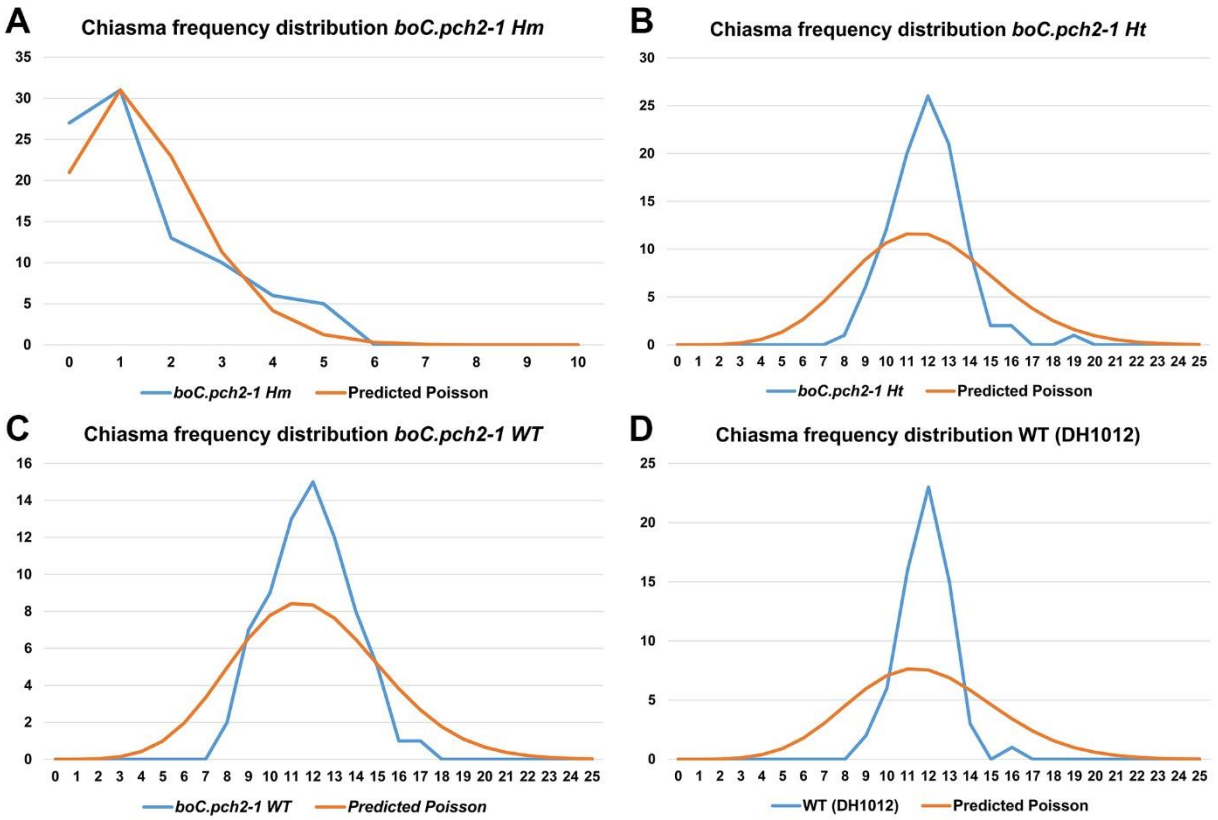


Figure 3.15. Analysis of the chiasma frequency distribution in *boC.pch2-1*. Graphs showing the distribution of the chiasma frequency per cell with respect to a predicted Poisson distribution in *boC.pch2-1* homozygous **(A)**, heterozygous, **(B)**, segregating WT **(C)**, and WT control plants **(D)**.

3.2.11. Analysis of the bivalent configurations and chiasma localisation in *boC.pch2-1*

To further understand how the reduction in CO formation was related to changes in the configurations of the bivalents in metaphase I, an analysis of the formation of ring and rod bivalents, together with the position of the chiasmata within the chromosome arms was conducted in the *boC.pch2-1* homozygous plants (Fig.3.16).

The results of the analysis of the bivalent configurations (Fig.3.16.A) revealed that in the case of the ring bivalents, these were almost completely absent in *boC.pch2-1*$^{-/-}$, which showed a much lower number of ring bivalents per cell than the WT control (0.08±0.03 and 2.68±0.15, respectively; Welch's T-test, t=17.45, df=69.69, p<0.0001). Similarly, the number of rod bivalents per cell was greatly reduced in the

boC.pch2-1 mutant in comparison with the WT control (1.36±0.13 and 6.15±0.16, respectively; Welch's T-test, t=23.15, df=140.8, p<0.0001). These results concur with the extremely low chiasma frequency registered for this mutant, also showing that the chiasmata observed are due to the residual occurrence of rod bivalents.

In a complementary way, the proportion between interstitially and distally located chiasmata was also studied in the *boC.pch2-1* mutant line (Fig.3.16.B). In this way, the results showed that the defects in CO formation observed in this mutant did not seem to influence the localisation of the remaining ones as the proportions remained the same between *boC.pch2-1* and the WT control (*boC.pch2-1*: IP=2.21% vs ID=97.79%, WT: IP=5.76% vs ID=94.24%; Fisher's exact test, p=0.1296).

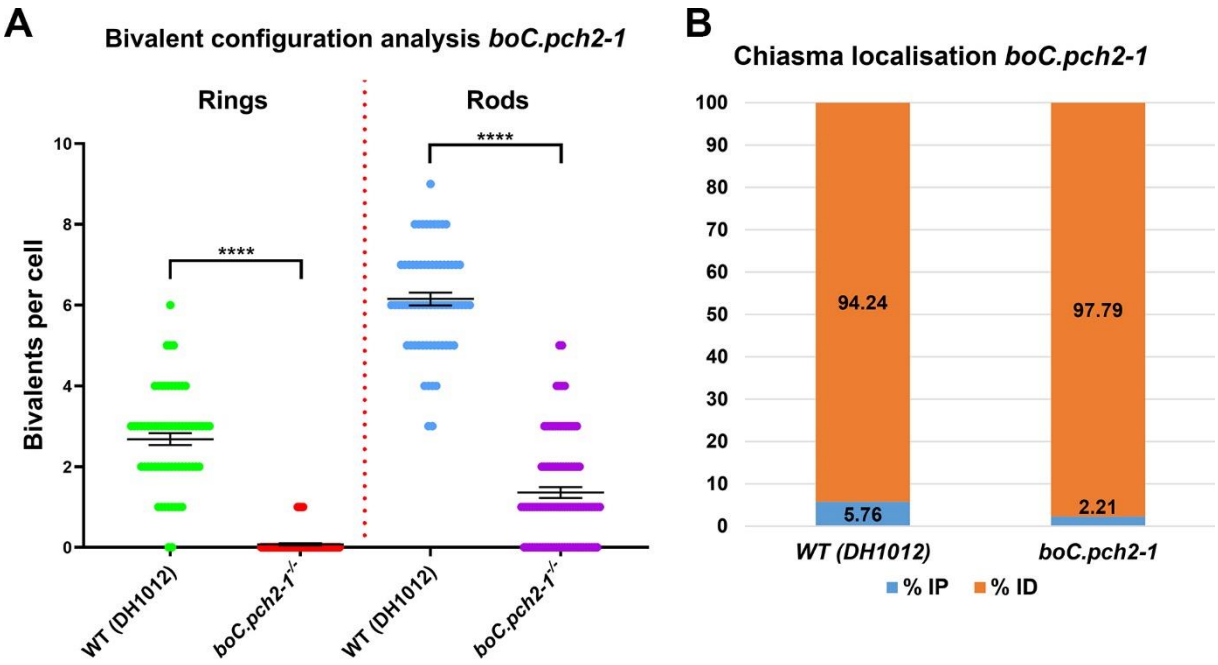


Figure 3.16. Bivalent configuration and chiasma localisation analyses in *boC.pch2-1*. (A) Scatter plot of the ring and rod bivalents per cell observed in *boC.pch2-1*. The bars represent the mean±S.E.M. **N.S.** Non-Significant. ********p<0.0001**. (B)** Bar graph showing the proportion between interstitial and distal chiasmata in *boC.pch2-1*.

3.2.12. PCH2 is absent in *boC.pch2-1* leading to defects in the association of ASY1 with the AEs and in the polymerisation of the synaptonemal complex

PCH2 has been described to be essential for the completion of synapsis between the homologs and the depletion of ASY1 from the LEs in parallel with the polymerisation of the SC (Lambing *et al.*, 2015; Cuacos *et al.*, 2021, section 3.2.4). Thus, the dynamics of ASY1, PCH2, and ZYP1 were studied by means of a triple immunolocalisation in different stages of meiosis in the WT control (Fig.3.17.) with the intention of using it as a reference to compare with the *boC.pch2-1* homozygous plants (Figs.3.18 and 3.20).

In this way, as shown in Fig.3.17 ASY1 polymerises during the leptotene stage, reaching a continuous signal in its transition to zygotene. During the zygotene stage, the signal of ASY1 becomes dimmer in the areas where synapsis between the homologs has been achieved due to the remodelling carried out by PCH2, resulting in a more diffuse and dimmer signal in pachytene. On the other hand, ZYP1 starts as foci in leptotene, and its signal extends through zygotene with the polymerisation of the SC, reaching its full extension in pachytene. Moreover, in agreement with the previous description by Lambing *et al.* (2015), PCH2 seems to consistently colocalise with ZYP1 through the different stages of prophase I.

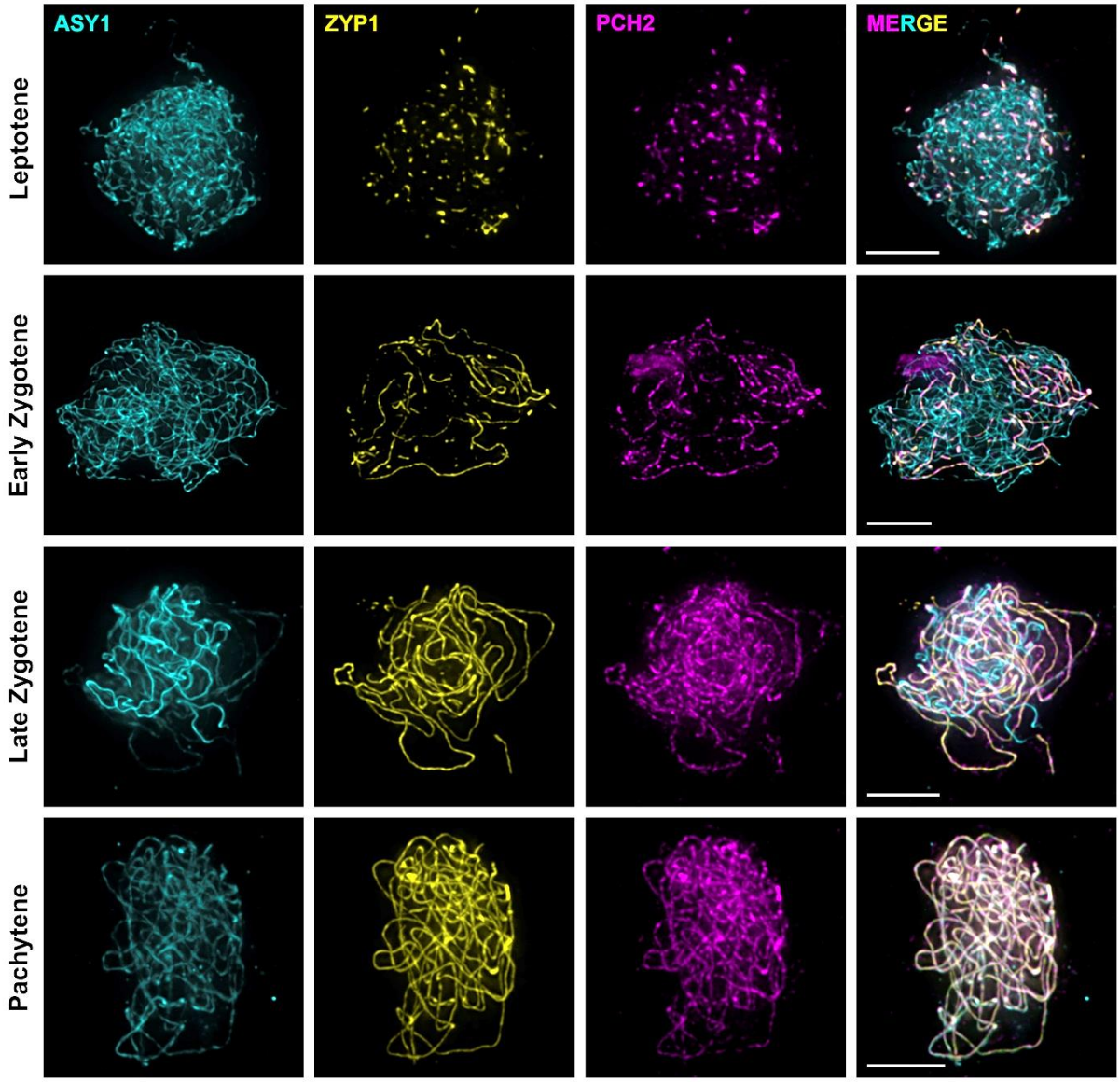


Figure 3.17. Atlas of the dynamics of ASY1, ZYP1 and PCH2 during different stages of meiosis in B. oleracea DH1012. 5µm bars.

Regarding the *boC.pch2-1* mutant plants, the immunolocalization of ASY1, ZYP1 and PCH2 showed severe defects the localisation of these proteins during prophase I (Fig.3.18). In the first place, ASY1 seemed to have difficulties with its localisation to the AEs and in its depletion from the synapsed areas. In this manner, it appears as an array of dim foci in the areas where synapsis is not present, whereas a slightly brighter and continuous signal is observed in the regions where the SC has been

able to polymerise, contrasting with its dynamics in the WT plants (Fig.3.17). In addition, the establishment of synapsis between the homologous chromosomes seems to be impaired in the *boC.pch2-1* mutant as the signal of ZYP1 does not fully extend, forming stretches of different length and aggregates (Figs.3.18-3.20). Both phenotypes are studied in more detail in sections 3.2.12 and 3.2.13. Moreover, the immunolocalization of PCH2 in the *boC.pch2-1* mutant was used as a negative control, revealing that no signal of PCH2 is present. Thus, this confirms that *boC.pch2-1* is effectively a null mutant since the predicted truncated product is unable to colocalise with ZYP1 and carry out its function.

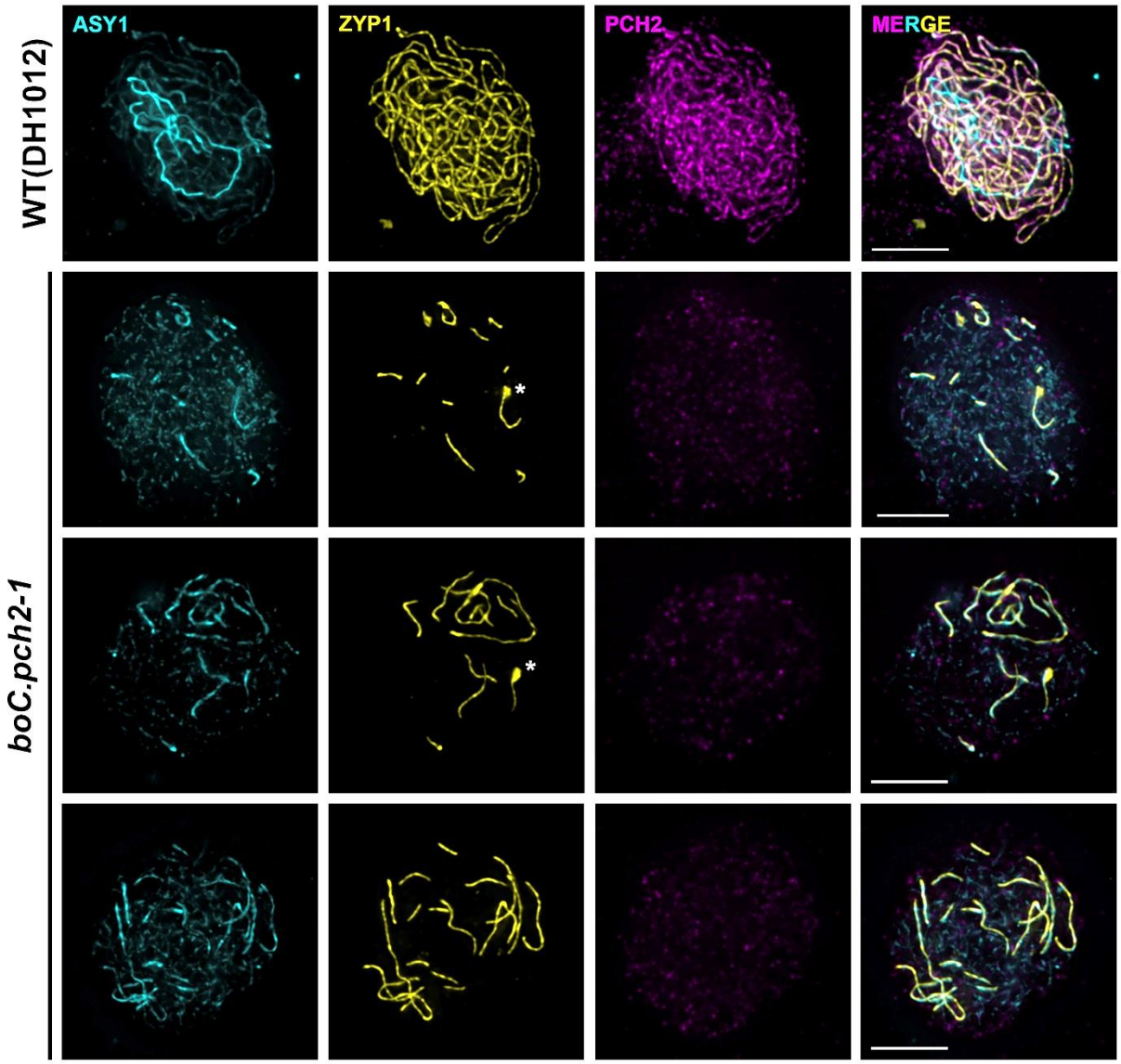


Figure 3.18. Immunolocalisation of ASY1, ZYP1 and PCH2 in prophase I of WT and *boC.pch2-1.*
* indicates the presence of ZYP1 aggregates. 5µm bars.

Interestingly, in a small subset of the *boC.pch2-1* cells analysed some ZYP1 aggregates were observed together with the short stretches of SC (Fig.3.18). Thus, to obtain a more detailed image of their structure these were analysed through Super-Resolution Structured Illumination Microscopy (SIM) (Fig.3.19). This revealed that the ZYP1 aggregates presented a highly organised stacked structure similar to the one present in the central element of the SC. These kinds of structural organisations are characteristic of SC protein aggregates named polycomplexes,

which consist of stacks of synaptonemal complexes (Fuge, 1979). The distance between the parallel lines of ZYP1 signal observed was ~150 nm. Polycomplexes have been previously observed in a number of species and mutant backgrounds (Hughes and Hawley, 2020) and most likely correspond with the structures observed.

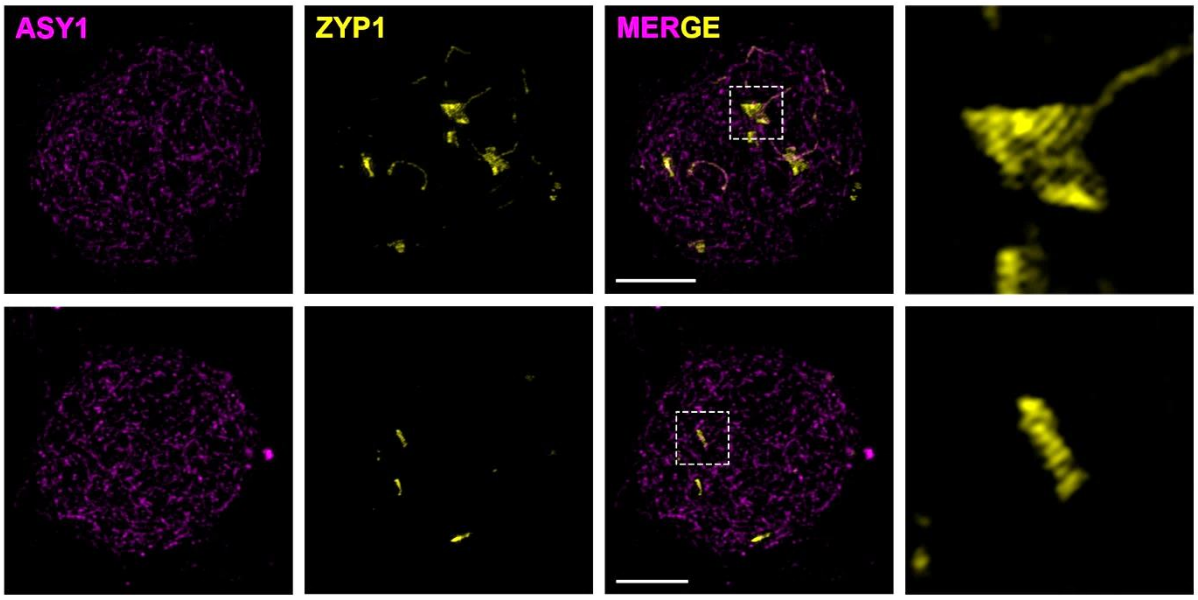


Figure 3.19. Analysis through Structure Illumination Microscopy of the polycomplex structures formed in *boC.pch2-1.* The dotted rectangles indicate the areas taken for the close-up images. 5µm bars

3.2.13. The absence of functional PCH2 in *boC.pch2-1* leads to a severe defect in the establishment of synapsis between the homologs

As for the defects in synapsis observed in the DAPI spreads of *boC.pch2-1* and the immunolocalisation of ZYP1, a more detailed study of synapsis was performed in this mutant (Figs.3.20 and 3.21). In this way, an immunolocalization of the axis-associated protein ASY1 and the TF component ZYP1 was performed, and the total SC extension was measured in the WT and *boC.pch2-1* meiocytes following the procedure described in section 2.4.4 (Figs.3.20 and 3.21.A,B, respectively). The results of this analysis revealed a great and significant reduction of the total SC length (Welch's T-test, t=30.12, df=39.65, p<0.0001) in the *boC.pch2-1* mutant line

(48.65±7.42 µm, 6.8-131.9 µm, n=25) in comparison with the WT control (395.9±8.83 µm, 342.4-500.1 µm, n=20). This represents an 87.71% decrease on average of the total SC length in the *boC.pch2-1* mutant of *B. oleracea.* Interestingly, this reduction is much higher than the one documented in *braA.pch2-9* (62%), described in section 3.2.4 and published by Cuacos *et al.* (2021), which also seems to correlate with the greater decrease of the chiasma frequency per cell observed in *boC.pch2-1* (88%).

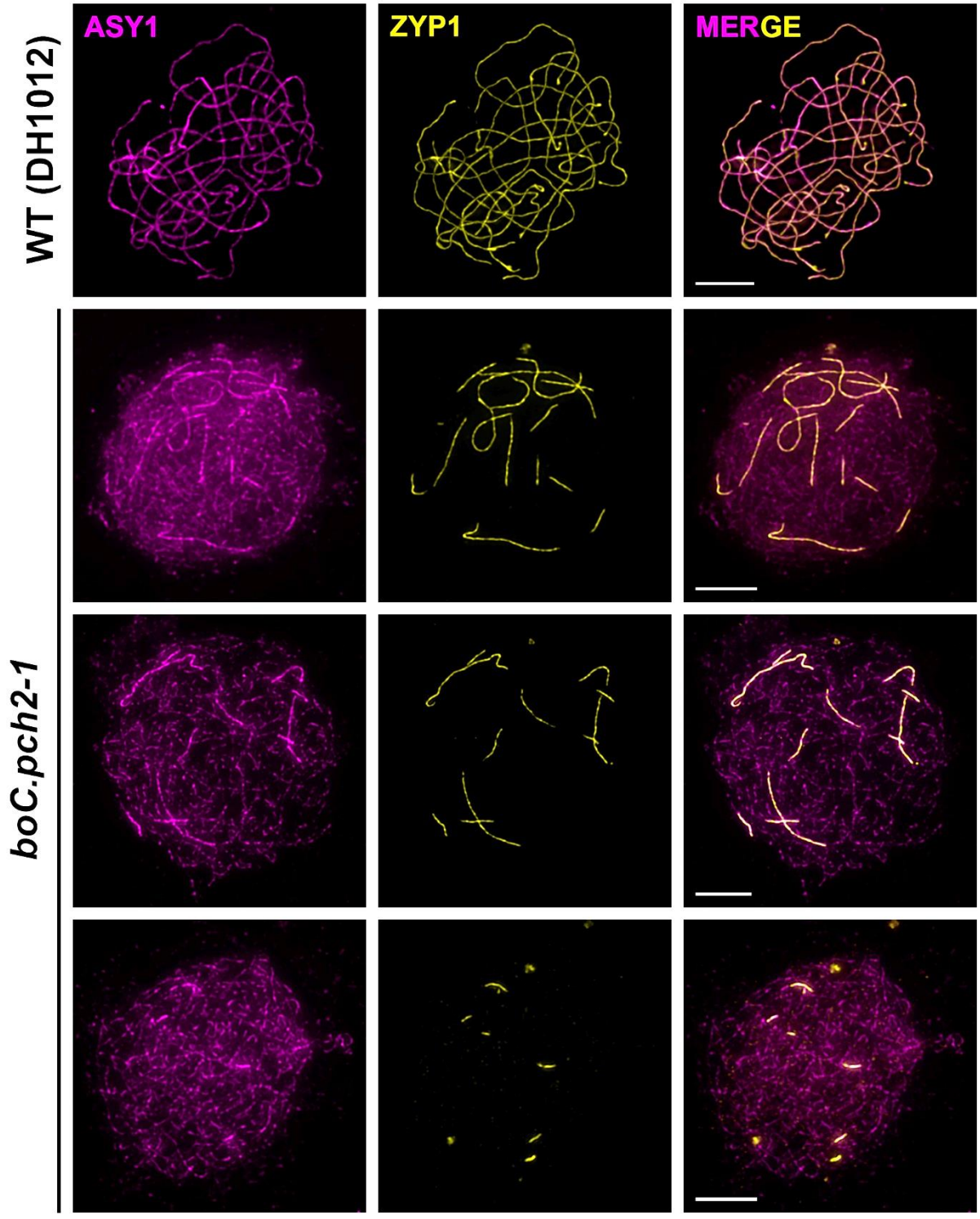


Figure 3.20. Immunolocalisation of ASY1 and ZYP1 prophase I of WT and *boC.pch2-1*. 5µm bars.

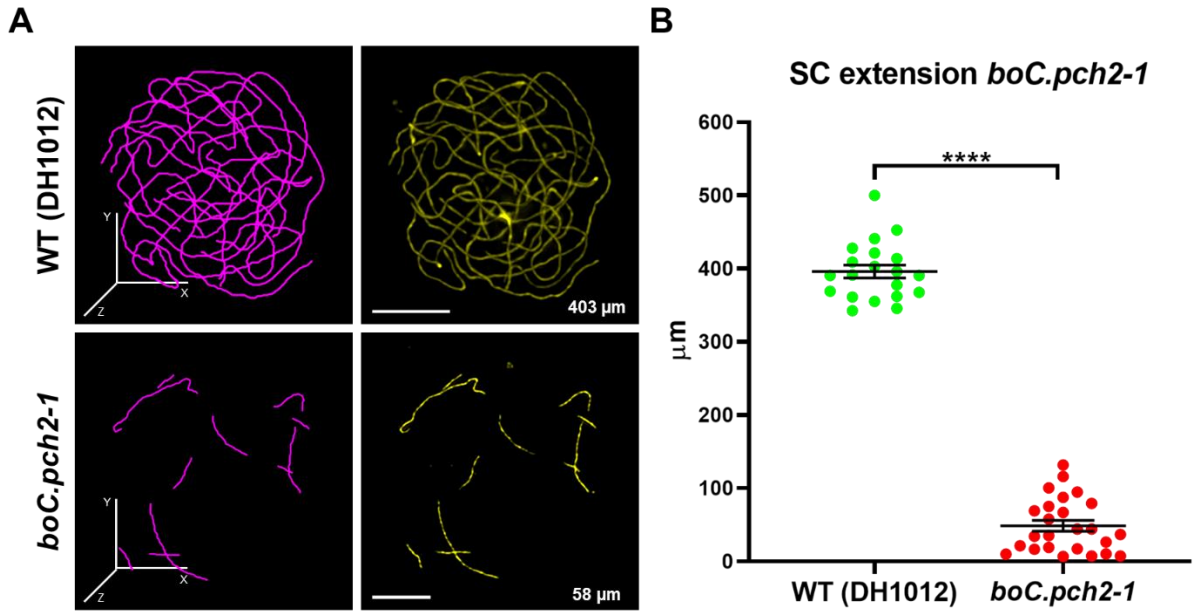


Figure 3.21. Analysis of the SC extension in *boC.pch2-1.* (A) SC tracking and reconstruction in WT and *boC.pch2-1* meiocytes using the Simple Neurite Tracer plugin of ImageJ. 5µm bars. **(B)** Scatter plot of the total SC extension in WT and *boC.pch2-1.* The bars represent the mean±S.E.M. ****p<0.0001.

3.2.14. The axis association of ASY1, its remodelling and the chromosome compaction during prophase I are abnormal in *boC.pch2-1*

Previous results of the characterisation of *pch2* mutants in *A. thaliana* and *B. rapa* suggest that PCH2 is necessary for the depletion of ASY1 from the synapsed regions, and for its loading to the AEs (Lambing *et al.*, 2015; Chao Yang *et al.*, 2020; Cuacos *et al.*, 2021). Moreover, the immunolocalisation of ASY1 in the *boC.pch2-1* plants (Fig.3.18) suggested that ASY1, apart from not being depleted from the synapsed areas, also appeared to have an abnormal association with the AEs. This was noted because the signal in the non-synapsed regions seemed dimmer and dottier than in the WT plants. Thus, to corroborate these results, a more detailed analysis of the intensity of ASY1 comparing the synapsed and non-synapsed areas was conducted in *boC.pch2-1.* In addition, the detection of the cohesin SMC3 was used as a reference since it does not suffer a PCH2 dependant remodelling process

as ASY1. In addition, ZYP1 was used as a guide to identify the synapsed regions (Fig.3.22.A).

Because the intensity of the signal was variable between cells, different parts of the same slide and between slides; the ratio of intensity between the synapsed and the non-synapsed areas per cell was calculated (S/NS, defined as "**ν**" from here onwards) as described in section 2.4.4. This allowed to normalise for those differences on intensity and to produce comparable results that could be statistically analysed. In this way: if 0< **ν** <1 then the intensity in the non-synapsed areas is higher than in the areas where the SC has polymerised; if **ν** >1 then the situation is the opposite; and if ν=1 then the intensities are the same.

The results show that in the case of ASY1, **ν** was significantly higher in the *boC.pch2-1* mutant plants than in the WT control (*boC.pch2-1:* **ν**=1.94±0.11, n=19; WT: ν= 0.33±0.03, n=14; Mann-Whitney U-test, U=0, p<0.0001; Fig.3.22.B). Therefore, the intensity of ASY1 was higher in the synapsed areas than in the non-synapsed areas in the *boC.pch2-1* mutant. This suggests that in the absence of functional BoC.PCH2, not only ASY1 is not removed from the areas where the SC has polymerised, but also seems to present difficulties on its association with the AEs. Moreover, the intensity analysis of the cohesin SMC3 revealed that the value of **ν** was significantly higher in *boC.pch2-1* than in the WT control (**ν**=2.04±0.10 and **ν**= 1.175±0.10, respectively; Mann-Whitney U-test, U=17, p<0.0001). These results point out that whereas in a WT situation the SMC3 signal has only a slight intensity increase in the synapsed areas, in *boC.pch2-1* the difference becomes more prononuced. This could suggest that the cycles of chromatin compaction during

prophase I are disrupted if PCH2 is not able to carry out its function, which has been previously mentioned by Lambing *et al.* (2015).

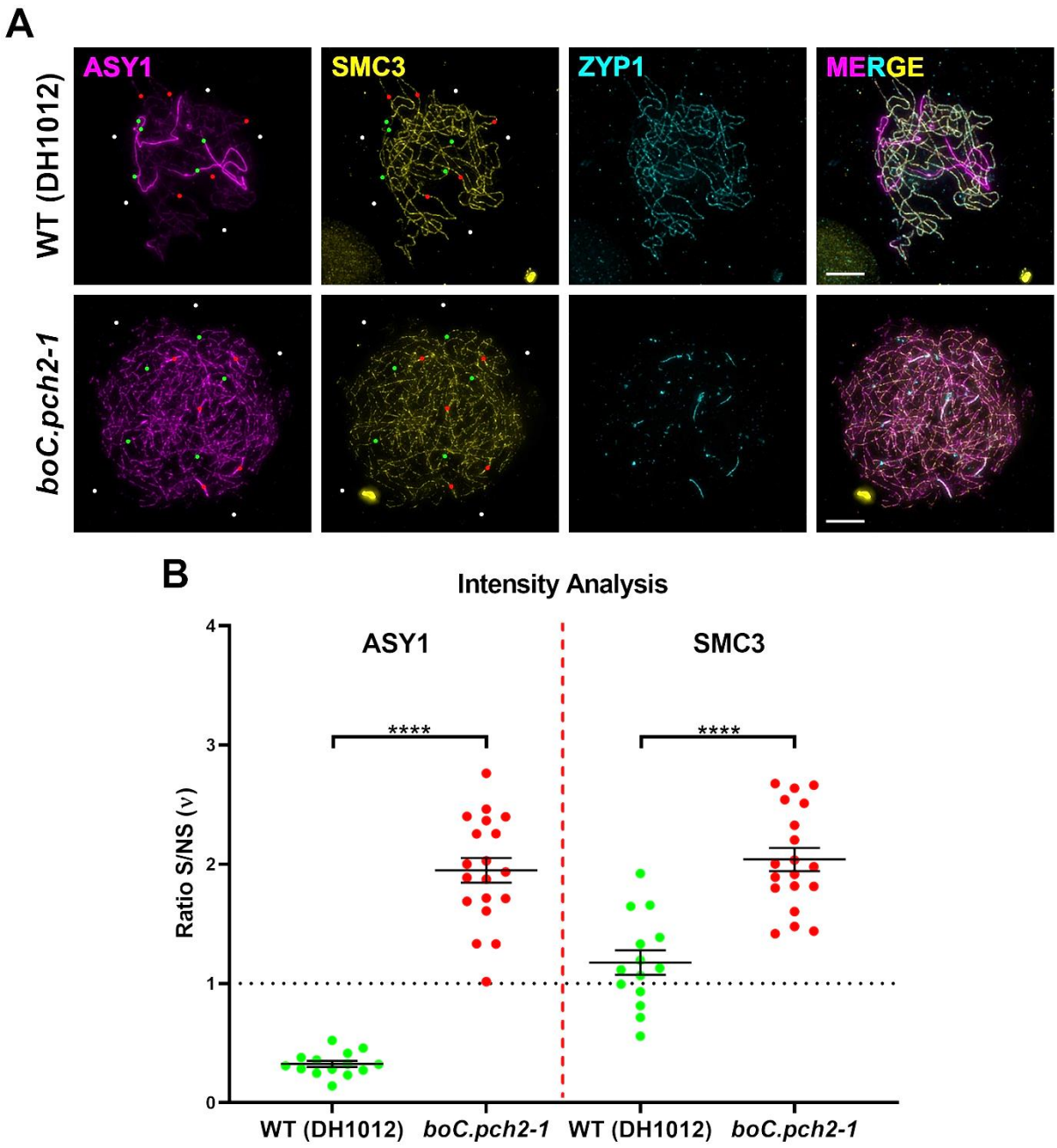


Figure 3.22. Analysis of the intensity signal of ASY1 and SMC3 in the synapsed and non-synapsed areas of prophase I meiocytes of WT and *boC.pch2-1.* (A) ASY1, SMC3, and ZYP1 immunolocalisation in WT and *boC.pch2-1.* The red dots indicate the synapsed areas. The green dots designate the non-synapsed regions, and the white dots label the background points. **(B)** Scatter plot of the intensity ratios per cell of ASY1 and SMC3 in WT and *boC.pch2-1.* The bars represent the mean±S.E.M. ****p<0.0001.

3.2.15. BoC.PCH2 is required for the timely processing of DSBs

To test whether the absence of a functional PCH2 affected DSB formation and processing in *B. oleracea*, an immunolocalisation of the phosphorylated histone variant H2AX (γH2AX) was conducted in the *boC.pch2-1* mutant line. During meiosis, this chromatin mark is deposited in the serine 139 of the histone H2AX by the checkpoint kinase complex ATM/ATR in the areas where a SPO11-catalysed DSB has been formed (Rogakou *et al.*, 1998; Abraham, 2001; Redon *et al.*, 2002; Bellani *et al.*, 2005). Thus, this allows to study DSB levels by analysing the numbers of γH2AX foci per cell. Moreover, this analysis was conducted through different stages of prophase I to analyse the effect of the *boC.pch2-1* mutantion in the dynamics of γH2AX.

In this manner, a triple immunolocalisation of γH2AX, SMC3, and ZYP1 was performed, using SMC3 as an axis marker and ZYP1 as a synapsis indicator (Fig.3.23). This allowed to distinguish between meiocytes in the stages of leptotene (fragmented SMC3 signal and no synapsis), early zygotene (continuous SMC3 signal as the AEs are completely polymerised), pachytene (full extension of the ZYP1 signal in WT), and pachytene-like (residual synapsis in *boC.pch2-1*).

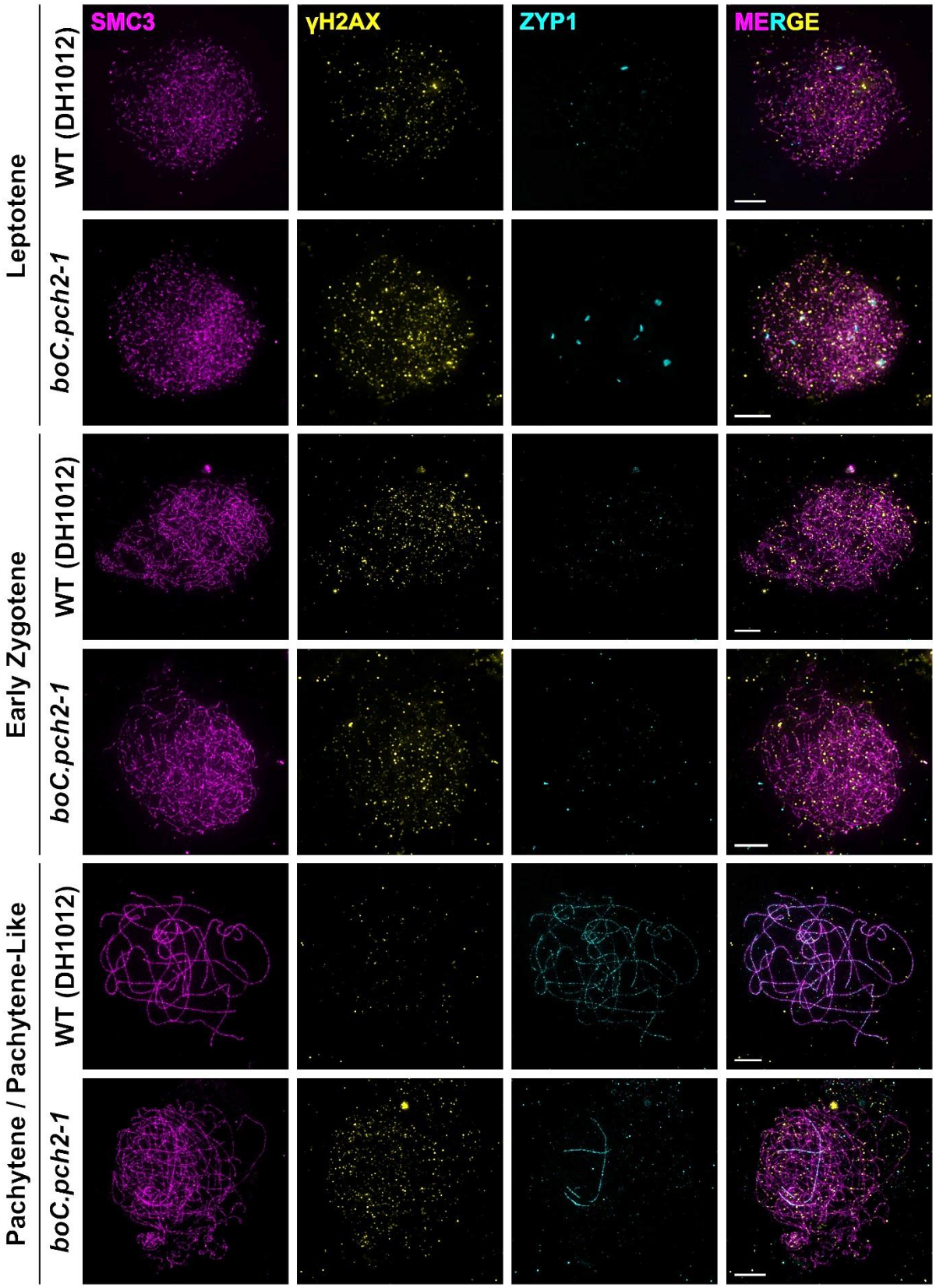


Figure 3.23. Immunolocalisation of γH2AX, SMC3, and ZYP1 in different stages of prophase I in WT and *boC.pch2-1* meiocytes. 5µm bars.

The results showed that the absence of PCH2 in *B. oleracea* led to altered dynamics in γH2AX in the late stages of prophase I (Fig.3.24). In this way, no signficant differences between *boC.pch2-1* and the WT control were found in the leptotene stage as both genotypes had similar number of γH2AX foci per cell (*boC.pch2-1*: 339.8±15.46, n=20; WT: 296.1±15.64, n=22; Welch's T-test, t=1.986, df=39.94, p=0.054). Likewise, the number of γH2AX foci per cell observed in early zygotene was similar between *boC.pch2-1* and the WT control (*boC.pch2-1*: 321.6±11.50, n=23; WT: 325.0±11.87, n=23; Welch's T-test, t=0.2078, df=43.96, p=0.84). Nevertheless, the pachytene-like stage cells of *boC.pch2-1* presented significantly higher levels of γH2AX foci per cell in comparison with the WT pachytene meiocytes (*boC.pch2-1*: 257.6±13.64, n=15; WT: 54.40±5.68, n=18; Welch's T-test, t=13.75, df=22.58, p<0.0001).

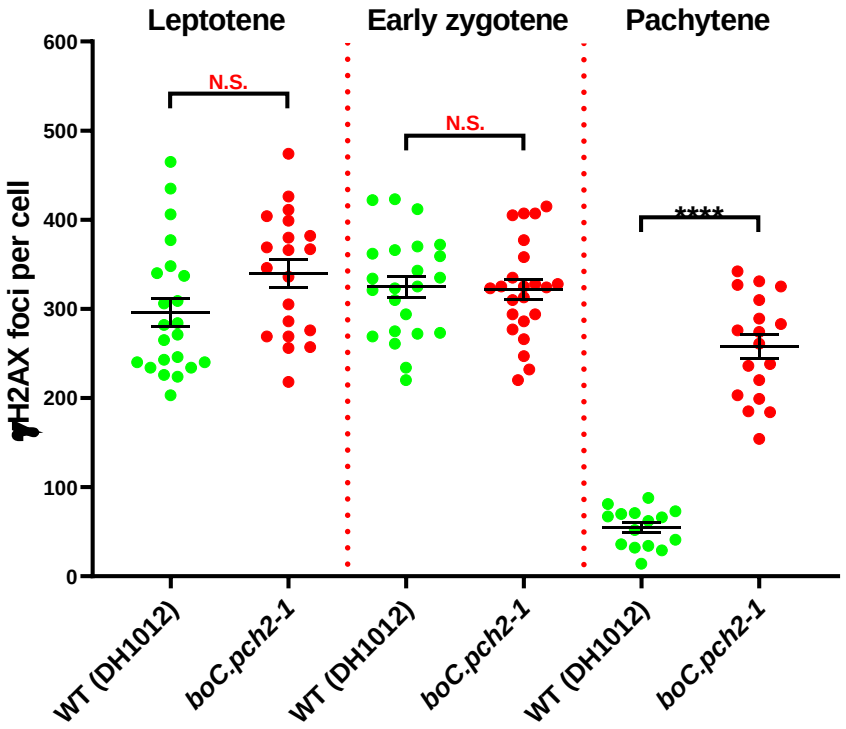


Figure 3.24. Analysis of DSB formation and processing in different stages of prophase I in WT and *boC.pch2-1.* Scatter plot of the number of γH2AX foci per cell in WT and boC.pch2-1. The bars represent the mean±S.E.M. **N.S.** Non-significant. ****p<0.0001.

This suggests that despite the number of DSBs initially formed is similar between the WT control and the *boC.pch2-1* mutant there could be a delay in DSB repair in the later.

3.2.16. Class I CO formation is severely compromised in *boC.pch2-1*

In order to study the effect of the absence of functional PCH2 on the formation of class I COs in *B. oleracea*, a more detailed analysis was conducted. This was achieved through the immunolocalization of the ZMM protein HEI10, which is widely used as Class I CO marker (Fig.3.25.A).

The statistical analysis of the number of HEI10 foci per cell revealed that the plants homozygous for the *boC.pch2-1* mutant allele presented a great and significant reduction of this variable in comparison with the WT control plants (2.40±0.21, n=37, and 12.58±0.30, n=33, respectively; Welch's T-test, t=27.66, df=58.41, p<0.0001; Fig.3.25.B). Interestingly, these values are close to the chiasma frequency observed in both genotypes indicating that Class I COs constitute the vast majority of the COs formed in WT *B. oleracea,* being the Class II greatly reduced; and that Class I CO formation is severely compromised in the *boC.pch2-1* mutant. In addition, the fact that the numbers of HEI10 foci per cell observed are slightly higher than the chiasma frequency could be anticipated as a result of the limitations inherent to the techniques used: i) underestimation of the chiasma frequency per cell in the metaphase I spreads due to the difficulties in resolving closely located chiasmata; ii) overestimation of HEI10 foci in the immunolocalisation analysis due to the presence of background signals. Nevertheless, it is clear that the disruption of PCH2 in *B. oleracea* has a major impact in CO formation as an ~80% reduction has been observed. This constitutes a much more drastic phenotype than what was previously

reported in *pch2* mutant lines of *A. thaliana* and *B. rapa,* where reductions of ~30% and ~40% were observed (Lambing *et al.*, 2015; Cuacos *et al.*, 2021, section 3.2.5).

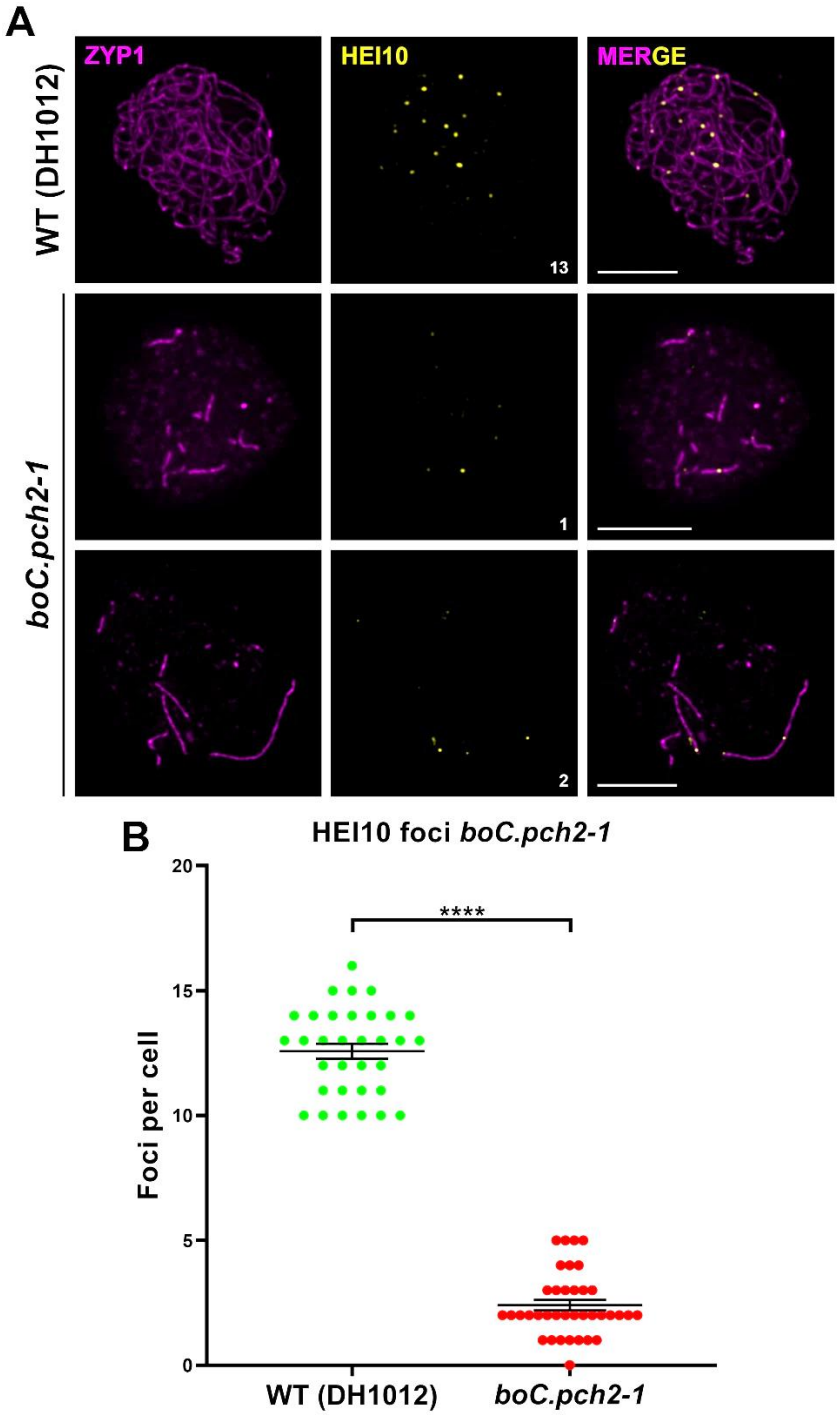


Figure 3.25. Analysis of class I CO formation in WT and *boC.pch2-1.* (A) Immunolocalisation of HEI10 and ZYP1 in WT and *boC.pch2-1* late prophase I meiocytes. The numbers indicate the HEI10 foci observed. 5µm bars. **(B)** Scatter plot of the HEI10 foci per cell in WT and *boC.pch2-1*. The bars represent the mean±S.E.M. ****p<0.0001.

Table 3.1. Summary of the cytological analysis of meiosis of *braA.pch2-9 and boC.pch2-1*

	Bivalent formation						Chiasmata (Xta) analysis			
Genotype	**% Cells w/ univalents**	**% I (pairs) /cell**	**Average I (pairs) /cell**	**Average II /cell**	**Average ring bivalents /cell**	**Average rod bivalents /cell**	**Mean Xta frequency /cell**	**% IP Xta**	**% ID Xta**	**n**
***B. rapa* (R-o-18)**	**0**	**0**	**0**	**10**	**5.44±0.22**	**4.56±0.22**	**15.79±0.27**	**9.1**	**90.9**	**34**
braA.pch2-9	91.7	37	3.98±0.26	6.02±0.26	1.87±0.17	4.14±0.20	8.13±0.39	10.6	89.4	108
braA.asy1-14	100	79	7.88±0.20	2.12±0.20	0.14±0.05	1.98±0.18	2.31±0.22	3	97	56
braA.asy1-14 braA.pch2-9	100	84	8.38±0.13	1.63±0.13	0.16±0.05	1.46±0.12	1.83±0.15	1	99	80
***B. oleracea* (DH1012)**	**16.67**	**0.02**	**0.17±0.05**	**8.83±0.05**	**2.68±0.15**	**6.15±0.16**	**11.86±0.15**	**5.62**	**94.38**	**66**
boC.pch2-1	100	76	7.57±0.14	1.43±0.14	0.08±0.03	1.36±0.13	1.48±0.15	2	98	92

3.4. Discussion

3.4.1. BraA.PCH2 and BoC.PCH2 constitute the orthologs of PCH2 in *B. rapa* and *B. oleracea*

In this chapter, two orthologs of PCH2 in the wild relatives of the crop species *B. rapa* and *B. oleracea*, previously identified by (Osman *et al.*, 2018) have been identified: *BraA.PCH2*, and *BoC.PCH2*; and their role in meiosis has been characterised through a reverse genetic approach based on the cytological analysis of meiosis in mutant lines of these genes. This has revealed that as in other organisms such PCH2 is essential for the normal development of the meiotic programme, as the plants mutant for these genes presented severe defects in meiosis at different levels. Overall, a common phenotype was found between the *braA.pch2* and the *boC.pch2* mutant lines consisting of severe defects in chromosome segregation due to a lack of CO formation, together with problems in the polymerisation of the SC between the homologs and meiotic axis remodelling. Interestingly, despite presenting a common phenotype in general lines, great differences with respect to the severity if this were found between the *braA.pch2-9* and *boC.pch2-1* mutants. In this way, the absence of functional PCH2 in *B. oleracea* seemed to have a more deleterious phenotype than in *B. rapa* and the plant model organism *A. thaliana* (Lambing *et al.*, 2015; Cuacos *et al.*, 2021), suggesting common but slightly different functions of this protein in this species with respect to the others. Moreover, it seems clear now the divergence on the role of PCH2 between monocots such as rice and dicots as *Brassica* and *Arabidopsis* since in the first one it seems to have a more upstream role as OsCRC1 is essential for the formation of DSBs and the axis association of the ASY1 ortholog

PAIR2, whereas in the others only facilitates ASY1 association with the axis and acts much later in recombination (Miao *et al.*, 2013).

In the following sections the results of the functional characterisation of the PCH2 ortholog of *B. rapa* and *B. oleracea* are examined, exploring the possible implications on the role of this protein in plant meiosis. This discussion is extended in chapter 6.

3.4.2. The defects in CO formation observed in *braA.pch2-9* and *boC.pch2-1* are due to a severe decrease in class I CO formation

As shown in sections 3.2.1-2 and 3.2.9-10, chromosome segregation was greatly impaired in *braA.pch2-9* and *boC.pch2*-1 due to defects in chiasma formation, which was reduced in both of them. Remarkably, the reduction in chiasma formation was proportionally much greater in *boC.pch2*-1 than in *braA.pch2-9* as it accounted for an ~88% reduction in the first one and a ~50% in the second one. In both cases, the defects in chiasma formation were more severe than previous reports of the *pch2* mutant of *A. thaliana*, which presented only a ~30% decrease of the chiasma frequency per cell. However, despite being a good indicator of CO formation, the scoring of the chiasma frequency per cell does not offer any information about the type of the COs observed. Thus, the formation of class I COs was investigated in both *braA.pch2-9* and *boC.pch2-1* mutants through the immunolocalization of the ZMM protein HEI10 (sections 3.2.5 and 3.2.16), which reported two main conclusions. In the first place, that the few remaining COs observed in both cases mainly belong to the Class I, which contrasts with the fact that chiasmata were randomly distributed in *braA.pch2-9* and *boC.pch2-1*, suggesting that Class I COs adopted a random behaviour in these backgrounds. And secondly, that the Class II COs are greatly diminished if not almost absent in these *Brassica* species; which is in

conflict with the fact that the *braA.msh4* mutants present a significant number of remaining COs (chapter 5; Gonzalo *et al.*, 2019). Nevertheless, this could be due to closely spaced chiasmata that cannot be distinguished in the metaphase I spreads as explained by Gonzalo *et al.* (2019).

3.4.3. SC polymerisation is greatly reduced in *braA.pch2-9* and *boC.pch2-1*, correlating with the CO levels observed

In the DAPI spreads of *the pch2* mutants of *B. rapa* and *B. oleracea* a clear absence of meiocytes reaching the pachytene stage was observed, suggesting that the absence of functional PCH2 in these species caused defects in SC polymerisation (sections 3.2.1, 3.2.9). This phenotype concurred with previous reports from the analysis of *pch2* mutants in *A. thaliana* (Lambing *et al.*, 2015). Therefore**,** SC polymerisation was examined by tracing and measuring the ZYP1 signal in late prophase I meiocytes of the *braA.pch2-9* and *boC.pch2-1* mutant lines (sections 3.2.12 and 3.2.13). As expected, a substantial decrease of the total SC length per cell was observed in these mutants, indicating that PCH2 is required in *B. rapa* and *B. oleracea* for the completion of synapsis between the homologs. Intriguingly, the reduction of the SC extension correlated with the reduction in CO formation observed in *braA.pch2-9* and *boC.pch2-1*. In this manner, a much greater decrease (~88%) was found in the *pch2* mutant of *B. oleracea*, in comparison with the one observed in the *B. rapa* mutant (~62%). In *A. thaliana* the reduction in SC length reported by Lambing *et al.* (2015) was of ~68%, similar to the one of *braA.pch2-9*. This correlation between the reduced levels of synapsis and CO formation observed in these mutants does not necessarily imply that they are directly related as ZYP1 does not seem essential for CO formation as shown in the *zyp1* mutants of *A. thaliana* and

the *zep1* mutants of rice (Higgins, Sanchez-Moran, Armstrong, Jones and F. Chris H. Franklin, 2005; Wang *et al.*, 2010; Capilla-Pérez *et al.*, 2021; France *et al.*, 2021). Moreover**,** to further test this hypothesis a correlation study was performed in *braA.pch2-9* by scoring HEI10 foci and measuring the SC length per cell in prophase I meioctes (section 3.2.6). The outcome of this analysis confirmed that no correlation was observed between these two variables as HEI10 foci appeared associated with ZYP1 strands regardless of their length. This suggests that there might not be a minimal SC length for a recombination intermediate determined to form a Class I CO to be finally resolved as such, and that since Class I COs behave randomly, the establishment of interference between them could be disrupted. Two possible complementary explanations for this can be deduced: i) since the SC appears to be necessary for the establishment of interference (Capilla-Pérez *et al.*, 2021; France *et al.*, 2021) and its formation is incomplete in these mutants, the transmission of the interference signal could be interrupted, leading to a random behaviour of the Class I COs; ii) alternatively, the areas where synapsis has occurred most likely correspond with regions where the processes of pairing and strand invasion were successful, and any recombination intermediate committed to form a Class I CO in these regions would be resolved as such. Therefore, the difference observed between *braA.pch2-9* and *boC.pch2-1* would be due to more severe difficulties to establish a more stable pairing and SEI in the later, leading to lower levels of synapsis and CO formation as both depend on these previous steps.

In addition, some ZYP1 aggregates were observed in *boC.pch2-1* that, when examined in more detail with the help of SIM super-resolution microscopy, appeared to correspond with polycomplexes (section 3.2.12). These are structures composed

of stacked SC fragments, and appear in a wide range of conditions as WT and mutant backgrounds and in abiotic stress conditions such as high temperatures (Fuge, 1979; Loidl, 1989; Morgan *et al.,* 2017; Hughes and Hawley, 2020; Ren *et al.*, 2021). The presence of polycomplexes in this mutant could be the result of excess of ZYP1 protein in the nucleoplasm of the meiocytes as the SC polymerisation is incomplete or due to defects in SC remodelling as recently reported by Ren *et al.* (2021).

3.4.4. AE remodelling and ASY1 axis-association are defective in *boC.pch2-1*

PCH2 carries out a double role during meiosis based on its ability to change the conformation of the HORMA domain protein ASY1. PCH2 achieves this by disengaging the interaction of the HORMA domain of ASY1 with its closure motif (Yang *et al.*, 2020). In this way, during the early stages of prophase I PCH2 is necessary to change the configuration of ASY1 from closed to open, facilitating its entrance to the nucleus and its association with the AEs (Yang *et al.*, 2020). By contrast, during zygotene, with the progression of the SC polymerisation, PCH2 is required for the depletion of ASY1 from the synapsed regions by breaking the interactions between ASY1 and ASY3 (Yang *et al.*, 2020).

These processes were cytologically studied in in *boC.pch2-1* where it was observed that the intensity of ASY1 was twice as high in the synapsed areas than in the non-synapsed ones, as reported by the analysis of the intensity ratio between them (section 3.2.14). This indicates that not only ASY1 is not depleted from these regions but also shows its difficulties to associate with the chromosome axis in the absence of PCH2 as otherwise the intensities would be similar between both regions. Moreover, it was also observed that ASY1 presented a more disorganised dottier

appearance in the non-synapsed areas (Figs.3.18 and 3.20). These results concur with the observations of the *braA.pch2-9* mutant from the Heckmann group (Cuacos *et al.*, 2021). A possible explanation for the fact that the signal of ASY1 appears more linear and intense in the synapsed areas could be that by chance ASY1 has been able to engage in a more stable association with the axis in these regions, thus facilitating the pairing and synapsis between the homologs. Moreover, the outcomes of this analysis further confirm the conservation of the roles of PCH2 in plant meiosis, as in *A. thaliana, B. rapa* and rice it is required for the association of the HORMA domain proteins to the AEs, and in the two first ones for its removal from the LEs of the SC (Miao *et al.*, 2013; Lambing *et al.*, 2015; Chao Yang *et al.*, 2020; Cuacos *et al.*, 2021).

Interestingly, the fact that ASY1 axis association is defective in *pch2* might be the cause of the recombination and pairing problems observed. In this way, as was reported by Sanchez-Moran *et al.* (2007), ASY1 appears to be necessary to stabilise the recombinase DMC1 *in A. thaliana*, which is responsible of establishing the IH Bias by catalysing the SEI process towards the homolog. Thus, it seems reasonable to think that an unstable DMC1 due to the improper axis loading of ASY1 in a *pch2* background might be behind the problems in CO formation and SC polymerisation. This is supported by the fact that Hop1 in yeast is necessary for the establishment of the IH Bias as IHR (CO ad NCO) is greatly reduced in the *hop1* mutants in favour of IS repair (Hollingsworth and Byers, 1989b).

In addition, the analysis of the intensity of the cohesin component SMC3 revealed that condensation might be affected in some manner in the *boC.pch2-1* mutant as a higher intensity ratio between the synapsed and non-synapsed regions was reported

in the mutant in comparison with the WT plants. This was briefly mentioned by Lambing *et al.* (2015) and as it was explained in the article it could be due to a delay in the condensation of the chromosomes.

3.4.5. DSB repair is delayed in the absence of functional PCH2

The formation and processing of DSBs was studied in the *boC.pch2-1* mutant through the immunolocalization of the DSB marker γH2AX in different stages of prophase I. This analysis revealed that, despite presenting no changes in the total levels of DSBs formed, their repair in *boC.pch2-1* was delayed in comparison with the WT control as the number of γH2AX foci per cell was much higher in the pachytene-like cells of the mutant whereas they were greatly reduced in the WT. This could be due, as we have previously pointed out, to the inability to recombine with the homologous chromosome due to de defects in ASY1 loading originated by the disruption of PCH2. Interestingly, these results concur with previous observations of the mice *trip13* mutants, where a delay in DSB repair was also found (Roig *et al.*, 2010). Nevertheless, the DSBs are always repaired in *boC.pch2-1*, possibly through IS repair or SDSA, as no chromosome fragmentation is observed in the chromosome spreads.

Chapter 4. Axis structure in *Brassica* crops: The role of the coiled-coil domain protein ASY3 in *B. rapa*

4.1. Introduction

The role of the axis-associated coiled-coil domain proteins in meiosis has been very well established across different model organisms comprising different taxa within the tree of life as it was previously explained in section 1.3.1.3.

In this manner, Ferdous *et al.* (2012) identified ASY3, an ortholog of the RED1 protein of budding yeast, in the plant model organism *A. thaliana*. AtASY3 was shown to be necessary for CO formation and the establishment of the SC between the homologous chromosomes, also participating in the formation of DSBs. Thus, being essential for the correct segregation of the homologous chromosomes and the maintenance of fertility. Moreover, it was revealed that AtASY3 was necessary for the correct association of the HORMA domain protein ASY1 to the chromosome axis. Additionally, Ferdous *et al.* (2012) demonstrated that both proteins physically interact, and that ASY1 is epistatic over ASY3 since the double mutant displayed CO formation levels similar to *atasy1* rather than to *atasy3.* The physical interaction between AtASY3 and AtASY1 was further explored by West *et al.* (2019), who showed that ASY3 interacts with the HORMA domain of ASY1 through a putative closure domain, and that ASY3 is able to self-polymerise via its C-terminal coiled-coil domain, which also interacts with the small coiled-coil domain protein AtASY4, required for the stabilisation of ASY1 and ASY3 in the AEs (Chambon *et al.*, 2018). In addition, ASY3 has been found to play a role in the diploidisation process in *A. arenosa* and *A. lyrata* as derived alleles of tetraploid populations of these plants were associated with a higher meiotic stability (Morgan *et al.*, 2020; Seear *et al.*, 2020). Therefore, given that ASY3 is a critical factor essential for CO formation and the maintenance of fertility in plants, also participating in the diploidisation process

together with ASY1, it is of outstanding interest to find and characterise orthologs of these proteins in crop species as they can potentially become a tool of great importance in breeding programmes.

Thus, the main goal of this project is to identify an ASY3 ortholog in the crop wild-relative *B. rapa* and to characterise its role in meiosis through a wide range of cytological techniques such as PMC spreads and immunolocalization of recombination and AE proteins. Moreover, given that orthologs of the axis-associated protein ASY1 and PCH2 have been recently described in *B. rapa* (see chapter 3; Cuacos *et al.*, 2021), and that their mutants showed a similar phenotype to the ones previously characterised in *A. thaliana* (Armstrong *et al.*, 2002; Lambing *et al.*, 2015), we also aim to further study the functional relations between these proteins and ASY3 in this crop species. We seek to achieve this by analysing meiosis in plants combining null alleles of *ASY1* and *PCH2* in an *ASY3* defective background, studying into more detail their putative epistatic relationships. The results obtained point out at similar roles of *BraA.ASY3* to those formerly described in *A. thaliana*, despite observing differences in terms of DSB formation and its epistatic relation with *BraA.ASY1*.

4.2. Results

4.2.1. Identification of a possible ASY3 ortholog in *B. rapa*

ASY3 is a well-known meiosis specific coiled-coil domain protein whose function has been previously characterised in the model organism *A. thaliana* (Ferdous *et al.*, 2012). Thus, as explained in section 4.1, given the critical roles in meiosis and recombination, together with its potential for plant breeding we wondered if we could find one or various orthologues of this protein in the crop species *B. rapa*, which is a

close relative of *A. thaliana* (Brassicaceae); and if the functions of these orthologs would be conserved.

In this way, the DNA sequence of *AtASY3* was used as a reference to seek for orthologues in the most recent assembly of the *B. rapa* genome (Wang *et al.*, 2011). By means of a classic homology BLAST search, one possible ASY3 orthologue was found in *B. rapa,* Bra004486, which showed an 87.3 %ID. The alignment of the amino acid sequences of both proteins in the annotation software Geneious confirmed a high similarity between them of a 74.9 %ID (Fig.4.1; section 2.5). Moreover, regarding their structural domains, both showed the characteristic coiled-coil domain located in the same region, near the C-terminal end of the protein. Also, both presented similar predicted molecular weights of 84.5 kDa (BraA.ASY3) and 87.9 kDa (AtASY3) and number of amino acid residues (BraA.ASY3=769; AtASY3=793). Consequently, once the putative ortholog of ASY3 in *B. rapa* was identified, a search for mutant lines was conducted in the RevGenUK service (John Innes Centre, Norwich, UK), which counts with a germplasm bank including a large collection of TILLING mutant lines of *B. rapa* (section 2.2.1). Two mutant lines for BraA.ASY3 were identified (ji30893-b, ji30254-a, here named as *asy3-2* and *asy3-3* for the sake of simplicity), both bearing point mutations that would generate stop codons in the first exon of *BraA.ASY3* (Fig.2.2; section 2.1.1), which subsequently would result in truncated protein products.

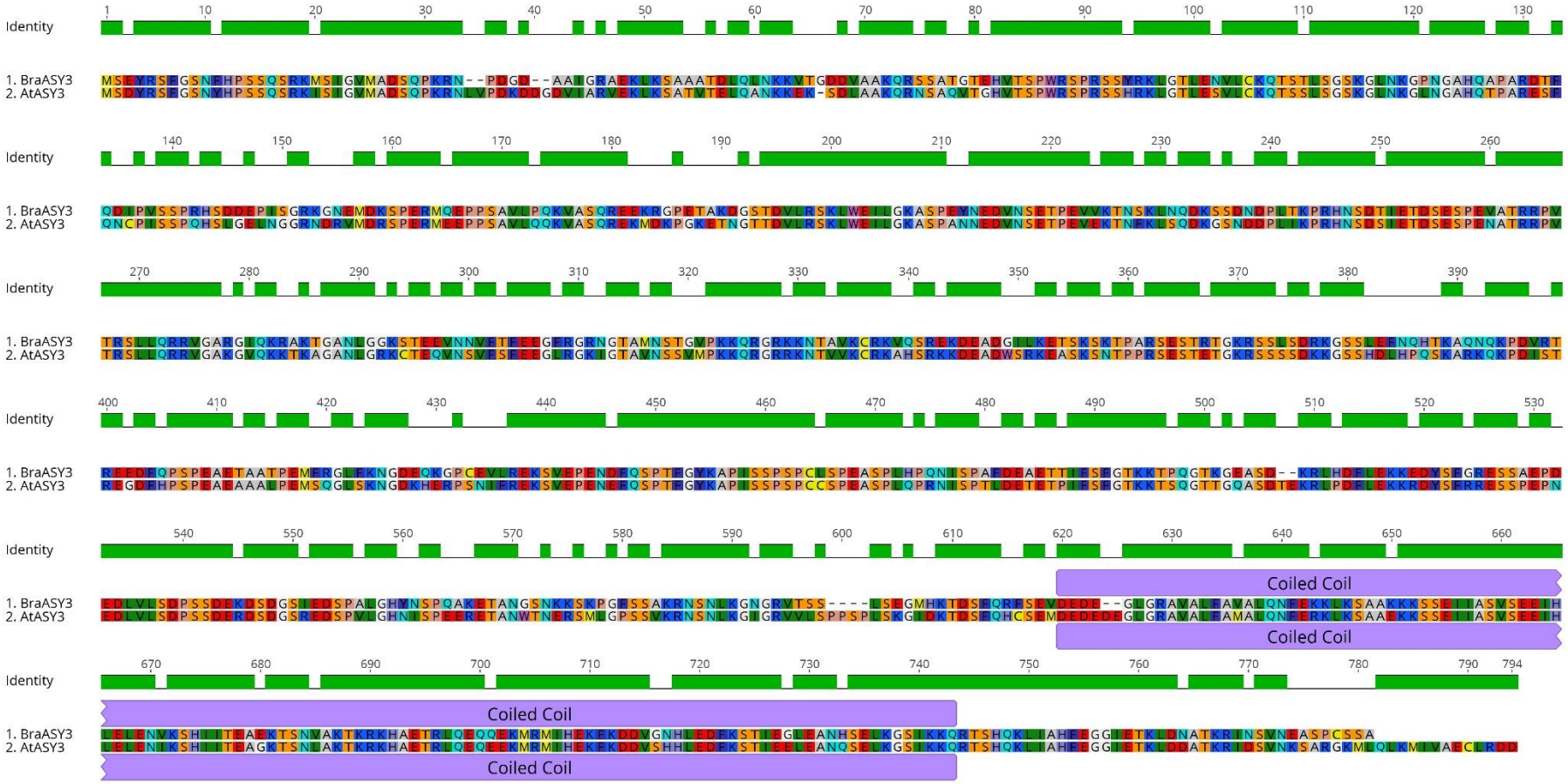


Figure 4.1. Protein sequence alignment between AtASY3 and the putative *B. rapa* ortholog BraA.ASY3 (Bra004486). This image was generated in Genious.

4.2.2. Defects in BraA.ASY3 lead to complete sterility in *B. rapa*

ASY3 is known to be a key factor for the maintenance of fertility in plants (Ferdous *et al.*, 2012). In this manner, an analysis of seed production and silique length was conducted to study the impact on fertility of the mutant alleles *asy3-2* and *asy3-3* (Figs. 4.2 and 4.3). For this study, all the possible genotypes of the mutant lines were considered: homozygous (*asy3-2*$^{-/-}$; *asy3-3*$^{-/-}$), heterozygous (*asy3-2*$^{+/-}$; *asy3-3*$^{+/-}$) and segregating WT (*asy3-2*$^{+/+}$; *asy3-3*$^{+/+}$). The data is summarised in the Table 4.1 at the end of this section.

Regarding the *asy3-2* line, the analysis of seed production showed that the plants homozygous for the mutation were completely sterile, producing siliques completely devoid of seeds. Thus, these were not included in the statistical analysis as invariably the siliques were found empty. On the other hand, significant differences were found among the other three different genotypes studied (Welch's One-Way ANOVA; W= 15.45 [2.000, 57.45]; p<0.0001). To perform a pairwise comparison between these genotypes the Dunnet's T3 *post-hoc* test was conducted, revealing a significant decrease in the number of seeds per silique in the heterozygous plants in comparison with the WT (R-o-18) and the segregating WT plants (13.57±0.92, 19.53±0.90, 20.70±1.14, respectively; p<0.0001; Fig.4.2.A). This analysis also showed that the segregating WT plants did not present significant differences with respect to the WT control plants (p=0.81). In a complementary way, the silique length was also studied as a fertility marker related to seed production (Fig.4.2.C). The statistical analysis showed significant differences between the four genotypes, in this case also including the plants homozygous for the mutation (Welch's One-Way ANOVA; W= 135.4 [3.000, 64.25]; p<0.0001). The *post-hoc* pairwise comparison (Dunnet's T3 test) between the different genotypes revealed a great and significant

decrease of the silique length in the homozygous plants in comparison with the WT (R-o-18), heterozygous and WT segregating plants (35.87±1.13, 59.63±1.14, 60.13±0.92, and 64.10±0.99 mm, respectively; $p<0.0001$). This analysis also revealed a slight but significant increase ($p<0.05$) of the seed pod length of the segregating WT plants with respect to the WT control and the heterozygous plants, which did not present any differences between them ($p=0.99$).

The same analyses were performed to assess fertility in the plants of the *asy3-3* line. In this way, seed production was studied in all genotypes, showing that, consistently with the results obtained for the *asy3-2* line, the plants homozygous for the *asy3-3* mutant variant were sterile, consistently producing completely empty seed pods, and thus, were excluded from the statistical analysis (Fig 4.2.B). On the other hand, the statistical analysis of seed production in the heterozygous, segregating WT and WT control revealed significant differences within the group (Welch's One-Way ANOVA; $W= 7.076$ [2.000, 57.76]; $p<0.01$). The outcome of the Dunnet's T3 multiple comparisons test indicated that only the segregating WT plants presented a significant decrease in seed production (14.87±0.85; $p<0.01$) when compared to the WT control, whereas seed production in the heterozygous plants was maintained in similar levels (17.13±0.99; $p=0.27$). In addition, a statistical analysis of the silique length including all four genotypes of the *asy3-3* line was performed and revealed that significant differences were present among them (Fig.4.2.D, Welch's One-Way ANOVA; $W= 369$ [3.000, 61.09]; $p<0.0001$). Subsequently, a Dunnet's T3 pairwise comparison was conducted revealing that only the plants homozygous for the mutation displayed a significant decrease of the seed pod length (28.67±0.67 mm; $p<0.0001$) in comparison with the WT control (59.63±1.14 mm), WT segregating (61.73±1.82 mm), and heterozygous plants (62.57±1.20 mm).

Altogether, these results undoubtedly indicate that the depletion of BraA.ASY3 has a severe effect in fertility as the plants bearing both mutant copies of the gene are unable to set seed, being this the same for the two lines analysed. Moreover, the decrease in seed production observed in the *asy3-2* heterozygous plants could suggest a dosage effect of BraA.ASY3. However, this possibility seems improbable as the changes in yield and seed pod length observed in the *asy3-2* and *asy3-3* WT and heterozygous plants seem more likely to be a result either of the variability present within the population or due to disparities in the growth conditions rather than a dosage effect.

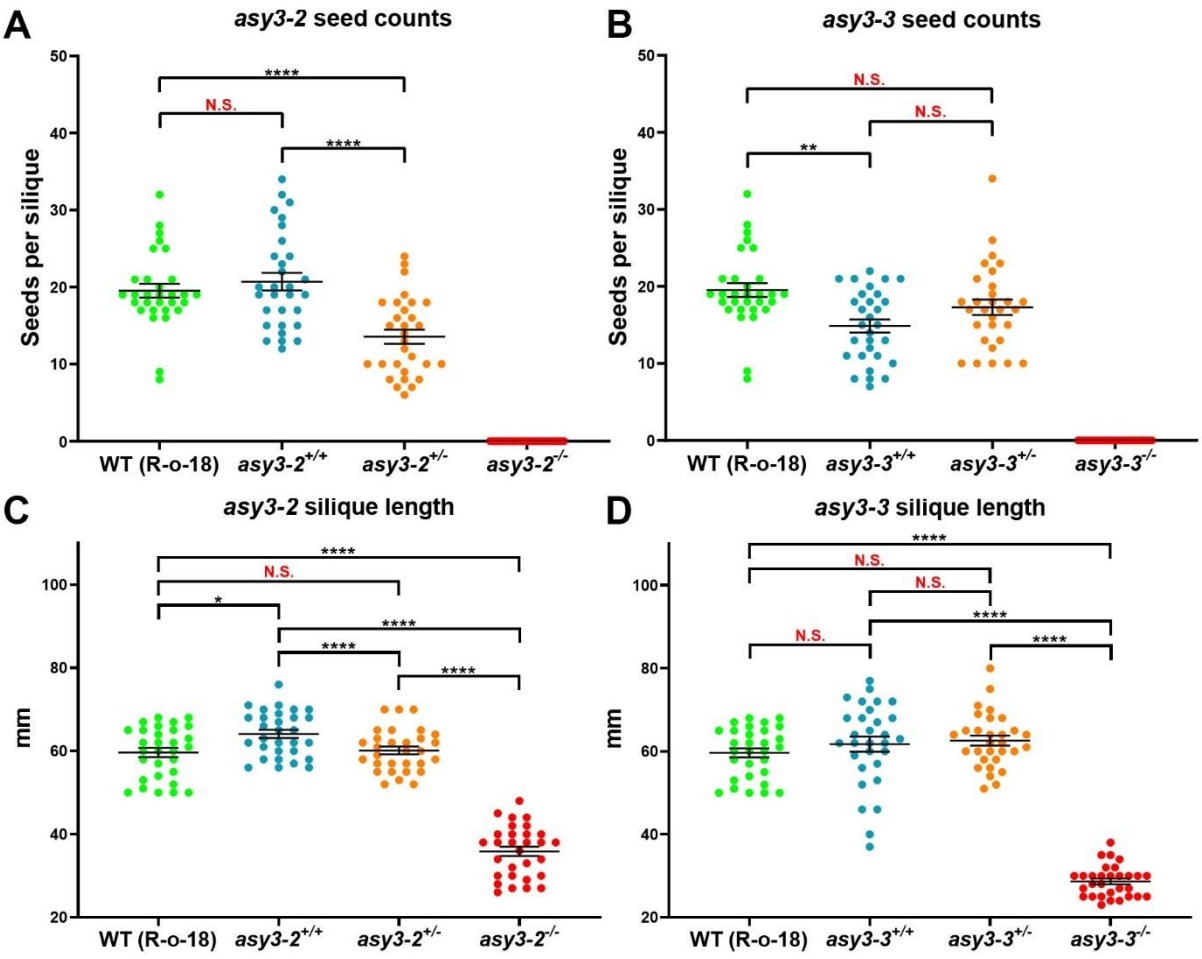


Figure 4.2. Analysis of seed production and silique length in *asy3-2* and *asy3-3*. Scatter plot of the number of seeds per silique in the different genotypes of the *asy3-2* **(A)**, and *asy3-3* **(B)** lines. Scatter plot of the silique length in the different genotypes of the *asy3-2* **(C)**, and *asy3-3* **(D)** lines. ********p<0.0001. ******p<0.01. *****p<0.05. The bars represent the mean ± S.E.M.

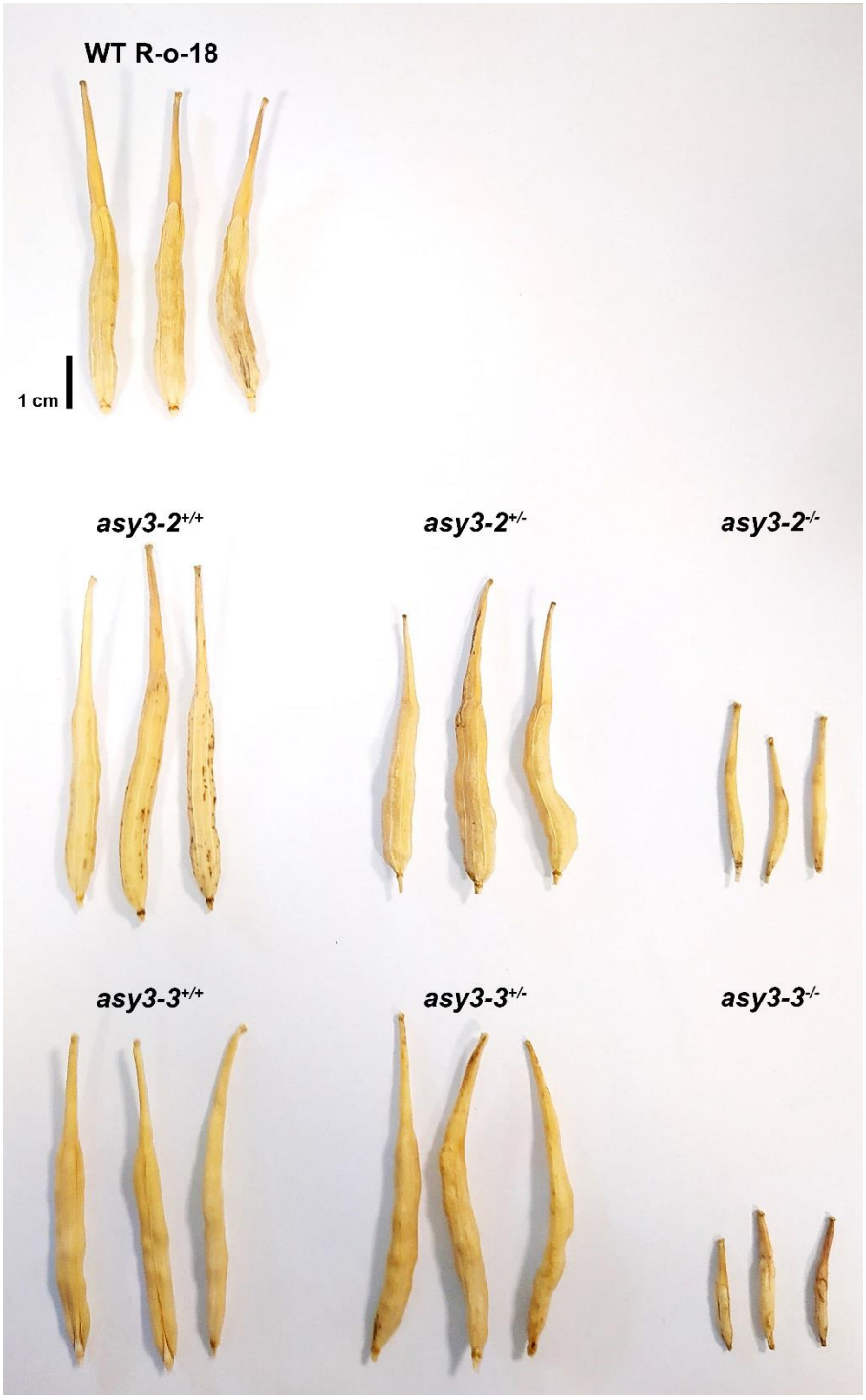


Figure 4.3. Comparison of the silique length between the WT (R-o-18) plants and the different genotypes of the *asy3-2* and *asy3-3* mutant lines. 1 cm bar.

Table 4.1. Summary of the fertility analysis data of the *braA.asy3* mutant lines

	Seeds per silique			Silique length (mm)			
Genotype	**Average ± S.E.M.**	**Min**	**Max**	**Average ± S.E.M.**	**Min**	**Max**	**n**
Wt (R-o-18)	19.53±0.90	8	32	59.63±1.14	50	68	30
asy3-2$^{-/-}$	0	0	0	35.87±1.13	26	48	30
asy3-2$^{+/-}$	13.57±0.92	6	24	60.13±0.92	52	70	30
asy3-2$^{+/+}$	20.70±1.14	12	34	64.10±0.99	56	76	30
asy3-3$^{-/-}$	0	0	0	28.67±0.67	23	38	30
asy3-3$^{+/-}$	17.13±0.99	10	34	62.57±1.20	51	80	30
asy3-3$^{+/+}$	14.87±0.85	7	15	61.73±1.82	37	77	30

4.2.3. Characterisation of the phenotype in meiosis of two different *BraA.ASY3* TILLING mutant lines shows defects in synapsis and bivalent formation.

In order to study whether the mutant lines showed a phenotype in meiosis, DAPI spreads were performed in all the three possible genotypes of the *asy3-2* and *asy3-3* mutant lines (Figs.4.2 and 4.3). In this manner, no defects were observed in the leptotene and zygotene stages of the homozygous plants of both mutant lines (Figs.4.3. and 4.4. A-B), which resembled those of a WT plant (Figs.1.1 and 3.1, sections 1.2 and 3.2.1). However, in the same way as the *BraA.PCH2* mutants (chapter 3), no complete synapsis at pachytene was found, reaching a late zygotene/pachytene-like stage (Figs.4.3.C and 4.4.C), where synapsed regions were uncommon and non-synapsed chromosomes were frequently found (Figs.4.3.D and

4.4.D). This could indicate difficulties in the polymerisation of the SC (studied in more detail in section 4.2.7). The aberrant meiotic phenotype of these mutant lines becomes more evident from diakinesis onwards when a severe deficiency in bivalent formation can be observed. This is characterised by a high proportion of univalents rather than bivalents in diakinesis and metaphase I (Figs.4.3.E,F and 4.4.E,F). In this manner, all the metaphases I observed presented univalents (*asy3-2*$^{-/-}$, n=100; *asy3-3*$^{-/-}$, n=58), and the average number of univalent pairs per cell observed was 7.8±0.16 in *asy3-2*$^{-/-}$ and 7.8±0.21 in *asy3-3*$^{-/-}$, not finding differences between both mutant alleles (Welch's T-test; t=0.6662; p=0.51). Conversely, the average number of bivalents per cell was 2.20±0.16 and 2.2±0.21, respectively. The appearance of univalents causes non-disjunction of chromosomes, that can be seen in metaphase II and telophase II (Figs.4.3.G,H and 4.4.G,H), in which instead of the classic tetrads, polyads are present due to the failures in the segregation of the homologs and the generation of unreduced nuclei. Nevertheless, and concurring with the outcomes of the fertility analysis (section 4.2.2), the asynaptic phenotype seems to be present only in the plants homozygous for each of the mutant alleles, constituting therefore monogenic recessive characters as the meiotic stages of the plants heterozygous for the mutations (Figs.4.3 and 4.4.I-O) are indistinguishable from the WT (R-o-18). Moreover, the fact that the segregating WT plants (Figs.4.3. and 4.4.P-V), of the *asy3*-2 and *asy3-3* TILLING lines, do not show any defects in meiosis, leads us to think that the possible background mutations caused by the mutagenesis process are not affecting any other meiotic gene.

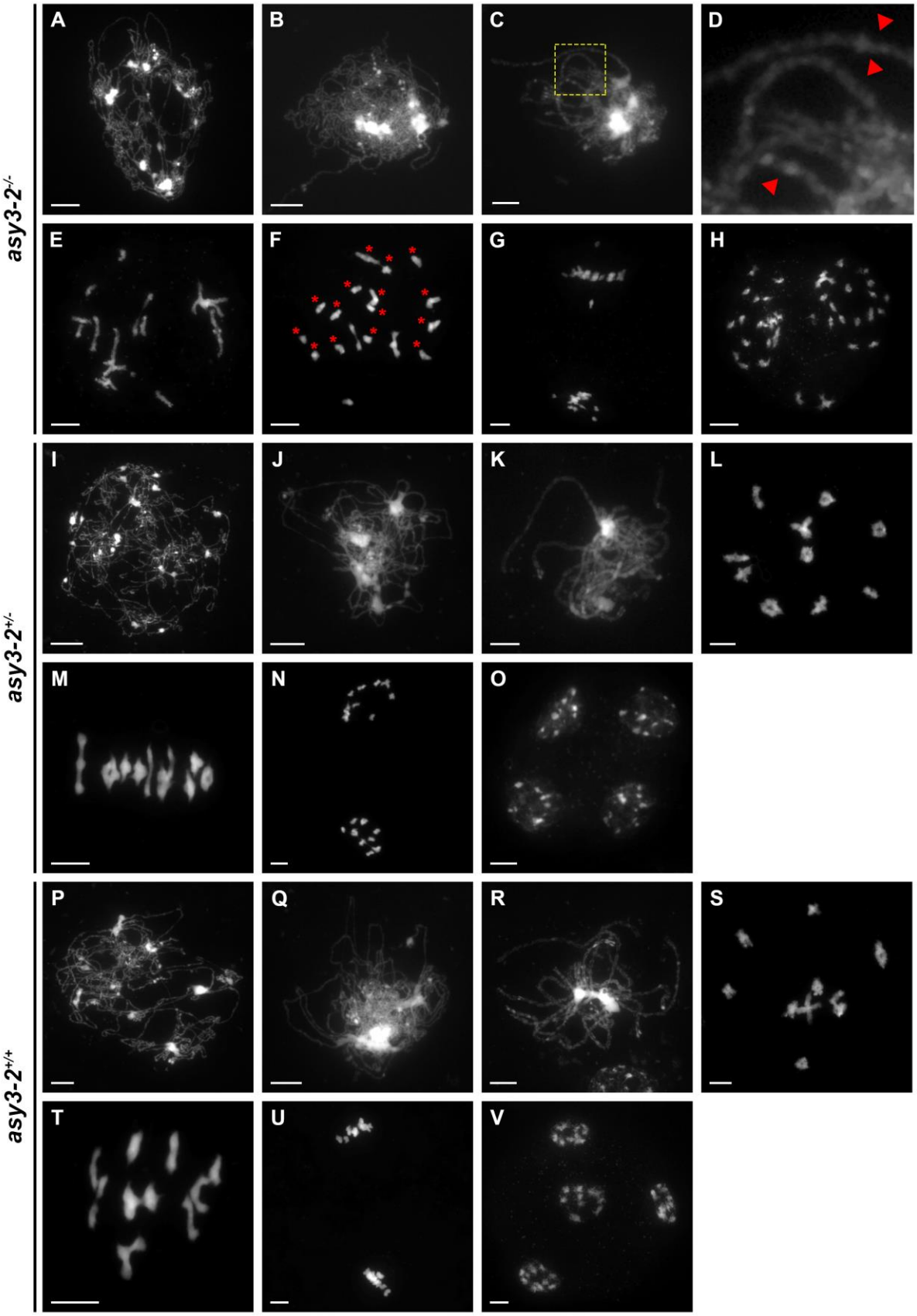


Figure 4.4. Stages of meiosis in homozygous, heterozygous, and segregating WT plants of the *asy3-2* TILLING mutant line. (A, I, P) Leptotene. **(B, J, Q)** Zygotene. **(C)** Pachytene-like**. (D)** Close-up of synapsed, white arrowheads, and non-synapsed regions, red arrowheads. **(K, S)** Pachytene. **(E, L, R)** Diakinesis. **(F, M, T)** Metaphase I, the red asterisks indicate the presence of univalents. **(G, N, U)** Metaphase II. **(H, O, V)** Telophase II/Tetrad. 5µm bars.

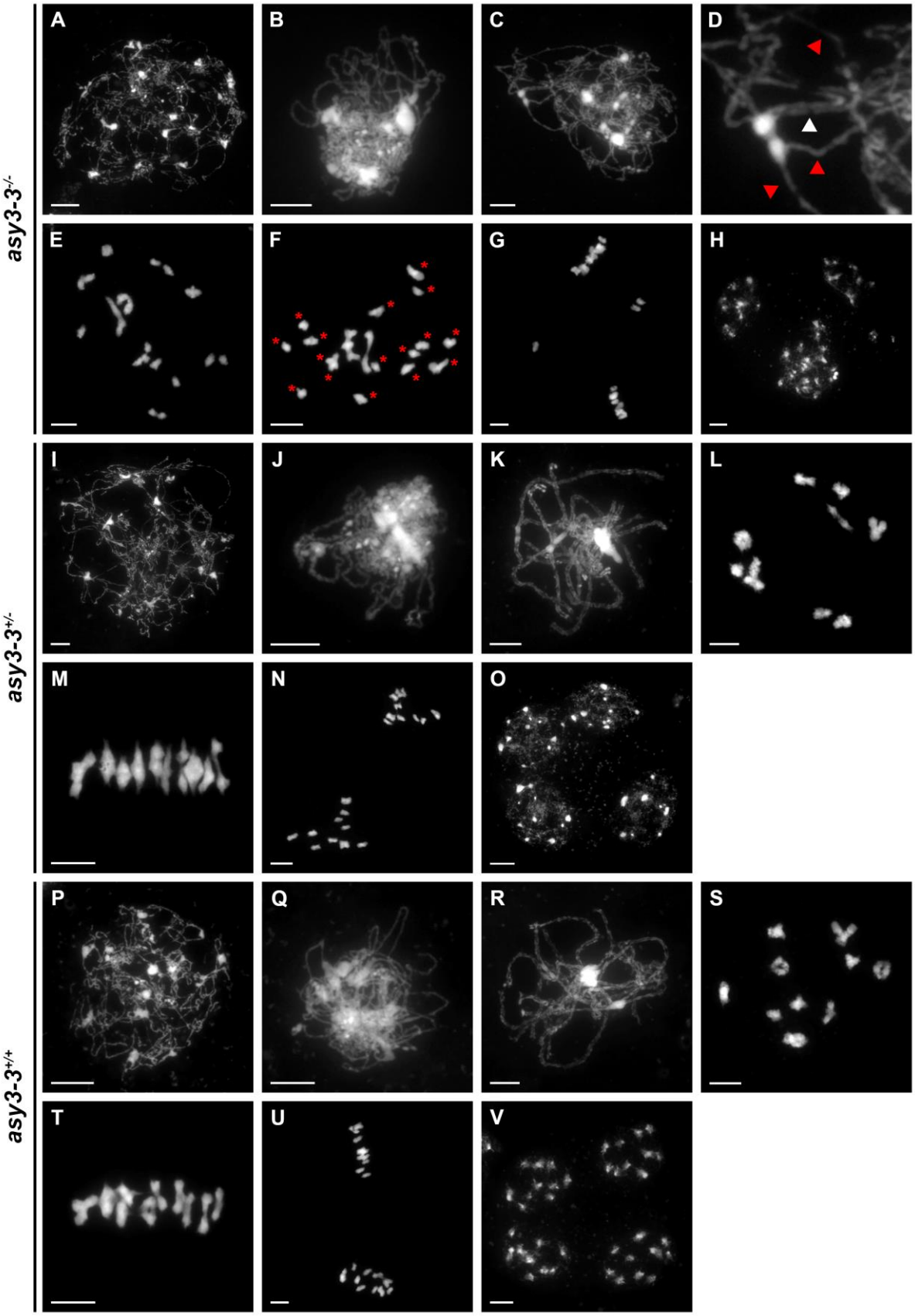


Figure 4.5. Stages of meiosis in homozygous, heterozygous, and segregating WT plants of the *asy3-3* TILLING mutant line. (A, I, P) Leptotene. **(B, J, Q)** Zygotene. **(C)** Pachytene-like**. (D)** Close-up of synapsed, white arrowheads, and non-synapsed regions, red arrowheads. **(K, S)** Pachytene. **(E, L, R)** Diakinesis. **(F, M, T)** Metaphase I, the red asterisks indicate the presence of univalents. **(G, N, U)** Metaphase II. **(H, O, V)** Telophase II/Tetrad. 5µm bars.

4.2.4. Chiasma frequency analysis in the *braA.asy3* mutant lines reveals a strong defect in recombination

After observing the major disruption in bivalent formation in the *asy3-2* and *asy3-3* homozygous lines an analysis of chiasma formation was performed as a means to measure CO formation in the context of these mutant genotypes. Thus, the chiasma frequency per cell was determined in the three possible genotypes of each line and compared it to the WT (R-o-18) control plants (Fig.4.6.A,C). The results of the cytological analysis of meiosis in the *asy3* lines are summarised in Table 4.2 at the end of the results section.

In the first place, the statistical analysis of the chiasma frequency per cell in the plants of the *asy3-2* line indicated that significant differences were present between the genotypes studied (Welch's One-Way ANOVA; W= 1486 [3.000, 106.6]; p<0.0001; Fig. 4.6.A). The subsequent *post-hoc* test for multiple comparisons (Dunnet's T3 test) showed a significant reduction in the chiasma frequency per cell in the *asy3-2* homozygous plants (2.28±0.16; n=100; p<0.0001), in comparison with the WT control (15.79±0.27; n=34), segregating WT (15.96±0.16; n=50), and heterozygous plants (15.56±0.21; n=62). By contrast, this analysis did not find significant changes in chiasma formation between the segregating WT and heterozygous plants when compared between them and to the WT control (R-o-18). In the same way, the statistical analysis of chiasma formation in the plants of the *asy3-3* line revealed significant differences among the genotypes studied (Welch's One-Way ANOVA; W= 926.7 [3.000, 92.84]; p<0.0001; Fig. 4.6.C). In accordance with the previous results from the *asy3-2* line, the outcome of the Dunnet's T3 multiple comparisons test showed that the *asy3-3* homozygous plants had a significantly lower chiasma frequency per cell (2.36±0.23; n=58; p<0.0001) with

respect to the WT control, the segregating WT (15.80±0.21; n=44), and the heterozygous plants (15.71±0.22; n=45). On the other hand, no differences were found between the other genotypes. Thus, these results show a major defect in CO formation in the *braA.asy3* plants, and also concur with the phenotype observed in the *atasy3* mutants by Ferdous *et al.* (2012).

In a complementary way, the distribution of the chiasma frequency per cell was analysed in the homozygous plants of both lines, comparing it to a predicted Poisson distribution generated with the chiasma frequency data (Fig.4.6.B,D). In this way, the chiasma frequency distributions of *asy3-2*$^{-/-}$ and *asy3-3*$^{-/-}$ did not significantly differ from a Poisson distribution (Kolmogorov-Smirnov test for cumulative distributions; $p<0.05$). Thus, as explained in section 3.3.2, the remaining COs in *braA.asy3* have a high random component that can be due to a high proportion of class II COs or to a random level of stable recombination intermediates that eventually are resolved as COs.

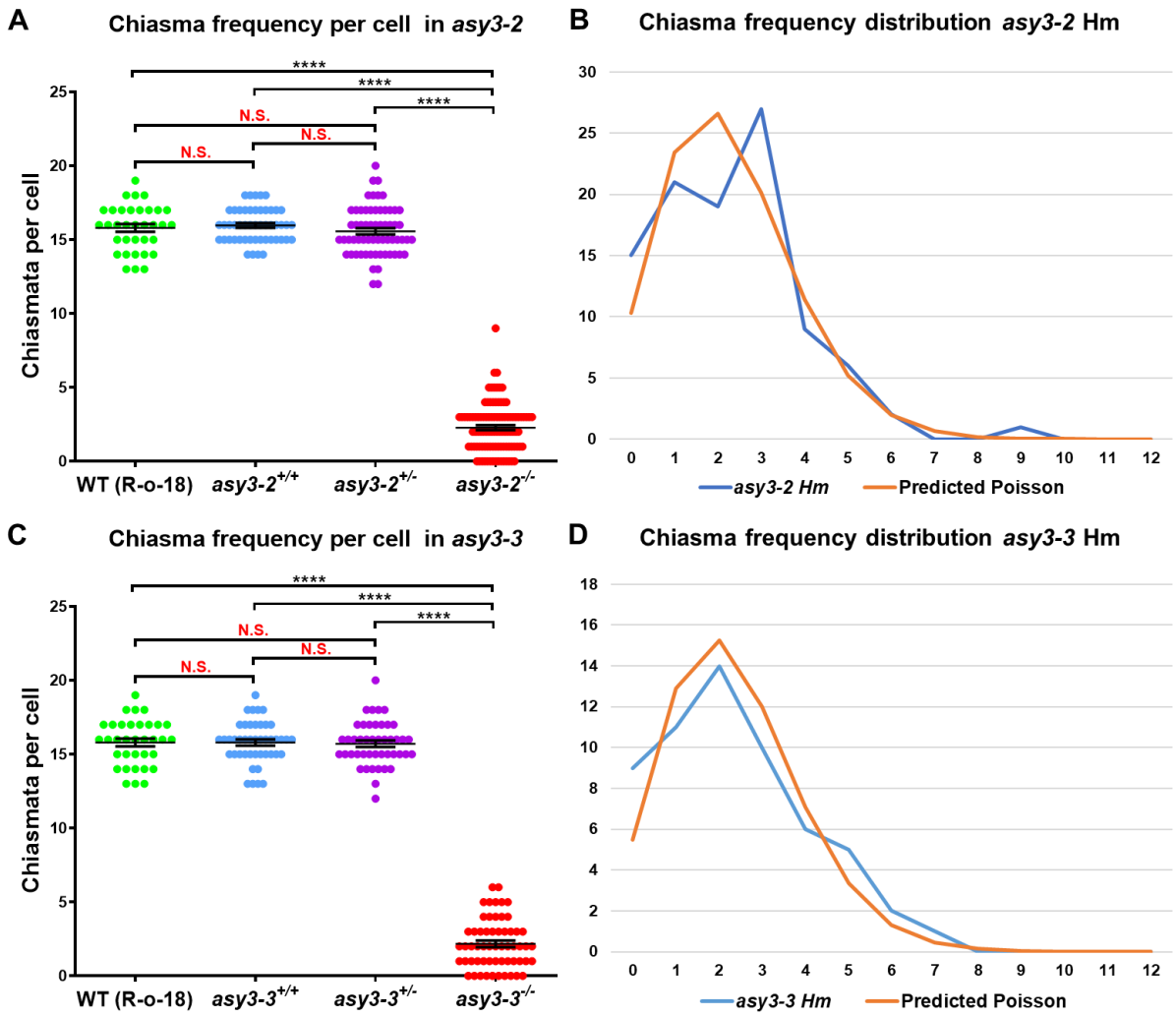


Figure 4.6. Chiasma frequency analysis and chiasma frequency distribution analysis in the *B. rapa asy3* mutants. (A & C). Scatter plots of the chiasma frequency per cell in all the genotypes studied of the *asy3-2* and *asy3-3* lines and the WT control (R-o-18). The bars represent the mean and S.D. **N.S**. Non-significant. ********p<0.0001. **(B & D).** Chiasma frequency distribution graphs of the *asy3-2* and *asy3-3* homozygous plants compared with their respective predicted Poisson distributions.

4.2.5. The *braA.asy3* mutants show a decrease in ring and rod bivalent formation despite no changes in the localisation of COs

In the same way as in the *braA.pch2-9* mutant line (section 3.1.3) to study how the reduction in CO formation was acting at the chromosomal level, the formation of ring and rod bivalents and the location of chiasmata within the chromosome arms was studied in both *braA.asy3* mutant lines, comparing it to that of the WT control plants (Fig.4.7). In this way, the results of the statistical analysis of the number of ring bivalents per cell showed that significant differences were present among the three

genotypes (Welch's One-Way ANOVA; W= 287.9 [2.000, 65.46]; p<0.0001; Fig. 4.7.C). Successively, the *post-hoc* pairwise comparison test revealed that, as expected given the low chiasma frequency per cell, ring bivalents were almost absent in *asy3*-2 and *asy3-3*, being their number significantly lower than in the WT control plants (0.08±0.03, 0.18±0.04, and 5.44±0.22 ring bivalents per cell, respectively; Dunnett's T3 multiple comparisons test; p<0.0001), also showing no significant differences between the mutant genotypes (p=0.37). A similar situation is found for the rod bivalents (Fig.4.7.B), where the Welch's One-Way ANOVA test also indicated that there were significant differences between the three genotypes (W= 48.64 [2.000, 89.11]; p<0.0001). Consequently, the result of the Dunnet's T3 multiple comparisons test revealed that the number of rod bivalents per cell was significantly reduced in the *asy3-2* and *asy3-3* homozygous plants with respect to the WT (R-o-18) plants (2.12±0.15, 2.03±0.19, and 4.56±0.22 rod bivalents per cell, respectively; p<0.0001) and that no differences were present among both mutants (p=0.97).

The localisation of the chiasmata within the chromosome arms was also studied (Fig.4.7.A), following the same criteria as in section 3.3.3. In this way, Fisher's exact test was used as a means to compare whether the distribution of COs within the chromosome arms was altered in the *asy3-2* and *asy3-3* mutant lines, comparing both with respect to the WT control and between them.

This analysis did not reveal any significant change in the proportion between interstitial and distal chiasmata in the *asy3-2* line with respect to the WT control (p>0.9999) as the proportions are similar between them (*asy3-2*: IP=8.81% vs ID=91.19%, WT: IP=9.12% vs ID=90.88%). By contrast, the *asy3-3* line, presented a significant change with respect to the WT control in the proportions between the chiasmata located in the ID and IP intervals of the chromosome arms (IP=3.65% vs

ID= 96.35%, p<0.05), showing a decrease of the proportion of IP. Nevertheless, no differences were found between the *asy3-2* and the *asy3-3* lines (p=0.08), which seems to contrast with the previous analysis. This could be due to a lack of sample size as even though 58 cells were analysed only a fraction of them presented chiasmata and could be used in this study.

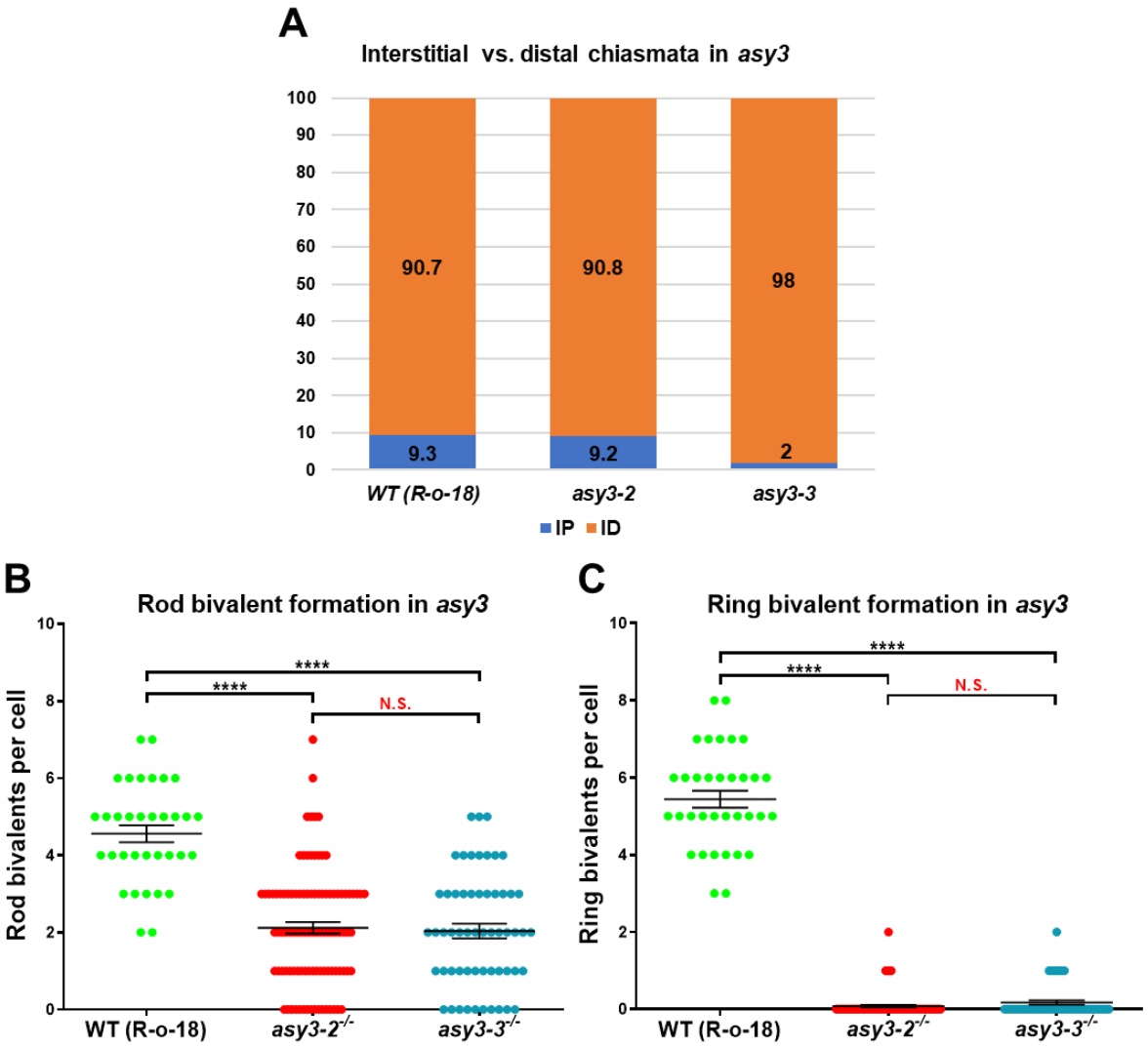


Figure 4.7. Bivalent shape and chiasma localisation analysis in *asy3-2* and *asy3-3* mutant lines. (A). Analysis of the position of COs within the chromosome arms. The numbers inside the columns represent percentages of the total. **IP.** Interstitial-Proximal interval. **ID.** Interstitial-Distal interval. **(B & C).** Scatter plots of the number of rod and ring bivalents per cell (respectively) in *asy3-2* and *asy3-3* homozygous plants. ********P<0.0001

4.2.6. The allelism test between *asy3-2* and *asy3-3* demonstrates that the *B. rapa* ortholog of ASY3 is essential for meiosis

To confirm that the asynaptic phenotype observed in *asy3*-2 and *asy3-3* was due to the mutation of ASY3 an allelism test was performed by crossing plants bearing both mutant alleles and analysing whether there was complementation of the meiotic phenotype in the heteroallelic individuals. Thus, the meiotic cell division and the mean chiasma frequency were analysed in DAPI spreads of meiocytes of the plants bearing one copy of each both mutant alleles (Figs.4.8 and 4.9). As expected, no complementation between both alleles was observed as the *asy3-2 x asy3-3* plants presented the same phenotype observed in the parental mutant lines: i) lack of the pachytene stage due to the absence of full synapsis (Fig.4.8.A-C); ii) high proportion of univalents in diakinesis and metaphase I (Fig.4.8.D,E); iii) unbalanced nuclei and polyads in metaphase II and telophase II (Fig.4.8.F,G).

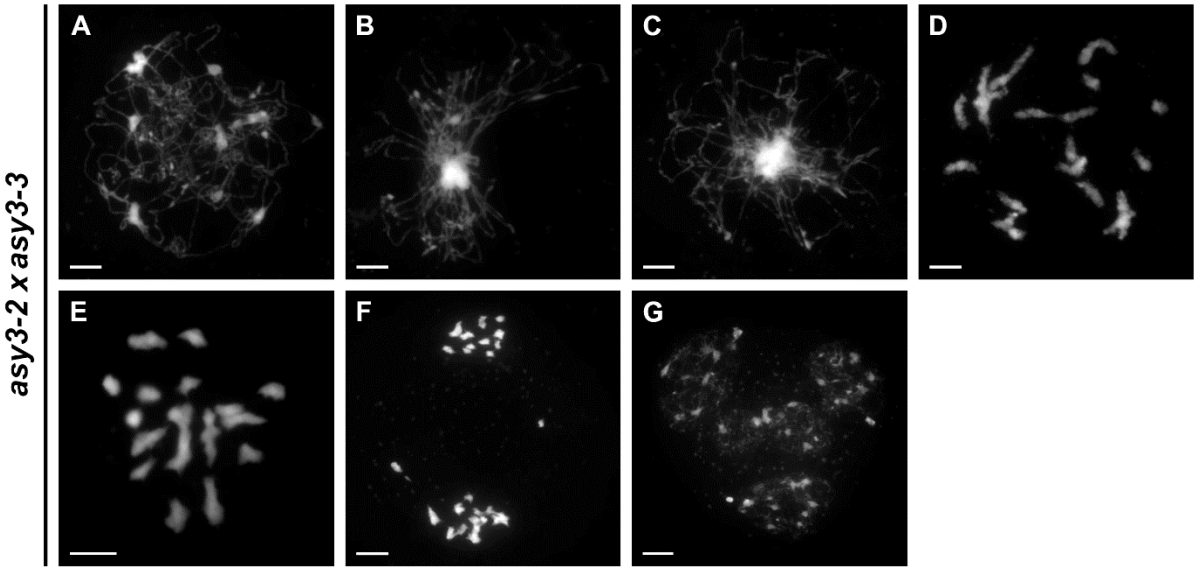


Figure 4.8. Meiotic cell division in the *asy3-2 x asy3-3* cross. (A) Leptotene. (B) Zygotene. (C) Late Zygotene. (D) Diakinesis. (E) Metaphase I. (F) Metaphase II. (G) Telophase II. 5 µm bars.

To perform the statistical analysis of the chiasma frequency the Welch's ANOVA test was used, revealing that significant differences ($W= 649.7$ [3.000,186.0]; $p<0.0001$)

were present among the genotypes analysed. Subsequently, a pairwise comparison (Dunnet's T3 test) of the *asy3-2 x asy3-3* plants with respect to the WT control and each of its mutant parental lines was conducted, also comparing the *asy3-2* and *asy3-3* plants. In this way, a significant reduction of the chiasma frequency per cell (2.40±0.25; n=47 p<0.0001) was found in the plants bearing both mutant alleles in comparison to the WT control, whereas no differences were detected with respect to the *asy3-2* (p=0.99) and *asy3-3* (p=0.93) homozygous plants, and neither between these two (p=0.99). The results of the cytological analysis of meiosis in the *asy3-2 x asy3-3* genotype are summarised in Table 4.2 at the end of the results section.

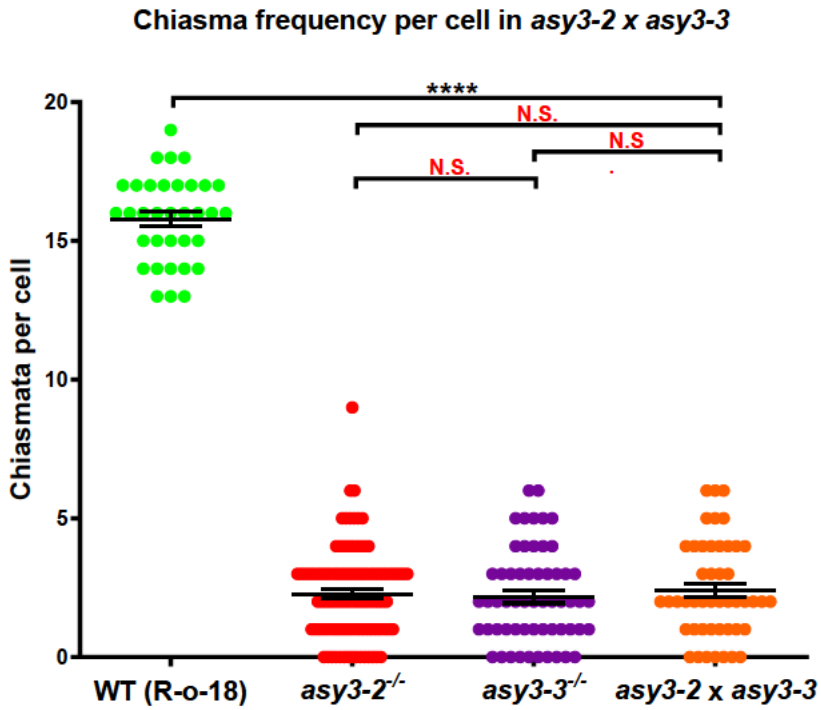


Figure 4.9. Scatter plot of the chiasmata frequency analysis of *asy3-2 x asy3-3*. The bars represent the mean and S.D. **N.S**. Non-significant. ****P<0.0001.

Therefore, these results of the cytological analysis of the allelism test of *asy3-2* and *asy3-3* demonstrate that both alleles constitute mutant variants (loss of function) of the same gene, and that the phenotype observed in meiosis is due to the disruption of *BraA.ASY3*.

4.2.7. ASY3 is essential for the correct formation of the meiotic chromosome axis and the establishment of synapsis in *B. rapa*

Given that the cytological analysis through spreading of PMCs in the *braA.asy3* mutant lines revealed an asynaptic phenotype consisting of a total absence of full pachytenes during prophase I and defects in CO formation, the structure of the AEs and the formation of the SC was studied in more detail in these mutants. In this way, immunolocalisation analyses of the axis-associated proteins ASY1 and ASY3, together with the SC TF protein ZYP1 were performed in the *asy3-2* mutant line (taken as a reference from here onwards).

In the first place, an analysis of the distribution of these three proteins through different stages of prophase I was carried out in the WT (R-o-18) plants (Fig.4.10). This analysis showed that during the leptotene stage, synchronously with the formation of the meiotic chromosome axis, ASY1 and ASY3 start to become associated with the AEs, appearing as a dense cloud of foci and short stretches as the AEs linearise. On the other hand, ZYP1 forms a series of bright foci variable in number prior to the onset of the SC polymerisation in early zygotene. As meiosis advances towards the zygotene stage ASY1 and ASY3 emerge as a linear signal once the AEs are fully formed, here some differences in the distribution of these proteins start to become visible. In this way, whereas the signal of ASY3 appears as a continuous line following the chromosome axes, ASY1 loses its intensity in the areas where the polymerisation of the SC, shown by ZYP1, is starting to take place. This reduction in the intensity of the ASY1 signal in the synapsed regions becomes clearer with the advance of the polymerisation of ZYP1 in the late zygotene stage. As previously explained in section 1.3.1.4 this is the result of the remodelling process of the meiotic chromosome axes conducted by the AAA+ ATPase PCH2 concomitant

with the formation of the SC. Finally, during the late pachytene stage the signal of ZYP1 completely colocalises with that of ASY3 and a much dimmer labelling of ASY1 as the homologous chromosomes are fully synapsed and the formation of the SC is completed. It is worth to mention that in some regions the signal of ASY1 appears slightly brighter, this phenomenon has been recently studied with greater detail in *A. thaliana* (Lambing *et al.*, 2020) where it was shown that ASY1 tends to be enriched towards the centromeric regions together with the cohesin REC8.

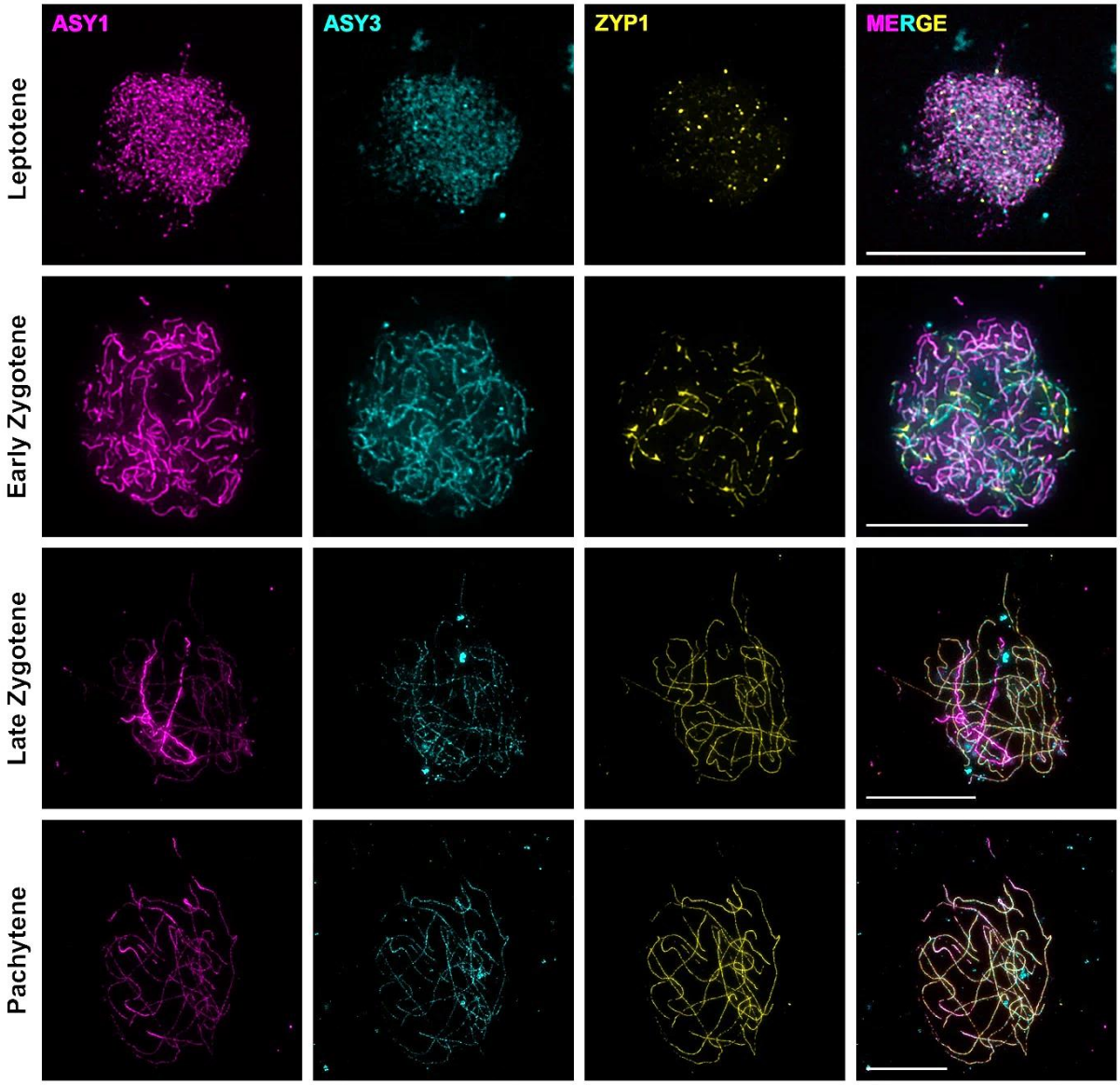


Figure 4.10. Triple immunolocalisation of ASY1 (magenta), ASY3 (cyan) and ZYP1 (yellow) through different stages of prophase I in WT (R-o-18) plants. 5 µm bars.

As a negative control, an immunolocalisation of the ASY3 protein was conducted in prophase I meiocytes of the *asy3-2* mutant line (Fig.4.11). The results showed that the antibody failed to recognise any trace of the ASY3 protein in the meiocytes of the *asy3-2* plants, demonstrating that the truncated version of the protein fails to localise to the meiotic chromosome axes.

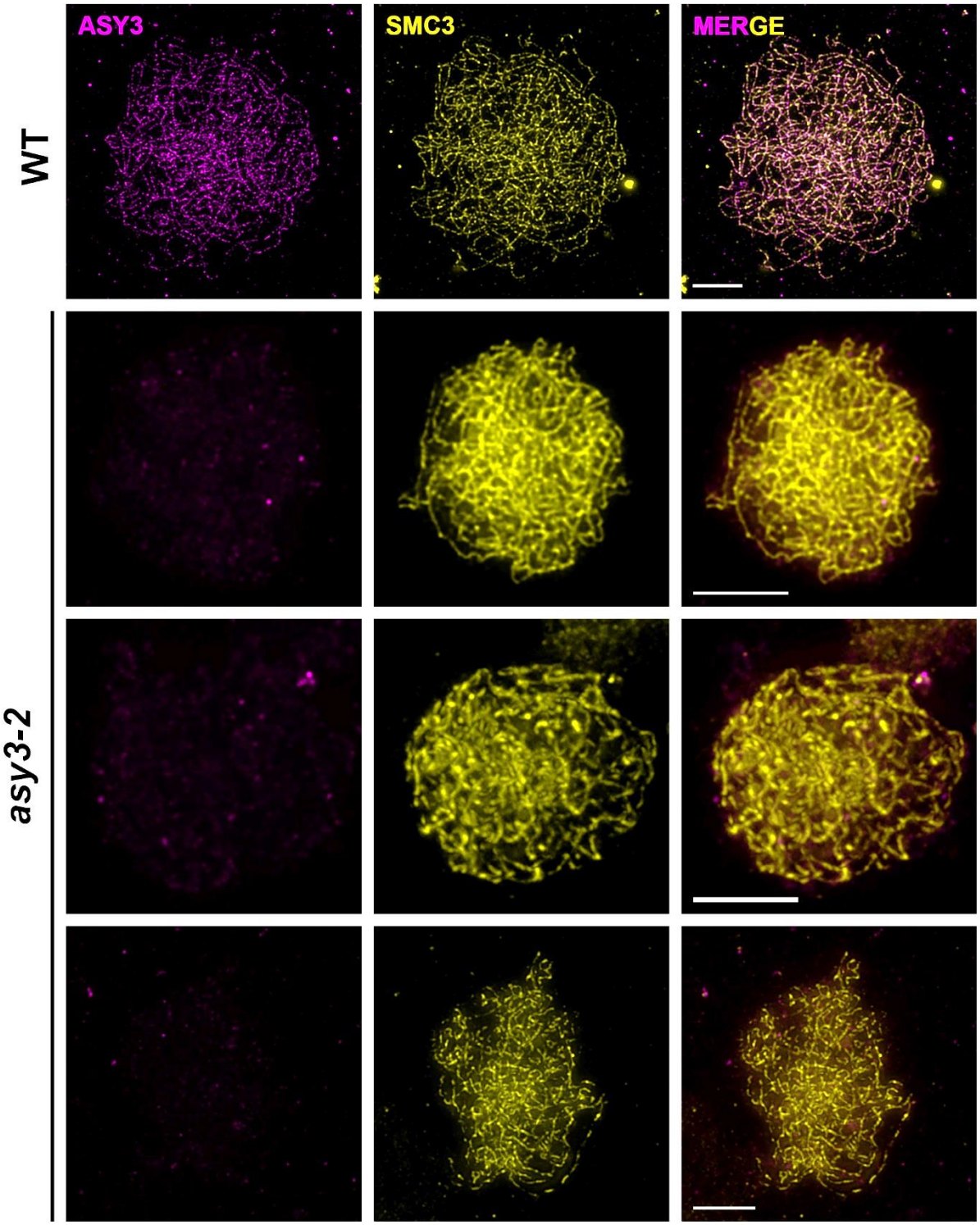


Figure 4.11. ASY3 immunolocalisation (magenta) in prophase I meiocytes of the *asy3-2* line. The cohesin SMC3 was used as a chromosome axis marker. 5 µm bars.

Since ASY3 has previously been described in *A. thaliana* as necessary for the correct association of ASY1 to the AEs during meiosis (Ferdous *et al.*, 2012), a double immunolocalisation of ASY1 and the cohesin SMC3 was performed in the WT control and *asy3-2* prophase I PMCs (Fig.4.12). In agreement with prior results, ASY3 seems to be also essential for the stable association of ASY1 to the meiotic chromosome axis of *B. rapa*, as in the meiocytes of the *asy3-2* line ASY1 appears as either a series of foci and short stretches without a clear organisation or as a “fuzzy” signal associated with the chromatin. These findings concur with the previous observations conducted in the *asy3* mutants of *A. thaliana*, where ASY1 was found as foci associated to the chromatin rather than as a linear signal (Ferdous et al., 2012).

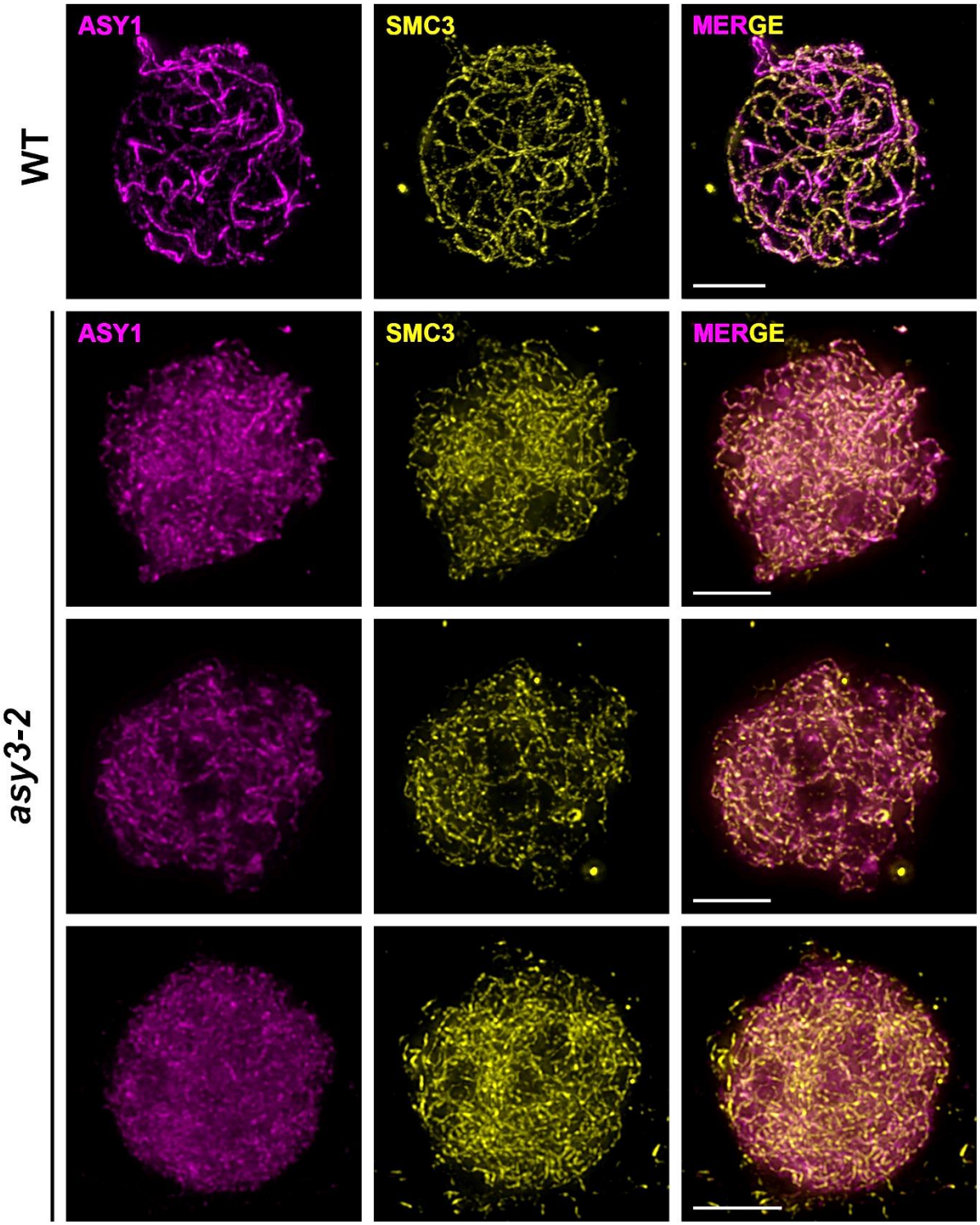


Figure 4.12. Double immunolocalisation of ASY1 (magenta) and SMC3 (yellow) in prophase I PMCs of *asy3-2* and the WT (R-o-18) control. 5 µm bars.

To study in more detail the asynaptic phenotype of the *asy3-2* mutant reported in section 4.2.2, a double immunolocalisation of the SC TF protein ZYP1 together with the SMC3 cohesin was carried out in *asy3-2* meiocytes (Fig. 4.13). As expected, the polymerisation of the SC is severely compromised as shown by ZYP1 appearing as foci and short stretches rather than as a continuous signal indicating the completion of synapsis as observed in the WT cells. Thus, ASY3 seems essential for the establishment of synapsis between the homologous chromosomes in *B. rapa.*

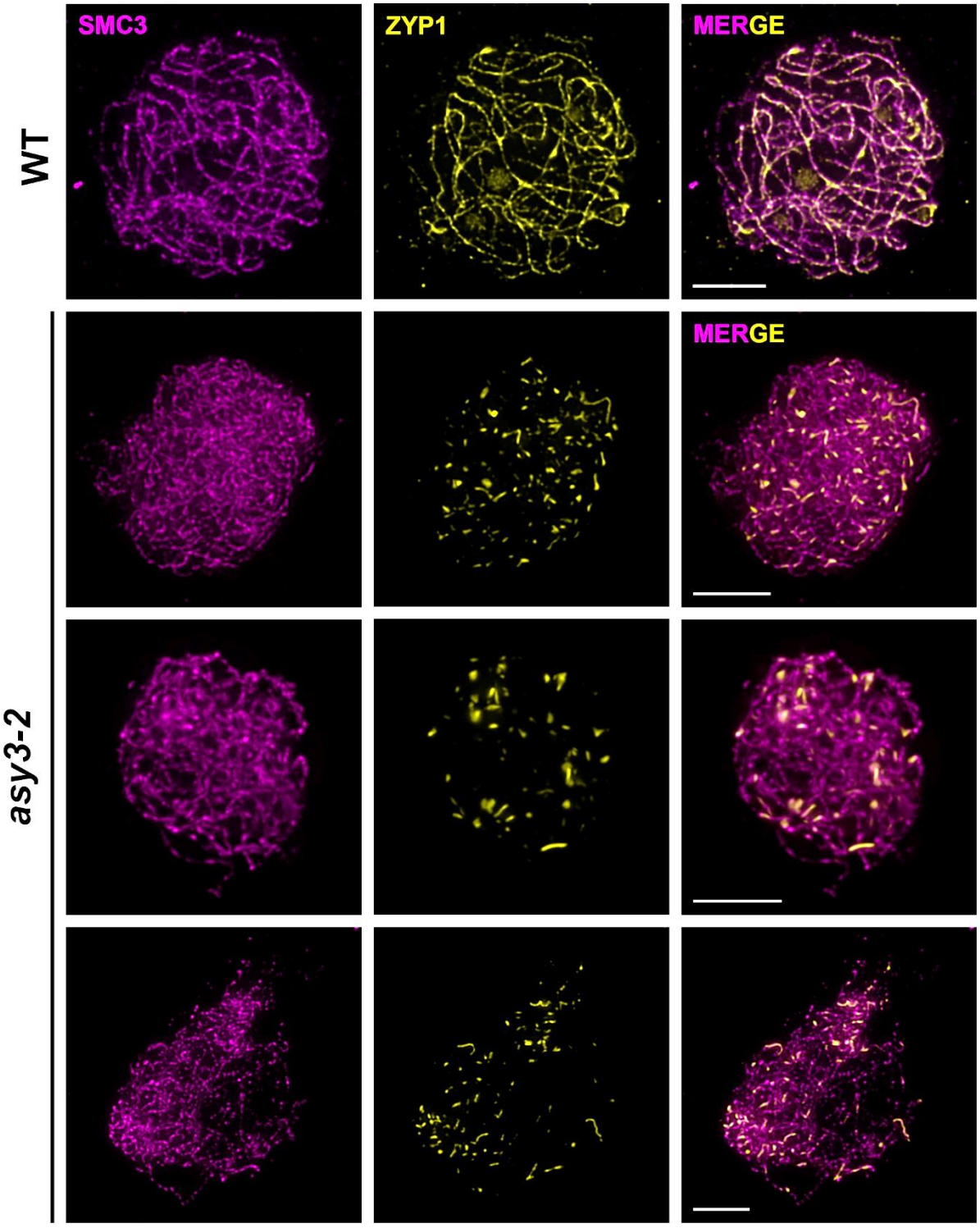


Figure 4.13. Immunolocalisation of SMC3 (magenta) and ZYP1 (yellow) in prophase I meiocytes of *asy3-2* and the WT control (R-o-18). 5 µm bars.

4.2.8. DSB processing is delayed in *braA.asy3*

Given that the formation of DSBs occurs in the context of the AEs according to the "tethered-loop" model (section 1.2.1.2) and that in *A. thaliana* it has been observed that the absence of ASY3 results in a 30% decrease in the formation of DSBs (Ferdous et al., 2012), the formation of these early recombination intermediates was studied in the *B. rapa asy3-2* mutant line. This analysis was preformed through the immunolocalization of the phosphorylation of the H2AX histone variant (γH2AX) as this is a commonly used DSB marker (section 3.2.15)

In this way, to conduct this analysis a triple immunolocalization of γH2AX together with the cohesin SMC3 (used as an axis marker) and the SC component ZYP1 (employed as a synapsis indicator) was carried out. This allowed to distinguish between meiocytes in the leptotene stage, when the AEs are still not completely polymerised, giving a dottier SMC3 signal, and PMCs in the very early stages of zygotene, when synapsis still has not taken place (no ZYP1 stretches) and the AEs are completely polymerised (linear signal of SMC3). Thus, the dynamics of DSB formation and processing could be analysed in more detail in the *asy3-2* mutant plants. It is worth mentioning that this comparative could not be done in the pachytene stage due to the inability to cytologically distinguish between *asy3* meiocytes in the zygotene stage and the later pachytene-like stage as a result of the complete absence of synapsis, also limiting the resolution of our analysis.

To statistically analyse the outcome of the γH2AX foci scoring, a One-Way Welch's ANOVA test was performed to find differences between the two genotypes tested for the two stages analysed, finding significant changes in the number of γH2AX foci among them ($W=5.444$ [3.000, 45.56]; $p<0.01$). The Dunnet's T3 multiple comparison's test was used to seek for differences between the WT and the *asy3-2*

mutant within the different stages and to compare between the two stages of the same genotype. This analysis revealed that there was a significant increase in the number of γH2AX foci per cell in the *asy3-2* meiocytes during the zygotene stage (226.3±10.33; n=28) with respect to the WT meiocytes in the same stage (182.5±11.72; n=20; $p<0.05$) and the *asy3-2* leptotene PMCs (168.7±12.99; n=18; $p<0.01$). By contrast, no significant changes were detected between the WT and *asy3-2* meiocytes in the leptotene stage ($p=0.96$) and the WT leptotene (177.8±10.27; n=25) cells with respect to its own zygotene PMCs ($p=0.99$).

Thus, it seems that there is a higher number of DSBs in the *asy3-2* early zygotene meiocytes, which could be explained as a result of delays in the processing of the DSBs due to the problems in their repair using the homologous chromosome as a template. Nonetheless, these are eventually repaired, possibly with the sister chromatid or through the SDSA pathway, as no chromosome fragmentation is observed in the DAPI spreads.

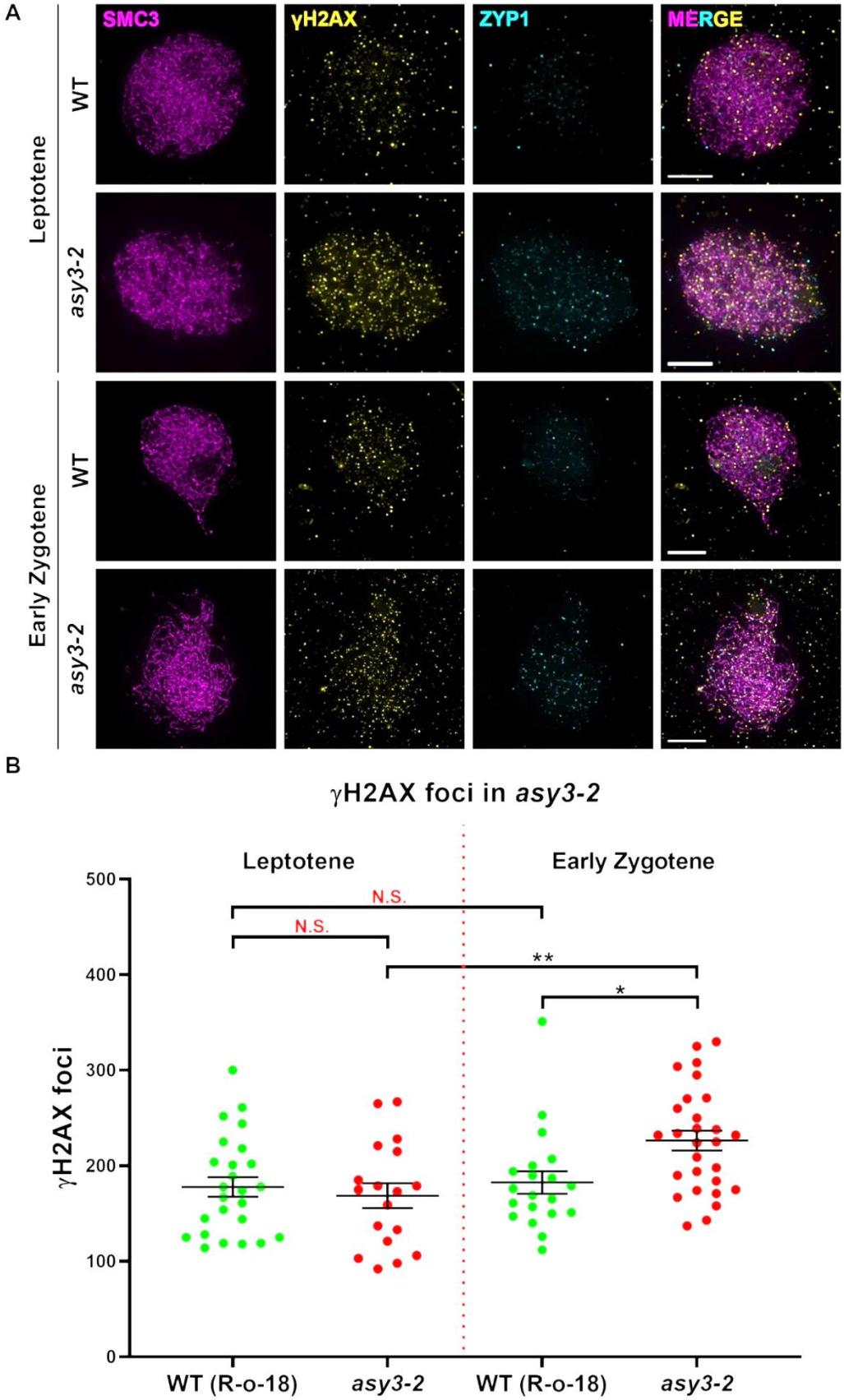


Figure 4.14. DSB formation and repair analysis in *braA*.*asy3*. A. Triple immunolocalisation of γH2AX, SMC3, and ZYP1 in the leptotene and early zygotene stages of WT and *asy3-2* PMCs. 5µm bars. **B.** Scatter plot of the number of γH2AX foci per cell in the leptotene and early zygotene stages of WT and *asy3-2* meiocytes. The bars represent the mean and S.D. **N.S**. Non-significant. ******p<0.01. *****p<0.05.

4.2.9. Class I CO formation is severely impaired in *asy3-2*

As has been shown in section 4.2.3, the *braA.asy3* mutant plants have a great decrease in the mean chiasma frequency per cell pointing out that CO formation is largely reduced in this genotype. Thus, in order to understand how the absence of BraA.ASY3 affects the establishment of COs, a more detailed analysis through the immunolocalisation of the ZMM protein HEI10, used as a class I CO marker (sections 1.2.3.1 and 3.1.5), was performed (Fig.4.15).

The results show a significant decrease (Student's T-test with Welch's correction; $p<0.0001$; Fig.15.B) in the number of HEI10 foci per cell in the plants of the *asy3-2* line (2.66±0.28; n=47) in comparison with the WT (R-o-18) plants (14.92±0.21; n=83). This indicates that class I CO formation is greatly diminished in the absence of ASY3 in *B. rapa*. Interestingly, the number of HEI10 foci observed in *asy3-2* coincides with the mean chiasma frequency per cell, suggesting that the remaining COs in this mutant mostly belong to the interference-sensitive class I, and therefore, that the class II CO route is greatly reduced.

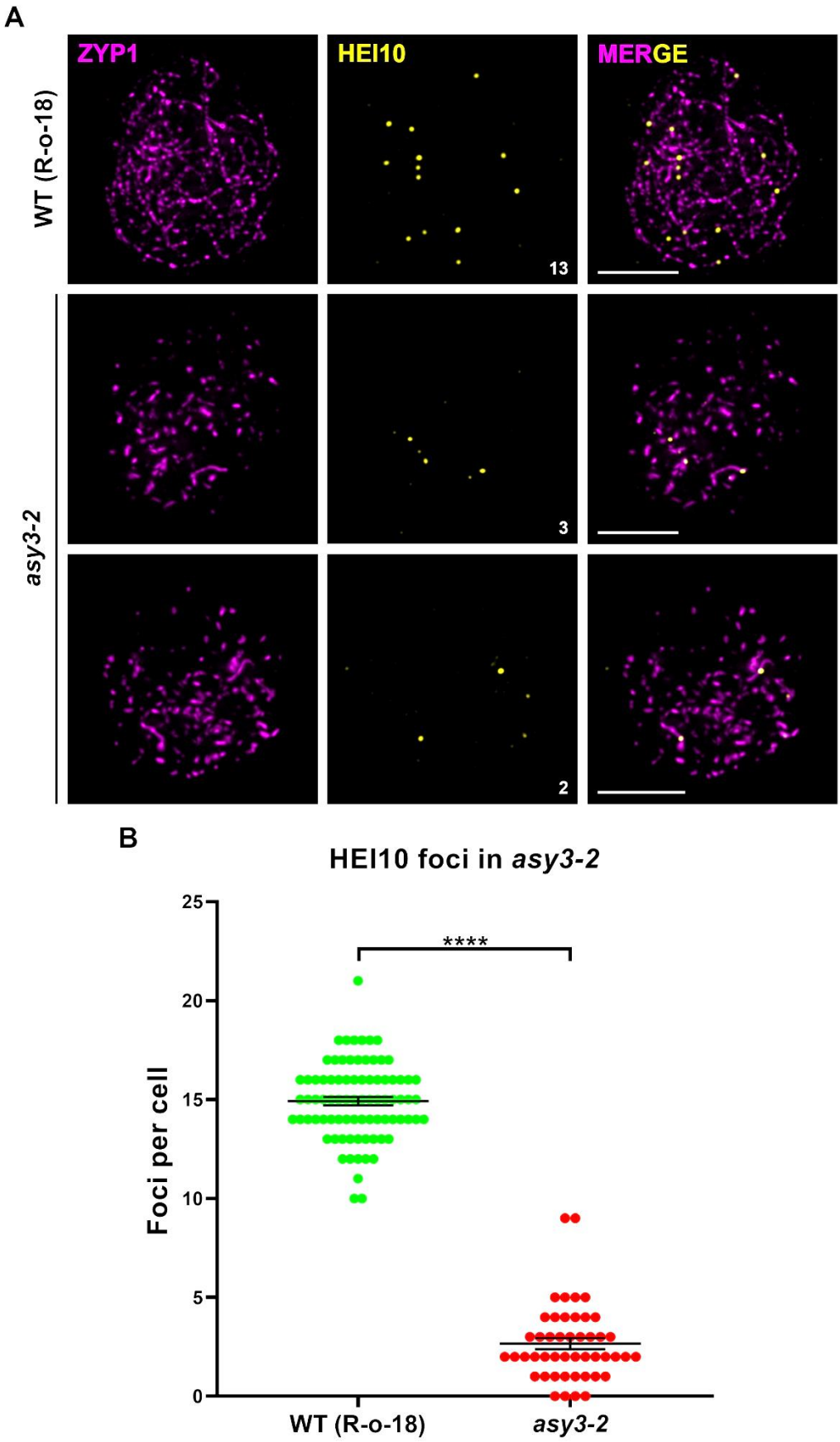


Figure 4.15. HEI10 foci analysis in *asy3-2* and the WT control (R-o-18). A. Comparison between the WT and *asy3-2* meiocytes, the number in the lower right corner indicates the number of foci. 5 µm bars. **B.** Scatter plot showing the HEI10 foci counts per cell in WT and *asy3-2*. The bars represent the mean and S.E.M. ****p<0.0001.

4.2.10. ASY1 and ASY3 contribute equally to CO formation in *B. rapa*

The relation between the axis associated proteins ASY1 and ASY3 has been studied in detail in the plant model organism *Arabidopsis thaliana*, showing an epistatic relation between the genes encoding both proteins (Ferdous *et al.*, 2012). In this way, double mutants bearing T-DNA insertions in *AtASY1* and *AtASY3* showed a predominance of the *asy1* mutant phenotype over that of *asy3*, consisting of lower levels of CO formation between the homologous chromosomes. To study whether this epistatic relation is maintained across different species, double mutants carrying point mutations in both ASY1 and ASY3 orthologs of *B. rapa* have been generated. For this purpose, plants bearing the *asy1-14* mutant allele of *BraA.ASY1*, recently described by Cuacos *et al.* (2021), have been crossed with plants from the *asy3-2* line; and the chiasma frequency per cell has been analysed in the double mutant comparing it with that of the single mutants and the WT control (Fig.4.16). The results of the cytological analysis of meiosis in *asy1-14 asy3-2* are summarised in Table 4.2 at the end of the results section.

The statistical analysis of the chiasma frequency per cell reported that, as expected, significant differences were present between the genotypes studied (Welch's One-Way ANOVA; W= 762.2 [3.000, 109,8]; p<0.0001; Fig.4.16.B). Subsequently, the outcome of the Dunnet's T3 multiple comparisons test showed that the *asy1-14 asy3-2* double mutants and the *asy1-14* single mutant presented a significantly lower chiasma frequency with respect to the WT control (1.72±0.17, n=65; 2.31±0.22, n=58; and 15.79±0.26 n=35, respectively; p<0.0001). On the other hand, no significant differences were found between the *asy1-14 asy3-2* plants and either of the single mutants (*asy1-14*: p=0.16; *asy3-2*: 2.17±0.17, n=100, p=0.10) and neither between the *asy1-14* and *asy3-2* plants (p>0.99).

Therefore, the outcome of this analysis points out that, by contrast with what has been previously described in *A. thaliana*, ASY1 and ASY3 are equally necessary for CO formation in *B. rapa.*

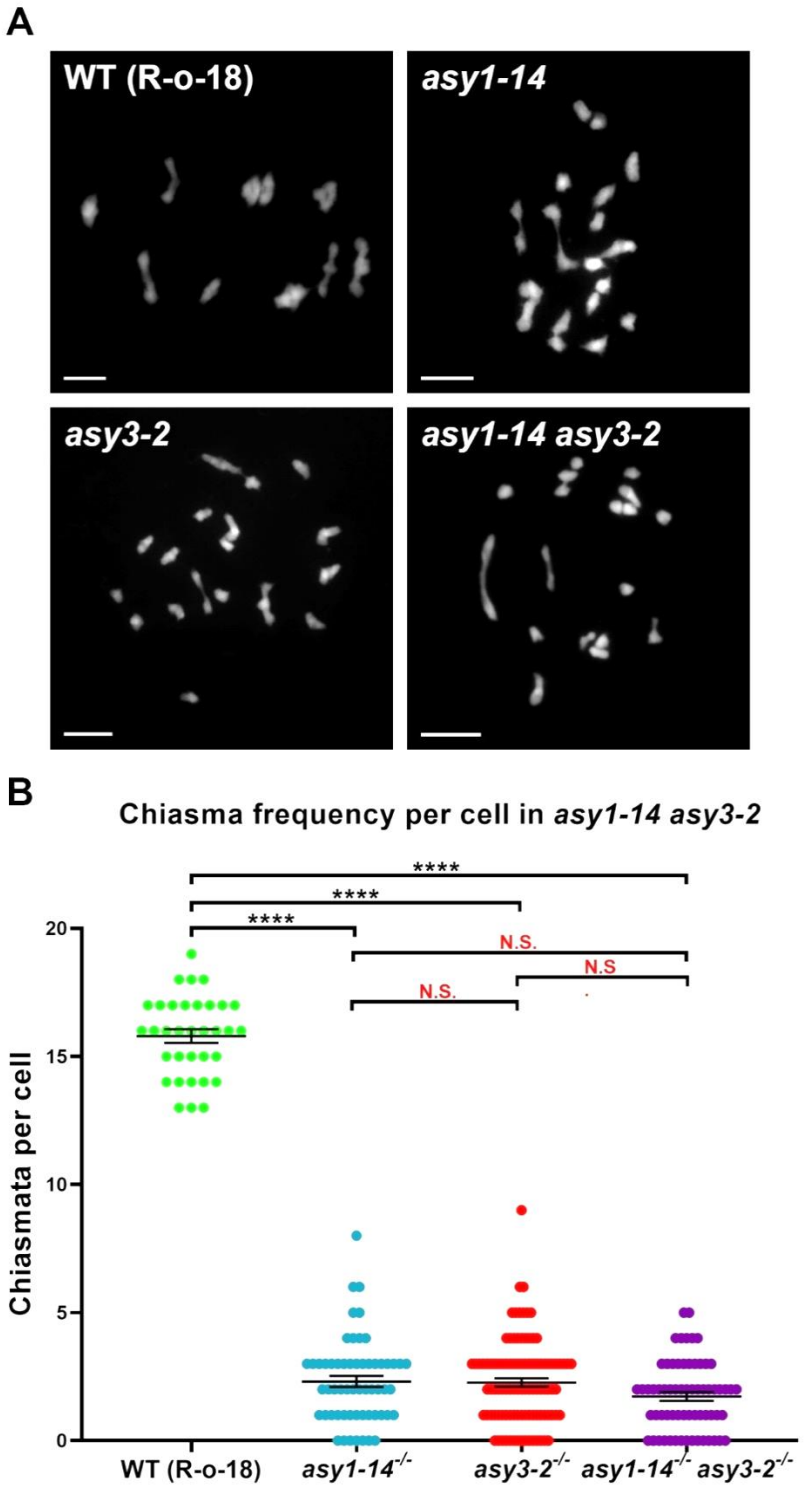


Figure 4.16. Chiasma frequency analysis in the *asy1-14 asy3-2* double mutant. A. Metaphase I meiocytes of the single mutants *asy1-14* and *asy3-2,* the double mutant *asy1-14 asy3-2*, and the WT control. **B.** Scatter plot of the mean chiasma frequency per cell in the aforementioned genotypes. ********p<0.0001. **N.S.** Non-Significant.

4.2.11. *braA.asy3* is epistatic with respect to *braA.pch2*

ASY3 is essential for the correct loading of ASY1 to the chromosome axis and, as it has recently been published, PCH2 appears to favour the localisation of ASY1 to the nucleus as well as its loading to the AEs (Ferdous *et al.*, 2012; Yang *et al.*, 2020). In this manner, we wanted to analyse whether there was an epistatic relation between *ASY3* and *PCH2* in *B. rapa*, in which the phenotype of one would predominate over the other, or if the combination of both mutations would produce a different phenotype. Thus, we generated an *asy3-2 pch2-9* double mutant and analysed the chiasma frequency per cell, comparing it to that of the single mutants *asy3-2* and *pch2-9*, and to the WT control (Fig.4.17).

The Welch's One-Way ANOVA test was used to seek for changes in the chiasma frequency per cell among the four genotypes analysed, revealing that significant differences were present between them (W= 724.0 [3.000, 126.6]). The pairwise comparison analysis (Dunnet's T3) showed that the *asy3-2 pch2-9* double mutant plants had a significant reduction of the chiasma frequency per cell (2.14±0.19; n=64) in comparison to the WT control (15.79±0.26; n=35; p<0.0001) and the single mutant *pch2-9* (8.13±0.39; n=108; p<0.0001). Nevertheless, no changes were found with respect to the single mutant *asy3-2* (2.27±0.17; n=100; p=0.94). These results may suggest that the role of BraA.ASY3 in the loading of BraA.ASY1 to the meiotic chromosome axis is predominant over the role of BraA.PCH2, which participates in the conformational changes of BraA.ASY1, ensuring a transition from a closed configuration to an open conformation, necessary for its correct loading to the AEs. Thus, even if BraA.ASY1 is in its open configuration, BraA.ASY3 is still essential for its association with the meiotic chromosome axis and to carry out its function.

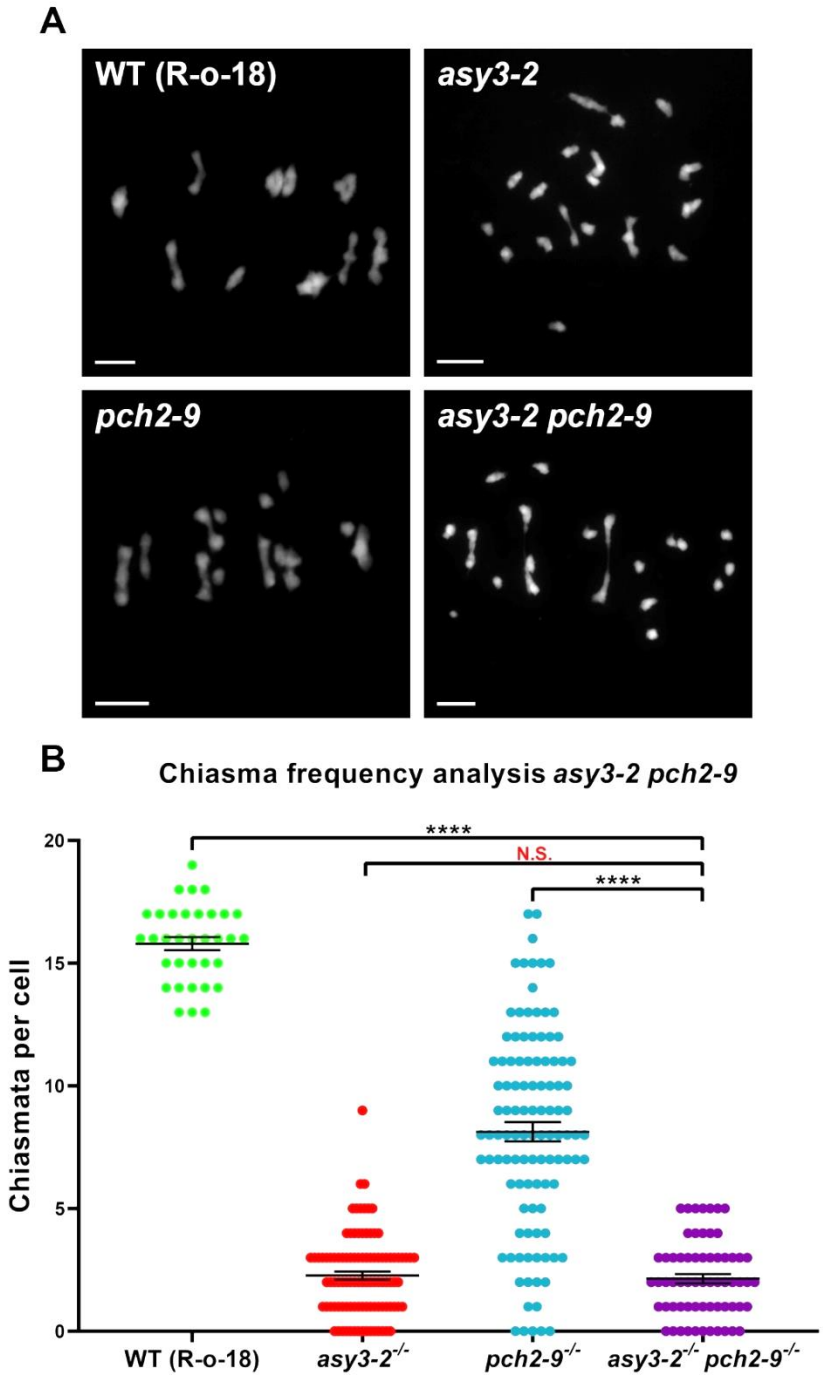


Figure 4.17. Chiasma frequency analysis in the *asy3-2 pch2-9* double mutant. A. Metaphase I meiocytes of the single mutants *asy3-2* and *pch2-9,* the double mutant *asy3-2 pch2-9*, and the WT control. **B.** Scatter plot of the mean chiasma frequency per cell in the previously mentioned genotypes. ********p<0.0001. **N.S.**Non-Significant.

Table 4. 2. Summary of the cytological analysis of meiosis of *braA.asy3*.

	Bivalent formation						Chiasmata (Xta) analysis			
Genotype	**% cells w/ univalents**	**% I (pairs) /cell**	**Average I (pairs) /cell**	**Average II /cell**	**Average ring bivalents /cell**	**Average rod bivalents /cell**	**Mean Xta frequency /cell**	**% IP Xta**	**% ID Xta**	**n**
WT (R-o-18)	**0**	**0**	**0**	**10**	**5.44±0.22**	**4.56±0.22**	**15.79±0.27**	**9.1**	**90.9**	**34**
asy3-2	100	78	7.8±0.16	2.2±0.16	0.08±0.03	2.12±0.15	2.27±0.17	9.2	90.8	100
asy3-3	100	78	7.8±0.21	2.2±0.21	0.18±0.04	2.04±0.15	2.36±0.23	2	98	58
asy3-2 x asy3-3	100	77.2	7.72±0.21	2.28±0.21	0.13±0.06	2.15±0.20	2.45±0.25	5	95	47
asy1-14	100	79	7.88±0.20	2.12±0.20	0.14±0.05	1.98±0.18	2.31±0.22	3	97	56
pch2-9	91.7	37	3.98±0.26	6.02±0.26	1.87±0.17	4.14±0.20	8.13±0.39	10.6	89.4	108
asy1-14 asy3-2	100	84.2	8.42±0.13	1.58±0.13	0.06±0.02	1.52±0.12	1.72±0.17	1	99	65
asy3-2 pch2-9	100	80	8.00±0.18	2.00±0.18	0.14±0.05	1.86±0.18	2.14±0.19	5	95	64

4.3. Discussion

In this chapter, a key component of the meiotic chromosome axis, the coiled coil domain protein BraA.ASY3 (Bra004486) has been identified and thoroughly characterised in the crop wild-relative *B. rapa* by means of a reverse genetic approach. In this manner, after the identification of a candidate gene through an *in-silico* analysis of homology, mutant lines bearing defective alleles of the gene have been cytologically analysed to unveil its functions during meiosis. This has revealed conserved functions of ASY3 in *B. rapa* as it is essential for: i) the maintenance of fertility; ii) the correct segregation of the homologous chromosomes; iii) the formation of COs between the homologous chromosomes; iv) the correct association of BraA.ASY1 to the AEs; v) the polymerisation of the SC.

Further experimentation is carried out in the chapter 5 regarding the role of BraA.ASY3 in the formation of both classes of COs: interference sensitive (Class I) and non-sensitive (Class II). Thus, a more detailed discussion over the roles of ASY3 is presented within that chapter and in chapter 6.

4.3.1. BraA.ASY3 is essential for the maintenance of fertility as it participates in the segregation of the homologous chromosomes

As it was observed in section 4.2.2 the plants homozygous for either of the mutant alleles of *BraA.ASY3* presented complete sterility as were completely unable to produce seeds. Moreover, this seems to be related with defects in the segregation of the chromosomes as it was shown in the section 4.2.2, where the analysis of meiosis through DAPI spreads of PMCs showed that the *asy3-2* plants presented unreduced nuclei at the end of meiosis as a result of the missegregation of chromosomes at the end of the first meiotic division. The non-disjunction of the chromosomes was due to

problems in the formation of bivalents as it was observed in the metaphase I spreads of the *braA.asy3* mutants. Consequently, the homologous chromosomes appeared as univalents unable to orient to opposite poles, preventing their accurate segregation. The defects in bivalent formation and chromosome segregation were the direct consequence of a severe reduction in chiasma formation as these allow the segregation of the homologs to opposite poles in anaphase I by counteracting the pulling forces of the spindle. Thus, the lack of chiasma formation seems to be the cause of the non-disjunction problems observed in these mutants, ultimately having its origin in problems in the establishment of COs between the homologs during prophase I, which were studied in more detail in section 4.2.9, and are discussed below.

4.3.2. BraA.ASY3 is necessary for the correct structure of the AEs (ASY1 loading) and the polymerisation of the SC

Given that the axis-associated coiled-coil domain proteins are known for their role in favouring the axis-association of the meiotic HORMA domain proteins and the polymerisation of the SC in several organisms such as: RED1 in yeast, SYCP2 in mouse, DSY2 in maize, PAIR3 in rice, and ASY3 in *A. thaliana*; a detailed analysis of these processes was carried out in the *braA.asy3* mutant (Rockmill and Roeder, 1990; Friedman, Hollingsworth and Byers, 1994; Smith and Roeder, 1997; Yang *et al.*, 2006; K. Wang *et al.*, 2011; Ferdous *et al.*, 2012; Lee *et al.*, 2015; MacQueen *et al.*, 2019; Fujiwara *et al.*, 2020). This revealed that, in agreement with previous results, BraA.ASY3 is necessary for the correct association of BraA.ASY1 to the AEs as in the absence of the former ASY1 appears as either a disorganised signal associated with the chromatin or forming foci and short stretches rather than

following a continuous pattern. This might be due to an early association with the cohesin axis, which later on requires BraA.ASY3 to maintain the stability of that interaction, as has been recently suggested in mouse (Fujiwara *et al.*, 2020).

In the same way, as the axis-associated coiled-coil domain proteins have been described to be essential for the establishment of synapsis between the homologous chromosomes, SC formation was studied in *braA.asy3.* This analysis showed that the putative ASY3 ortholog of *B. rapa* is necessary for the polymerisation of the SC, which instead of forming a continuous signal, appears as short stretches. This further confirms its homology with the other axis-associated coiled-coil domain proteins. Moreover, regarding the deleterious effect in the formation of the SC that the absence of BraA.ASY3 has, this might be due to defects in the pairing process mediated by SEI process catalysed by DMC1. In this way, it has been previously observed in *A. thaliana* that the DMC1/RAD51 nucleoprotein filament becomes unstable in the absence of ASY1, thus abrogating the recognition between the homologs since this is the main drive for the homology search during meiosis (Sanchez-Moran *et al.*, 2007, 2008). Consequently, due to the inability of reaching a stable pairing, the formation of the SC is prevented together with the ability to recombine with the homologous chromosome, also severely affecting CO formation as discussed below. To summarise, the absence of BraA.ASY3 prevents a stable association of BraA.ASY1 to the AEs, which leads to difficulties in the establishment of the IH Bias, and the strand invasion process, preventing the formation of the SC and the recombination with the homologous chromosome.

4.3.3. BraA.ASY3 is necessary for CO formation and contributes to the establishment of the *Inter-Homolog Bias* and DSB repair dynamics

As the analysis of metaphase I spreads showed, chiasma formation was severely impaired in the *braA.asy3* mutant lines, thus pointing out that CO formation between the homologous chromosomes was severely compromised. The immunolocalization of the ZMM protein HEI10 allowed for a more detailed characterisation of CO formation in the *braA.asy3* mutants. In this way, it revealed that the vast majority of the remaining COs belonged to the interference-sensitive class I, and that their formation was greatly impaired. As pointed out in the previous section this is most likely due to difficulties in the establishment of the IH Bias, directing the repair of the SPO11-dependant DSBs by HR using the sister chromatid as a template rather than the homologous chromosome. This has previously been observed in *S. cerevisiae*, where it has been shown that RED1 (the budding yeast ortholog of ASY3) counteracts the action of the cohesin REC8 which favours the repair of the meiotic DSBs with the sister chromatid rather than with the homolog (Schwacha and Kleckner, 1997; Kim *et al.*, 2010). Moreover, yeast mutants of both *HOP1* and *RED1* present a reduction of both types of recombination with the homologous chromosome, COs and NCOs (Hollingsworth and Byers, 1989; Rockmill and Roeder, 1990).

In addition, given that in *A. thaliana* it was observed a possible role for ASY3 in promoting the formation of DSBs, their levels and dynamics through prophase I were assessed in the *braA.asy3* mutants through the immunolocalization of the DSB marker γH2AX. This analysis revealed that, by contrast with previous results from Ferdous *et al.* (2012), DSB formation was not altered in *braA.asy3.* Nevertheless, an

increase in the levels of γH2AX in the early zygotene stage of the mutant was observed, suggesting that the dynamics of DSB processing could be affected by the absence of BraA.ASY3, leading to an accumulation of these early recombination intermediates due to a delay in their processing. This could be related to the difficulties in the repair of the DSBs using the homologous chromosome as a template as previously discussed. Nevertheless, the DSBs are always repaired, possibly by HR with the sister chromatid or as NCOs since no chromosome fragmentation is observed in *braA.asy3.* An alternative explanation could be that DSB formation could be extended in *braA.asy3,* which could be supported by the observation in budding yeast that many DSB factors are removed from synapsed chromosomes by different feedback loops (reviewed in Yadav and Bouuaert, 2021).

4.3.4. BraA.ASY1 stable localisation to the AEs mediated by BraA.ASY3 is essential for BraA.ASY1 to carry out its function.

In yeast and *Arabidopsis*, an epistatic relation has been described by which the phenotype of either *hop1* or *asy1* predominates over the one of *red1* or *asy3* (Rockmill and Roeder, 1990; Ferdous *et al.*, 2012). In both cases it consists of lower levels of recombination between the homologous chromosomes.

In this way a *braA.asy1 braA.asy3* double mutant was generated in *B. rapa* to test whether this epistatic relation was conserved. Interestingly, no differences in CO formation were found between the double mutant with respect to the single mutants and neither between themselves. This indicates that by contrast with *A. thaliana* and yeast, in *B. rapa*, the stable association of the HORMA domain protein BraA.ASY1 to the AEs mediated by BraA.ASY3 is absolutely necessary for its role in HR, thus losing the epistatic relation between both. In this way, it could be argued that in *B.*

rapa ASY1 is not able to retain any activity in the absence of BraA.ASY3, whereas *A. thaliana* ASY1 and *S. cerevisiae* HOP1 are able to keep some residual activity in the absence of ASY3/RED1 (Smith and Roeder, 1997; Ferdous *et al.*, 2012).

Moreover, it was recently published in *A. thaliana* that the AAA+ ATPase PCH2 is necessary for the conversion of ASY1 to an open active conformation which facilitates its loading to the chromosome axes (Chao Yang *et al.*, 2020). In this manner, a *braA.asy3 braA.pch2* double mutant was generated to analyse the relation between the function of PCH2 in facilitating the axis loading of ASY1 and the one of ASY3 stabilising it. The predominance of the *asy3* phenotype pointed out that ASY3 is epistatic to PCH2, concurring with the phenotype of the *asy1 asy3* double mutant, which demonstrated that the role of ASY3 in the axis association of ASY1 is key for its activity in *B. rapa*, regardless of whether ASY1 is present in an active open conformation.

Chapter 5. Relation between the meiotic axis structure, its remodelling and crossover formation in *B. rapa*

5.1. Introduction

In this chapter, the influence of the axis-associated proteins ASY1 and ASY3, and the axis remodelling protein PCH2 over the formation of both classes of COs is explored into more detail. This is achieved through the combination of mutations for the genes encoding these proteins with genetic backgrounds defective for the anti-recombinase FANCM, and the ZMM protein MSH4.

The role of the FANCM helicase in plant meiosis is well known as it has been described in different plant organisms as *A. thaliana*, *B. rapa*, *B. napus*, and lettuce (Crismani *et al.*, 2012a; Knoll *et al.*, 2012; Blary *et al.*, 2018; Li *et al.*, 2021a). In this way, FANCM acts as an anti-recombinase factor that limits the formation of the interference non-sensitive Class II COs during meiosis by favouring the repair of DNA intermediates as NCOs through the SDSA pathway, limiting their repair as COs by the structure specific nuclease MUS81 (Crismani *et al.*, 2012; Knoll *et al.*, 2012). Moreover, it has recently been found that FANCM is also necessary to regulate CO distribution (Li *et al.*, 2021a; Li *et al.*, 2021b). In this way, the combination of a *fancm* mutant background together with a class I CO defective one as the *zmm* mutants results in a recovery of chiasma formation by increasing the numbers of class II COs (Crismani *et al.*, 2012; Blary *et al.*, 2018). The mutation of FANCM in *B. rapa* does not seem to have a clear phenotype unless combined with other genetic backgrounds defective for the formation of Class I COs such as the *msh4* mutant (Blary *et al.*, 2018). Therefore, the objective of obtaining plants with defects in axis-associated proteins and AE remodelling (*asy1-14*, *asy3-2* and *pch2-9* respectively) in a *fancm* mutant background was to study whether the increase in Class II CO formation due to the disruption of the anti-CO helicase FANCM (Crismani *et al.*,

2012; Blary *et al.*, 2018) was affected by the structure of the AEs and their remodelling, or if both classes of COs are equally affected.

On the other hand, MSH4 is a well-known pro-class I CO factor as it is a ZMM protein involved in the resolution of the dHjs as interference-sensitive Class I COs as explained in section 1.2.3.1. The role of MHS4 in plant meiosis has been studied in detail through the analysis of *msh4* mutants in *A. thaliana* and *Brassica*, which presented a severe reduction in CO formation as class I COs are absent and these account for the majority of COs in plants (Higgins *et al.*, 2004; Blary *et al.*, 2018; Gonzalo *et al.*, 2019). In this way, double mutants between the axis defective genes named above and the *msh4-1* mutant of *B. rapa* were also obtained and chiasma together with bivalent formation were studied in these mutants. This allowed us to further understand the impact on class I CO formation of the loss of function of the axis associated proteins ASY1 and ASY3, and the axis remodelling protein PCH2.

This work has been done in collaboration with Dr Maria Cuacos and Dr Stefan Heckmann (IPK Gatersleben, Germany). The *asy1-14 fancm-11* and *pch2-9 fancm-11* double mutants were obtained by Dr Maria Cuacos by crossing plants of the corresponding genetic backgrounds as described in section 2.1.4, and their seeds were donated to us to continue with the cytological characterisation of these mutant lines.

5.2. Results

To study how the combination of the mutant backgrounds named above influenced chromosome segregation and CO formation at the meiocyte and chromosome levels, the following cytological markers were taken into consideration for analysis in

metaphase I spreads of PMCs (Fig.5.1): chiasma frequency per cell, chromosome configurations (ring and rod bivalents per cell) and number of univalents per cell. In some cases, as the *pch2-9 fancm-11* double mutant, further analyses were carried out, which appear at the end of section 5.2.1.

The results of the cytological analysis of meiosis in the different single and double mutants are summarised in Fig.5.3.A,B and in the Table 5.19. The outcomes of the different statistical analyses are summarised in the Tables 5.1-18, throughout the chapter. For some genotypes, no comparison was carried out as it was already performed in previous sections of this thesis, thus, the corresponding cell of the table appears as "-".

It is worth to mention in advance that the *fancm-11* mutant line is a novel allele, not related to the one described by Blary *et al.* (2018). Therefore, to confirm that it corresponds to a null mutant of the anti-recombinase FANCM, and that the phenotype of the mutant is the same as in previous publications, a double mutant *msh4-1 fancm-11* was generated (Fig.A1, Appendix). The analysis of this double mutant revealed a significant increase in chiasma formation in comparison with the *msh4-1* single mutant (11.69±0.32 and 2.97±0.22, respectively; Welch's T-test, $t=22.17$, $df=96.13$, $p<0.0001$), corroborating that the *fancm-11* line constitutes a null mutant of FANCM.

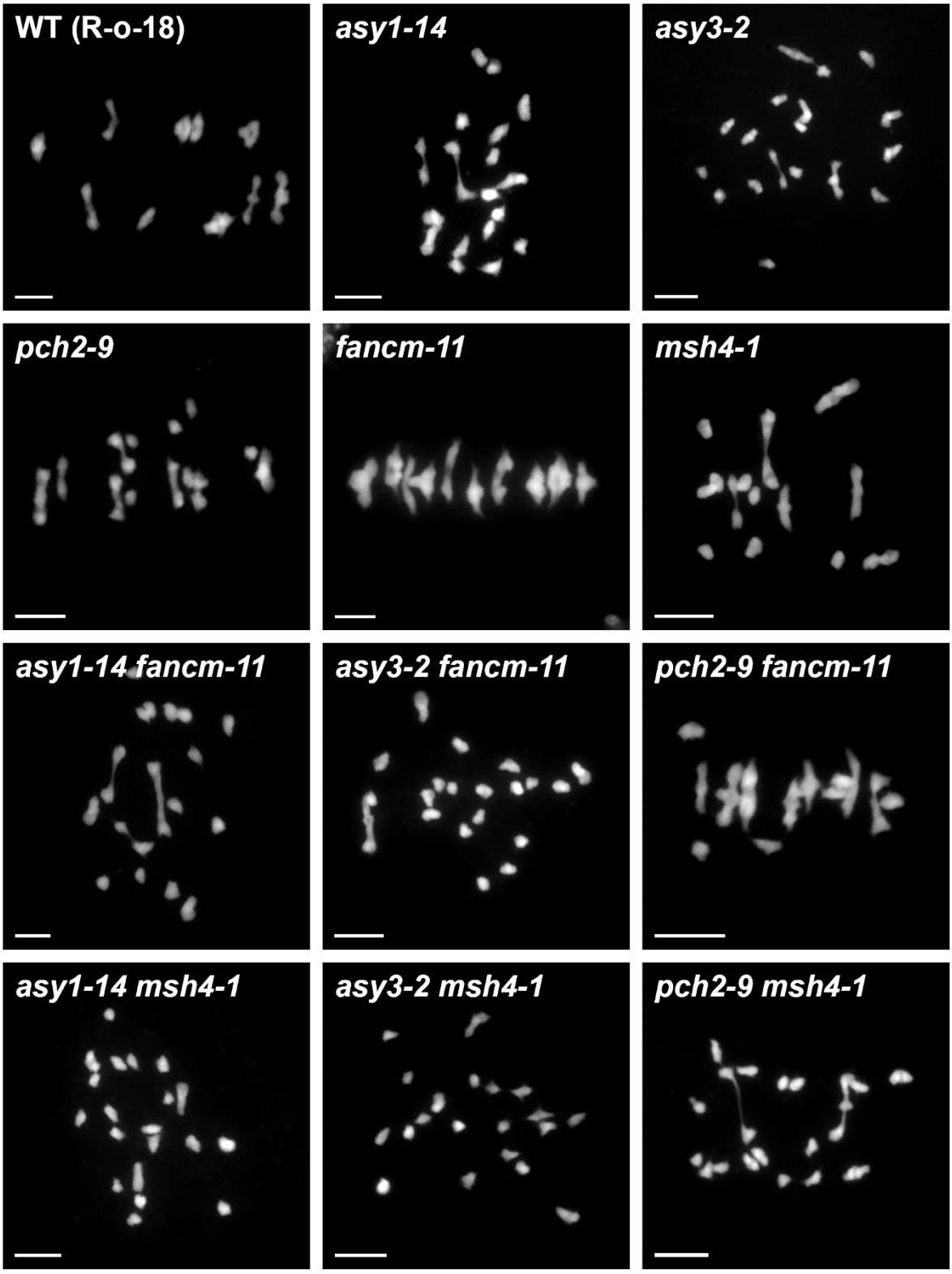


Figure 5.1. Metaphase I chromosome spreads of PMCs of the double and single mutants analysed in the chapter. 5µm bars.

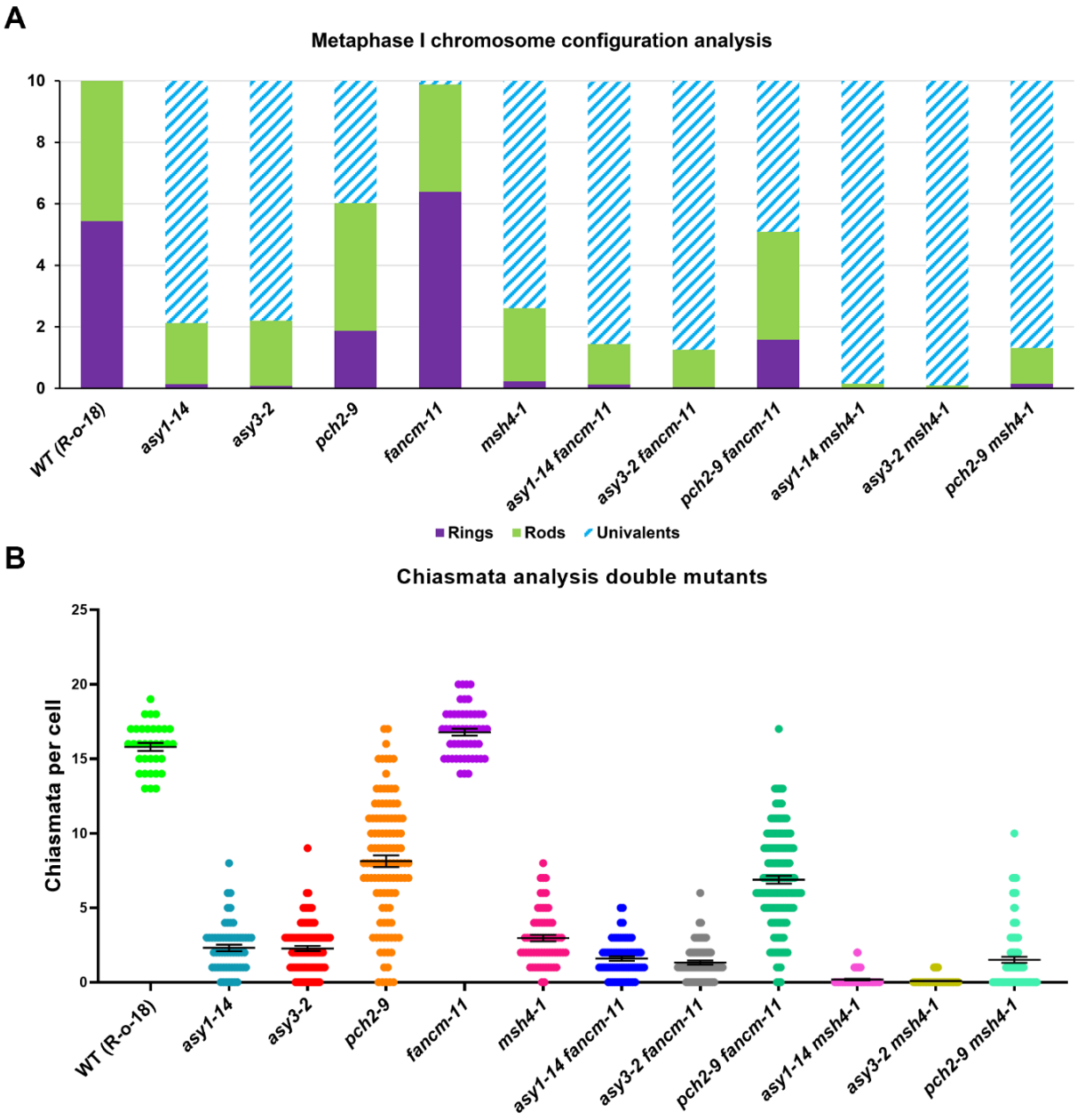


Figure 5.2. Summary of the cytological analysis of metaphase I spreads carried out in the single and double mutants analysed in the chapter **A.** Column graphs of the analysis of ring, rods and univalents per cell in the single and double mutants. **B.** Scatter plot showing the chiasma frequency per cell in the single and double mutants. The bars represent the mean ± S.E.M.

Table 5.1. Summary of the results of the cytological analysis of single and double mutants.

	Bivalent formation						Chiasmata (Xta) analysis			
Genotype	**% cells w/ univalents**	**% I (pairs) /cell**	**Average I (pairs) /cell**	**Average II /cell**	**Average ring bivalents /cell**	**Average rod bivalents /cell**	**Mean Xta frequency /cell**	**% IP Xta**	**% ID Xta**	**n**
WT (R-o-18)	**0**	**0**	**0**	**10**	**5.44±0.22**	**4.56±0.22**	**15.79±0.27**	**9.1**	**90.9**	**34**
asy1-14	100	79	7.88±0.20	2.12±0.20	0.14±0.05	1.98±0.18	2.31±0.22	3	97	56
pch2-9	91.7	37	3.98±0.26	6.02±0.26	1.87±0.16	4.15±0.21	8.12±0.39	10	90	108
asy3-2	100	78	7.8±0.16	2.2±0.16	0.08±0.03	2.12±0.15	2.27±0.17	9.2	90.8	100
fancm-11	7.8	12	0.12±0.06	9.88±0.06	6.39±0.17	3.49±0.17	16.78±0.23	9	91	51
msh4-1	100	73.9	7.39±0.18	2.61±0.18	0.23±0.06	2.38±0.17	2.97±0.22	7.1	92.9	66
asy1-14 fancm-11	100	85.3	8.53±0.12	1.47±0.12	0.12±0.04	1.32±0.12	1.59±0.15	6	94	66
asy3-2 fancm-11	100	87.5	8.75±0.12	1.25±0.12	0.04±0.02	1.21±0.12	1.32±0.14	4	96	71
pch2-9 fancm-11	99.32	49.1	4.91±0.17	5.05±0.17	1.58±0.11	3.5±0.15	6.92±0.26	16.5	84.1	148
asy1-14 msh4-1	100	99	9.85±0.04	0.15±0.04	0.01±0.01	0.14±0.04	0.18±0.05	0	100	88
asy3-2 msh4-1	100	99	9.91±0.03	0.09±0.03	0	0.09±0.03	0.09±0.03	0	100	86
pch2-9 msh4-1	100	87	8.68±0.17	1.32±0.17	0.15±0.04	1.17±0.15	1.51±0.20	2	98	114

5.2.1. The combination of axis defective backgrounds with the loss of function of the class II anti-CO factor FANCM results in a decrease of CO formation

The chiasma frequency per cell was analysed in the double mutant *asy1-14 fancm-11* and compared to that of the single mutants and the WT control (Table 5.2). In this way, the statistical analysis revealed that significant differences were present among the genotypes studied (Welch's One-Way ANOVA, W= 1529 [3.000, 171.1], p<0.0001). Subsequently, the Dunnet's T3 *post-hoc* test was used to conduct pairwise comparisons between them. This showed that the *asy1-14 fancm-11* double mutant presented a significantly lower chiasma frequency per cell (1.59±0.15, n=66) in comparison with the WT control (15.79±0.27, n=34, p<0.0001) and the single mutants *asy1-14* (2.31±0.22, n=58, p<0.05) and *fancm-11* (16.78±0.23, n=51, p<0.0001). Interestingly, the *fancm-11* single mutant showed a significant increase in the chiasma frequency per cell when compared to the WT control (p<0.05), that had not been reported in previous studies (Blary *et al.*, 2018).

Table 5. 2. Outcomes of the Dunnet'sT3 test comparing the chiasma frequency per cell between the *asy1-14 fancm-11* double mutant, the single mutants, and the WT control.

	WT (R-o-18)		
asy1-14	-	***asy1-14***	
fancm-11	*	-	***fancm-11***
asy1-14 fancm-11	****	*	****

***p<0.05, ****p<0.0001

The analysis of the number of univalent pairs per cell in *asy1-14 fancm-11* also showed that significant differences were present between the *asy1-14*, *fancm-11*, and *asy1-14 fancm-11* backgrounds (Welch's One-Way ANOVA, W= 2378 [2.000,

100.0], P<0.0001; Table 5.3). The multiple comparisons test (Games-Howell's test) revealed that concurring with the decrease in chiasma formation, the double mutant *asy1-14 fancm-11* also presented significantly more univalent pairs per cell (8.53±0.12) that the single mutants *fancm-11* (0.12±0.06, p<0.0001) and *asy1-14* (7.88±0.19, p<0.05).

Table 5. 3. Results of the Games-Howell's test comparing the number of univalent pairs per cell between the *asy1-14 fancm-11* double and single mutants.

	asy1-14	
fancm-11	-	***fancm-11***
asy1-14 fancm-11	*	****

*p<0.05, ****p<0.0001

To conclude with the cytological analysis of meiosis in metaphase I spreads, the formation of ring and rod bivalents was studied in the *asy1-14 fancm-11* plants to understand how the changes in the chiasma frequency per cell were related to the bivalent shapes in this genotype (Table 5.4). Regarding the number of ring bivalents per cell, the Welch's One-Way ANOVA test showed that differences in this cytological marker were present between the genotypes studied (W=600.8 [3.000, 86.76], p<0.0001). In this way, the *post-hoc* multiple comparisons test (Dunnet's T3 test) revealed in a first instance that the single mutant *asy1-14* presented a great reduction in the number of ring bivalents per cell with respect with the WT control (0.14±0.05 and 5.44±0.22, respectively, p<0.0001) whereas *fancm-11* showed an increase of these with respect to the WT plants (6.39±0.17, p<0.001). Secondly, this analysis revealed that the *asy1-14 fancm-11* double mutant presented a significantly lower number of ring bivalents per cell in comparison with the WT (0.12±0.04,

p<0.0001) and *fancm-11* (p<0.0001) plants, whereas no differences were found with respect to the single mutant *asy1-14* (p=0.9997). Similarly, the analysis of the number of rod bivalents per cell showed that significant differences were present among these genotypes (Welch's ANOVA test, W=74.77 [3.000, 97.74], p<0.0001). In this way, the consecutive pairwise comparison test (Dunnet's T3 test) revealed that the single mutant *asy1-14* had a significantly lower number of rod bivalents per cell in comparison with the WT plants due to its defects in CO formation (1.98±0.18 and 4.56±0.22, respectively; p<0.0001). The single mutant *fancm-11* also presented a lower number of rod bivalents per cell in comparison with the WT plants but due to the opposite situation (3.49±0.17; p<0.01). In this way, the higher number of chiasmata formed in *fancm-11* resulted in an increase in the proportion of ring bivalents, reducing the number of rod bivalents per cell. This *post-hoc* test also revealed that the *asy1-14 fancm-11* plants presented a significant decrease in the number of rod bivalents per cell with respect to the WT control, *fancm-11* and *asy1-14* plants (1.32±0.12; p<0.0001, p<0.0001, and p<0.05, respectively).

Table 5. 4. Results of the Dunnet'sT3 test comparing the number of ring and rod bivalents per cell between the *asy1-14 fancm-11* double mutant, the single mutants and the WT control.

Ring bivalents per cell				**Rod bivalents per cell**			
	WT (R-o-18)				**WT (R-o-18)**		
asy1-14	****	***asy1-14***		***asy1-14***	****	***asy1-14***	
fancm-11	**	-	***fancm-11***	***fancm-11***	**	****	***fancm-11***
asy1-14 fancm-11	****	**N.S.**	****	***asy1-14 fancm-11***	****	*	****

***p<0.05, **p<0.01, ****p<0.0001. **N.S.** Non-Significant.

Similar results were found in the cytological analysis of the metaphase I spreads of the double mutant *asy3-2 fancm-11*. In this way, starting with the chiasma frequency per cell (Table 5.5), the Welch's One-Way ANOVA test showed that significant differences (W=1695 [3.000,105.4], p<0.0001) were present between the double mutant *asy3-2 fancm-11*, each of the single mutants and the WT control. This was followed by a pairwise comparisons test between the genotypes by means of the Dunnett's T3 test. The results of the test showed that the *asy3-2 fancm-11* plants displayed a significantly lower chiasma frequency per cell (1.32±0.14, n=71) in comparison with the WT control, *asy3-2,* and *fancm-11* plants (p<0.0001).

Table 5. 5. Summary of the Dunnet'sT3 test outcome comparing the chiasma frequency per cell between the *asy3-2 fancm-11* double mutant, the single mutants, and the WT control.

	WT (R-o-18)		
asy3-2	-	***asy3-2***	
fancm-11	-	-	***fancm-11***
asy3-2 fancm-11	****	****	****

****p<0.0001

The decrease in the chiasma frequency per cell observed in the *asy3-2 fancm-11* plants had an influence in the number of univalent pairs per cell observed in this genotype. In this way, the statistical analysis showed that there were significant differences between *asy3-2 fancm-11* and the single mutants (Welch's One-Way ANOVA, W=2630 [2.000, 137.5], p<0.0001; Table 5.6). The Games-Howell's multiple comparisons test revealed that the *asy3-2 fancm-11* plants presented a significant increase in the number of univalent pairs per cell in comparison with the *asy3-2* and *fancm-11* plants (8.75±0.12, p<0.0001)

Table 5. 6. Results of the Games-Howell's test comparing the number of univalent pairs per cell between the *asy3-2 fancm-11* double mutant and the single mutants.

	asy3-2	
fancm-11	-	***fancm-11***
asy3-2 fancm-11	****	****

****p<0.0001

In a complementary way, the number of ring and rod bivalents per cell was analysed in *asy3-2 fancm-11* to understand how the changes in the chiasma frequency and the number of univalent pairs per cell could be affecting the bivalent configurations. In the first place, the analysis of the number of ring bivalents per cell revealed that significant differences were present among the *asy3-2 fancm-11, asy3-2, fancm-11*, and the WT plants (Welch's One-Way ANOVA, W=637.7 [3.000, 90.00], p<0.0001). However, the pairwise comparisons test (Dunnett's T3, Table 5.7) showed that whereas the *asy3-2 fancm-11* double mutant presented a significant decrease of the number of ring bivalents per cell (0.42±0.02), in comparison with the WT control (p<0.0001) and *fancm-11* mutant (p<0.0001), no differences were found with respect to the *asy3-2* plants (p=0.7044).

Regarding the number of rod bivalents per cell, the statistical analysis revealed that significant differences were present between the double mutant *asy3-2 fancm-11*, either of the single mutants and the WT control (Welch's One-Way ANOVA, W=79.64 [3.000, 107.1], p<0.0001). The subsequent *post hoc* test (Dunnet's T3) showed that the *asy3-2 fancm-11* double mutant had a significantly lower (p<0.0001) number of rod bivalents per cell (1.211±0.12) than the *asy3-2* and *fancm-11* single mutants, and the WT control.

Table 5. 7. Results of the Dunnet'sT3 test comparing the number of ring and rod bivalents per cell between the *asy3-2 fancm-11* double mutant, the single mutants, and the WT control.

Ring bivalents per cell				Rod bivalents per cell			
	WT (R-o-18)				WT (R-o-18)		
asy3-2	-	***asy3-2***		***asy3-2***	-	***asy3-2***	
fancm-11	-	-	***fancm-11***	***fancm-11***	-	-	***fancm-11***
asy3-2 fancm-11	****	**N.S.**	****	***asy3-2 fancm-11***	****	****	****

****p<0.0001. **N.S.** Non-Significant

The last of the *B. rapa* double mutants with a FANCM defective background was the *pch2-9 fancm-11* double mutant, in which the combination of the *pch2-9* mutation with the *fancm-11* allele had a similar effect to the one observed in the *asy1-14 fancm-11* and *asy3-2 fancm-11* double mutants. In this manner, the study of the chiasma frequency per cell in *pch2-9 fancm-11*, the single mutants, and the WT control showed that significant differences were present between them (Welch's One-Way ANOVA, W=356.7 [3.000, 139.3], p<0.0001; Table 5.8). The subsequent Dunnet's T3 multiple comparisons test revealed that the *pch2-9 fancm-11* plants had a significant decrease in the chiasma frequency per cell (6.88±0.26, n=148) with respect to the *pch2-9* (p<0.05), *fancm-11* (p<0.0001), and WT control plants (p<0.0001).

Table 5. 8. Summary of the Dunnet'sT3 test comparing the chiasma frequency per cell between the *pch2-9 fancm-11* double mutant, the single mutants, and the WT control.

	WT (R-o-18)		
pch2-9	-	***pch2-9***	
fancm-11	-	-	***fancm-11***
pch2-9 fancm-11	****	*	****

***p<0.05, ****p<0.0001

Significant differences in the number of univalent pairs were also found between the double mutant *pch2-9 fancm-11* and the single mutants (Welch's One-Way ANOVA, W=4269 [2.000,185.0]). In this way, the Games-Howell's multiple comparisons test indicated that concurring with the greater defects in chiasma formation (Table 5.9), a significantly higher number of univalents per cell was observed in the *pch2-9 fancm-11* double mutant (4.91±0.17) in comparison with the *pch2-9* (3.98±0.26, p>0.01) and *fancm-11* plants (p<0.0001).

Table 5. 9. Results of the Games-Howell's test comparing the number of univalent pairs per cell between the *pch2-9 fancm-11* double and single mutants.

	pch2-9	
fancm-11	-	***fancm-11***
pch2-9 fancm-11	**	****

**p<0.01, ****p<0.0001

The chromosome configurations were also studied in the *pch2-9 fancm-11* double mutant plants and compared with the single mutant and WT control plants (Table 5.10). In the first place, regarding the number of ring bivalents per cell, significant differences were found between the four genotypes (Welch's One-Way ANOVA,

W=245.8 [3.000,112.2]). The following pairwise comparisons test (Dunnet's T3) showed that the number of ring bivalents per cell was significantly lower in the *pch2-9 fancm-11* plants (1.58±0.11) in comparison with the *fancm-11* mutant plants (p<0.0001) and the WT control (p<0.0001). By contrast, no differences were found when compared to the single mutant *pch2-9* (p=0.3370). Secondly, the Welch's One-Way ANOVA test of the number of rod bivalents per cell also showed that significant differences were present among the *pch2-9 fancm-11* double mutant, the single, and the WT plants (W=7.265 [3.000, 277.0], p<0.001). Subsequently, the multiple comparisons test (Dunnet's T3) revealed that the *pch2-9 fancm-11* double mutant presented a significantly lower number of rod bivalents per cell (3.51±0.15) than the *pch2-9* (4.15±0.21; p<0.05) and WT control (p<0.001) plants, but not with respect to the *fancm-11* plants (p=0.9908).

Table 5. 10. Results of the Dunnet'sT3 test comparing the number of ring and rod bivalents per cell between the *pch2-9 fancm-11* double mutant, the single mutants and the WT control.

Ring bivalents per cell				Rod bivalents per cell			
	WT (R-o-18)				WT (R-o-18)		
pch2-9	-	***pch2-9***		***pch2-9***	-	***pch2-9***	
fancm-11	-	-	***fancm-11***	***fancm-11***	-	-	***fancm-11***
pch2-9 fancm-11	****	**N.S.**	****	***pch2-9 fancm-11***	***	*	**N.S.**

*****p<0.05, ***p<0.001, ****p<0.0001. **N.S.** Non-Significant

The combination of the axis remodelling defective *pch2-9* mutation with the class II anti-recombinase defective *fancm-11* background resulted in a significant decrease of the chiasma frequency per cell in the double mutants. In this manner, CO formation was examined with greater detail through the immunolocalisation of the ZMM protein HEI10 in the *pch2-9 fancm-11* plants, comparing it to that of the single

mutant *pch2-9* (Fig 5.2.A,B). The statistical analysis of the number of HEI10 foci per cell revealed that no significant differences were present between the two genotypes (*pch2-9*: 7.31±0.56, n=61, *pch2-9 fancm-11*: 8.02±0.63, n=54*;* Welch's T-test, t=0.8432, df=109.7, p=0.40). This suggests that the decrease in the chiasma frequency per cell observed in the double mutant *pch2-9 fancm-11* with respect to the single mutant *pch2-9* might not be due to a lower number of class I COs but to a decrease in class II CO formation.

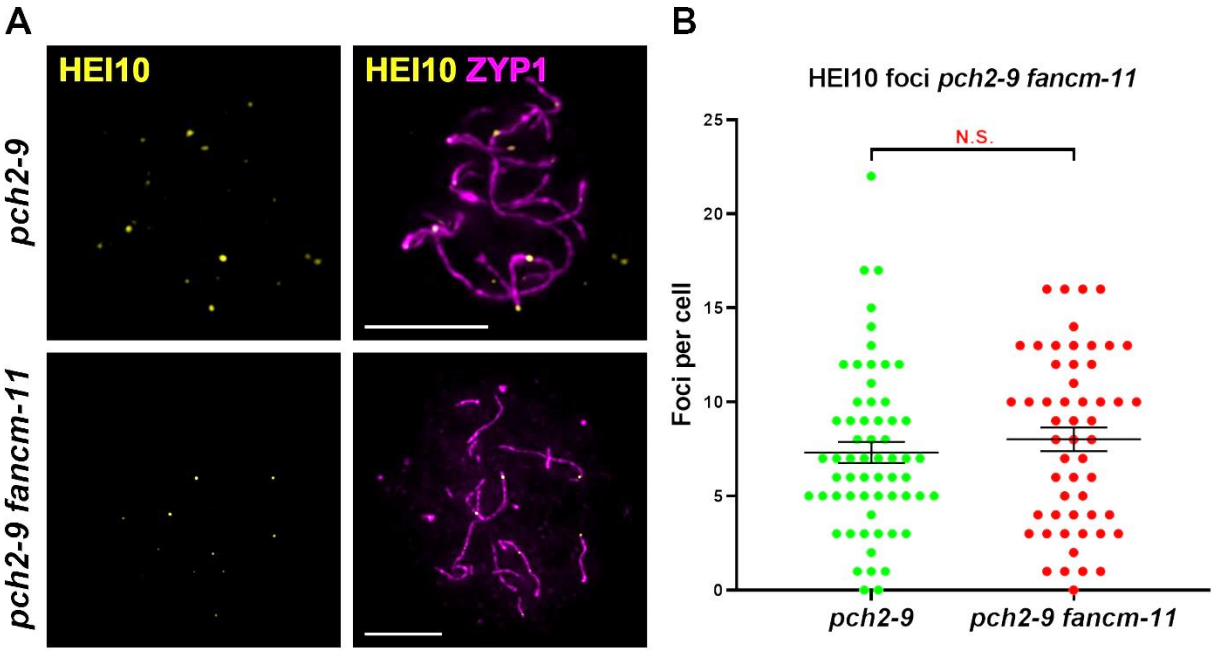


Figure 5.3. HEI10 foci analysis in the *pch2-9 fancm-11* double mutant and the single mutant *pch2-9*. A. HEI10/ZYP1 double immunolocalization in late prophase I PMCs of *pch2-9 fancm-11* and *pch2-9* plants. 5 µm bars. **B.** Scatter plot showing the HEI10 foci counts per cell in *pch2-9 fancm-11* and *pch2-9*. The bars represent the mean and S.E.M. **N.S.** Non-significant.

5.2.2. The combination of axis defective backgrounds with the loss of function of the ZMM protein MSH4 results in almost complete abrogation of CO formation

The analysis of the chiasma frequency per cell in the double mutant *asy1-14 msh4-1*, in comparison with the single mutants *asy1-14*, and *msh4-1*, and the WT control revealed that significant differences were present within the group (Welch's One-Way ANOVA, W=1444 [3.000, 84.73, p<0.0001). The following Dunnet's T3 pairwise comparison among the genotypes (Table 5.11) showed that the *asy1-14 msh4-1* plants had a significantly lower chiasma frequency per cell (0.18±0.05, n=88) in comparison with the WT (p<0.0001), *asy1-14* (p<0.0001), and *msh4-1* (2.97±0.22, n=66; p<0.0001) plants as chiasma formation was almost completely abrogated in the double mutant. The later also showed a great decrease of the chiasma frequency per cell with respect to the WT control (p<0.0001), concurring with the previous results from Blary *et al.* (2018).

Table 5.11. Summary of the Dunnet'sT3 test outcome comparing the chiasma frequency per cell between the *asy1-14 msh4-1* double mutant, the single mutants, and the WT control.

	WT		
asy1-14	-	***asy1-14***	
msh4-1	****	-	***msh4-1***
asy1-14 msh4-1	****	****	****

****p<0.0001

Following the analysis of the chiasma frequency a study of the number of univalent pairs per cell was carried out in the double mutant *asy1-14 msh4-1*, comparing it to the single mutants (Table 5.12). In this way, significant differences were found between the *asy1-14 msh4-1*, *asy1-14*, and *msh4-1* plants (Welch's One-Way

ANOVA, W=131.3 [2.000, 88.41], p<0.0001). The subsequent Games-Howell's multiple comparisons test showed that the double mutant *asy1-14 msh4-1* presented a significant increase of the number of univalent pairs per cell (9.85±0.04) with respect to the single mutants *asy1-14* (p<0.0001), and *msh4-1* (7.39±0.18, p<0.0001), in agreement with the decrease in chiasma formation previously observed (Table 5.11).

Table 5.12. Results of the Games-Howell's test comparing the number of univalent pairs per cell between the *asy1-14 msh4-1* double mutant and the single mutants.

	asy1-14	
msh4-1	-	***msh4-1***
asy1-14 msh4-1	****	****

****p<0.0001

The bivalent conformations were also studied in the *asy1-14 msh4-1* to analyse how the decrease in chiasma formation was influencing the formation of ring and rod bivalents (Table 5.13). In this way, starting with the analysis of ring bivalents per cell, the Welch's One-Way ANOVA test reported that significant differences were present between the genotypes analysed (W=203.8 [3.000, 82.44]). Next, the pairwise comparison amongst the genotypes (Dunnet's T3 test) showed that the *asy1-14 msh4-1* double mutant had a significantly lower number of ring bivalents per cell (0.01±0.01) than the WT control (p<0.0001) and the *msh4-1* single mutant (0.22±0.06, p<0.01). Also, the single mutant *msh4-1* presented a significant decrease in the number of ring bivalents per cell in comparison with the WT plants (p<0.0001). By contrast, no differences were found with respect to the single mutant *asy1-14* (p=0.08) as ring bivalents were almost completely absent in both genotypes. The

analysis of rod bivalents per cell in the *asy1-14 msh4-1* plants showed similar results. In this way, significant differences were found between the double mutant, the WT control, and the single mutants (Welch's One-Way ANOVA, W=198.1 [3.000, 85.11], p<0.0001). The subsequent Dunnet's T3 multiple comparisons test revealed that, in agreement with the decrease in chiasma formation observed in *asy1-14 msh4-1*, the number of rod bivalents per cell (0.14±0.04) was significantly lower with respect to the WT (p<0.0001), *asy1-14* (p<0.0001), and *msh4-1* plants (2.38±0.17, p<0.0001). The later also showed a significant reduction of the number of rod bivalents per cell in comparison with the WT control (p<0.0001).

Table 5.13. Results of the Dunnet'sT3 test comparing the number of ring and rod bivalents per cell between the *asy1-14 msh4-1* double mutant, the single mutants, and the WT control.

Ring bivalents per cell			
	WT (R-o-18)		
asy1-14	-	***asy1-14***	
msh4-1	****	-	***msh4-1***
asy1-14 msh4-1	****	**N.S.**	****

Rod bivalents per cell			
	WT (R-o-18)		
asy1-14	-	***asy1-14***	
msh4-1	****	-	***msh4-1***
asy1-14 msh4-1	****	****	****

****p<0.0001. **N.S.** Non-significant

The analysis of chiasma formation, univalent pairs per cell and bivalent configuration in the *asy3-2 msh4-1* double mutant showed a similar phenotype as the one observed in *asy1-14 msh4-1.*

In this way, starting with the analysis of the chiasma frequency per cell (Table 5.14), the Welch's One-Way ANOVA test revealed that significant differences were present between the genotypes studied (W=1216 [3.000,157.7], p<0.0001). The following pairwise comparisons between the genotypes (Dunnet's T3 test), showed that the

asy1-14 msh4-1 double mutant presented a significant decrease in chiasma formation (0.09±0.03, n=86) in comparison with the WT (p<0.0001), *asy3-2* (p<0.0001), and *msh4-1* plants (p<0.0001) as chiasmata were almost entirely absent (Table 5.1). This result concurs from previous reports from the *asy3 msh4* double mutant of *A. thaliana*, in which chiasma formation was completely abolished (Ferdous *et al.*, 2012).

Table 5.14. Summary of the Dunnet'sT3 test comparing the chiasma frequency per cell between the *asy3-2 msh4-1* double mutant, the single mutants, and the WT control.

	WT (R-o-18)		
asy3-2	-	***asy3-2***	
msh4-1	-	-	***msh4-1***
asy3-2 msh4-1	****	****	****

****p<0.0001

Similarly, the number of univalent pairs per cell was studied in the double mutant *asy3-2 msh4-1*, comparing it to the single mutants *asy3-2* and *msh4-1*. The statistical analysis revealed that significant differences were present among the genotypes studied (Welch's One-Way ANOVA, W=176.2 [2.000, 160.3], p<0.0001). Next, the Dunnet's T3 *post-hoc* test was used conduct pairwise comparisons between the genotypes (Table 5.15). This revealed that the *asy3-2 msh4-1* plants presented a significant increase in the number of univalent pairs per cell (9.91±0.03) in comparison with the *asy1-14* (p<0.0001) and the *msh4-1* plants (p<0.0001), in accordance with the decrease in chiasma formation previously observed.

Table 5.15. Results of the Games-Howell's test comparing the number of univalent pairs per cell between the *asy3-2 msh4-1* double and single mutants.

	asy3-2	
msh4-1	-	***msh4-1***
asy3-2 msh4-1	****	****

****p<0.0001

The chromosome configuration analysis also revealed substantial changes in the double mutant *asy3-2 msh4-1* with respect to the *asy3-2*, *msh4-1*, and WT plants (Table 5.16). In this way, the formation of ring bivalents was completely abolished in all the *asy3-2 msh4-1* metaphase I meiocytes analysed, and thus no statistical analysis was conducted. Similarly, the formation of rod bivalents in the *asy3-2 msh4-1* double mutant plants was severely compromised as it was also observed in the *asy1-14 msh4-1* double mutant. In this manner, significant differences were found between the genotypes studied (W=232.8 [3.000, 94.25], p<0.0001). The pairwise comparisons test (Dunnet's T3) showed that, in agreement with the decrease in the chiasma frequency per cell, the *asy3-2 msh4-1* plant also presented a significant reduction in the number of rod bivalents per cell (0.09±0.03) with respect to the single mutants *asy1-14* (p<0.0001) and *msh4-1* (p<0.0001), and the WT plants (p<0.0001).

Table 5.16. Results of the Dunnet'sT3 test comparing the number of rod bivalents per cell between the *asy3-2 msh4-1* double mutant, the single mutants and the WT control.

Rod bivalents per cell

	WT (R-o-18)		
asy3-2	-	***asy3-2***	
msh4-1	-	-	***msh4-1***
asy3-2 msh4-1	****	****	****

****p<0.0001

Finally, the last double mutant to be analysed was *pch2-9 msh4-1,* which combined the defects in the axis remodelling with the loss of function of the pro-class I CO ZMM protein MSH4. The analysis of the chiasma frequency per cell in this double mutant in comparison with the single mutants and the WT control revealed significant differences among the four genotypes (Welch's One-Way ANOVA, W=683.3 [3.000, 134.7], p<0.0001). Subsequently, the Dunnet's T3 multiple comparisons test (Table 5.17) showed that the *pch2-9 msh4-1* double mutant plants presented a significantly lower chiasma frequency per cell (1.51±0.20, n=114) in comparison with the *pch2-9* (p<0.0001), *msh4-1* (p<0.0001), and WT control plants (p<0.0001). Thus, this result suggests that the majority of COs in the *pch2-9* mutant belong to the class I, as only a small fraction of the total remained in the *pch2-9 msh4-1* double mutant. This concurs with the results of the HEI10 immunolocalisation of section 3.4.5, which showed that despite being reduced, the majority of COs remaining in the absence of PCH2 in *B. rapa*, belong to the class I.

Table 5.17. Summary of the Dunnet'sT3 test outcome comparing the chiasma frequency per cell between the *pch2-9 msh4-1* double mutant, the single mutants, and the WT control.

	WT (R-o-18)		
pch2-9	-	***pch2-9***	
msh4-1	-	-	***msh4-1***
pch2-9 msh4-1	****	****	****

****p<0.0001

The decrease in the chiasma frequency per cell was translated into changes in the number of univalent pairs in the *pch2-9 msh4-1* metaphase I meiocytes when compared to the *pch2-9* and *msh4-1* single mutants, and the WT control as was

revealed by the statistical analysis (Welch's One-Way ANOVA, W=112.7 [2.000,179.0], p<0.0001). In this manner, the following Games-Howell's *post-hoc* test (Table 5.18) reported that, in agreement with the reduction chiasma formation, the *pch2-9 msh4-1* plants presented a significant increase in the number of univalent pairs per cell (8.68±0.17) with respect to the *pch2-9* (p<0.0001), *msh4-1* (p<0.0001), and WT plants (p<0.0001).

Table 5.18. Results of the Games-Howell's test comparing the number of univalent pairs per cell between the *pch2-9 msh4-1* double mutant and the single mutants.

	pch2-9	
msh4-1	-	***msh4-1***
pch2-9 msh4-1	****	****

****p<0.0001

Bivalent configurations were also studied in the *pch2-9 msh4-1* double mutant to analyse the effects of the decrease in chiasma formation in the numbers of ring and rod bivalents per cell (Table 5.19). In the first place, the statistical analysis of ring bivalent formation revealed significant differences between the genotypes analysed (Welch's One-Way ANOVA, W=217.8 [3.000, 106.5], p<0.0001). In this way, the pairwise comparison test (Dunnet's T3; Table 5.19) showed that the *pch2-9 msh4-1* plants presented a significant decrease in the number of ring bivalents per cell (0.15±0.04) when compared to the WT (p<0.0001) and *pch2-9* plants (p<0.0001). However, no changes were found with respect to the *msh4-1* single mutant (p=0.6161), as the formation of ring bivalents was greatly compromised in both cases. Similarly, the Welch's One-Way ANOVA test of the number of rod bivalents per cell in the double, single mutant, and WT plants revealed that differences were

present within the group (W=75.88 [3.000, 128.9], p<0.0001). The following Dunnet's T3 multiple comparisons test showed that accordingly with the decrease in the chiasma frequency, the number of rod bivalents per cell was greatly reduced in the *pch2-9 msh4-1* double mutant (1.17±0.15) in comparison with the *pch2-9* (p<0.0001), *msh4-1* (p<0.0001), and the WT plants (p<0.0001).

Table 5.19. Results of the Dunnet'sT3 test comparing the number of ring and rod bivalents per cell between the *pch2-9 msh4-1* double mutant, the single mutants, and the WT control.

Ring bivalents per cell				Rod bivalents per cell			
	WT (R-o-18)				**WT (R-o-18)**		
pch2-9	-	***pch2-9***		***pch2-9***	-	***pch2-9***	
msh4-1	-	-	***msh4-1***	***msh4-1***	-	-	***msh4-1***
pch2-9 msh4-1	****	**N.S.**	****	***pch2-9 msh4-1***	****	****	****

****p<0.0001. **N.S.** Non-Significant

5.3. Discussion

In this chapter, the relation between CO formation and the structure of the meiotic chromosome axis and its remodelling has been explored by means of the cytological analysis of double mutants. This analysis revealed that Class II COs might be greatly dependant in the AEs and their remodelling. These results are further discussed in chapter 6.

5.2.1. The combination of a FANCM defective background with mutations disrupting the axis-associated proteins ASY1/3, and the AAA ATPase PCH2 results in further defects in CO formation.

The cytological analysis of meiosis of the *asy1-14 fancm-11, asy3-2 fancm-11,* and the *pch2-9 fancm-11* double mutants has revealed that: i) the hyper-recombinant phenotype of the loss of function of FANCM is lost when combined with mutations that affect the meiotic chromosome axis structure and its remodelling; ii) the loss of the inhibition mechanisms of class II CO formation in an axis defective context leads to further defects in chiasma formation.

In this way, the analysis of the chiasma frequency per cell in these double mutants showed a reduction of around one chiasma per cell on average in all of them in comparison with their respective *asy1-14, asy3-2,* and *pch2-9* double mutants. This was also translated in a higher increase in the number of univalent pairs per cell observed in these mutants with respect to the single mutants, indicating further defects in bivalent formation. Moreover, this also had an impact in the chromosome configurations observed in the double mutants analysed. In this way, in the case of the *asy1-14 fancm-11* and *asy3-2 fancm-11* double mutants, the number of rod bivalents per cell was reduced with respect to the single mutants *asy1-14* and *asy3-*

2, which correlates with the increase in the number of univalents observed. By contrast, no differences in the number of ring bivalents per meiocyte were observed as these were almost completely absent in both, single and double mutants. On the other hand, the formation of both, ring and rod bivalents, was further decreased in the *pch2-9 fancm-11* double mutant with respect to the *pch2-9* line.

Moreover, the formation of class I COs was examined in closer detail in the *pch2-9 fancm-11* double mutant through the immunolocalization of the HEI10 ZMM protein, involved in CO formation. This revealed that despite showing a decrease in chiasma formation, the number of class I COs remained stable in this genotype, suggesting that a reduction in class II CO formation could be the behind these differences observed between the single and double mutants.

Altogether, these results suggest that the formation of class II COs is greatly impaired in situations where the AE composition or its remodelling are altered. In this way, it could be hypothesised that the FANCM-limited class II COs cannot be formed in the absence of a functional axis. Thus, it is possible that in these double mutants, the class II CO route limited by FANCM is overexpressed, sequestering intermediates that otherwise would have been resolved as COs by other class II CO pathways. Nevertheless, these intermediates are not able to be resolved as COs due to the lack of functional AEs, resulting in a slight decrease in chiasma formation. Moreover, the fact that no chromosome fragmentation is observed indicates that the intermediates are eventually resolved, most likely through IS repair or dHj resolution as SDSA and Class II CO formation are abolished in these mutants. An alternative explanation could be that the absence of FANCM results in a change in the distribution of COs. In this manner, more closely located COs that could not be distinguished as chiasmata,

resulting in an overall decrease of chiasma formation together with a further increase in the number of univalent pairs observed. This explanation fits with the results recently published by Li *et al.* (2021), who observed that in the absence of the class II anti-recombinases FANCM, FIGL1 and RM1, class I CO distribution was altered, resulting in closely located COs.

5.2.2. MSH4-dependant class I COs account for the vast majority of COs in *asy1-14, asy3-2*, and *pch2-9*

The cytological analysis of *asy1-14 msh4-1, asy3-2 msh4-1,* and *pch2-9 msh4-1* has revealed that most of the COs formed when the structure and remodelling of the AEs is compromised belong to the interference-sensitive class I. In this manner, in the *asy1-14 msh4-1*, and *asy3-2 msh4-1* double mutants, the formation of COs between the homologous chromosomes is almost completely abolished as the chiasma frequency per cell is close to zero. These results concur with previous observations of the *asy3 msh4-1* double mutant of *A. thaliana*, in which CO formation seemed to be completely abrogated (Ferdous *et al.*, 2012). The severe lack of chiasma formation observed in these double mutants results in an almost complete absence of bivalent formation.

Similarly, the *pch2-9 msh4-1* double mutant suffered a great decrease in chiasma formation, concurring with the lack of class I COs due to the depletion of the ZMM protein MSH4. Moreover, the remaining chiasmata in this double mutant coincide with the difference observed in the single mutant *pch2-9* between the number of HEI10 foci per cell and the chiasma frequency per cell. This further confirms the results obtain in the characterisation of *pch2-9* in chapter 3.

In addition, the results of the analysis of these double mutants further suggest the idea previously mentioned that in the double mutants with a *fancm-11* background, the distribution of class I COs might be altered since the remaining CO in *asy1-14, asy3-2*, and *pch2-9* belong to the class I.

Chapter 6. General Discussion

In this thesis, we have produced a detailed characterisation of the meiotic role of the AAA+ ATPase PCH2 orthologs of both, *B. rapa* and *B. oleracea*; and of the coiled-coil domain protein ASY3 in *B. rapa.* Moreover, the relation between the axis-associated components, axis remodelling, and the formation of COs has also been investigated. In this chapter, the implications of the results obtained are fully discussed, set in the context of research in plant meiosis, and future lines of research are proposed to try to answer the new interrogates that have arisen.

6.1. PCH2 is a key axis remodelling factor in plant meiosis

The analysis of PCH2 in *B. rapa* and *B. oleracea* has revealed that the functions of this protein in meiosis are conserved in general lines across different taxa. In this way, the analysis of meiosis in DAPI spreads of PMCs of the *braA.pch2-9* and *boC.pch2-1* mutants showed that PCH2 is essential for the correct progression of meiosis in both *Brassica* species. In the first place, the absence of pachytene stages pointed out defects in synapsis, and the defects in bivalent formation and chromosome segregation suggested that CO formation was also compromised in these mutants. Secondly, the detailed analysis of chiasma formation in these lines confirmed this phenotype as the mean chiasma frequency per cell was greatly reduced in *braA.pch2-9* and *boC.pch2-1*. This already revealed some differences in terms of CO formation between both PCH2 orthologs as *boC.pch2-1* showed a greater decrease in the mean chiasma frequency per cell (~88%), than *braA.pch2-9* (~42%), suggesting a more critical role of PCH2 in CO formation in *B. oleracea*. This was further confirmed through the immunolocalisation of the ZMM protein HEI10, which showed that class I COs were the main class of COs in both species, and that

their formation was severely defective in both mutants, also corroborating a differential need for PCH2 in Class I CO formation between both species.

In addition, the function of PCH2 in the establishment of synapsis between the homologs was further analysed through the immunolocalisation of the TF protein ZYP1, and the careful measure of the total SC extension per cell in both mutant lines: *braA.pch2-9* and *boC.pch2-1.* In a first instance, this analysis revealed that SC polymerisation was greatly reduced in the absence of PCH2 in both species of *Brassica*. Moreover, this also showed a more severe phenotype in *boC.pch2-1* than in *braA.pch2-9*, as the reductions in the total SC length were ~88% and ~62%. Interestingly, the differences in SC extension also correlated with the ones in chiasma formation, further confirming the more severe phenotype of *boC.pch2-1*. However, this does not necessarily mean that one is the cause of the other, as SC polymerisation is not essential for CO formation as demonstrated by the analysis of *zyp1* mutants in *A. thaliana* (Higgins *et al.*, 2005; Capilla-Pérez *et al.*, 2021; France *et al.*, 2021). Thus, most likely they have a common origin as explained below.

Further analysis of the role of PCH2 in axis remodelling was carried out in the *boC.pch2-1* mutant through the analysis of the signal intensities of ASY1 and SMC3 in synapsed and non-synapsed regions of WT and mutant plants. This revealed that in the absence of PCH2 the axis-associated protein ASY1 is not depleted from the synapsed areas, also showing greater signal intensity. Moreover, ASY1 also appeared dottier and more disorganised in the non-synapsed axes in *boC.pch2-1*, suggesting loading defects. Interestingly, the analysis of the signal intensity of the cohesin SMC3 suggested abnormal chromosome condensation as, similar to ASY1, its intensity appeared to be higher in the synapsed regions of the *boC.pch2-1* mutant.

Finally, to try to find an explanation for the defects in recombination and SC formation observed in *boC.pch2-1* an analysis of DSB formation was conducted to test whether the formation of this early recombination intermediates was defective as in the *crc1* mutants of rice (Miao *et al.*, 2013). Nevertheless, the immunolocalisation of the DSB marker γH2AX (phosphorylation of the H2AX histone variant) did not reveal defects in the formation of DSBs, but in their processing as a greater foci number was observed in the late prophase I cells of the mutant.

Despite showing different degrees of severity, the phenotypes observed in the *pch2* mutants of *B. rapa* and *B. oleracea* are similar to the one described for the *pch2* mutant of *A. thaliana*, which presented a 40% decrease in chiasma formation, a 68% reduction in the total SC length, and no depletion of ASY1 from the synapsed areas (Lambing *et al.*, 2015). This indicates that, although there might be different requirements of PCH2 depending on the organism, it seems to accomplish the same functions in the three of them. By contrast, the *crc1* mutant of rice presents a much more severe phenotype as chiasma formation, SC polymerisation, and PAIR2 (ASY1 ortholog) axis association are completely abrogated. However, this difference is due to the absence of DSB formation observed in this mutant. In this way, it seems that PAIR2 loading is essential for DSB formation in rice as CO formation is completely abolished in the *pair2* mutants (Miao *et al.*, 2013). The phenotype of the mutants for the different PCH2 orthologs described in plants are summarised in Table 6.1.

Table 6.1. Summary of the mutant phenotypes of different PCH2 orthologs described in plants

Mutant	CO formation (% of WT)	SC extension (% of WT)	ASY1/PAIR2 loading	DSB formation	References
boC.pch2-1	~12%	~12%	defective	Yes	This thesis
braA.pch2-9	~50%	~38%	defective	?	This thesis; Cuacos *et al.*, 2021
atpch2-1	~70%	~32%	defective	Yes	Lambing *et al.*, 2015; Yang *et al.*, 2020
oscrc1	0%	0%	absent	No	Miao *et al.*, 2013

The different phenotypes observed in the *pch2* mutants of the different species in which it has been analysed could be explained as the consequence of the role of PCH2 in ASY1 axis loading during early prophase I and the function of ASY1 in stabilising DMC1 to facilitate the IH Bias, or in DSB formation in the case of rice (Sanchez-Moran *et al.*, 2007; Miao *et al.*, 2013). In this way, in *B. rapa, B. oleracea* and *A. thaliana*, in the absence of PCH2 the loading of ASY1 during the early stages of prophase I is defective as it cannot transition from an inactive closed configuration to an active open conformation (Yang *et al.*, 2020). Thus, if ASY1 cannot be loaded in an adequate and stable way to the AEs, the recombinase DMC1 would become unstable as described by Sanchez-Moran *et al.* (2007). As a consequence, the processes of pairing, synapsis and CO formation would be compromised since DMC1 is responsible of establishing the IH Bias by catalysing the SEI towards the homolog, which is necessary for pairing and recombination (Da Ines *et al.*, 2012). The DSBs would then be repaired with the sister chromatid as the IH Bias cannot be established. This is supported by the phenotype of the *hop1* mutant in yeast, where IHR is greatly diminished in favour of IS repair (Hollingsworth and Byers, 1989b).

This explanation can also account for the differences in the severity of the mutant phenotype observed between *B. oleracea, B. rapa* and *A. thaliana* (Fig. 6.1). In this way, whereas in the WT situation the pool of ASY1 molecules in open and closed conformation is displaced towards an open active form by PCH2, in the mutants there is a balance between both due to the spontaneous changes in the conformation leading to lower levels of available O-ASY1. In the case of the *pch2* mutants of *B. rapa* and *A. thaliana* this equilibrium is enough to reach between 50-70% of WT levels of CO formation and 38-32% of total SC extension, respectively (Lambing *et al.*, 2015; Cuacos *et al.*, 2021; this thesis). On the other hand, in *B. oleracea* the balance between the open and closed conformations of ASY1 in the absence of PCH2 would be displaced towards a closed inactive conformation, leading to lower levels of CO formation (~12% of WT) and SC polymerisation (~12% of WT).

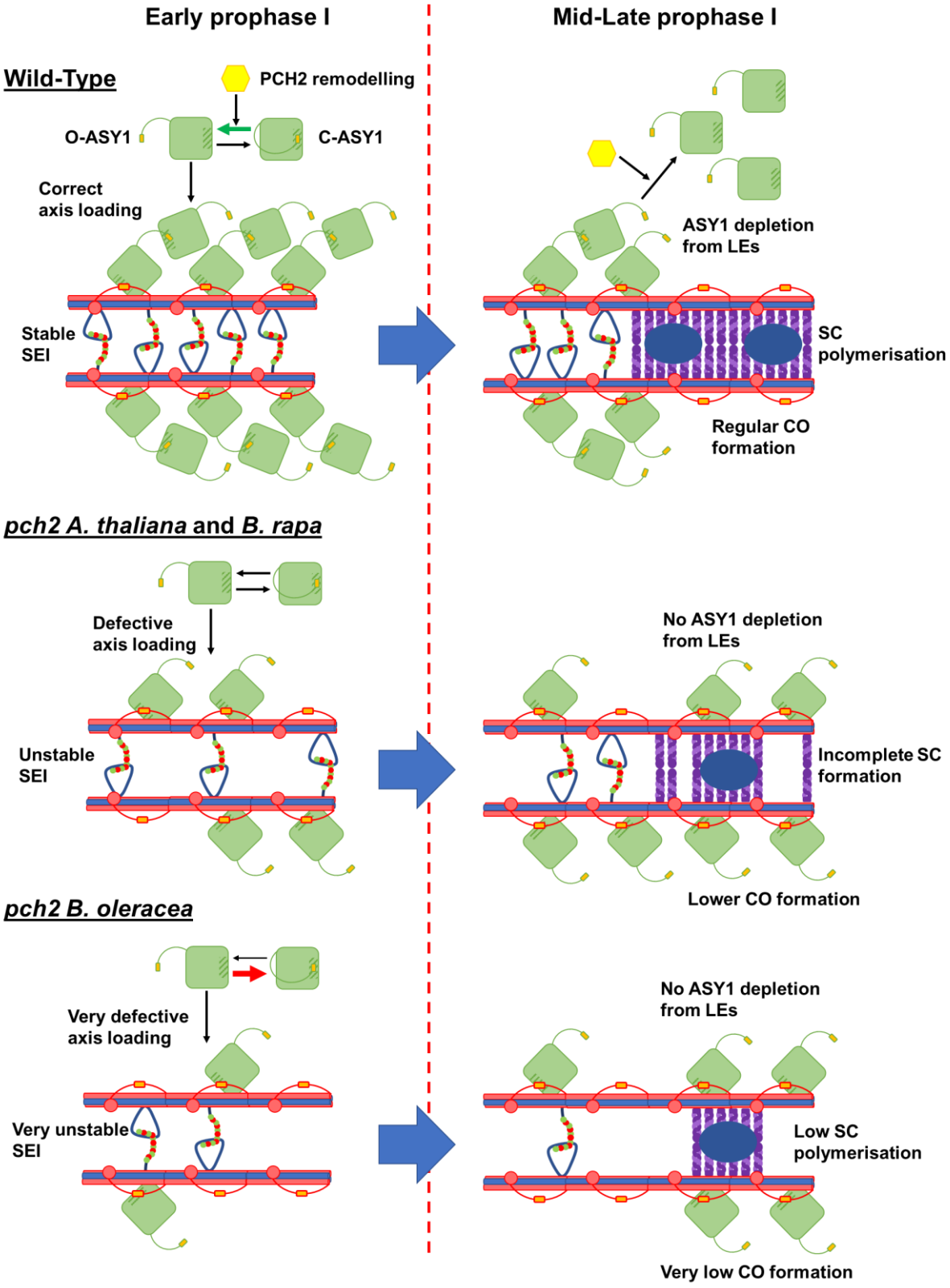


Figure 6.1. Proposed model of differential ASY1 loading in the *pch2* mutants of *A. thaliana*, *B. rapa*, and *B. oleracea*

6.2. *B. rapa* ASY3 ortholog is essential for meiosis progression

The identification and cytological characterisation of the ASY3 ortholog of *B. rapa* revealed that the functions of this axis-associated coiled-coil domain protein are conserved, also showing some differences with respect to the *A. thaliana* and yeast orthologs. In this way, the *braA.asy3* mutant lines presented complete sterility as they were unable to set seed. Further cytological analysis revealed that this was due to a severe disruption of meiosis. This consisted of an absence of meiocytes in the pachytene stage, which pointed out to defects in SC polymerisation, and more importantly, an almost complete abrogation of bivalent formation that resulted in missegregation of the chromosomes due to the inability of establishing COs between the homologs. As shown by the chiasma frequency analysis and the immunolocalisation of the ZMM protein HEI10, CO formation was greatly reduced, and the few remaining COs belonged to the Class I. This was further confirmed in the *braA.asy3-2 braA.msh4* double mutant in which chiasma formation was almost completely absent. These results showed that ASY3 is essential for the formation of both classes of COs. Interestingly, by contrast with the results of the HEI10 immunolocalisation in the *braA.asy1* mutant published by Cuacos *et al.* (2021), no foci were observed that did not colocalise with an SC signal.

The immunolocalisation of the axis-associated protein ASY1 and the TF protein ZYP1 in the *braA.asy3-2* mutant further confirmed the conserved role of ASY3 in *B. rapa*. In this way, ASY1 could not properly localise to the AEs in the absence of ASY3 as its signal appeared fuzzy and disorganised, concurring with the results obtained by Ferdous *et al.* (2012) in *A. thaliana*. However, since ASY1 still appeared associated with the chromatin, although in a disorganised manner**,** we cannot rule

out that ASY1 might have an early association with the axis due to an interaction with its cohesin components that requires ASY3 for its stabilisation. This suggestion is supported by the results shown by Fujiwara *et al.* (2020) in the analysis of the chromosomal localisation of HORMAD1/2 in mice. Moreover, the ChiP-Seq analysis of ASY1 and REC8 carried out by Lambing *et al.* (2020) in *A. thaliana* revealed that both presented the same loading pattern along the chromosomes. However, further work needs to be done to elucidate the physical interactions between the axis associated proteins ASY1 and ASY3 with the cohesin REC8. Also, as previously shown in the *asy3* mutant of *A. thaliana* (Ferdous *et al.*, 2012), the polymerisation of the SC was completely abrogated, only appearing as foci and very short stretches in the *braA.asy3-2* mutant.

Altogether these results concur with previous analysis of the meiotic role of the axis-associated coiled coil domain protein ASY3 in *A. thaliana* and its respective orthologs in rice (PAIR3), maize (DSY2), budding yeast (RED1), and mouse (SYCP2)(Rockmill and Roeder, 1988b, 1990; Smith and Roeder, 1997; Yang *et al.*, 2006; Yuan *et al.*, 2009; K. Wang *et al.*, 2011; Ferdous *et al.*, 2012; Lee *et al.*, 2015). In this manner, in general the coiled-coil domain protein ASY3 is essential for: i) the correct axis association of ASY1; ii) the polymerisation of the SC; iii) CO formation between the homologs. However, it is worth to mention that in *B. rapa* no difference in terms of chiasma formation was observed between the *braA.asy1* and *braA.asy3* mutants. Moreover, the double mutant presented no difference with respect to either single mutant, suggesting that in *B. rapa* the axis association of ASY1 mediated by ASY3 is essential for CO formation. This, contrasts with the results previously obtained in *A, thaliana* which showed that ASY1 seems able to retain some pro-CO activity in the

absence of ASY3 as the *atasy3* single mutants show higher chiasma frequency than the *atasy1* mutant, and also the phenotype of *atasy1* is epistatic over the one of *atasy3* in the *atasy1 atasy3* double mutant (Ferdous *et al.*, 2012). Furthermore, no role in DSB formation has been observed for BraA.ASY3 as the mutant *braA.asy3-2* presented similar levels of DSB formation as the WT plants, opposite to the results found in *A. thaliana asy3* and yeast *red1* mutants (Xu, Weiner and Kleckner, 1997; Ferdous *et al.*, 2012). Moreover, as explained in section 4.3.2, the role of ASY3 in CO formation and SC polymerisation might be related to the function of the axis associated proteins in the establishment of the IH Bias. In this manner, in yeast meiosis the axis associated proteins HOP1 and RED1 are necessary to direct HR towards the homolog as in their absence, IHR is greatly diminished in favour of IS repair (Rockmill and Roeder, 1990). Moreover, RED1 seems to counteract the action of the meiosis-specific cohesion REC8, which promotes recombination with the sister chromatid (Kim *et al.*, 2010). In addition, following the same reasoning as in the previous section, ASY3 is needed for the correct localisation of ASY1 and the later was shown to stabilise the recombinase DMC1 (Sanchez-Moran *et al.*, 2007). Thus, an interesting possibility is that the defects in SC polymerisation and CO formation of the *asy3* mutants are due to the unstable load of DMC1 due to the defects in ASY1 axis association. In this way, if DMC1 is unstable, the SEI towards the homolog would be negatively affected, generating defects in pairing, synapsis and recombination as shown in the *dmc1* mutants (Couteau *et al.*, 1999; da Ines *et al.*, 2012; Da Ines *et al.*, 2013). This explanation could also account for the delay in DSB repair observed in the *braA.asy3* mutant. However, further research about the dynamics of DMC1 in this mutant needs to be conducted to confirm this hypothesis.

6.3. The formation of both classes of COs is severely compromised in the context of deficient AEs

The combination in *B. rapa* of mutations for the axis-associated proteins (ASY1 and ASY3) and for the axis remodelling ATPase PCH2 with genetic backgrounds presenting hyper-recombinant phenotypes as *fancm*, and defective for the formation of class I COs as *msh4,* has clarified the relation between the AEs and CO formation (Higgins *et al.*, 2004; Crismani *et al.*, 2012; Knoll *et al.*, 2012; Blary *et al.*, 2018).

In this way, the *asy1 fancm, asy3 fancm,* and *pch2 fancm* double mutants have revealed a critical role of the AEs in Class II CO formation as rather than presenting an increase in CO formation the chiasma frequency was significantly reduced in comparison with the single mutants. This was translated in higher numbers of univalents per meiocyte and changes in the bivalent configurations observed. Moreover, the immunolocalisation of HEI10 in the *pch2-9 fancm-11* double mutant revealed that the decrease in chiasma formation observed was not due to a reduction in Class I CO formation as their number remained unchanged with respect to the *pch2-9* single mutant. This suggested that the decrease in the chiasma frequency per cell reported in the double mutants with *fancm* was likely a result of further difficulties in CO formation depending on the context. In this way, Class I CO formation was decreased in *asy1 fancm* and *asy3 fancm*, whereas Class II CO formation was further impaired in *pch2 fancm*. In addition, these results could further confirm the role of the AEs in favouring the IH Bias. In this way, given that: i) no increase in CO formation is observed in these double mutants, ii) that the SDSA pathway is disrupted due to the absence of FANCM, iii) and that no fragmentation is observed in meiosis; the recombination intermediates must be repaired using the sister chromatid

as a template. An alternative possibility is that they are resolved as NCOs through dHj dissolution by the RTR complex (section 1.3.4.2). We disfavour this second possibility given that is in conflict with the decrease in CO and NCO formation of *hop1* and *red1* mutants in yeast, and the role of ASY1 in stabilising DMC1, which acts upstream to dHJ formation (Rockmill and Roeder, 1990; Sanchez-Moran et al., 2007).

The analysis of the *asy1-14 msh4-1*, *asy3-2 msh4-1,* and *pch2-9 msh4-1* double mutants revealed some key information about Class I CO formation in these mutants. In the first place**,** Class I COs are the vast majority of the COs present in *asy1-14*, *asy3-2,* and *pch2-9.* Concurring with the results of the HEI10 immunolocalisation in the *asy3-2* and *pch2-9* single mutants conducted in the chapters 3 and 4, and with the results obtained in the analyses if the *Arabidopsis asy3 msh4* double mutant and the *B. rapa asy1* mutant published by Ferdous *et al.* (2012) and Cuacos *et al.* (2021), respectively. However, it is worth to mention that whereas in the *asy1-14* and *asy3-2* mutants the remaining COs belonged only to the Class I, suggesting a completely absent Class II. In *pch2-9,* Class II CO formation seemed to be affected to a much lower extent as the chiasma frequency observed in the *pch2-9 msh4-1* double mutant correlated with the difference between the number of HEI10 foci and the chiasma frequency per cell in *pch2-9.* Altogether these results point out the essential role of the AEs and their remodelling in the formation of both classes of COs. In this way, as previously suggested in section 5.3.1, the decrease in the chiasma frequency per cell observed when axis defective backgrounds are combined with the depletion of the *FANCM* Class II anti-recombinase could be the result of the competition of both routes of CO formation for the same recombination intermediates. In this way, the

absence of FANCM would cause the overexpression of the Class II CO pathway, which could then subtract intermediates form the Class I pathway despite these are not eventually resolved as Class II COs since the AEs and their remodelling are defective in these double mutants. This could also be related to the defects in IHR observed in the absence of the axis-associated proteins as explained in previous sections. However, an alternative possibility could be that the absence of the anti-recombinase FANCM could be affecting the distribution of class I COs as recently found by Li *et al.* (2021a, 2021b). Thus, this could lead to more closely located COs that cannot be identified in the chiasma scoring, leading to lower chiasma frequencies in the mutants.

6.4. Future research

The results obtained in this thesis have raised some interesting new questions that could potentially led to future lines of research. In this way, it would be interesting to investigate the reasons for the differences observed between the *pch2* mutants of *B. oleracea*, *B. rapa*, and *A. thaliana*. One option would be to transform the *PCH2* copies of the two *Brassica* species in the *pch2* mutant of *A. thaliana.* This could give an idea of the extent to which PCH2 could have diverged in its functions in these species. Moreover, the ASY1 copies of *B. oleracea* and *B. rapa* could also be transformed in the *Arabidopsis asy1 pch2* mutant to study whether the differences between the phenotypes of the *pch2* mutants in these species are due to a higher dependence on PCH2 for the proper axis loading of ASY1 as proposed by the model described in section 6.1. Furthermore, this analysis could be complemented with a study of the structure of the AEs and the localisation of ASY1 in the different *pch2* mutants of *Arabidopsis* and *Brassica*. This could be achieved by means of super-

resolution microscopy, of which the techniques based on Single Molecule Localisation Microscopy (SMLM) such as the direct Stochastic Optical Reconstruction Microscopy (dSTORM), could be of great use as they reach resolutions of ~20nm and offer the possibility of analysing the stoichiometry of the molecule interactions. In addition, it would be of great interest to characterise in more detail the protein-protein interactions between the axis-associated proteins ASY1 and ASY3 and the cohesin REC8. This could be achieved through the combination of molecular techniques and cytological techniques as Y2H (Yeast-Two-Hybrid) and dSTORM super-resolution microscopy. Together these could shed some light on the interactions that take place within the AEs and the structures that they give rise. This could elucidate the reason behind the differences observed between the *asy3* mutants of *A. thaliana* and *B. rapa*, also confirming whether the HORMA domain protein ASY1 interacts with the cohesin axes as it has been suggested in other organisms as mouse (Fujiwara *et al.*, 2020). Moreover, as previously proposed for *PCH2* the transformation of the ASY1 and ASY3 orthologs of *B. rapa* in the *asy1 asy3* mutant of *A. thaliana* could show whether the differences between the phenotypes of both mutants are due to a higher dependency on the ASY3 mediated axis localisation of ASY1 to carry out its function in *B. rapa*. Finally, it would be interesting to further investigate the relation between the axis associated proteins and the IH Bias in plants, in particular, the putative interaction between ASY1 and the recombinase DMC1 as previously suggested in *A. thaliana* (Sanchez-Moran *et al.*, 2007). In this way, as the anti-recombinase FIGL1 has a role in limiting the SEI process by disassembling the RAD51/DMC1 nucleoprotein filament (Girard *et al.*,

2015), the combination of a *figl1* defective background with the depletion of ASY1 could shed light on this matter.

6.5. Conclusions

- PCH2 remodelling of ASY1 is essential for the establishment of synapsis and the formation of COs in *Brassica.*
- The depletion of PCH2 in *B. oleracea* leads to a more severe phenotype than that observed in *B. rapa* and *A. thaliana.*
- There are divergences in the requirement of PCH2 for ASY1 axis localisation, CO formation and synapsis among the Brassicaceae family.
- ASY3 is a key component of the meiotic chromosome axis in *Brassica rapa* with conserved functions in meiosis.
- ASY3 is not required for normal DSB formation in *B. rapa.*
- ASY3-mediated axis localisation of ASY1 is essential for its role in meiosis as both contribute equally to CO formation in *B. rapa.*
- The AEs and their remodelling are essential for the establishment of both classes of COs in plants.
- The hyper-recombinant phenotype resulting from the depletion of FANCM is lost when combined with mutations of AE component and remodelling proteins.
- CO formation is negatively affected when defects in axis-associated or axis remodelling proteins are combined with *fancm* hyper-recombinant backgrounds.
- Class I COs seem to be the main COs formed when the AE composition or its remodelling are defective.

References

Abe, K. *et al.* (2005) 'Arabidopsis RAD51C gene is important for homologous recombination in meiosis and mitosis', *Plant Physiology*, 139(2), pp. 896–908. doi: 10.1104/pp.105.065243.

Abraham, R. T. (2001) 'Cell cycle checkpoint signaling through the ATR and ATM kinases', *Genes and Development*. IEEE, 1(15), pp. 2177–2196. doi: 10.1109/ICISE.2010.5689338.

Acquaviva, L. *et al.* (2013) 'The COMPASS Subunit Spp1 Links Histne Methylation to Initiation of Meiotic Recombination', *Science*, 399, pp. 215–218. doi: 10.1007/7050.

Agarwal, S. and Roeder, G. S. (2000) 'Zip3 provides a link between recombination enzymes and synaptonemal complex proteins', *Cell*, 102(2), pp. 245–255. doi: 10.1016/S0092-8674(00)00029-5.

Albini, S. M. and Jones, G. H. (1987) 'Synaptonemal complex spreading in Allium cepa and A. fistulosum - I. The initiation and sequence of pairing', *Chromosoma*, 95(5), pp. 324–338. doi: 10.1007/BF00293179.

Alexandratos, N. and Bruinsma, J. (2012) *World agriculture towards 2030/2050. The 2012 revision*, *FAO*. doi: 10.1002/jso.2930300113.

Allers, T. and Lichten, M. (2001a) 'Differential timing and control of noncrossover and crossover recombination during meiosis', *Cell*, 106(1), pp. 47–57. doi: 10.1016/S0092-8674(01)00416-0.

Allers, T. and Lichten, M. (2001b) 'Intermediates of yeast meiotic recombination contain heteroduplex DNA', *Molecular Cell*, 8(1), pp. 225–231. doi: 10.1016/S1097-2765(01)00280-5.

Anderson, L. K. *et al.* (2014) 'Combined fluorescent and electron microscopic imaging unveils the specific properties of two classes of meiotic crossovers', *Proceedings of the National Academy of Sciences*, 111(37), pp. 13415–13420. doi: 10.1073/pnas.1406846111.

Armstrong, S. J. *et al.* (2002) 'Asy1, a protein required for meiotic chromosome synapsis, localizes to axis-associated chromatin in Arabidopsis and Brassica', *Journal of Cell Science*, 115(18), pp. 3645–3655. doi: 10.1242/jcs.00048.

Armstrong, S. J. *et al.* (no date) 'Asy1, a protein required for meiotic chromosome synapsis, localizes to axis-associated chromatin in Arabidopsis and Brassica', 115(18), pp. 3645–3655. doi: 10/bn7r3w.

Armstrong, S. J., Franklin, F. C. H. and Jones, G. H. (2001) 'Nucleolus-associated telomere clustering and pairing precede meiotic chromosome synapsis in Arabidopsis thaliana', *Journal of Cell Science*, 114(23), pp. 4207–4217. doi: 10.1525/bio.2010.60.7.5.

Armstrong, S. J., Franklin, F. C. H. and Jones, G. H. (2003) 'A meiotic time-course for Arabidopsis thaliana', *Sexual Plant Reproduction*, 16, pp. 141–149. doi: 10.1007/s00497-003-0186-4.

Asela J. Wijeratne *et al.* (2006) 'The Arabidopsis thaliana PARTING DANCERS Gene Encoding a Novel Protein Is Required for Normal Meiotic Homologous Recombination□', *Molecular Biology of the Cell*, 17, pp. 1331–1343. doi: 10.1091/mbc.E05.

Atcheson, C. L. *et al.* (1987) 'Isolation, DNA sequence, and regulation of a meiosis-specific eukaryotic recombination gene.', *Proceedings of the National Academy of Sciences of the United States of America*, 84(22), pp. 8035–8039. doi: 10.1073/pnas.84.22.8035.

Baker, S. M. *et al.* (1996) 'Involvement of mouse Mlh1 in DNA mismatch repair and meiotic crossing over', *Nature Genetics*, 13(3), pp. 336–342. doi: 10.1038/ng0796-336.

Balboni, M. *et al.* (2020) 'COMET Functions as a PCH2 Cofactor in Regulating the HORMA Domain Protein ASY1', *Current Biology*. Elsevier Ltd., 30(21), pp. 4113-4127.e6. doi: 10.1016/j.cub.2020.07.089.

Barakate, A. *et al.* (2014) 'The synaptonemal complex protein ZYP1 is required for imposition of meiotic crossovers in barley', *Plant Cell*, 26(2), pp. 729–740. doi: 10.1105/tpc.113.121269.

Baudat, F. *et al.* (2010) 'PRDM9 is a major determinant of meiotic recombination hotspots in humans and mice', *Science*, 327(5967), pp. 836–840. doi: 10.1126/science.1183439.

Bellani, M. A. *et al.* (2005) 'SPO11 is required for sex-body formation, and Spo11 heterozygosity rescues the prophase arrest of Atm-/- spermatocytes', *Journal of Cell Science*, 118(15), pp. 3233–3245. doi: 10.1242/jcs.02466.

Bennett, M. D. (1977) 'The time and duration of meiosis', *Phil. Trans. R. Soc. Lond. B*, 277, pp. 201–226.

Berchowitz, L. E. *et al.* (2007) 'The role of AtMUS81 in interference-insensitive crossovers in A. thaliana', *PLoS Genetics*, 3(8), pp. 1355–1364. doi: 10.1371/journal.pgen.0030132.

Bergerat, A. *et al.* (1997) 'An atypical topoisomerase II from archaea with implications for meiotic recombination', *Nature*, 386(27), pp. 414–417. doi: 10.1038/386414a0.

Bhalla, N. and Dernburg, A. F. (2005) 'A Conserved Checkpoint Monitors Meiotic Chromosome Synapsis in Caenorhabditis elegans', *Science*, 310(5754), pp. 1683–1687.

Bhatt, A. M. *et al.* (1999) 'The DIF1 gene of Arabidopsis is required for meiotic chromosome segregation and belongs to the REC8/RAD21 cohesin gene family', *Plant Journal*, 19(4), pp. 463–472. doi: 10.1046/j.1365-313X.1999.00548.x.

Bishop, D. K. *et al.* (1992) 'DMC1: A meiosis-specific yeast homolog of E. coli recA required for recombination, synaptonemal complex formation, and cell cycle progression', *Cell*, 69(3), pp. 439–456. doi: 10.1016/0092-8674(92)90446-J.

Blary, A. *et al.* (2018) 'FANCM Limits Meiotic Crossovers in Brassica Crops', *Frontiers in Plant Science*, 9(March), pp. 1–13. doi: 10.3389/fpls.2018.00368.

Blary, A. and Jenczewski, E. (2019) 'Manipulation of crossover frequency and distribution for plant breeding', *Theoretical and Applied Genetics*. Springer Berlin Heidelberg, 132(3), pp. 575–592. doi: 10.1007/s00122-018-3240-1.

Blat, Y. *et al.* (2002) 'Physical and functional interactions among basic chromosome organizational features govern early steps of meiotic chiasma formation', *Cell*, 111(6), pp. 791–802. doi: 10.1016/S0092-8674(02)01167-4.

Bleuyard, J. Y. *et al.* (2005) 'Differing requirements for the Arabidopsis Rad51 paralogs in meiosis and DNA repair', *Plant Journal*, 41(4), pp. 533–545. doi: 10.1111/j.1365-313X.2004.02318.x.

Bleuyard, J. Y., Gallego, M. E. and White, C. I. (2004) 'Meiotic defects in the Arabidopsis rad50 mutant point to conservation of the MRX complex function in early stages of meiotic recombination', *Chromosoma*, 113(4), pp. 197–203. doi: 10.1007/s00412-004-0309-1.

Bleuyard, J. Y. and White, C. I. (2004) 'The Arabidopsis homologue of Xrcc3 plays an essential role in meiosis', *EMBO Journal*, 23(2), pp. 439–449. doi: 10.1038/sj.emboj.7600055.

Boateng, K. A. *et al.* (2008) 'SWI1 Is Required for Meiotic Chromosome Remodeling Events', *Molecular Plant*. The Authors 2008, 1(4), pp. 620–633. doi: 10.1093/mp/ssn030.

Boden, S. A. *et al.* (2007) 'Expression and functional analysis of TaASY1 during meiosis of bread wheat (Triticum aestivum)', *BMC Molecular Biology*, 8, pp. 1–14. doi: 10.1186/1471-2199-8-65.

Bohuon, E. J. R. *et al.* (1996) 'Alignment of the conserved C genomes of Brassica oleracea and Brassica napus', *Theoretical and Applied Genetics*, (93), pp. 833–839.

Bolaños-Villegas, P. *et al.* (2013) 'Arabidopsis CHROMOSOME TRANSMISSION FIDELITY 7 (AtCTF7/ECO1) is required for DNA repair, mitosis and meiosis', *Plant Journal*, 75(6), pp. 927–940. doi: 10.1111/tpj.12261.

Bolaños-Villegas, P. *et al.* (2017) 'In favor of establishment: Regulation of chromatid cohesion in plants', *Frontiers in Plant Science*, 8(May), pp. 1–12. doi: 10.3389/fpls.2017.00846.

Borde, V. *et al.* (2009) 'Histone H3 lysine 4 trimethylation marks meiotic recombination initiation sites', *EMBO Journal*, 28(2), pp. 99–111. doi: 10.1038/emboj.2008.257.

Borde, V. and de Massy, B. (2013) 'Programmed induction of DNA double strand breaks during meiosis: Setting up communication between DNA and the chromosome structure', *Current Opinion in Genetics and Development*, 23(2), pp. 147–155. doi: 10.1016/j.gde.2012.12.002.

Borner, G. V., Barot, A. and Kleckner, N. (2008) 'Yeast Pch2 promotes domainal axis organization, timely recombination progression, and arrest of defective recombinosomes during meiosis', *Proceedings of the National Academy of Sciences*, 105(9), pp. 3327–3332. doi: 10.1073/pnas.0711864105.

Botstein, D. *et al.* (1980) 'Construction of a Genetic Linkage Map in Man Using Restriction Fragment Length Polymorphisms', *Am J Hum Gen*, 32, pp. 314–331. Available at: papers2://publication/uuid/0B80518E-A22B-41F3-BE43-171F51007E42.

Boveri, T. (1893) 'Ein geschlechtlich erzeugter Organismus ohne mütterliche Eigenschaften. Gesel. für Morph. und Physiol. München 5: 73–83 (translated by T. H. Morgan 1893, as "An organ ism produced sexually without characteristics of the mother").', *Am. Nat.*, 27(315), pp. 222–232.

Cai, C. *et al.* (2017) 'Brassica rapa Genome 2.0: A Reference Upgrade through Sequence Re-assembly and Gene Re-annotation', *Molecular Plant*, 10(4), pp. 649–651. doi: 10.1016/j.molp.2016.11.008.

Cai, X. *et al.* (2003) 'The Arabidopsis SYN1 cohesin protein is required for sister chromatid arm cohesion and homologous chromosome pairing', *Journal of Cell Science*, 116(14), pp. 2999–3007. doi: 10.1242/jcs.00601.

Cao, L., Alani, E. and Kleckner, N. (1990) 'A pathway for generation and processing of double-strand breaks during meiotic recombination in S. cerevisiae', *Cell*, 61(6), pp. 1089–1101. doi: 10.1016/0092-8674(90)90072-M.

Capilla-Pérez, L. *et al.* (2021) 'The synaptonemal complex imposes crossover interference and heterochiasmy in Arabidopsis', *Proceedings of the National Academy of Sciences of the United States of America*, 118(12), pp. 1–11. doi: 10.1073/pnas.2023613118.

Carpenter, A. T.C. (1975) 'Electron microscopy of meiosis in Drosophila melanogaster females: II: The recombination nodule, a recombination associated structure at pachytene?', *Proceedings of the National Academy of Sciences of the United States of America*, 72(8), pp. 3186–3189. doi: 10.1073/pnas.72.8.3186.

Carpenter, Adelaide T.C. (1975) 'Electron microscopy of meiosis in Drosophila melanogaster females - I. Structure, arrangement, and temporal change of the synaptonemal complex in wild-type', *Chromosoma*, 51(2), pp. 157–182. doi: 10.1007/BF00319833.

Carpenter, A. T. C. (1981) 'EM autoradiographic evidence that DNA synthesis occurs at recombination nodules during meiosis in Drosophila melanogaster females', *Chromosoma*, 83(1), pp. 59–80. doi: 10.1007/BF00286016.

Carpenter, A. T. C. (1994) 'Chiasma function', *Cell*, 77(7), pp. 959–962. doi: 10.1016/0092-8674(94)90434-0.

Caryl, A. P. *et al.* (2000) 'A homologue of the yeast HOP1 gene is inactivated in the Arabidopsis meiotic mutant asy1', *Chromosoma*, 109(1–2), pp. 62–71. doi: 10.1007/s004120050413.

Chambon, A., West, A., Vezon, D., Horlow, C., De Muyt, A., Chelysheva, L., Ronceret, A., Darbyshire, A. R., *et al.* (2018) 'Identification of ASYNAPTIC4, a component of the meiotic chromosome axis', *Plant Physiology*, 178(September), p. pp.01725.2017. doi: 10.1104/pp.17.01725.

Chambon, A., West, A., Vezon, D., Horlow, C., De Muyt, A., Chelysheva, L., Ronceret, A., Darbyshire, A., *et al.* (2018) 'Identification of ASYNAPTIC4, a Component of the Meiotic Chromosome Axis', *Plant Physiology*, 178(1), pp. 233–246. doi: 10.1104/pp.17.01725.

Chan, K. L. *et al.* (2013) 'Pds5 promotes and protects cohesin acetylation', *Proceedings of the National Academy of Sciences of the United States of America*, 110(32), pp. 13020–13025. doi:

10.1073/pnas.1306900110.

Chelysheva, L. *et al.* (2005) 'AtREC8 and AtSCC3 are essential to the monopolar orientation of the kinetochores during meiosis', *Journal of Cell Science*, 118(20), pp. 4621–4632. doi: 10.1242/jcs.02583.

Chelysheva, L. *et al.* (2007) 'Zip4/Spo22 is required for class I CO formation but not for synapsis completion in Arabidopsis thaliana', *PLoS Genetics*, 3(5), pp. 802–813. doi: 10.1371/journal.pgen.0030083.

Chelysheva, L. *et al.* (2008) 'The Arabidopsis BLAP75/Rmi1 homologue plays crucial roles in meiotic double-strand break repair', *PLoS Genetics*, 4(12). doi: 10.1371/journal.pgen.1000309.

Chelysheva, L. *et al.* (2012) 'The Arabidopsis HEI10 is a new ZMM protein related to Zip3', *PLoS Genetics*, 8(7). doi: 10.1371/journal.pgen.1002799.

Chen, C. *et al.* (2013) 'Pch2 is a hexameric ring ATPase that remodels the chromosome axis protein Hop1', *Proceedings of the National Academy of Sciences*, 111(1), pp. E44–E53. doi: 10.1073/pnas.1310755111.

Cheng, F. *et al.* (2014) 'Genome triplication drove the diversification of Brassica plants', *Horticulture Research*, 1(14024), pp. 1–24. doi: 10.1007/978-3-662-47901-8_10.

Chi, J. *et al.* (2014) 'Meiosis gene inventory of four ciliates reveals the prevalence of a synaptonemal complex-independent crossover pathway', *Molecular Biology and Evolution*, 31(3), pp. 660–672. doi: 10.1093/molbev/mst258.

Choi, K. *et al.* (2018) 'Nucleosomes and DNA methylation shape meiotic DSB frequency in Arabidopsis thaliana transposons and gene regulatory regions', *Genome Research*, 4(28), pp. 532–546. doi: 10.1101/gr.225599.117.28.

Choi, K. and Henderson, I. R. (2015) 'Meiotic recombination hotspots - A comparative view', *Plant Journal*, 83(1), pp. 52–61. doi: 10.1111/tpj.12870.

Chua, P. R. and Roeder, G. S. (1998) 'Zip2, a Meiosis-Specific Protein Required for the Initiation of Chromosome Synapsis', 93, pp. 349–359.

Colaiácovo, M. P. (2006) 'The many facets of SC function during C. elegans meiosis', *Chromosoma*, 115(3), pp. 195–211. doi: 10.1007/s00412-006-0061-9.

Colas, I. *et al.* (2017) 'Observation of extensive chromosome axis remodeling during the "Diffuse-phase" of Meiosis in large genome cereals', *Frontiers in Plant Science*, 8(July), pp. 1–9. doi: 10.3389/fpls.2017.01235.

Colbert, T. *et al.* (2001) 'High-throughput screening for induced point mutations', *Plant Physiology*, 126(2), pp. 480–484. doi: 10.1104/pp.126.2.480.

Cooper, T. J., Garcia, V. and Neale, M. J. (2016) 'Meiotic DSB patterning: A multifaceted process', *Cell Cycle*. Taylor & Francis, 15(1), pp. 13–21. doi: 10.1080/15384101.2015.1093709.

Couteau, F. *et al.* (1999) 'Random Chromosome Segregation without Meiotic Arrest in Both Male and Female Meiocytes of a dmc1 Mutant of Arabidopsis', *The Plant Cell*, 11(9), p. 1623. doi: 10.2307/3871042.

Creighton, H. B. and Mcclintock, B. (1935) 'The Correlation of Cytological and Genetical Crossing-Over in Zea Mays. A Corroboration', *Proceedings of the National Academy of Sciences*, 21, pp. 148–150.

Creighton, H. B. and McClintock, B. (1931) 'A Correlation of Cytological and Genetical Crossing-Over in Zea Mays', *Proceedings of the National Academy of Sciences*, 17, pp. 492–497. doi: 10.1073/pnas.21.3.148.

Crismani, W. *et al.* (2012a) 'FANCM Limits Meiotic Crossovers. Sup. material', *Science*, 336(6088),

pp. 1588–1590. doi: 10.1126/science.1220381.

Crismani, W. *et al.* (2012b) 'FANCM Limits Meiotic Crossovers', *Science*, 336(6088), pp. 1588–1590. doi: 10.1126/science.1220381.

Cuacos, M. *et al.* (2021) 'Meiotic chromosome axis remodelling is critical for meiotic recombination in Brassica rapa', *Journal of Experimental Botany*, 72(8), pp. 3012–3027. doi: 10.1093/jxb/erab035.

Dangel, N. J., Knoll, A. and Puchta, H. (2014) 'MHF1 plays Fanconi anaemia complementation group M protein (FANCM)-dependent and FANCM-independent roles in DNA repair and homologous recombination in plants', *Plant Journal*, 78(5), pp. 822–833. doi: 10.1111/tpj.12507.

Daoudal-Cotterell, S., Gallego, M. E. and White, C. I. . (2002) 'The plant Rad50-Mre11 protein complex', *FEBS Letters*, 516, pp. 164–166.

De, K. *et al.* (2014) 'Arabidopsis thaliana WAPL Is Essential for the Prophase Removal of Cohesin during Meiosis', *PLoS Genetics*, 10(7). doi: 10.1371/journal.pgen.1004497.

Demmerle, J. *et al.* (2017) 'Strategic and practical guidelines for successful structured illumination microscopy', *Nature protocols*, 12(5), pp. 988–1010. doi: 10.1038/nprot.2017.019.

Desjardins, S. D. *et al.* (2020) 'MutS homologue 4 and MutS homologue 5 maintain the obligate crossover in wheat despite stepwise gene loss following polyploidization1[CC-BY]', *Plant Physiology*, 183(4), pp. 1545–1558. doi: 10.1104/pp.20.00534.

Dion, É. *et al.* (2007) 'An Arabidopsis MLH1 mutant exhibits reproductive defects and reveals a dual role for this gene in mitotic recombination', *Plant Journal*, 51(3), pp. 431–440. doi: 10.1111/j.1365-313X.2007.03145.x.

Dissmeyer, N. *et al.* (2007) 'T-loop phosphorylation of Arabidopsis CDKA;1 is required for its function and can be partially substituted by an aspartate residue', *Plant Cell*, 19(3), pp. 972–985. doi: 10.1105/tpc.107.050401.

Dong, F., Cai, X. and Makaroff, C. A. (2001) 'Cloning and characterization of two Arabidopsis genes that belong to the RAD21/REC8 family of chromosome cohesin proteins', *Gene*, 271(1), pp. 99–108. doi: 10.1016/S0378-1119(01)00499-1.

Dong, H. and Roeder, G. S. (2000) 'Organization of the yeast Zip1 protein within the central region of the synaptonemal complex', *Journal of Cell Biology*, 148(3), pp. 417–426. doi: 10.1083/jcb.148.3.417.

Dubois, E. *et al.* (2019) 'Building bridges to move recombination complexes', *Proceedings of the National Academy of Sciences of the United States of America*, 116(25), pp. 12400–12409. doi: 10.1073/pnas.1901237116.

FAO (2017) *The future of food and agriculture - Trends and challenges*, *The future of food and agriculture: trends and challenges*. Rome: Food and Agriculture Organization of the United Nations (FAO). Available at: www.fao.org/publications%0Ahttp://www.fao.org/3/a-i6583e.pdf%0Ahttp://siteresources.worldbank.org/INTARD/825826-1111044795683/20424536/Ag_ed_Africa.pdf%0Awww.fao.org/cfs%0Ahttp://www.jstor.org/stable/4356839%0Ahttps://ediss.uni-goettingen.de/bitstream/han.

FAO *et al.* (2018) *The State of Food Security and Nutrition in the World. Building climate resilience for food security and Nutrition*. Rome. Available at: www.fao.org/publications.

Fawcett, D. W. (1956) 'The Fine Structure of Chromosomes in the Meiotic Prophase of Vertebrate Spermatocytes', *J. Biophys. and Biochem. Cytol.*, 2(4), pp. 403–406.

Ferdous, M. *et al.* (2012) 'Inter-homolog crossing-over and synapsis in arabidopsis meiosis are dependent on the chromosome axis protein atasy3', *PLoS Genetics*, 8(2), p. e1002507. doi: 10.1371/journal.pgen.1002507.

Fernandes, J. B. *et al.* (2017) 'Unleashing meiotic crossovers in hybrid plants', *Proceedings of the National Academy of Sciences*, p. 201713078. doi: 10.1073/pnas.1713078114.

Fernandes, J. B. *et al.* (2018) 'FIGL1 and its novel partner FLIP form a conserved complex that regulates homologous recombination.', *PLoS Genetics*, 14(4), p. e1007317. doi: 10.1101/107821.

France, M. G. *et al.* (2021) 'ZYP1 is required for obligate crossover formation and crossover interference in Arabidopsis', *Proceedings of the National Academy of Sciences*, 118(14), pp. 1–11. doi: 10.1073/pnas.2021671118/-/DCSupplemental.Published.

Friedman, D. B., Hollingsworth, N. M. and Byers, B. (1994) 'Insertional mutations in the yeast HOP1 gene: Evidence for multimeric assembly in meiosis', *Genetics*, 136(2), pp. 449–464.

Fuge, H. (1979) 'Synapsis, desynapsis, and formation of polycomplex-like aggregates in male meiosis of Pales ferruginea (diptera, tipulidae)', *Chromosoma*, 70(3), pp. 353–373. doi: 10.1007/BF00328772.

Fujiwara, Y. *et al.* (2020) 'Meiotic cohesins mediate initial loading of HORMAD1 to the chromosomes and coordinate SC formation during meiotic prophase', *PLoS Genetics*, 16(9), pp. 1–26. doi: 10.1371/journal.pgen.1009048.

Furness, C. A. and Rudall, P. J. (1999) 'Microsporogenesis in Monocotyledons', *Annals of Botany*, 84(4), pp. 475–499. doi: 10.1006/anbo.1999.0942.

Gangloff, S. *et al.* (1994) 'The yeast type I topoisomerase Top3 interacts with Sgs1, a DNA helicase homolog: a potential eukaryotic reverse gyrase', *Molecular and Cellular Biology*, 14(12), pp. 8391–8398. doi: 10.1128/mcb.14.12.8391.

Gari, K. *et al.* (2008) 'The Fanconi Anemia Protein FANCM Can Promote Branch Migration of Holliday Junctions and Replication Forks', *Molecular Cell*, 29(1), pp. 141–148. doi: 10.1016/j.molcel.2007.11.032.

Geuting, V. *et al.* (2009) 'Two Distinct MUS81-EME1 Complexes from Arabidopsis Process Holliday Junctions', *Plant Physiology*, 150(2), pp. 1062–1071. doi: 10.1104/pp.109.136846.

Girard, C. *et al.* (2015) 'AAA-ATPase FIDGETIN-LIKE 1 and Helicase FANCM Antagonize Meiotic Crossovers by Distinct Mechanisms', *PLoS Genetics*, 11(7), pp. 1–22. doi: 10.1371/journal.pgen.1005369.

Golubovskaya, I. N. *et al.* (2006) 'Alleles of afd1 dissect REC8 functions during meiotic prophase I', *Journal of Cell Science*, 119(16), pp. 3306–3315. doi: 10.1242/jcs.03054.

Gonzalo, A. *et al.* (2018) 'Meiotic effects of MSH4 copy number variation support an adaptive role for post - polyploidy gene loss'.

Gonzalo, A. *et al.* (2019) 'Reducing MSH4 copy number prevents meiotic crossovers between non-homologous chromosomes in Brassica napus', *Nature Communications*. Springer US, 10(1), pp. 1–9. doi: 10.1038/s41467-019-10010-9.

Grandont, L., Jenczewski, E. and Lloidl, A. (2013) 'Meiosis and its deviations in polyploid plants', *Cytogenetic and Genome Research*, 140(2–4), pp. 185–203. doi: 10.1159/000351731.

Gray, S. and Cohen, P. E. (2016) 'Control of Meiotic Crossovers: From Double-Stand Break Formation to Designation', *Annual Review of Genetics*, 50(1), p. annurev-genet-120215-035111. doi: 10.1146/annurev-genet-120215-035111.

Grelon, M. *et al.* (2001) 'AtSPO11-1 is necessary for eficient meiotic recombination in plants', *EMBO Journal*, 20(3), pp. 589–600.

Griffiths, S. *et al.* (2006) 'Molecular characterization of Ph1 as a major chromosome pairing locus in polyploid wheat', *Nature letters*, 439(7077), p. 749. doi: 10/fp7ssb.

Gu, Y., Desai, A. and Corbett, K. D. C. (2022) 'Evolutionary Dynamics and Molecular Mechanisms of HORMA Domain Protein Signaling', *Annu. Rev. Biochem.*, 91, pp. 1.1-1.29.

Haber, J. E. (2007) 'Evolution of Models of Homologous Recombination', in *Recombination and meiosis*, pp. 1–67. doi: 10.1007/7050.

Haliassos, A. *et al.* (1989) 'Modification of enzymaticaly amplified DNA for the detection of point mutations', *Nucleic Acids Research*, 17(9), pp. 3606–3606.

Hamant, O., Ma, H. and Cande, W. Z. (2006) 'Genetics of Meiotic Prophase I in Plants', *Annual Review of Plant Biology*, 57(1), pp. 267–302. doi: 10.1146/annurev.arplant.57.032905.105255.

Hartung, F. *et al.* (2006) 'The role of AtMUS81 in DNA repair and its genetic interaction with the helicase AtRecQ4A', *Nucleic Acids Research*, 34(16), pp. 4438–4448. doi: 10.1093/nar/gkl576.

Hartung, F. *et al.* (2007) 'The catalytically active tyrosine residues of both SPO11-1 and SPO11-2 are required for meiotic double-strand break induction in Arabidopsis', *Plant Cell*, 19(10), pp. 3090–3099. doi: 10.1105/tpc.107.054817.

Hartung, F. *et al.* (2008) 'Topoisomerase 3α and RMI1 suppress somatic crossovers and are essential for resolution of meiotic recombination intermediates in Arabidopsis thaliana', *PLoS Genetics*, 4(12). doi: 10.1371/journal.pgen.1000285.

Hartung, F., Suer, S. and Puchta, H. (2007) 'Two closely related RecQ helicases have antagonistic roles in homologous recombination and DNA repair in Arabidopsis thaliana', *Proceedings of the National Academy of Sciences*, 104(47), pp. 18836–18841. doi: 10.1073/pnas.0705998104.

Hartung, Frank, Suer, S. and Puchta, H. (2007) 'Two closely related RecQ helicases have antagonistic roles in homologous recombination and DNA repair in Arabidopsis thaliana', *Proceedings of the National Academy of Sciences of the United States of America*, 104(47), pp. 18836–18841. doi: 10.1073/pnas.0705998104.

He, Y. *et al.* (2017) 'Genomic features shaping the landscape of meiotic double-strand-break hotspots in maize', *Proceedings of the National Academy of Sciences of the United States of America*, 114(46), pp. 12231–12236. doi: 10.1073/pnas.1713225114.

Hernandez Sanchez-Rebato, M. *et al.* (2021) 'RAD54 is essential for RAD51-mediated repair of meiotic DSB in Arabidopsis', *PLoS Genetics*, 17(5), pp. 1–24. doi: 10.1371/journal.pgen.1008919.

Heyting, C. (1996) 'Synaptonemal complexes: Structure and function', *Current Opinion in Cell Biology*, 8(3), pp. 389–396. doi: 10.1016/S0955-0674(96)80015-9.

Higgins, J. D. *et al.* (2004) 'The Arabidopsis MutS homolog AtMSH4 functions at an early step in recombination: Evidence for two classes of recombination in Arabidopsis', *Genes and Development*, 18(20), pp. 2557–2570. doi: 10.1101/gad.317504.

Higgins, J. D., Sanchez-Moran, E., Armstrong, S. J., Jones, G. H. and Franklin, F. Chris H. (2005) 'The Arabidopsis synaptonemal complex protein ZYP1 is required for chromosome synapsis and normal fidelity of crossing over', *Genes and Development*, 19(20), pp. 2488–2500. doi: 10.1101/gad.354705.

Higgins, J. D., Sanchez-Moran, E., Armstrong, S. J., Jones, G. H. and Franklin, F. Chris H (2005) 'The Arabidopsis synaptonemal complex protein ZYP1 is required for chromosome synapsis and normal fidelity of crossing over', *Genes and Development*, 19(20), pp. 2488–2500. doi: 10.1101/gad.354705.

Higgins, J. D., Vignard, J., *et al.* (2008) 'AtMSH5 partners AtMSH4 in the class I meiotic crossover pathway in Arabidopsis thaliana, but is not required for synapsis', *Plant Journal*, 55(1), pp. 28–39. doi: 10.1111/j.1365-313X.2008.03470.x.

Higgins, J. D., Buckling, E. F., *et al.* (2008) 'Expression and functional analysis of AtMUS81 in Arabidopsis meiosis reveals a role in the second pathway of crossing-over', *Plant Journal*, 54(1), pp. 152–162. doi: 10.1111/j.1365-313X.2008.03403.x.

Hirano, T. (2012) 'Condensins: Universal organizers of chromosomes with diverse functions', *Genes and Development*, 26(15), pp. 1659–1678. doi: 10.1101/gad.194746.112.

Holliday, R. (1964) 'A mechanism for gene conversion in fungi', *Genetics Research*, 5, pp. 282–304. doi: 10.1017/S0016672308009476.

Holliday, R. (1974) ‘Molecular aspects of genetic exchange and gene conversion’, *Genetics*, 78(1), pp. 273–287.

Hollingsworth, N. M. and Brill, S. J. (2004) ‘The Mus81 solution to resolution: Generating meiotic crossovers without Holliday junctions’, *Genes and Development*, 18(2), pp. 117–125. doi: 10.1101/gad.1165904.

Hollingsworth, N. M. and Byers, B. (1989a) ‘HOP1: a yeast meiotic pairing gene.’, *Genetics*, 121(3), pp. 445–462. doi: 10.1093/genetics/121.3.445.

Hollingsworth, N. M. and Byers, B. (1989b) ‘HOP1: a yeast meiotic pairing gene.’, *Genetics*, 121(3), pp. 445–462.

Hollingsworth, N. M. and Ponte, L. (1997) ‘Genetic interactions between HOP1, RED1 and MEK1 suggest that MEK1 regulates assembly of axial element components during meiosis in the yeast Saccharomyces cerevisiae’, *Genetics*, 147(1), pp. 33–42. doi: 10.1093/genetics/147.1.33.

Hollingsworth, N. M., Ponte, L. and Halsey, C. (1995) ‘MSH5, a novel MutS homolog, facilitates meiotic reciprocal recombination between homologs in Saccharomyces cerevisiae but not mismatch repair’, *Genes and Development*, 9(14), pp. 1728–1739. doi: 10.1101/gad.9.14.1728.

Holloway, J. K. *et al.* (2010) ‘Mammalian BLM helicase is critical for integrating multiple pathways of meiotic recombination’, *Journal of Cell Biology*, 188(6), pp. 779–789. doi: 10.1083/jcb.200909048.

Hughes, S. E. and Hawley, R. S. (2020) ‘Alternative Synaptonemal Complex Structures: Too Much of a Good Thing?’, *Trends in Genetics*. Elsevier Ltd, 36(11), pp. 833–844. doi: 10.1016/j.tig.2020.07.007.

Hunter, N. (2015) ‘Meiotic Recombination : The Essence of Heredity’, *Cold Spring Harb Perspect Biol*, 7, pp. 1–34.

Hunter, N. and Borts, R. H. (1997) ‘Mlh1 is unique among mismatch repair proteins in its ability to promote crossing-over during meiosis’, *Genes and Development*, 11(12), pp. 1573–1582. doi: 10.1101/gad.11.12.1573.

Hunter, N. and Kleckner, N. (2001) ‘The single-end invasion: An asymmetric intermediate at the double-strand break to double-holliday junction transition of meiotic recombination’, *Cell*, 106(1), pp. 59–70. doi: 10.1016/S0092-8674(01)00430-5.

da Ines, O. *et al.* (2012) ‘Differing requirements for RAD51 and DMC1 in meiotic pairing of centromeres and chromosome arms in Arabidopsis thaliana’, *PLoS Genetics*, 8(4). doi: 10.1371/journal.pgen.1002636.

Da Ines, O. *et al.* (2012) ‘Differing requirements for RAD51 and DMC1 in meiotic pairing of centromeres and chromosome arms in Arabidopsis thaliana’, *PLoS Genetics*, 8(4). doi: 10.1371/journal.pgen.1002636.

Da Ines, O. *et al.* (2013) ‘Meiotic Recombination in Arabidopsis Is Catalysed by DMC1, with RAD51 Playing a Supporting Role’, *PLoS Genetics*, 9(9). doi: 10.1371/journal.pgen.1003787.

IPCC. (2014) *Climate Change 2014: Synthesis Report. Contribution of Working Groups I, II and III to the Fifth Assessment Report of the Intergovernmental Panel on Climate Change*, *Managing the Risks of Extreme Events and Disasters to Advance Climate Change Adaptation: Special Report of the Intergovernmental Panel on Climate Change*. Geneva, Switzerland. doi: 10.1017/CBO9781139177245.003.

IPCC. (2019) *Climate Change and Land: an IPCC special report on climate change, desertification, land degradation, sustainable land management, food security, and greenhouse gas fluxes in terrestrial ecosystems*, *Climate Change and Land: an IPCC special report on climate change, desertification, land degradation, sustainable land management, food security, and greenhouse gas fluxes in terrestrial ecosystems*. Available at: https://burundi-food securityhealthywealthywise.weebly.com/food-security.html.

Jackson, N. *et al.* (2006) ‘Reduced meiotic crossovers and delayed prophase I progression in

AtMLH3-deficient Arabidopsis', *The EMBO Journal*, 25(6), pp. 1315–1323. doi: 10.1038/sj.emboj.7600992.

Janssens, F. A. (1909) 'La Theorie de la Chiasmatypie nouvelle interprétation des cinèses de maturation', *La Cellule*, 25, pp. 389–411. doi: 10.1534/genetics.112.139725.

Jenczewski, E. *et al.* (2003) 'PrBn, a major gene controlling homeologous pairing in oilseed rape (Brassica napus) haploids', *Genetics*, 164(2), pp. 645–653. doi: 10.1093/genetics/164.2.645.

Jenczewski, E. and Alix, K. (2004) 'From Diploids to Allopolyploids: The Emergence of Efficient Pairing Control Genes in Plants', *Critical Reviews in Plant Sciences*, 23(1), pp. 21–45. doi: 10.1080/07352680490273239.

Jenczewski, E., Chèvre, A. M. and Alix, K. (2013) 'Polyploid and Hybrid Genomics', in Chen, Z. J. and Birchler, J. A. (eds) *Polyploid and Hybrid Genomics*. 1st edn. Iowa, USA: Wiley-Blackwell, pp. 171–183. doi: 10.1002/9781118552872.

Jessop, L. *et al.* (2006) 'Meiotic chromosome synapsis-promoting proteins antagonize the anti-crossover activity of sgs1', *PLoS Genetics*, 2(9), pp. 1402–1412. doi: 10.1371/journal.pgen.0020155.

Jessop, L. and Lichten, M. (2008) 'Mus81/Mms4 Endonuclease and Sgs1 Helicase Collaborate to Ensure Proper Recombination Intermediate Metabolism during Meiosis', *Molecular Cell*, 31(3), pp. 313–323. doi: 10.1016/j.molcel.2008.05.021.

Jones, G. H. (1971) 'The analysis of exchanges in tritium-labelled meiotic chromosomes - II. Stethophyma grossum', *Chromosoma*, 34(4), pp. 367–382. doi: 10.1007/BF00326312.

Joshi, N. *et al.* (2009) 'Pch2 links chromosome axis remodeling at future crossover sites and crossover distribution during yeast meiosis', *PLoS Genetics*, 5(7). doi: 10.1371/journal.pgen.1000557.

Joyce, E. F. and Mckim, K. S. (2009) 'Drosophila PCH2 Is Required for a Pachytene Checkpoint That Monitors Double-Strand-Break-Independent Events Leading to Meiotic Crossover Formation', 51(January), pp. 39–51. doi: 10.1534/genetics.108.093112.

Keeney, S., Giroux, C. N. and Kleckner, N. (1997) 'Meiosis-specific DNA double-strand breaks are catalyzed by Spo11, a member of a widely conserved protein family', *Cell*, 88(3), pp. 375–384. doi: 10.1016/S0092-8674(00)81876-0.

Kim, D. H. *et al.* (2017) 'The AAA+ ATPase TRIP13 remodels HORMA domains through N-terminal engagement and unfolding', *The EMBO Journal*, 36(16), pp. 2419–2434. doi: 10.15252/embj.201797291.

Kim, K. P. *et al.* (2010) 'Sister cohesion and structural axis components mediate homolog bias of meiotic recombination', *Cell*. Elsevier Inc., 143(6), pp. 924–937. doi: 10.1016/j.cell.2010.11.015.

Kim, Y. *et al.* (2014) 'The chromosome axis controls meiotic events through a hierarchical assembly of HORMA domain proteins', *Developmental Cell*. Elsevier Inc., 31(4), pp. 487–502. doi: 10.1016/j.devcel.2014.09.013.

Kleckner, N. *et al.* (2004) 'A mechanical basis for chromosome function.', *Proceedings of the National Academy of Sciences of the United States of America*, 101(34), pp. 12592–12597. doi: 10.1073/pnas.0402724101.

Kleckner, N. (2006) 'Chiasma formation: Chromatin/axis interplay and the role(s) of the synaptonemal complex', *Chromosoma*, 115(3), pp. 175–194. doi: 10.1007/s00412-006-0055-7.

Klein, F. *et al.* (1999) 'A Central Role for Cohesins in Sister Chromatid Cohesion, Formation of Axial Elements, and Recombination during Yeast Meiosis Genetic and biochemical analyses have identified', *Cell*, 98, pp. 91–103.

Knoll, A. *et al.* (2012) 'The Fanconi Anemia Ortholog FANCM Ensures Ordered Homologous Recombination in Both Somatic and Meiotic Cells in *Arabidopsis*', *The Plant Cell*, 24(4), pp. 1448–1464. doi: 10.1105/tpc.112.096644.

Knoll, A., Schröpfer, S. and Puchta, H. (2014) 'The RTR complex as caretaker of genome stability and its unique meiotic function in plants', *Frontiers in Plant Science*, 5(February), pp. 1–6. doi: 10.3389/fpls.2014.00033.

Konieczy, A. and Ausubel, F. M. (1993) 'A procedure for mapping Arabidopsis mutations Using co-dominant ecotype-specific PCR-based markers', *The Plant Journal*, 4(2), pp. 403–410.

Kueng, S. *et al.* (2006) 'Wapl Controls the Dynamic Association of Cohesin with Chromatin', *Cell*, 127(5), pp. 955–967. doi: 10.1016/j.cell.2006.09.040.

Kurzbauer, M.-T. *et al.* (2018) 'Arabidopsis thaliana FANCD2 Promotes Meiotic Crossover Formation', *The Plant Cell*, 4, p. tpc.00745.2017. doi: 10.1105/tpc.17.00745.

Lambing, C. *et al.* (2015) 'Arabidopsis PCH2 Mediates Meiotic Chromosome Remodeling and Maturation of Crossovers', *PLoS Genetics*, 11(7), pp. 1–27. doi: 10.1371/journal.pgen.1005372.

Lambing, C., Kuo, P. C., *et al.* (2020) 'ASY1 acts as a dosage-dependent antagonist of telomere-led recombination and mediates crossover interference in Arabidopsis.', *Proceedings of the National Academy of Sciences of the United States of America*. doi: 10.1073/pnas.1921055117.

Lambing, C., Tock, A. J., Topp, S. D., Choi, K., Kuo, P. C., Zhao, X., Osman, K., Higgins, J. D., Franklin, F. H. C., *et al.* (2020) 'Interacting genomic landscapes of REC8-cohesin, chromatin, and meiotic recombination in arabidopsis', *Plant Cell*, 32(4), pp. 1218–1239. doi: 10.1105/TPC.19.00866.

Lambing, C., Tock, A. J., Topp, S. D., Choi, K., Kuo, P. C., Zhao, X., Osman, K., Higgins, J. D., Franklin, F. C. H., *et al.* (2020) 'Interacting Genomic Landscapes of REC8-Cohesin, Chromatin, and Meiotic Recombination in Arabidopsis', *The Plant cell*, 32(4), pp. 1218–1239. doi: 10.1105/tpc.19.00866.

Lambing, C., Franklin, F. C. H. and Wang, C.-J. R. (2017) 'Understanding and manipulating meiotic recombination in plants', *Plant Physiology*, 173(March), p. pp.01530.2016. doi: 10.1104/pp.16.01530.

Latypov, V. *et al.* (2010) ' Roles of Hop1 and Mek1 in Meiotic Chromosome Pairing and Recombination Partner Choice in Schizosaccharomyces pombe ', *Molecular and Cellular Biology*, 30(7), pp. 1570–1581. doi: 10.1128/mcb.00919-09.

Lee, D. H. *et al.* (2015) 'The axial element protein desynaptic2 mediates meiotic double-strand break formation and synaptonemal complex assembly in maize', *Plant Cell*, 27(9), pp. 2516–2529. doi: 10.1105/tpc.15.00434.

Li, H. *et al.* (2018) 'Fast-Forwarding Genetic Gain', *Trends in Plant Science*. Elsevier Ltd, 23(3), pp. 184–186. doi: 10.1016/j.tplants.2018.01.007.

Li, W. *et al.* (2004) 'The Arabidopsis AtRAD51 gene is dispensable for vegetative development but required for meiosis', *Proceedings of the National Academy of Sciences of the United States of America*, 101(29), pp. 10596–10601. doi: 10.1073/pnas.0404110101.

Li, W. *et al.* (2005) 'The AtRAD51C gene is required for normal meiotic chromosome synapsis and double-stranded break repair in Arabidopsis', *Plant Physiology*, 138(2), pp. 965–976. doi: 10.1104/pp.104.058347.

Li, X., Yu, M., *et al.* (2021) 'Fanconi anemia ortholog FANCM regulates meiotic crossover distribution in plants', *Plant Physiology*, 186(1), pp. 344–360. doi: 10.1093/plphys/kiab061.

Li, X., Zhang, J., Huang, J., Xu, J., *et al.* (2021) 'Regulation of interference-sensitive crossover distribution ensures crossover assurance in Arabidopsis.', *Proceedings of the National Academy of Sciences of the United States of America*, 118(47), pp. 1–9. doi: 10.1073/pnas.2107543118.

Li, X., Zhang, J., Huang, J., Chen, Z., *et al.* (2021) 'Regulation of interference-sensitive crossover distribution ensures crossover assurance in Arabidopsis', *Proceedings of the National Academy of Sciences*, 118(47), pp. 1–9. doi: 10.1073/pnas.2107543118/-/DCSupplemental.Published.

Liu, J., Wu, T. C. and Lichten, M. (1995) 'The location and structure of double-strand DNA breaks

induced during yeast meiosis: evidence for a covalently linked DNA-protein intermediate.', *The EMBO Journal*, 14(18), pp. 4599–4608. doi: 10.1002/j.1460-2075.1995.tb00139.x.

Liu, S. *et al.* (2014) 'The brassica oleracea genome reveals the asymmetrical evolution of polyploid genomes', *Nature Communications*. Nature Publishing Group, 5(3930), pp. 1–11. doi: 10.1038/ncomms4930.

Lloyd, A. *et al.* (2018) 'Homoeologous exchanges cause extensive dosage-dependent gene expression changes in an allopolyploid crop', *New Phytologist*, 217(1), pp. 367–377. doi: 10.1111/nph.14836.

Lloyd, A. H. *et al.* (2014) 'Meiotic gene evolution: Can you teach a new dog new tricks?', *Molecular Biology and Evolution*, 31(7), pp. 1724–1727. doi: 10.1093/molbev/msu119.

Loidl, J. (1989) 'Effects of elevated temperature on meiotic chromosome synapsis in Allium ursinum', *Chromosoma*, 97(6), pp. 449–458. doi: 10.1007/BF00295029.

Lorenz, A. *et al.* (2004) 'S. pombe meiotic linear elements contain proteins related to synaptonemal complex components', *Journal of Cell Science*, 117(15), pp. 3343–3351. doi: 10.1242/jcs.01203.

De los Santos, T. *et al.* (2003) 'The MUS81/MMS4 endonuclease acts independently of double-holliday junction resolution to promote a distinct subset of crossovers during meiosis in budding yeast', *Genetics*, 164(1), pp. 81–94.

Lui, D. Y. and Colaiácovo, M. P. (2013) 'Meiotic Development in Caenorhabditis elegans', *Adv Exp Med Biol.*, 757, pp. 133–170. doi: 10.1007/978-1-4614-4015-4.

Lynn, A., Soucek, R. and Börner, G. V. (2007) 'ZMM proteins during meiosis: Crossover artists at work', *Chromosome Research*, 15(5), pp. 591–605. doi: 10.1007/s10577-007-1150-1.

Macaisne, N. *et al.* (2008) 'SHOC1, an XPF Endonuclease-Related Protein, Is Essential for the Formation of Class I Meiotic Crossovers', *Current Biology*, 18(18), pp. 1432–1437. doi: 10.1016/j.cub.2008.08.041.

MacQueen, A. J. *et al.* (2019) 'A conserved filamentous assembly underlies the structure of the meiotic chromosome axis', *eLife*, 8, pp. 1–27. doi: 10.7554/elife.40372.

Mainiero, S. and Pawlowski, W. P. (2014) 'Meiotic chromosome structure and function in plants', *Cytogenetic and Genome Research*, 143(1–3), pp. 6–17. doi: 10.1159/000365260.

Mandáková, T. *et al.* (2010) 'Fast Diploidization in Close Mesopolyploid Relatives of Arabidopsis', *The Plant Cell*, 22(July), pp. 2277–2290. doi: 10.1105/tpc.110.074526.

Manhart, C. M. and Alani, E. (2016) 'Roles for mismatch repair family proteins in promoting meiotic crossing over', *DNA Repair*. Elsevier B.V., 38, pp. 84–93. doi: 10.1016/j.dnarep.2015.11.024.

Mao, B. *et al.* (2021) 'Rice MutLγ, the MLH1–MLH3 heterodimer, participates in the formation of type I crossovers and regulation of embryo sac fertility', *Plant Biotechnology Journal*, 19(7), pp. 1443–1455. doi: 10.1111/pbi.13563.

Martín, A. C. *et al.* (2017) 'Dual effect of the wheat Ph1 locus on chromosome synapsis and crossover', *Chromosoma*. Chromosoma, 126(6), pp. 669–680. doi: 10.1007/s00412-017-0630-0.

Martín, A. C., Alabdullah, A. K. and Moore, G. (2021) 'A separation-of-function ZIP4 wheat mutant allows crossover between related chromosomes and is meiotically stable', *Scientific Reports*. Nature Publishing Group UK, 11(1), pp. 1–13. doi: 10.1038/s41598-021-01379-z.

Martínez-pérez, E. *et al.* (1999) 'Homologous chromosome pairing in wheat', *Journa of Cell Science*, 112(Pt 11), pp. 1761–1769.

Martinez-Perez, E. and Villeneuve, A. M. (2005) 'HTP-1-dependent constraints coordinate homolog pairing and synapsis and promote chiasma formation during C. elegans meiosis', *Genes and Development*, 19(22), pp. 2727–2743. doi: 10.1101/gad.1338505.

de Massy, B. (2013) ‘Initiation of Meiotic Recombination: How and Where? Conservation and Specificities Among Eukaryotes’, *Annual Review of Genetics*, 47(1), pp. 563–599. doi: 10.1146/annurev-genet-110711-155423.

Mazina, O. M. *et al.* (2004) ‘Saccharomyces cerevisiae Mer3 helicase stimulates 3′-5′ heteroduplex extension by Rad51: Implications for crossover control in meiotic recombination’, *Cell*, 117(1), pp. 47–56. doi: 10.1016/S0092-8674(04)00294-6.

McCallum, Claire M. *et al.* (2000) ‘Targeted screening for induced mutations’, *Nature Biotechnology*, 18(4), pp. 455–457. doi: 10.1038/74542.

McCallum, C. M. *et al.* (2000) ‘Targeting induced local lesions IN genomes (TILLING) for plant functional genomics’, *Plant Physiology*, 123(2), pp. 439–442. doi: 10.1104/pp.123.2.439.

McMahill, M. S., Sham, C. W. and Bishop, D. K. (2007) ‘Synthesis-dependent strand annealing in meiosis’, *PLoS Biology*, 5(11), pp. 2589–2601. doi: 10.1371/journal.pbio.0050299.

Mendel, G. (1865) ‘Versuche über Pflanzen-Hybriden’, *Abhandlungen des naturfordschenden Vereines in Brünn*, (4), pp. 3–47.

Mercier, R. *et al.* (2001) ‘SWITCH1 (SWI1): a novel protein required for the establishment of sister chromatid cohesion and for bivalent formation at meiosis’, *Genes and Development*, 1, pp. 1859–1871. doi: 10.1101/gad.203201.cohesion.

Mercier, R. *et al.* (2015) ‘The Molecular Biology of Meiosis in Plants’, *Annual Review of Plant Biology*, 66(1), pp. 297–327. doi: 10.1146/annurev-arplant-050213-035923.

Miao, C. *et al.* (2013) ‘Central region component1, a novel synaptonemal complex component, Is essential for meiotic recombination initiation in RiceC’, *Plant Cell*, 25(8), pp. 2998–3009. doi: 10.1105/tpc.113.113175.

Michaels, S. D. and Amasino, R. M. (1998) ‘A robust method for detecting single-nucleotide changes as polymorphic markers by PCR’, *Plant Journal*, 14(3), pp. 381–385. doi: 10.1046/j.1365-313X.1998.00123.x.

Mieulet, D. *et al.* (2018) ‘Unleashing meiotic crossovers in crops’, *Nature Plants*. Springer US, 4(12), pp. 1010–1016. doi: 10.1038/s41477-018-0311-x.

Moens, P. B. (1978) ‘Lateral element cross connections of the synaptonemal complex and their relationship to chiasmata in rat spermatocytes’, *Canadian Journal of Genetics and Cytology*, 20(4), pp. 567–597. doi: 10.1139/g78-066.

Moens, P. B. *et al.* (2002) ‘The time course and chromosomal localization of recombination-related proteins at meiosis in the mouse are compatible with models that can resolve the early DNA-DNA interactions without reciprocal recombination’, *Journal of Cell Science*, 115(8), pp. 1611–1622.

Moens, P. B. *et al.* (2007) ‘Initiation and resolution of interhomolog connections: Crossover and non-crossover sites along mouse synaptonemal complexes’, *Journal of Cell Science*, 120(6), pp. 1017–1027. doi: 10.1242/jcs.03394.

Moens, P. B. and Pearlman, R. E. (1988) ‘Chromatin organization at meiosis’, *BioEssays*, 9(5), pp. 151–153. doi: 10.1002/bies.950090503.

Moose, S. P. and Mumm, R. H. (2008) ‘Molecular plant breeding as the foundation for 21st century crop improvement’, *Plant Physiology*, 147(3), pp. 969–977. doi: 10.1104/pp.108.118232.

Morgan, C. *et al.* (2020) ‘Derived alleles of two axis proteins affect meiotic traits in autotetraploid Arabidopsis arenosa’, *Proceedings of the National Academy of Sciences of the United States of America*, 117(16), pp. 8980–8988. doi: 10.1073/pnas.1919459117.

Morgan, C., Fozard, J. A., *et al.* (2021) ‘Diffusion-mediated HEI10 coarsening can explain meiotic crossover positioning in Arabidopsis’, *Nature Communications*. Springer US, 12(1). doi: 10.1038/s41467-021-24827-w.

Morgan, C., White, M. A., *et al.* (2021) 'Evolution of crossover interference enables stable autopolyploidy by ensuring pairwise partner connections in Arabidopsis arenosa', *Current Biology*. Elsevier Ltd., 31(21), pp. 4713-4726.e4. doi: 10.1016/j.cub.2021.08.028.

Morgan, C. H., Zhang, H. and Bomblies, K. (2017) 'Are the effects of elevated temperature on meiotic recombination and thermotolerance linked via the axis and synaptonemal complex?', *Philosophical Transactions of the Royal Society B: Biological Sciences*, 372(1736). doi: 10.1098/rstb.2016.0470.

Moses, M. J. (1956) 'Cromosomal Structures in Crayfish Spermatocytes', *J. Biophys. and Biochem. Cytol.*, 2, pp. 215–219.

De Muyt, A. *et al.* (2009) 'A high throughput genetic screen identifies new early meiotic recombination functions in Arabidopsis thaliana', *PLoS Genetics*, 5(9). doi: 10.1371/journal.pgen.1000654.

Nageswaran, D. C. *et al.* (2021) 'HIGH CROSSOVER RATE1 encodes PROTEIN PHOSPHATASE X1 and restricts meiotic crossovers in Arabidopsis', *Nature Plants*. Springer US, 7(4), pp. 452–467. doi: 10.1038/s41477-021-00889-y.

Nakagawa, T. and Kolodner, R. D. (2002) 'Saccharomyces cerevisiae Mer3 Is a DNA Helicase Involved in Meiotic Crossing Over', *Molecular and Cellular Biology*, 22(10), pp. 3281–3291. doi: 10.1128/mcb.22.10.3281-3291.2002.

Nakagawa, T. and Ogawa, H. (1999) 'The Saccharomyces cerevisiae MER3 gene, encoding a novel helicase-like protein, is required for crossover control in meiosis', *EMBO Journal*, 18(20), pp. 5714–5723. doi: 10.1093/emboj/18.20.5714.

Nasmyth, K. and Haering, C. H. (2005) 'the Structure and Function of Smc and Kleisin Complexes', *Annual Review of Biochemistry*, 74(1), pp. 595–648. doi: 10.1146/annurev.biochem.74.082803.133219.

Nassif, N. *et al.* (1994) 'Efficient copying of nonhomologous sequences from ectopic sites via P-element-induced gap repair.', *Molecular and Cellular Biology*, 14(3), pp. 1613–1625. doi: 10.1128/mcb.14.3.1613.

Neale, M. J., Pan, J. and Keeney, S. (2005) 'Endonucleolytic processing of covalent protein-linked DNA double-strand breaks', *Nature*, 436(7053), pp. 1053–1057. doi: 10.1038/nature03872.

Neff, M. M. *et al.* (1998) 'dCAPS, a simple technique for the genetic analysis of single nucleotide polymorphisms: Experimental applications in Arabidopsis thaliana genetics', *Plant Journal*, 14(3), pp. 387–392. doi: 10.1046/j.1365-313X.1998.00124.x.

Neff, M. M., Turk, E. and Kalishman, M. (2002) 'Web-based primer design for single nucleotide polymorphism analysis', *Trends in Genetics*, 18(12), pp. 613–615. doi: 10.1016/S0168-9525(02)02820-2.

Nonomura, K. *et al.* (2004) 'The Novel Gene HOMOLOGOUS PAIRING ABERRATION IN RICE MEIOSIS1 of Rice Encodes a Putative Coiled-Coil Protein Required for Homologous Chromosome Pairing in Meiosis', *The Plant Cell*, 16(April), pp. 1008–1020. doi: 10.1105/tpc.020701.of.

Nonomura, K. I. *et al.* (2004) 'An insertional mutation in the rice PAIR2 gene, the ortholog of Arabidopsis ASY1, results in a defect in homologous chromosome pairing during meiosis', *Molecular Genetics and Genomics*, 271(2), pp. 121–129. doi: 10.1007/s00438-003-0934-z.

Novak, J. E., Ross-Macdonald, P. B. and Shirleen Roeder, G. (2001) 'The budding yeast Msh4 protein functions in chromosome synapsis and the regulation of crossover distribution', *Genetics*, 158(3), pp. 1013–1025.

Oleykowski, C. A. *et al.* (1998) 'Mutation detection using a novel plant endonuclease', *Nucleic Acids Research*, 26(20), pp. 4597–4602. doi: 10.1093/nar/26.20.4597.

Osman, K. *et al.* (2006) 'Chromosome synapsis in Arabidopsis: Analysis of the transverse filament protein ZYP1 reveals novel functions for the synaptonemal complex', *Chromosoma*, 115(3), pp. 212–219. doi: 10.1007/s00412-005-0042-4.

Osman, K. *et al.* (2009) 'Replication protein A (AtRPA1a) is required for class I crossover formation but is dispensable for meiotic DNA break repair', *EMBO Journal*, 28(4), pp. 394–404. doi: 10.1038/emboj.2008.295.

Osman, K. *et al.* (2018a) 'Affinity proteomics reveals extensive phosphorylation of the Brassica chromosome axis protein ASY1 and a network of associated proteins at prophase I of meiosis', *Plant Journal*, 93(1), pp. 17–33. doi: 10.1111/tpj.13752.

Osman, K. *et al.* (2018b) 'Affinity proteomics reveals extensive phosphorylation of the Brassica chromosome axis protein ASY1 and a network of associated proteins at prophase I of meiosis', *Plant Journal*, 93(1), pp. 17–33. doi: 10.1111/tpj.13752.

Osman, K. *et al.* (2021) 'Distal Bias of Meiotic Crossovers in Hexaploid Bread Wheat Reflects Spatio-Temporal Asymmetry of the Meiotic Program', *Frontiers in Plant Science*, 12(February), pp. 1–20. doi: 10.3389/fpls.2021.631323.

Østergaard, L. and King, G. J. (2008) 'Standardized gene nomenclature for the Brassica genus', *Plant Methods*, 4(1), pp. 2–5. doi: 10.1186/1746-4811-4-10.

Panizza, S. *et al.* (2011) 'Spo11-accessory proteins link double-strand break sites to the chromosome axis in early meiotic recombination', *Cell*. Elsevier, 146(3), pp. 372–383. doi: 10.1016/j.cell.2011.07.003.

Pâques, F. and Haber, J. E. (1999) 'Multiple Pathways of Recombination Induced by Double-Strand Breaks in Saccharomyces cerevisiae', *Microbiology and Molecular Biology Reviews*, 63(2), pp. 349–404. doi: 10.1128/mmbr.63.2.349-404.1999.

Perry, J., Kleckner, N. and Börner, G. V. (2005) 'Bioinformatic analyses implicate the collaborating meiotic crossover/chiasma proteins Zip2, Zip3, and Spo22/Zip4 in ubiquitin labeling', *Proceedings of the National Academy of Sciences of the United States of America*, 102(49), pp. 17594–17599. doi: 10.1073/pnas.0508581102.

Pochart, P., Woltering, D. and Hollingsworth, N. M. (1997) 'Conserved properties between functionally distinct MutS homologs in yeast', *Journal of Biological Chemistry*, 272(48), pp. 30345–30349. doi: 10.1074/jbc.272.48.30345.

Pradillo, M. *et al.* (2007) 'An analysis of univalent segregation in meiotic mutants of Arabidopsis thaliana: A possible role for synaptonemal complex', *Genetics*, 175(2), pp. 505–511. doi: 10.1534/genetics.106.067595.

Pradillo, M. *et al.* (2012) 'Together yes, but not coupled: New insights into the roles of RAD51 and DMC1 in plant meiotic recombination', *Plant Journal*, 69(6), pp. 921–933. doi: 10.1111/j.1365-313X.2011.04845.x.

Pradillo, M. *et al.* (2014) 'On the role of AtDMC1, AtRAD51 and its paralogs during Arabidopsis meiosis.', *Frontiers in plant science*, 5(23), pp. 1–13. doi: 10.3389/fpls.2014.00023.

Pradillo, M. *et al.* (2015) 'Involvement of the cohesin cofactor PDS5 (SPO76) during meiosis and DNA repair in Arabidopsis thaliana', *Frontiers in Plant Science*, 6(DEC), pp. 1–14. doi: 10.3389/fpls.2015.01034.

Prinz, S., Amon, A. and Klein, F. (1997) 'Isolation of COM1, a new gene required to complete meiotic double- strand break-induced recombination in Saccharomyces cerevisiae', *Genetics*, 146(3), pp. 781–795.

Prusicki, M. A. *et al.* (2019) 'Live cell imaging of meiosis in Arabidopsis thaliana', *eLife*, 8(e42834), pp. 1–31.

Prusicki, M. A. *et al.* (2021) 'Caught in the Act : Live-Cell Imaging of Plant Meiosis', *Frontiers in Plant Science*, 12(December), p. 718346. doi: 10.3389/fpls.2021.718346.

Redon, C. *et al.* (2002) 'Histone H2A variants H2AX and H2AZ', *Current Opinion in Genetics & Development*, 12(1), pp. 162–169. doi: 10.1016/j.febslet.2004.12.092.

Ren, L. *et al.* (2021) ‘The E3 ubiquitin ligase DESYNAPSIS1 regulates synapsis and recombination in rice meiosis’, *Cell Reports*, 37(5), p. 109941. doi: 10.1016/j.celrep.2021.109941.

Resnick, M. A. (1976) ‘The repair of double-strand breaks in DNA: A model involving recombination’, *Journal of Theoretical Biology*, 59(1), pp. 97–106. doi: 10.1016/S0022-5193(76)80025-2.

Rey, M. D. *et al.* (2017) ‘Exploiting the ZIP4 homologue within the wheat Ph1 locus has identified two lines exhibiting homoeologous crossover in wheat-wild relative hybrids’, *Molecular Breeding*. Molecular Breeding, 37(8). doi: 10.1007/s11032-017-0700-2.

Riley, R. and Chapman, V. (1958) ‘Genetic Control of the Cytologically Diploid Behaviour of Hexaploid Wheat’, *Nature*, (182), pp. 713–715.

Robert, T. *et al.* (2016) ‘The TopoVIB-Like protein family is required for meiotic DNA double-strand break formation’, *Science*, 351(6276), pp. 943–949.

Rockmill, B. and Roeder, G. S. (1988a) ‘RED1: a yeast gene required for the segregation of chromosomes during the reductional division of meiosis.’, *Proceedings of the National Academy of Sciences of the United States of America*, 85(16), pp. 6057–6061. doi: 10.1073/pnas.85.16.6057.

Rockmill, B. and Roeder, G. S. (1988b) ‘RED1: a yeast gene required for the segregation of chromosomes during the reductional division of meiosis.’, *Proceedings of the National Academy of Sciences of the United States of America*, 85(16), pp. 6057–6061. doi: 10.1073/pnas.85.16.6057.

Rockmill, B. and Roeder, G. S. (1990) ‘Meiosis in asynaptic yeast’, *Genetics*, 126(3), pp. 563–574.

Rogakou, E. P. *et al.* (1998) ‘DNA double-stranded breaks induce histone H2AX phosphorylation on serine 139’, *Journal of Biological Chemistry*. Â© 1998 ASBMB. Currently published by Elsevier Inc; originally published by American Society for Biochemistry and Molecular Biology., 273(10), pp. 5858–5868. doi: 10.1074/jbc.273.10.5858.

Roig, I. *et al.* (2010) ‘Mouse TRIP13/PCH2 is required for recombination and normal higher-order chromosome structure during meiosis’, *PLoS Genetics*, 6(8). doi: 10.1371/journal.pgen.1001062.

Rosenberg, S. C. and Corbett, K. D. (2015) ‘The multifaceted roles of the HOR MA domain in cellular signaling’, *Journal of Cell Biology*, 211(4), pp. 745–755. doi: 10.1083/jcb.201509076.

Ross-Macdonald, P. and Roeder, G. S. (1994) ‘Mutation of a meiosis-specific MutS homolog decreases crossing over but not mismatch correction’, *Cell*, 79(6), pp. 1069–1080. doi: 10.1016/0092-8674(94)90037-X.

Ross, K. J. *et al.* (1997) ‘Cytological characterization of four meiotic mutants of Arabidopsis isolated from T-DNA-transformed lines’, *Chromosome Research*, 5(8), pp. 551–559. doi: 10.1023/A:1018497804129.

Ross, K. J., Fransz, P. and Jones, G. H. (1996) ‘A light microscopic atlas of meiosis inArabidopsis thaliana’, *Chromosome Research*, 4(7), pp. 507–516. doi: 10.1007/BF02261778.

Rusholme, R. L. *et al.* (2007) ‘Genetic control of broad-spectrum resistance to turnip mosaic virus in Brassica rapa (Chinese cabbage)’, *Journal of General Virology*, 88(11), pp. 3177–3186. doi: 10.1099/vir.0.83194-0.

Saintenac, C. *et al.* (2009) ‘Detailed recombination studies along chromosome 3B provide new insights on crossover distribution in wheat (Triticum aestivum L.)’, *Genetics*, 181(2), pp. 393–403. doi: 10.1534/genetics.108.097469.

San-Segundo, P. A. and Shirleen Roeder, G. (1999) ‘Pch2 links chromatin silencing to meiotic checkpoint control’, *Cell*, 97(3), pp. 313–324. doi: 10.1016/S0092-8674(00)80741-2.

Sanchez-Moran, E. *et al.* (2001) ‘Chiasma formation in Arabidopsis thaliana accession Wassileskija and in two meiotic mutants’, *Chromosome Research*, 9(2), pp. 121–128. doi: 10.1023/A:1009278902994.

Sanchez-Moran, E. *et al.* (2007) 'ASY1 mediates AtDMC1-dependent interhomolog recombination during meiosis in Arabidopsis', *Genes and Development*, 21(17), pp. 2220–2233. doi: 10.1101/gad.439007.

Sanchez-Moran, E. *et al.* (2008) 'ASY1 coordinates early events in the plant meiotic recombination pathway', *Cytogenetic and Genome Research*, 120(3–4), pp. 302–312. doi: 10.1159/000121079.

Scheller, J. *et al.* (2000) 'MPH1, a yeast gene encoding a DEAH protein, plays a role in protection of the genome from spontaneous and chemically induced damage', *Genetics*, 155(3), pp. 1069–1081.

Schürer, K. A. *et al.* (2004) 'Yeast MPH1 Gene Functions in an Error-Free DNA Damage Bypass Pathway That Requires Genes from Homologous Recombination, but Not from Postreplicative Repair', *Genetics*, 166(4), pp. 1673–1686. doi: 10.1534/genetics.166.4.1673.

Schwacha, A. and Kleckner, N. (1997) 'Interhomolog bias during meiotic recombination: Meiotic functions promote a highly differentiated interhomolog-only pathway', *Cell*, 90(6), pp. 1123–1135. doi: 10.1016/S0092-8674(00)80378-5.

Sebastian, J. *et al.* (2009) 'The plant adherin AtSCC2 is required for embryogenesis and sister-chromatid cohesion during meiosis in Arabidopsis', *Plant Journal*, 59(1), pp. 1–13. doi: 10.1111/j.1365-313X.2009.03845.x.

Seear, P. J. *et al.* (2020) 'A novel allele of ASY3 is associated with greater meiotic stability in autotetraploid Arabidopsis lyrata', *PLoS Genetics*, 16(7), pp. 1–21. doi: 10.1371/journal.pgen.1008900.

Séguéla-Arnaud, M. *et al.* (2015) 'Multiple mechanisms limit meiotic crossovers: TOP3α and two BLM homologs antagonize crossovers in parallel to FANCM', *Proceedings of the National Academy of Sciences of the United States of America*, 112(15), pp. 4713–4718. doi: 10.1073/pnas.1423107112.

Shen, Y. *et al.* (2012) 'ZIP4 in homologous chromosome synapsis and crossover formation in rice meiosis', *Journal of Cell Science*, 125(11), pp. 2581–2591. doi: 10.1242/jcs.090993.

Shinohara, A., Ogawa, H. and Ogawa, T. (1992) 'Rad51 protein involved in repair and recombination in S. cerevisiae is a RecA-like protein', *Cell*, 69(3), pp. 457–470. doi: 10.1016/0092-8674(92)90447-K.

Sims, J., Copenhaver, G. P. and Schlögelhofer, P. (2019) 'Meiotic DNA repair in the nucleolus employs a nonhomologous end-joining mechanism', *Plant Cell*, 31(9), pp. 2259–2275. doi: 10.1105/TPC.19.00367.

Skibbens, R. V. *et al.* (1999) 'Ctf7p is essential for sister chromatid cohesion and links mitotic chromosome structure to the DNA replication machinery', *Genes and Development*, 13(3), pp. 307–319. doi: 10.1101/gad.13.3.307.

Smith, A. V. and Roeder, G. S. (1997) 'The yeast Red1 protein localizes to the cores of meiotic chromosomes', *Journal of Cell Biology*, 136(5), pp. 957–967. doi: 10.1083/jcb.136.5.957.

Smith, S. J., Osman, K. and Franklin, F. C. H. (2014) 'The condensin complexes play distinct roles to ensure normal chromosome morphogenesis during meiotic division in Arabidopsis', *Plant Journal*, 80(2), pp. 255–268. doi: 10.1111/tpj.12628.

Solari, A. J. and Moses, M. J. (1973) 'The structure of the central region in the synaptonemal complexes of hamster and cricket spermatocytes', *Journal of Cell Biology*, 56(1), pp. 145–152. doi: 10.1083/jcb.56.1.145.

Sommermeyer, V. *et al.* (2013) 'Spp1, a Member of the Set1 Complex, Promotes Meiotic DSB Formation in Promoters by Tethering Histone H3K4 Methylation Sites to Chromosome Axes', *Molecular Cell*, 49(1), pp. 43–54. doi: 10.1016/j.molcel.2012.11.008.

Soustelle, C. *et al.* (2002) 'Replication protein A is required for meiotic recombination in Saccharomyces cerevisiae', *Genetics*, 161(2), pp. 535–547.

Stacey, N. J. *et al.* (2006) 'Arabidopsis SPO11-2 functions with SPO11-1 in meiotic recombination',

Plant Journal, 48(2), pp. 206–216. doi: 10.1111/j.1365-313X.2006.02867.x.

Stack, S. M., Anderson, L. K. and Sherman, J. D. (1989) ' Chiasmata and recombination nodules in Lilium longiflorum ', *Genome*, 32(3), pp. 486–498. doi: 10.1139/g89-473.

Stephenson, P. *et al.* (2010) 'A rich TILLING resource for studying gene function in Brassica rapa', *BMC Plant Biology*, 10, pp. 1–10. doi: 10.1186/1471-2229-10-62.

Storlazzi, A. *et al.* (2003) 'Meiotic double-strand breaks at the interface of chromosome movement, chromosome remodeling, and reductional division', *Genes and Development*, 17(21), pp. 2675–2687. doi: 10.1101/gad.275203.

Sturtevant, A. H. (1913) 'The linear arrangement of six sex-linked factors in Drosophila, as shown by their mode of association', *Journal of Experimental Zoology*, 14(1), pp. 43–59. doi: 10.1002/jez.1400140104.

Sturtevant, A. H. (1915) 'The behavior of the chromosomes as studied through linkage', *Zeitschrift für Induktive Abstammungs- und Vererbungslehre*, 13(1), pp. 234–287. doi: 10.1007/BF01792906.

Sun, H., Treco, D. and Szostak, J. W. (1991) 'Extensive 3′-overhanging, single-stranded DNA associated with the meiosis-specific double-strand breaks at the ARG4 recombination initiation site', *Cell*, 64(6), pp. 1155–1161. doi: 10.1016/0092-8674(91)90270-9.

Sung, P. *et al.* (2003) 'Rad51 Recombinase and Recombination Mediators', *Journal of Biological Chemistry*. Â© 2003 ASBMB. Currently published by Elsevier Inc; originally published by American Society for Biochemistry and Molecular Biology., 278(44), pp. 42729–42732. doi: 10.1074/jbc.R300027200.

Sutton, W. S. (1902) 'On the morphology of the chromosome group in Brachystola magna', *Biological Bulletin*, 4, pp. 24–39. doi: 10.1007/s12045-009-0041-5.

Sutton, W. S. (1903) 'The Chromosomes in Heredity', *Biologicall Bulletin*, 4, pp. 231–251.

Sybenga, J. (1969) 'Allopolyploidization of Autopolyploids I. Possibilities and Limitations', *Euphytica*, 18, pp. 355–371.

Sybenga, J. (1975) *Meiotic Configurations: A Source of Information for Estimating Genetic Parameters*. 1st edn. Edited by R. Frankel et al. Berlin Heidelberg New York: Springer-Verlag.

Sybenga, J. (1996) 'Chromosome pairing affinity and quadrivalent formation in polyploids: do segmental allopolyploids exist?', *Genome*, 39(6), pp. 1176–1184. doi: 10.1139/g96-148.

Sym, M., Engebrecht, J. A. and Roeder, G. S. (1993) 'ZIP1 is a synaptonemal complex protein required for meiotic chromosome synapsis', *Cell*, 72(3), pp. 365–378. doi: 10.1016/0092-8674(93)90114-6.

Szostak, J. W. *et al.* (1983) 'The double-strand-break repair model for recombination', *Cell*, 33(1), pp. 25–35. doi: 10.1016/0092-8674(83)90331-8.

Taagen, E., Bogdanove, A. J. and Sorrells, M. E. (2020) 'Counting on Crossovers: Controlled Recombination for Plant Breeding', *Trends in Plant Science*. The Authors, 25(5), pp. 455–465. doi: 10.1016/j.tplants.2019.12.017.

Tarsounas, M. *et al.* (1999) 'RAD51 and DMC1 form mixed complexes associated with mouse meiotic chromosome cores and synaptonemal complexes', *Journal of Cell Biology*, 147(2), pp. 207–219. doi: 10.1083/jcb.147.2.207.

Tock, A. J. and Henderson, I. R. (2018) 'Hotspots for Initiation of Meiotic Recombination', *Frontiers in Genetics*, 9(November). doi: 10.3389/fgene.2018.00521.

Tsubouchi, T., Zhao, H. and Roeder, G. S. (2006) 'The Meiosis-Specific Zip4 Protein Regulates Crossover Distribution by Promoting Synaptonemal Complex Formation Together with Zip2', *Developmental Cell*, 10(6), pp. 809–819. doi: 10.1016/j.devcel.2006.04.003.

Tung, K. S. and Roeder, G. S. (1998) 'Meiotic chromosome morphology and behavior in zip1 mutants of Saccharomyces cerevisiae', *Genetics*, 149(2), pp. 817–832.

Vader, G. (2015) 'Pch2TRIP13: controlling cell division through regulation of HORMA domains', *Chromosoma*, 124(3), pp. 333–339. doi: 10.1007/s00412-015-0516-y.

Vaur, S. *et al.* (2012) 'Pds5 promotes cohesin acetylation and stable cohesin-chromosome interaction', *EMBO Reports*, 13(7), pp. 645–652. doi: 10.1038/embor.2012.72.

Vrielynck, N. *et al.* (2016) 'A DNA topoisomerase VI – like complex initiates meiotic recombination', *Science (New York, NY)*, 351(6276), pp. 939–944.

Vrielynck, N. *et al.* (2021) ' Conservation and divergence of meiotic DNA double strand break forming mechanisms in Arabidopsis thaliana ', *Nucleic Acids Research*, 49(17), pp. 9821–9835. doi: 10.1093/nar/gkab715.

Wang, K. *et al.* (2009) 'MER3 is required for normal meiotic crossover formation, but not for presynaptic alignment in rice', *Journal of Cell Science*, 122(12), pp. 2055–2063. doi: 10.1242/jcs.049080.

Wang, K. *et al.* (2011) 'PAIR3, an axis-associated protein, is essential for the recruitment of recombination elements onto meiotic chromosomes in rice', *Molecular Biology of the Cell*, 22(1), pp. 12–19. doi: 10.1091/mbc.E10-08-0667.

Wang, K. *et al.* (2012) 'The role of rice HEI10 in the formation of meiotic crossovers', *PLoS Genetics*, 8(7). doi: 10.1371/journal.pgen.1002809.

Wang, M. *et al.* (2010) 'The central element protein ZEP1 of the synaptonemal complex regulates the number of crossovers during meiosis in rice', *Plant Cell*, 22(2), pp. 417–430. doi: 10.1105/tpc.109.070789.

Wang, T. F., Kleckner, N. and Hunter, N. (1999) 'Functional specificity of MutL homologs in yeast: Evidence for three Mlh1-based heterocomplexes with distinct roles during meiosis in recombination and mismatch correction', *Proceedings of the National Academy of Sciences of the United States of America*, 96(24), pp. 13914–13919. doi: 10.1073/pnas.96.24.13914.

Wang, X. *et al.* (2011) 'The genome of the mesopolyploid crop species Brassica rapa', *Nature Genetics*, 43(10), pp. 1035–1040. doi: 10.1038/ng.919.

Waterworth, W. M. *et al.* (2007) 'NBS1 is involved in DNA repair and plays a synergistic role with ATM in mediating meiotic homologous recombination in plants', *Plant Journal*, 52(1), pp. 41–52. doi: 10.1111/j.1365-313X.2007.03220.x.

Watson, B. I. D. and Callan, H. G. (1963) 'The Form of Bivalent Chromosomes in Newt Oocytes at First Metaphase of Meiosis', *Journal of Cell Science*, s3-104(66), pp. 281–295.

Watt, P. M. *et al.* (1996) 'SGS1, a homologue of the Blooms and Werner's syndrome genes, is required for maintenance of genome stability in Saccharomyces cerevisiae', *Genetics*, 144(3), pp. 935–945.

West, A. M. V. *et al.* (2019) 'A conserved filamentous assembly underlies the structure of the meiotic chromosome axis', *eLife*, 8, pp. 1–27. doi: 10.7554/elife.40372.

West, A. M. V., Komives, E. A. and Corbett, K. D. (2018) 'Conformational dynamics of the Hop1 HORMA domain reveal a common mechanism with the spindle checkpoint protein Mad2', *Nucleic Acids Research*. Oxford University Press, 46(1), pp. 279–292. doi: 10.1093/nar/gkx1196.

White, C. I. (2008) 'News from Arabidopsis on the Meiotic Roles of Blap75/Rmi1 and Top3α', *PLoS Genetics*, 4(12), p. e1000306. doi: 10.1371/journal.pgen.1000306.

Wijnker, E. *et al.* (2019) 'The Cdk1/Cdk2 homolog CDKA;1 controls the recombination landscape in Arabidopsis', *Proceedings of the National Academy of Sciences of the United States of America*, 116(25), pp. 12534–12539. doi: 10.1073/pnas.1820753116.

Wilson, E. B. and Morgan, T. H. (1920) 'Chiasmatype and Crossing Over', *American Naturalist*, 54(632), pp. 193–219.

Wojtasz, L. *et al.* (2009) 'Mouse HORMAD1 and HORMAD2, two conserved meiotic chromosomal proteins, are depleted from synapsed chromosome axes with the help of TRIP13 AAA-ATPase', *PLoS Genetics*, 5(10). doi: 10.1371/journal.pgen.1000702.

Xu, L., Weiner, B. M. and Kleckner, N. (1997) 'Meiotic cells monitor the status of the interhomolog recombination complex', *Genes and Development*, 11(1), pp. 106–118. doi: 10.1101/gad.11.1.106.

Yadav, V. K. and Claeys Bouuaert, C. (2021) 'Mechanism and Control of Meiotic DNA Double-Strand Break Formation in S. cerevisiae', *Frontiers in Cell and Developmental Biology*, 9(March), pp. 1–20. doi: 10.3389/fcell.2021.642737.

Yang, C. *et al.* (2019) ' The Arabidopsis Cdk1/Cdk2 homolog CDKA ;1 controls chromosome axis assembly during plant meiosis ', *The EMBO Journal*, pp. 1–19. doi: 10.15252/embj.2019101625.

Yang, C. *et al.* (2020) 'Closure motif-mediated state changes of the HORMA protein ASY1', *BioRxiv*. doi: 10.1016/j.solener.2019.02.027.

Yang, Chao *et al.* (2020) 'State changes of the HORMA protein ASY1 are mediated by an interplay between its closure motif and PCH2', *Nucleic Acids Research*. Oxford University Press, pp. 1–15. doi: 10.1093/nar/gkaa527.

Yang, F. *et al.* (2006) 'Mouse SYCP2 is required for synaptonemal complex assembly and chromosomal synapsis during male meiosis', *Journal of Cell Biology*, 173(4), pp. 497–507. doi: 10.1083/jcb.200603063.

Yin, J. *et al.* (2005) 'BLAP75, an essential component of Bloom's syndrome protein complexes that maintain genome integrity', *EMBO Journal*, 24(7), pp. 1465–1476. doi: 10.1038/sj.emboj.7600622.

Yuan, L. *et al.* (2000) 'The Murine SCP3 Gene Is Required for Synaptonemal Complex Assembly, Chromosome Synapsis, and Male Fertility', *Molecular Cell*, 5, pp. 73–83. doi: 10.1083/jcb.200603063.

Yuan, W. *et al.* (2009) 'Mutation of the rice gene PAIR3 results in lack of bivalent formation in meiosis', *Plant Journal*, 59(2), pp. 303–315. doi: 10.1111/j.1365-313X.2009.03870.x.

Zakharyevich, K. *et al.* (2010) 'Temporally and Biochemically Distinct Activities of Exo1 during Meiosis: Double-Strand Break Resection and Resolution of Double Holliday Junctions', *Molecular Cell*. Elsevier Inc., 40(6), pp. 1001–1015. doi: 10.1016/j.molcel.2010.11.032.

Zalevsky, J. *et al.* (1999) 'Crossing over during Caenorhabditis elegans meiosis requires a conserved MutS-based pathway that is partially dispensable in budding yeast', *Genetics*, 153(3), pp. 1271–1283.

Zhang, J. *et al.* (2008) 'Acetylation of Smc3 by Eco1 Is Required for S Phase Sister Chromatid Cohesion in Both Human and Yeast', *Molecular Cell*, 31(1), pp. 143–151. doi: 10.1016/j.molcel.2008.06.006.

Zhang, L. *et al.* (2014) 'Crossover Patterning by the Beam-Film Model: Analysis and Implications', *PLoS Genetics*, 10(1). doi: 10.1371/journal.pgen.1004042.

Zhao, D. *et al.* (2006) 'ASK1, a SKP1 homolog, is required for nuclear reorganization, presynaptic homolog juxtaposition and the proper distribution of cohesin during meiosis in Arabidopsis', *Plant Molecular Biology*, 62(1–2), pp. 99–110. doi: 10.1007/s11103-006-9006-1.

Zhong, X. B., De Jong, J. H. and Zabel, P. (1996) 'Preparation of tomato meiotic pachytene and mitotic metaphase chromosomes suitable for fluorescence in situ hybridization (FISH)', *Chromosome Research*, 4(1), pp. 24–28. doi: 10.1007/BF02254940.

Zickler, D and Kleckner, N. (1999) 'Meiotic chromosomes: integrating structure and function.', *Annual review of genetics*, 33, pp. 603–754. doi: 10.1146/annurev.genet.33.1.603.

Zickler, Denise and Kleckner, N. (1999) 'Meiotic chromosomes: integrating structure and function',

Annu. Rev. Genet., 33(1), pp. 603–754. doi: 10/djjgsx.

Zickler, D. and Kleckner, N. (2015) 'Recombination, Pairing, and Synapsis of Homologs during Meiosis', *Cold Spring Harbor Laboratory Press*, p. 1,2. doi: 10.1101/cshperspect.a016626.

Zickler, D. and Kleckner, N. (2016) 'A few of our favorite things: Pairing, the bouquet, crossover interference and evolution of meiosis', *Seminars in Cell and Developmental Biology*. Elsevier Ltd, 54, pp. 135–148. doi: 10.1016/j.semcdb.2016.02.024.

Zielinski, M.-L. and Mittelsten Scheid, O. (2012) 'Meiosis in Polyploid Plants', in *Polyploidy and Genome Evolution*. Springer Berlin Heidelberg, pp. 33–55. doi: 10.1007/978-3-642-31442-1_3.

Ziolkowski, P. A. *et al.* (2017) 'Natural variation and dosage of the HEI10 meiotic E3 ligase control Arabidopsis crossover recombination', *Genes and Development*, 31(3), pp. 306–317. doi: 10.1101/gad.295501.116.

Appendix

A.1. Cytological analysis of the *msh4-1 fancm-11* double mutant

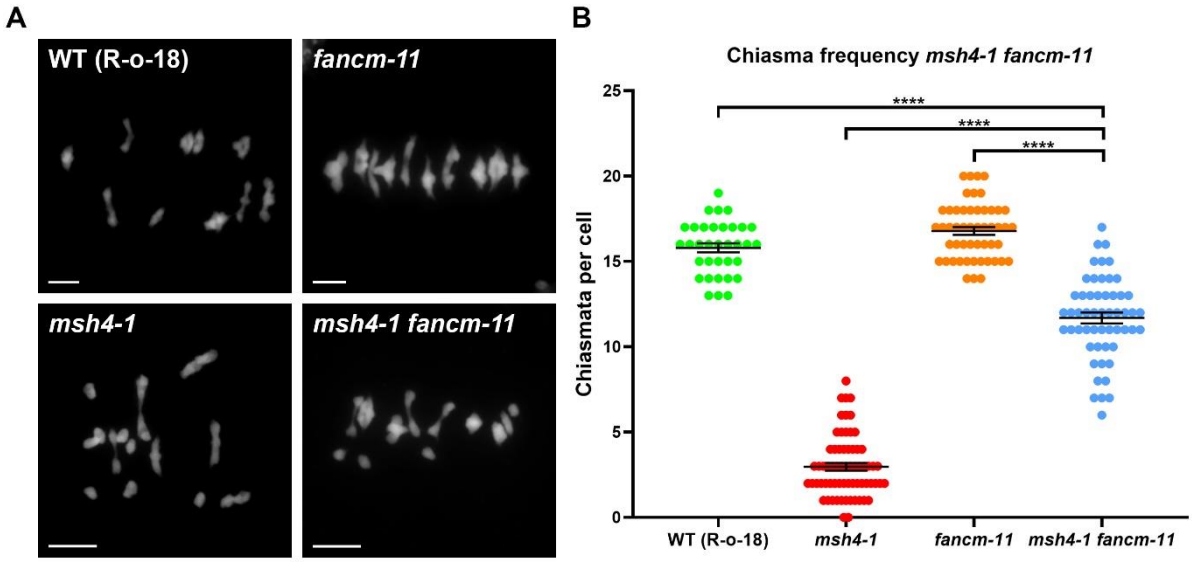


Figure A.1. Chiasma frequency analysis in the *msh4-1 fancm-11* double mutant. (A). Metaphase I nuclei spreads of WT, *fancm-11*, *msh4-1*, and *msh4-1 fancm-11* plants. 5 µm bars. **(B).** Scatter plot of the chiasma frequency per cell in the previously mentioned mutant lines. The *msh4-1 fancm-11* double mutant (n=54) presents an increase in the chiasma frequency per in comparison with the *msh4-1* plants (n=66), although this is significantly lower than in the *fancm-11* single mutant (n=51) and the WT control plants (n=34). ****p<0.0001. The statistical analysis employed to seek for differences within the group was a Welch's ANOVA (W=752.8 [3.000, 102.7]), this followed by pairwise comparisons between the genotypes using the Dunnet's T3 test.

A.2. Scientific communications

A.2.1. Conferences

SEB 2021 Annual Conference (29th June – 8th July 2021)

- Society of Experimental Biology. On-line conference.
- **Oral Presentation:** "Meiotic axis structure in Brassica crops: The role of the coiled-coil domain protein ASY3 in *B. rapa*"

The Students and Postdocs Meiosis Workshop v3.0 - PDSM 2021 (06th – 08th April 2021)

- On-line conference.
- **Oral Presentation:** "Meiotic axis structure in Brassica crops: The role of the coiled-coil domain protein ASY3 in *B. rapa*"

BGRS Symposium 2020 (12th – 13th November 2020)

- Biosciences Graduate Research School. University of Birmingham, Birmingham, UK. (On-line conference)

- **Oral presentation:** “Functional analysis of the meiotic chromosome axis morphogenesis in Brassica crops”.

EMBO Workshop of Meiosis 2019 (25th – 29th August 2019)

- EMBO Meiosis Organising Committee. La Rochelle, France.
- **Poster:** “Systematic analysis of the axial element organization in plant meiosis”

SymBioSE 2019 Scotland (29th July – 06th August 2019)

- Symposium of Biology Students of Europe. University of Glasgow, Glasgow, UK.
- **Oral presentation:** “Meiosis and Homologous Recombination: New Insights from Plant Cytogenetics Research”

11th British Meiosis Meeting (17th – 18th April 2019)

- University of Aberystwyth, Aberystwyth, Wales, UK.
- **Poster:** “Shedding Light on The Role of The Aminopeptidase MPA1 In *Arabidopsis thaliana* Meiotic Recombination”.

A.2.2. Seminars

Plant Science Seminar (15th December 2021)

- School of Biosciences, University of Birmingham, Birmingham, UK.
- **Presentation:** “Analysis of the meiotic chromosome axis remodelling in *Brassica* crops”

Plant Science Seminar (18th November 2020)

- School of Biosciences, University of Birmingham, Birmingham, UK.
- **Presentation:** “Functional analysis of the meiotic chromosome axis morphogenesis in *Brassica* crops”

A.2.3. Participation in outreach events

University Open Days (17th November 2021)

- University of Birmingham, Birmingham UK.
- **Objective:** Introduce Year 10 students to research in plant science and its applications

MEICOM Meet the Scientist Outreach Event (21st February 2019)

- Think Tank Museum, Birmingham, UK.
- Member of the organising committee
- **Objective:** Dissemination of plant science, biotechnology, and food security to the general public, particularly young children and their families.

SOCIETY FOR EXPERIMENTAL BIOLOGY

Journal of Experimental Botany, Vol. 72, No. 8 pp. 3012–3027, 2021
doi:10.1093/jxb/erab035 Advance Access Publication 27 January 2021
This paper is available online free of all access charges (see https://academic.oup.com/jxb/pages/openaccess for further details)

RESEARCH PAPER

Meiotic chromosome axis remodelling is critical for meiotic recombination in *Brassica rapa*

Maria Cuacos[1], Christophe Lambing[2], Miguel Pachon-Penalba[3], Kim Osman[3], Susan J. Armstrong[3], Ian R. Henderson[2], Eugenio Sanchez-Moran[3], F. Christopher H. Franklin[3] and Stefan Heckmann[1,*]

[1] Leibniz Institute of Plant Genetics and Crop Plant Research (IPK) OT Gatersleben, D-06466 Seeland, Germany
[2] Department of Plant Sciences, University of Cambridge, Cambridge CB2 3EA, UK
[3] School of Biosciences, University of Birmingham, Edgbaston, Birmingham B15 2TT, UK

* Correspondence: [redacted]

Received 7 September 2020; Editorial decision 18 January 2021; Accepted 21 January 2021

Editor: Anna Dobritsa, Ohio State University, USA

Abstract

Meiosis generates genetic variation through homologous recombination (HR) that is harnessed during breeding. HR occurs in the context of meiotic chromosome axes and the synaptonemal complex. To study the role of axis remodelling in crossover (CO) formation in a crop species, we characterized mutants of the axis-associated protein ASY1 and the axis-remodelling protein PCH2 in *Brassica rapa*. *asy1* plants form meiotic chromosome axes that fail to synapse. CO formation is almost abolished, and residual chiasmata are proportionally enriched in terminal chromosome regions, particularly in the nucleolar organizing region (NOR)-carrying chromosome arm. *pch2* plants show impaired ASY1 loading and remodelling, consequently achieving only partial synapsis, which leads to reduced CO formation and loss of the obligatory CO. PCH2-independent chiasmata are proportionally enriched towards distal chromosome regions. Similarly, in Arabidopsis *pch2*, COs are increased towards telomeric regions at the expense of (peri-) centromeric COs compared with the wild type. Taken together, in *B. rapa*, axis formation and remodelling are critical for meiotic fidelity including synapsis and CO formation, and in *asy1* and *pch2* CO distributions are altered. While *asy1* plants are sterile, *pch2* plants are semi-sterile and thus *PCH2* could be an interesting target for breeding programmes.

Keywords: ASY1, *Brassica rapa*, crossover, meiosis, meiotic chromosome axis remodelling, meiotic recombination, PCH2, synaptonemal complex.

Introduction

Meiosis is a specialized cell division in sexually reproducing organisms shuffling maternal and paternal genomes through homologous recombination (HR) and independent assortment of homologous chromosomes.

HR is initiated by programmed formation of SPO11-catalysed DNA double-strand breaks (DSBs) (Keeney and Kleckner, 1995; Keeney *et al.*, 1997; Neale *et al.*, 2005; Pan *et al.*, 2011). DSBs undergo a series of transitions, being

Abbreviations: CO, crossover; DSB, DNA double-strand break; FISH, fluorescence *in situ* hybridization; HR, homologous recombination; NCO, non-crossover; SC, synaptonemal complex; WT, wild type.

© The Author(s) 2021. Published by Oxford University Press on behalf of the Society for Experimental Biology.
This is an Open Access article distributed under the terms of the Creative Commons Attribution License (http://creativecommons.org/licenses/by/4.0/), which permits unrestricted reuse, distribution, and reproduction in any medium, provided the original work is properly cited.

repaired differently (Osman *et al.*, 2011; Mercier *et al.*, 2015; Wang and Copenhaver, 2018) into either a crossover (CO; reciprocal genetic exchange between homologous chromosomes) or a non-crossover (NCO), using as repair template either the sister chromatid or the homologous chromosome exchanging only short stretches of DNA. Erroneous meiotic DSB formation or repair may lead to univalent formation or chromosome breakage and thus genome instability, reducing fertility. In plants <10% of DSBs are repaired as COs, and DSBs/COs occur heterogeneously along chromosomes (Muyt *et al.*, 2009; Mercier *et al.*, 2015) limiting genetic variation generated during each meiotic cycle. In many crop species, COs are restricted to chromosome ends, inhibiting access to traits residing in 'cold' regions or creating 'linkage drag'; therefore, modulating CO number and distribution is of interest for plant breeding (Phillips *et al.*, 2013; Choulet *et al.*, 2014; Li *et al.*, 2015; Demirci *et al.*, 2017; Lambing and Heckmann, 2018; Dreissig *et al.*, 2019).

CO formation is tightly controlled in the following ways: (i) interhomologue bias, where recombination is favoured between homologous chromosomes; (ii) CO assurance, where at least one 'obligate' CO forms per chromosome essential for faithful chromosome segregation; and (iii) CO interference, where formation of one CO reduces the probability of another close by, thereby hampering CO clustering and limiting CO number per chromosome (Zickler and Kleckner, 2015). In Arabidopsis, at least two CO classes exist: ~85% of COs are catalysed by the ZMM proteins (MER3, HEI10, ZIP4, SHOC1, PTD, MSH4, and MSH5) and MLH1–MLH3 (Higgins *et al.*, 2004, 2008*b*; Chen *et al.*, 2005; Mercier *et al.*, 2005; Wijeratne *et al.*, 2006; Chelysheva *et al.*, 2007, 2012; Macaisne *et al.*, 2008), generating interference-sensitive class I COs; and part of the remaining ~15% are MUS81- or FANCD2-dependent interference-insensitive class II COs (Berchowitz *et al.*, 2007; Higgins *et al.*, 2008*a*; Kurzbauer *et al.*, 2018).

Concurrently with HR, the meiotic nucleus undergoes extensive reorganization of the chromatin. Following S phase, sister chromatids are linked by cohesins and, during leptotene, are organized in chromatin loops tethered to a linear proteinaceous structure called the meiotic chromosome axis (Kleckner, 2006). In Arabidopsis, this structure comprises, for example, ASY1, ASY3, ASY4, SMC3, and REC8 (Caryl *et al.*, 2000; Cai *et al.*, 2003; Chelysheva *et al.*, 2005; Lam *et al.*, 2005; Ferdous *et al.*, 2012; Chambon *et al.*, 2018). DSBs form at preferred sites (hotspots) in the chromatin loops which are then tethered to the axes where they are repaired as COs or NCOs (Panizza *et al.*, 2011). Following DSB formation, a proteinaceous structure, called the synaptonemal complex (SC), starts to form during zygotene by progressively polymerizing between homologous chromosome axes physically connecting them and promoting CO formation (Page and Hawley, 2004).

The Arabidopsis meiotic axis-associated protein ASY1 (Caryl *et al.*, 2000; Armstrong *et al.*, 2002; Sanchez-Moran *et al.*, 2007) is a HORMA domain-containing protein (yeast HOP1, mouse HORMAD1/2, or rice PAIR2; Hollingsworth *et al.*, 1990; Caryl *et al.*, 2000; Nonomura *et al.*, 2004; Fukuda *et al.*, 2010) required for synapsis and HR. In different organisms it is involved in the interhomologue bias (Martinez-Perez and Villeneuve, 2005; Niu *et al.*, 2005; Sanchez-Moran *et al.*, 2007; Carballo *et al.*, 2008; Kim *et al.*, 2010). In plants, *asy1* or *pair2* mutants display asynapsis and univalents due to reduced chiasma formation (Ross *et al.*, 1997; Caryl *et al.*, 2000; Nonomura *et al.*, 2004). In addition to axis and SC formation *per se*, dynamic regulation of these structures is critical for CO formation. Concomitant with ZYP1 loading, ASY1 becomes depleted from synapsed regions in a PCH2-dependent manner (Wojtasz *et al.*, 2009; Chen *et al.*, 2014; Lambing *et al.*, 2015). PCH2 is a conserved AAA-ATPase with diverse functions in different organisms. Initially reported as a checkpoint protein in yeast (San-Segundo and Roeder, 1999) and other species (Bhalla and Dernburg, 2005; Joyce and McKim, 2009), it has also been implicated in numerous meiotic processes, including DSB/CO formation, interhomologue bias, interference, axis morphogenesis, synapsis, and inhibition of DSB formation at rDNA borders (Börner *et al.*, 2008; Joshi *et al.*, 2009., 2015; Wojtasz *et al.*, 2009; Zanders and Alani, 2009; Vader *et al.*, 2011; Zanders *et al.*, 2011; Farmer *et al.*, 2012; Miao *et al.*, 2013; Lambing *et al.*, 2015; Subramanian *et al.*, 2016). In plants, Arabidopsis PCH2 is critical for axis remodelling as well as SC and CO formation (Lambing *et al.*, 2015; Yang *et al.*, 2020*a*, *b*) while rice PCH2 (CRC) is an integral component of the SC essential for DSB and CO formation as well as ASY1 assembly (Miao *et al.*, 2013). Interestingly, in Arabidopsis *pch2*, CO rates are altered in some chromosome regions (Lambing *et al.*, 2015).

To study the role of axis remodelling in a crop species, we characterized *asy1* and *pch2* mutants in *Brassica rapa* ($2n$=20). *asy1* plants form axes but SC formation is defective, leading to a reduction in CO frequency. Interestingly, residual chiasmata are proportionally increased towards chromosome ends and are enriched in the major 45S rDNA-carrying chromosome; in particular, chiasmata form within or close to the 45S rDNA locus while this is not the case in the wild type (WT) or in *pch2*. *pch2* plants form a partial SC while axes are not remodelled; that is, ASY1 loading during leptotene is reduced and ASY1 is not depleted from synapsed regions, leading to a reduction in CO frequency. PCH2-independent chiasmata are more skewed towards terminal chromosome regions. To corroborate this cytological observation, in Arabidopsis CO rates were established in different genetic intervals, revealing increased CO rates in telomeric chromosome regions at the expense of decreased (peri-)centromeric CO rates in *pch2* compared with the WT. We conclude that ASY1 and PCH2 are critical for SC and CO formation during meiosis in *B. rapa* and that *asy1* and *pch2* show altered CO patterning. Due to *pch2* showing only semi-sterility, it could potentially be an interesting target in breeding programmes to redistribute COs.

Materials and methods

Plant material

Brassica rapa cultivar R-o-18 and Arabidopsis ecotype Columbia (Col-0) were used as the WTs. The following *B. rapa* mutant lines were received from RevGenUK (https://www.jic.ac.uk/research-impact/technology-research-platforms/reverse-genetics/): *asy1-13* (JI32391-B), *asy1-14* (JI31044-B), *pch2-9* (JI32373-B), and *pch2-12* (JI32174-B). The following Arabidopsis T-DNA insertion lines (Alonso *et al.*, 2003) in the Col-0 background were obtained from the T-DNA mutant collection at the Salk Institute Genomics Analysis Laboratory (SIGnAL, http://signal.salk.edu/cgi-bin/tdnaexpress) via the NASC (http://arabidopsis.info/): *asy1-4* (SALK_046272) (Lambing *et al.*, 2020), *shoc1-1* (SALK_057589) (Macaisne *et al.*, 2008), *mus81-2* (SALK_107515) (Higgins *et al.*, 2008*a*), and *pch2-1* (Sail_1187_C06) (Lambing *et al.*, 2015). Plants were grown in greenhouses under 16 h day/8 h night, at 16 °C/14 °C (*B. rapa*) and 21 °C/18 °C (Arabidopsis) day/night temperatures.

Genotyping

In *B. rapa*, PCR-based genotyping was performed using derived cleaved amplified polymorphic sequences (dCAPS) (Neff *et al.*, 1998) with primers selected using the dCAPS Finder 2.0 tool (http://helix.wustl.edu/dcaps/) (Neff *et al.*, 2002). A list of primers and restriction enzymes is shown in Supplementary Table S1. After PCR amplification, the resulting amplicons were digested with corresponding restriction enzymes at 37 °C overnight and resolved on 2.5% agarose gels. Primers used to genotype Arabidopsis T-DNA mutants are indicated in Supplementary Table S1.

RNA extraction and reverse transcription–PCR

Total RNA of sample tissues was extracted with an RNeasy Plant Mini Kit (Qiagen) performing DNase digestion with the RNase-Free DNase Set (Qiagen). Reverse transcription was performed in a 20 µl reaction employing 750 ng of total RNA with a Tetro cDNA synthesis kit (Bioline) using oligo(dT) primers. Expression of *Actin* was evaluated as technical control for the integrity of the RNA/cDNA. A 5 µl aliquot of undiluted cDNA was used as template for 36 (*PCH2-12*) and 28 (*Actin*) PCR cycles. Primers used are listed in Supplementary Table S1.

Cytology and microscopy

Cytological procedures were carried out as described (Armstrong *et al.*, 2009) with minor modifications. 5S (pCT4.2; Campell *et al.*, 1992) and 45S (pTa71; Gerlach and Bedbrook, 1979) rDNA fluorescence *in situ* hybridization (FISH) probes were labelled by nick translation with Texas Red and Atto488 (NT labelling kits, Jena Biosciences). Chromosome spreading for immunostaining in *B. rapa* was done using five anthers per slide; digestion was done during 8 min in a moist chamber at 37 °C, disrupting the material with a brass rod after the first 4 min; and spreading was done with 1.5% lipsol. Immunostaining in Arabidopsis was performed on acid chromosome spreads from male meiocytes as described (Lambing *et al.*, 2020). The following antibodies and dilutions were used: anti-ASY1 (rabbit/rat, Sanchez-Moran *et al.*, 2007, 1:500), anti-ZYP1 (rat/guinea pig, Higgins *et al.*, 2005, 1:500), anti-SMC3 (rat, Ferdous *et al.*, 2012, 1:300), anti-ASY3 (rabbit, Ferdous *et al.*, 2012, 1:200), anti-MLH1 (for *B. rapa* rabbit, Jackson *et al.*, 2006; for Arabidopsis rabbit, Chelysheva *et al.*, 2010, 1:200), and anti-HEI10 (rat, Lambing *et al.*, 2015, 1:200). ASY1 intensity in *B. rapa* asynapsed versus synapsed regions was measured as described (Lambing *et al.*, 2015). Quantification of ASY1 signal intensity in Arabidopsis leptotene nuclei was performed according to Ziolkowski *et al.* (2017). In brief, Arabidopsis images were acquired as *z*-stacks of 10 images with an optical section of 0.2 µm each. The maximum fluorescence intensity projection for each cell was generated, and total signal intensity was quantified using ImageJ. A region adjacent to the chromatin was used to quantify the background level that was deducted from the total signal intensity. Each signal intensity was normalized by the mean WT signal intensity for comparison. Quantification of ASY1 signal intensity in *B. rapa* leptotene nuclei was performed in a similar way, but images were acquired as a single plane, and measurements were done with the corresponding microscope software. Images were acquired with a Nikon Eclipse 90i fluorescence microscope equipped with a Nikon DS-Qi1Mc digital camera and NIS-Elements-F software, or a Nikon Eclipse Ni-E equipped with a Nikon DS-Qi2 camera and NIS-Elements-AR version 4.60 software (Nikon, Tokyo, Japan). Images were processed with GIMP 2.10 (www.gimp.org).

Recombination measurement at genetic intervals

Recombination measurements for the intervals I5b, I2f, I2g, I5a, I5d, and I5c using fluorescent pollen (Berchowitz and Copenhaver, 2008) are from the study of Lambing *et al.* (2015); 420 and 5.11 are seed-based fluorescent assays (Melamed-Bessudo *et al.*, 2005; Wu *et al.*, 2015). Fluorescent seeds and recombination measurements were calculated using Cell Profiler as previously described (Ziolkowski *et al.*, 2015). CEN3 is a pollen-based fluorescent assay (Berchowitz and Copenhaver, 2008; Yelina *et al.*, 2012). Fluorescent pollen was manually recorded under an epifluorescence microscope. and recombination measurements were calculated as previously reported (Lambing *et al.*, 2015).

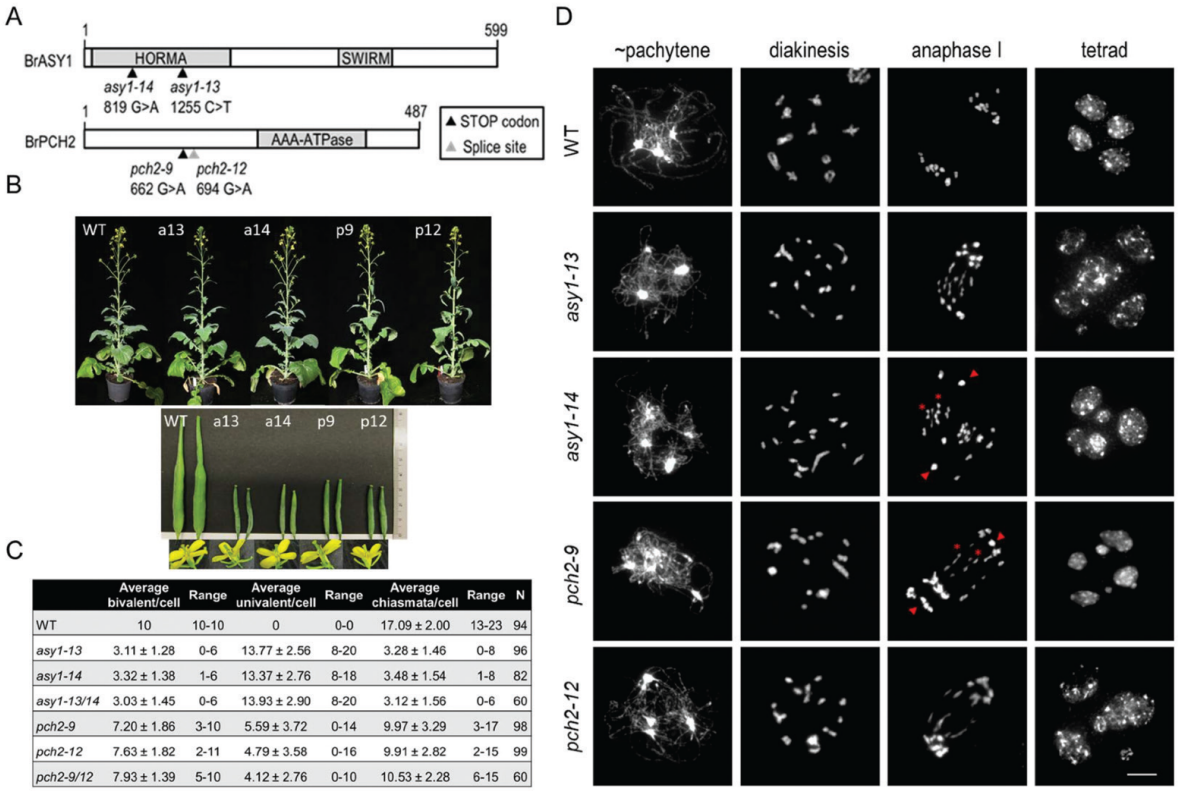
Results

Isolation of Brassica rapa asy1 *and* pch2

The *B. rapa* genome encodes *ASY1* (Bra004222) and *PCH2* (Bra013827) on chromosomes A07 and A01, respectively. One region spanning ~1 kb within *ASY1* and within *PCH2* were screened in a *B. rapa* R-o-18 TILLING (targeting induced local lesions in genomes) population (Stephenson *et al.*, 2010) by the RevGenUK TILLING service (https://www.jic.ac.uk/research-impact/technology-research-platforms/reverse-genetics/) to isolate putative *asy1* and *pch2* loss-of-function alleles.

For *ASY1*, two lines with predicted premature stop codons were selected (Fig. 1A): *asy1-13* (1255C>T, Q143>Stop) and *asy1-14* (819G>A, W72>Stop) predicted to encode 24% and 12% of the native protein length, respectively. Sequencing analysis in each line confirmed the presence of a single nucleotide polymorphism (SNP).

For *PCH2*, one line with a predicted premature stop codon and a second line with an SNP in an intron–exon boundary were selected (Fig. 1A): *pch2-9* (662G>A, W143>Stop), predicted to encode 29% of the native protein length, and *pch2-12* (694G>A, intron4–exon4 boundary). SNPs were confirmed by sequencing. Reverse transcription–PCR revealed the presence of alternative splice variants in *pch2-12* (Supplementary Fig. S1). Although the presence of the *PCH2* WT transcript cannot be excluded, *pch2-12* probably results in a null mutation as *pch2-12* is allelic to *pch2-9* in terms of meiotic fidelity (see below). *PCH2* expression is found in flower buds (containing cells undergoing meiosis) and also in leaves, similar to



	Average bivalent/cell	Range	Average univalent/cell	Range	Average chiasmata/cell	Range	N
WT	10	10-10	0	0-0	17.09 ± 2.00	13-23	94
asy1-13	3.11 ± 1.28	0-6	13.77 ± 2.56	8-20	3.28 ± 1.46	0-8	96
asy1-14	3.32 ± 1.38	1-6	13.37 ± 2.76	8-18	3.48 ± 1.54	1-8	82
asy1-13/14	3.03 ± 1.45	0-6	13.93 ± 2.90	8-20	3.12 ± 1.56	0-6	60
pch2-9	7.20 ± 1.86	3-10	5.59 ± 3.72	0-14	9.97 ± 3.29	3-17	98
pch2-12	7.63 ± 1.82	2-11	4.79 ± 3.58	0-16	9.91 ± 2.82	2-15	99
pch2-9/12	7.93 ± 1.39	5-10	4.12 ± 2.76	0-10	10.53 ± 2.28	6-15	60

Fig. 1. *asy1* and *pch2* plants display reduced fertility due to defects during meiosis. (A) Schematic representation of *Brassica rapa* ASY1 and PCH2 including mutations analysed (arrowheads). (B) *B. rapa* plant phenotypes (upper panel) including siliques and flowers (lower panel): WT, *asy1-13* (a13), *asy1-14* (a14), *pch2-9* (p9), and *pch2-12* (p12). (C) Average, SD, and range of bivalents, univalents, and chiasmata per cell in analysed lines. *n*=number of cells; a minimum of two independent plants per genotype. (D) *B. rapa* WT, *asy1*, and *pch2* male meiotic chromosome spreads. In both mutants, synapsis and chiasma formation are impaired, leading to the occurrence of univalents at diakinesis that results in unequal chromosome segregation and unbalanced tetrads. Note, univalents in the mutants could migrate complete to a pole (arrowheads) or separate chromatids (asterisks) during anaphase I. DNA is counterstained with DAPI and shown in grey. Scale bar=10μm.

the expression pattern found for other meiotic genes (Caryl *et al.*, 2000; Grelon *et al.*, 2001).

For all lines, three backcrosses to the WT (R-o-18) were performed in order to decrease the secondary mutation load. Data presented correspond to plants from the third backcross generation.

asy1 *and* pch2 *plants have reduced fertility due to defects in meiosis*

All plants exhibited normal vegetative growth and development (Fig. 1B). However, plants homozygous for any of the SNPs showed sterile anthers, short siliques, and reduced seed set, while corresponding heterozygous or WT TILLING plants were similar to the WT (Fig. 1B; Supplementary Table S2). To explore whether reduced fertility was due to meiotic defects, we performed male meiotic chromosome spread analysis. During WT meiosis (Fig. 1D; Supplementary Fig. S2a), unpaired chromosomes appear as thin threads during leptotene. During zygotene, chromosomes start to align and synapse, reaching full synapsis visible as thick threads at pachytene. At diakinesis, homologous chromosomes are visible as bivalents physically connected by chiasmata (cytological manifestation of COs). At metaphase I, 10 bivalents align at the equatorial plate and 10 homologous chromosomes migrate to opposite poles during anaphase I. During the second meiotic division, chromosomes align at metaphase II and 10 chromatids separate to opposite poles during anaphase II, producing four haploid products in a balanced tetrad.

In *asy1*, thick chromatin threads indicative of synapsis were not observed (Fig. 1D). During diakinesis and metaphase I, most chromosomes appeared as univalents, indicating a failure to form COs. During anaphase I, univalents either segregated to one pole or showed precocious separation of sister chromatids (Fig.

1D), leading to unbalanced tetrads and micronuclei. The WT showed invariably 10 bivalents with a mean of 17.1±2 chiasmata per cell, while *asy1* showed univalents in all cells. Reduced chiasma values for both *asy1* lines (3.28±1.46 and 3.48±1.54 chiasmata per cell for *asy1-13* and *asy1-14*, respectively) were not significantly different (Student's *t*-test, P=0.39, n=96 *asy1-13* and n=82 *asy1-14*) (Fig. 1C). Typically, bivalents formed rods (one chiasma). Only 12.4% of cells were found with one ring bivalent (at least one chiasma on each chromosome arm) and just 2.2% of cells had two ring bivalents (22/178 and 4/178 cells, respectively). No difference was found in *asy1-13/14* compared with each single mutant, confirming that the mutations are allelic (Fig. 1C; Supplementary Fig. S2c; Supplementary Table S2). Moreover, heterozygous *ASY1* plants pollinated with WT pollen produced long siliques with WT seed levels, while WT-pollinated homozygous *asy1* plants produced short siliques with zero seeds, suggesting that female meiosis is also defective. TILLING plants, WT or heterozygous for the mutations, showed WT-like meiosis (Supplementary Fig. S2b). Together, reduced fertility in *asy1* is based on defective synapsis and CO formation, and unbalanced chromosome segregation.

In *pch2* plants, cells with complete synapsis were never observed. At diakinesis/metaphase I, 89% of cells showed a mixture of bivalents and univalents (0–16 univalents per cell) that led to unbalanced tetrads and micronuclei (Fig. 1D). Univalents during anaphase I either separated chromatids or migrated to one pole (Fig. 1D). WT or heterozygous TILLING plants for *PCH2* showed WT-like meiosis (Supplementary Fig. S2b). The mean bivalent number was 7.20±1.86 (range 3–10) with an average of 9.97±3.29 (range 3–17) chiasmata per cell in *pch2-9*, and 7.63±1.82 (range 2–11) bivalents with an average of 9.91±2.82 (range 2–15) chiasmata per cell in *pch2-12* (Fig. 1C). Chiasma values for both lines were not significantly different (Student's *t*-test, P=0.89, n=98 *pch2-9* and n=99 *pch2-12*). Similar to *asy1*, ring bivalents co-existed with univalents. Notably, 46% of all cells showed ≥10 chiasmata per cell (a number that would be sufficient for all chromosome pairs to acquire at least one obligate CO), together with univalents. An allelism test crossing revealed no difference between *pch2-9/12* and *pch2-9* or *pch2-12* in terms of chiasma formation (Fig. 1C; Supplementary Fig. S2c), supporting that both mutations are allelic. However, in *pch2-12*, despite three backcrosses, a slight reduction in fertility was found among segregating families independent of *PCH2* (Supplementary Table S2). Thus, we focused our analysis on *pch2-9*.

Increased chiasmata in the major 45S rDNA locus-carrying chromosome in asy1

To identify whether in *asy1* bivalents formed preferentially between any particular chromosome pair(s), we performed FISH with 5S and 45S rDNA probes (Fig. 2). The number of 5S and 45S signals in *B. rapa* differs among varieties (Fukui *et al.*, 1998; Snowdon *et al.*, 2002; Koo *et al.*, 2004; Lim *et al.*, 2005; Mun *et al.*, 2010; Xiong and Pires, 2011; Perumal *et al.*, 2017) and has already been discussed (e.g. Hasterok *et al.*, 2006; Boutte *et al.*, 2020). In *B. rapa* R-o-18, we found four 45S and five 5S FISH signals, and assigned them to the chromosomes organized from the largest to the smallest, thereby distinguishing chromosome pairs #1 (largest chromosome, carrying 5S signals), #3 [large block of 45S, the nucleolar organizing region (NOR), and small 5S, probably corresponding to chromosome A03], #4 and #5 (both containing 5S and 45S, with a larger 45S locus in #4), #6 (45S only), and #10 (smallest chromosome, 5S only) (Fig. 2A).

In *asy1*, except for #3, all discernible chromosomes including the largest and the smallest appeared as univalents at similar frequencies (79–86%) (Supplementary Table S3). However, #3 which possesses the NOR with the largest 45S block, appeared as univalent in only 37% of cells. From the 63% #3 bivalents, 84% were rods and 16% rings; and from the #3 rod bivalents, in 64% of *asy1* cells the chiasma was cytologically associated with the 45S rDNA; that is, the chiasma was found either inside the NOR or distal to it (Fig. 2B). In contrast to *asy1*, in WT and *pch2* #3 rod bivalents, the single chiasma was never associated with the NOR but instead was invariably formed in the opposite arm (Fig. 2B).

Chromosome axes form in asy1 *but fail to assemble a synaptonemal complex*

The *asy1* mutants encode <25% of the native protein length, thus having a truncated or deleted HORMA domain and closure motif, critical for ASY1 localization (West *et al.*, 2019; Yang *et al.*, 2020*b*). To determine if the truncated ASY1 protein localizes to the axes and an SC forms in the *asy1* cells, we performed ASY1 and ZYP1 (transverse filament protein of the SC; Higgins *et al.*, 2005) immunolocalization. In the WT (Fig. 3), ASY1 localized to chromosome axes during leptotene. Once ASY1 was fully polymerized, ZYP1 initially formed foci and then short stretches which progressively elongated until all homologous chromosomes were fully synapsed. In *asy1* (Fig. 3), ASY1 could not be detected. ZYP1 predominantly formed foci (from <5 to >20, possibly in a stage-dependent manner) and rarely elongated beyond forming short stretches, indicating that SC formation is largely impaired. In late pachytene-/early diplotene-like cells, ZYP1 formed aggregates probably due to its inability to assemble the SC (Zickler and Kleckner, 1999).

To analyse axis morphogenesis in *asy1*, we performed immunolocalization of the cohesin subunit SMC3 (Lam *et al.*, 2005) and the coiled-coil protein ASY3 (Ferdous *et al.*, 2012). In the WT (Fig. 4), SMC3 was present from leptotene to pachytene, co-localizing initially with ASY1 and later on with ZYP1. Upon synapsis, ASY1 signals became faint while SMC3 persisted, gradually thickening as synapsis proceeded. ASY3 initially localized to the nucleolus during leptotene similar to Arabidopsis (Ferdous *et al.*, 2012) before it co-localized with ASY1 and then with ZYP1; however, ASY3 signals were patchier and less linear than those of ZYP1. In *asy1* (Fig. 4), both SMC3 and ASY3 localized to the axis following WT dynamics.

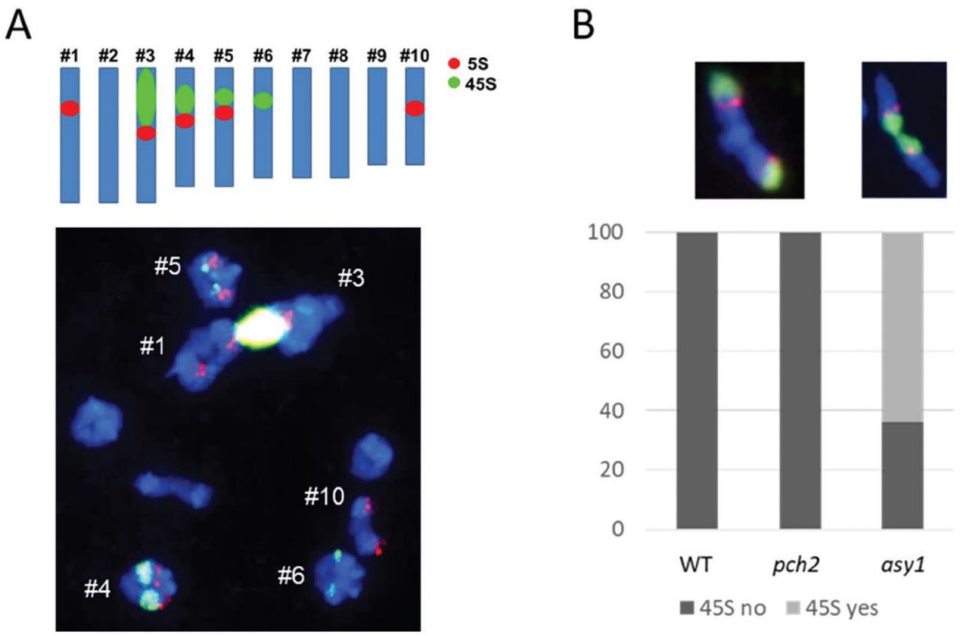


Fig. 2. The major 45S rDNA locus-carrying chromosome arm shows increased chiasmata in *asy1* but not in *pch2* or the WT. (A) Top: *B. rapa* chromosomes organized by size with 5S and 45S rDNA clusters detected by FISH. Bottom: a representative WT cell after FISH. (B) Percentage of #3 rod bivalents with a chiasma in the 45S-carrying arm ('45S yes', example FISH image right) or in the opposite arm ('45S no', example FISH image left). Total number of rod bivalents scored: WT 41, *pch2* 16, *asy1* 36. FISH images: 5S (red), 45S (green); DNA is counterstained with DAPI and shown in blue.

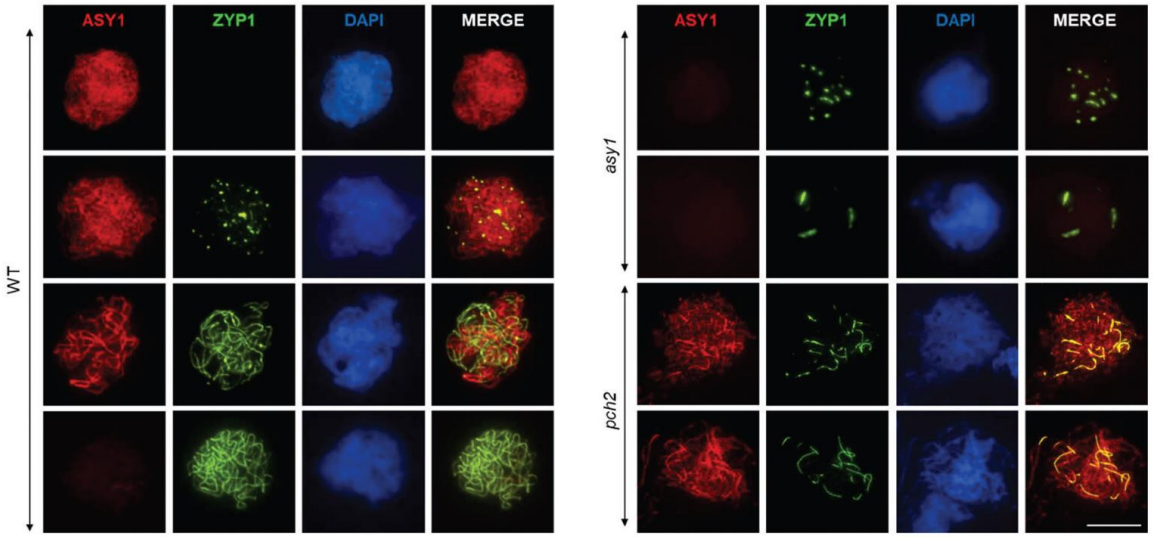


Fig. 3. Synapsis is defective in *asy1* and *pch2*. Immunolocalization of ASY1 (red) and ZYP1 (green) in the WT, *asy1*, and *pch2*. In *asy1*, ASY1 is not detected and ZYP1 forms foci in zygotene–pachytene cells and aggregates in late pachytene–diplotene cells. In *pch2*, different from the WT, ASY1 does not get depleted from the axes and appears highly abundant in limited synapsed regions co-localizing with ZYP1. DNA is counterstained with DAPI and shown in blue. Scale bar=10μm.

Thus, ASY1-independent axes form but are insufficient to support SC formation, resulting in reduced CO formation.

Class I and class II crossovers are reduced in asy1

CO formation was reduced but not abolished in *asy1*. From 178 *asy1* cells analysed, only one cell showed 20 univalents, whereas in all others between one and eight chiasmata were observed. To evaluate the nature of the remaining COs in *asy1*, we analysed the chiasma frequency distribution per cell. In the WT, the majority of COs are sensitive to interference, which leads to a non-random numerical distribution between cells. As a result, the mean chiasma frequency significantly deviates from a Poisson distribution [$\chi^2_{(R-o-18)}$=46.32, P<0.0001, n=94] (Fig. 5). However, in *asy1*, the chiasma frequency per cell was not significantly different from a Poisson distribution [$\chi^2_{(asy1-14)}$=7.79, P=0.25, n=82] (Fig. 5), suggesting that residual ASY1-independent COs are randomly distributed between cells.

To better understand CO formation in *asy1*, we performed immunolocalization of the class I CO marker MLH1 (Jackson *et al.*, 2006) together with ZYP1. We scored on average 9.44±0.72 (n=37) and 8.7±4.79 (n=10) MLH1 foci per cell in the WT and *asy1*, respectively (Fig. 6A). The MLH1 foci number per cell was highly variable in *asy1* (1–15) but not in the WT (8–11). While in the WT MLH1 foci typically overlapped with ZYP1, in *asy1* only an average of 3.9 MLH1 foci co-localized with residual ZYP1 foci (range 0–9). This manifested in different ways: ZYP1 stretches appeared to originate from MLH1 foci, two MLH1 foci were 'bridging' a ZYP1 stretch, or an MLH1 focus formed between two ZYP1 foci (Fig. 6A). Assuming that only ZYP1-associated MLH1 foci or a subset of these are CO competent, at least some of the residual chiasmata in *asy1* could be ZMM-dependent class I COs.

We also immunolocalized HEI10 (Chelysheva *et al.*, 2012; Wang *et al.*, 2012) together with ZYP1. In the WT, numerous small HEI10 foci found during early pachytene progressively fade, leaving on average 11.31±1.71 bright HEI10 foci per cell (n=27, range 8–15) during diplotene–diakinesis (Fig. 6B). In *asy1*, this number was significantly lower and more variable (9±3.3, n=19, range 4–14). This variability could be attributed to the difficulty in cytologically defining meiotic prophase stages in *asy1* and it is possible that some of the observed HEI10 foci will not mature in CO sites. However, as in the WT, in *asy1*, HEI10 foci typically co-localized with ZYP1. Similar to MLH1, short ZYP1 stretches originated from HEI10 foci or two HEI10 foci bridged a ZYP1 stretch. Altogether, our data suggest that interference-sensitive COs are designated in *asy1*, but the synaptic defect compromises CO maturation. As a result, an obligate CO fails to form between all chromosome pairs, and those COs that do mature exhibit a random distribution.

Next, we asked whether class II COs also form in the absence of ASY1 by taking advantage of available Arabidopsis resources. We crossed Arabidopsis *asy1* either with *shoc1* (involved in class I CO formation; Macaisne *et al.*, 2008, 2011) or with *mus81* (involved in class II CO formation; Berchowitz *et al.*, 2007; Higgins *et al.*, 2008*a*), and compared the chiasma frequency in these lines. Under our growth conditions, Arabidopsis *asy1* showed 2.3±0.88 bivalents and 2.77±1.22 chiasmata per cell (Table 1), *shoc1* showed 2.38±1.04 bivalents and 2.79±1.41

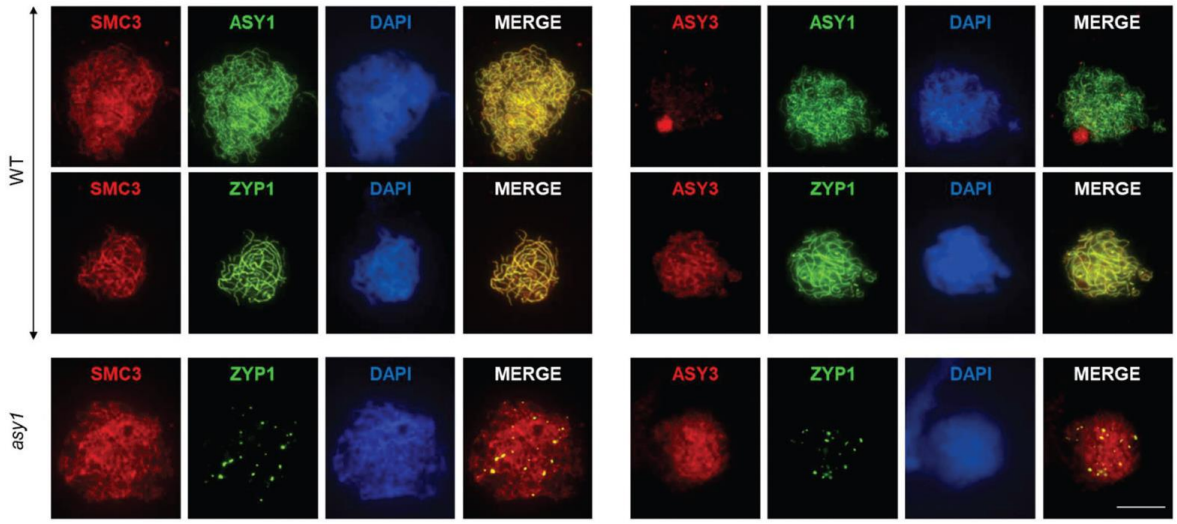


Fig. 4. ASY3 and SMC3 localize to chromosome axes in *asy1*. Immunolocalization of SMC3 (red, left) and ASY3 (red, right) together with ASY1 (green, WT top) and ZYP1 (green, WT bottom and *asy1*). ASY3 and SMC3 display similar dynamics in WT and *asy1* cells. DNA is counterstained with DAPI and shown in blue. Scale bar=10μm.

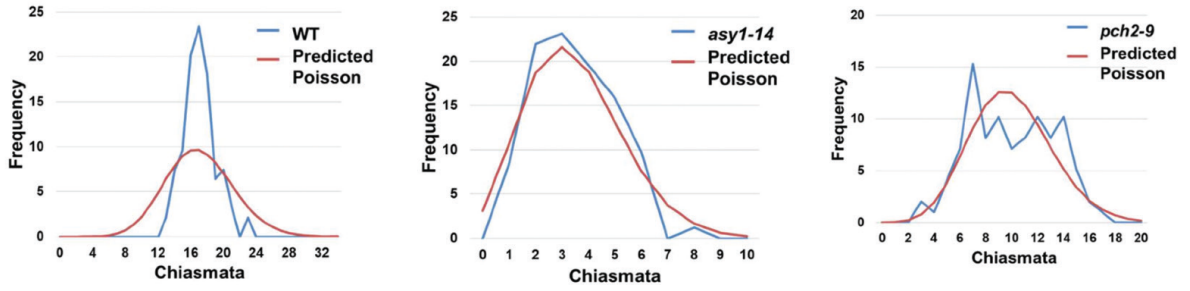


Fig. 5. Chiasma frequency distribution follows a Poisson distribution in *asy1* and *pch2*. Chiasma frequency distribution (blue) and predicted Poisson distribution (red) for the WT, *asy1-14*, and *pch2-9*. In the mutants, chiasma frequency distribution does not significantly deviate from a Poisson-predicted distribution.

chiasmata per cell, and *mus81* invariably showed five bivalents. In *asy1/shoc1* and in *asy1/mus81*, fewer chiasmata formed than in *asy1*; in *asy1/shoc1*, we found a reduction of ~72% and in *asy1/mus81* a reduction of ~21% compared with *asy1*. This suggests that residual COs in *asy1* are both class I and II.

Axis remodelling is defective in pch2

In *pch2*, ASY1 loaded onto chromosomes and, once ASY1 was fully polymerized, ZYP1 appeared initially as foci and later on as stretches. However, full ZYP1 polymerization was never observed (Fig. 3). Indeed, measuring ZYP1 extension in WT and *pch2-9* nuclei revealed a large variation in the extension of the SC across *pch2* cells and, on average, a reduction of 62% in SC length (Mann–Whitney–Wilcoxon test, $P<0.0001$, $n=13$ WT and $n=31$ *pch2*) (Fig. 7).

Furthermore, in contrast to the WT, in *pch2* ASY1 remained brightly stained following ZYP1 installation (Fig. 3), suggesting that ASY1 is not depleted from chromosome axes at synapsed regions. In various organisms including Arabidopsis, PCH2 is needed for the programmed removal of ASY1 during zygotene from chromosome axes concomitant with SC installation (Börner *et al.*, 2008; Martinez-Perez *et al.*, 2008; Wojtasz *et al.*, 2009; Lambing *et al.*, 2015). To validate this observation, we measured ASY1 intensity (Supplementary Table S4) and found that in the WT there was a 55% reduction in ASY1 intensity in synapsed versus asynapsed regions, whereas in *pch2* there was a 21% increase. This increase in *pch2* is probably based on the juxtaposition of the two homologous chromosome axes, leading to an increase in signal intensity per pixel.

Interestingly, in asynapsed regions, ASY1 intensity was consistently lower in *pch2* than in the WT. In Arabidopsis, PCH2 is involved not only in ASY1 removal, but also in its loading (Yang *et al.*, 2020*b*). To check whether ASY1 loading is also defective in *pch2*, we measured ASY1 intensity in leptotene whole nuclei. Despite substantial variation in ASY1 intensity values among slides/experiments, ASY1 intensity was consistently lower in *pch2* than in the WT (range 14–76%). To corroborate this cytological observation, we also immunostained ASY1 in Arabidopsis WT and *pch2*, and found that ASY1 signal intensity was significantly reduced at leptotene in Arabidopsis *pch2* (Mann–Whitney–Wilcoxon test, $P=4.01^{e-03}$, $n=24$ Col-0 and $n=24$ *pch2*) (Supplementary Fig. S3). In summary, our data indicate that PCH2 in *B. rapa* is important for initial ASY1 loading during leptotene and programmed removal of ASY1 from chromosome axes concomitant with SC installation during zygotene.

Crossover patterning in pch2*: distalized crossover at the expense of interstitial crossover*

In *pch2*, chiasma frequency was highly variable and in ~50% of cells the obligatory CO was lost. To better understand how CO control is altered, we analysed CO frequency distribution. We found that chiasma frequency in *pch2* did not significantly deviate from a Poisson-predicted distribution [$\chi^2_{(pch2\text{-}9)}=14.70$, $P=0.26$, $n=98$)] (Fig. 5), revealing a random distribution of chiasmata between cells. To identify whether interference-sensitive class I COs form in *pch2*, we performed immunolocalization of HEI10 together with ZYP1 (Fig. 6B). In *pch2-9*, we found an average of 10.5±3.15 (range 4–15) HEI10 foci during diplotene–diakinesis. These values are comparable with the average chiasma number in *pch2-9* (9.97±3.29, range 3–17). Interestingly, we found nuclei where several HEI10 foci localized in close proximity onto one ZYP1 stretch (Fig. 6B, asterisks) together with ZYP1 stretches devoid of HEI10 foci. Thus, a majority of COs in *pch2* showing a random distribution according a Poisson-predicted distribution probably belong to class I COs (marked by HEI10 foci).

We next asked whether residual chiasmata in *pch2* are positioned differently compared with the WT. We scored the number of terminal versus interstitial chiasmata and found that the percentage of interstitial chiasmata among all chiasmata was 8% in *pch2* and 14% in the WT (Fig. 8A, B). Similarly, in *asy1*, among residual chiasmata, only 6% were interstitial while the majority were found towards chromosome ends (Fig. 8B). Thus, cytologically residual chiasmata in *pch2* and *asy1* are proportionally more frequently located in terminal chromosome regions compared with the WT.

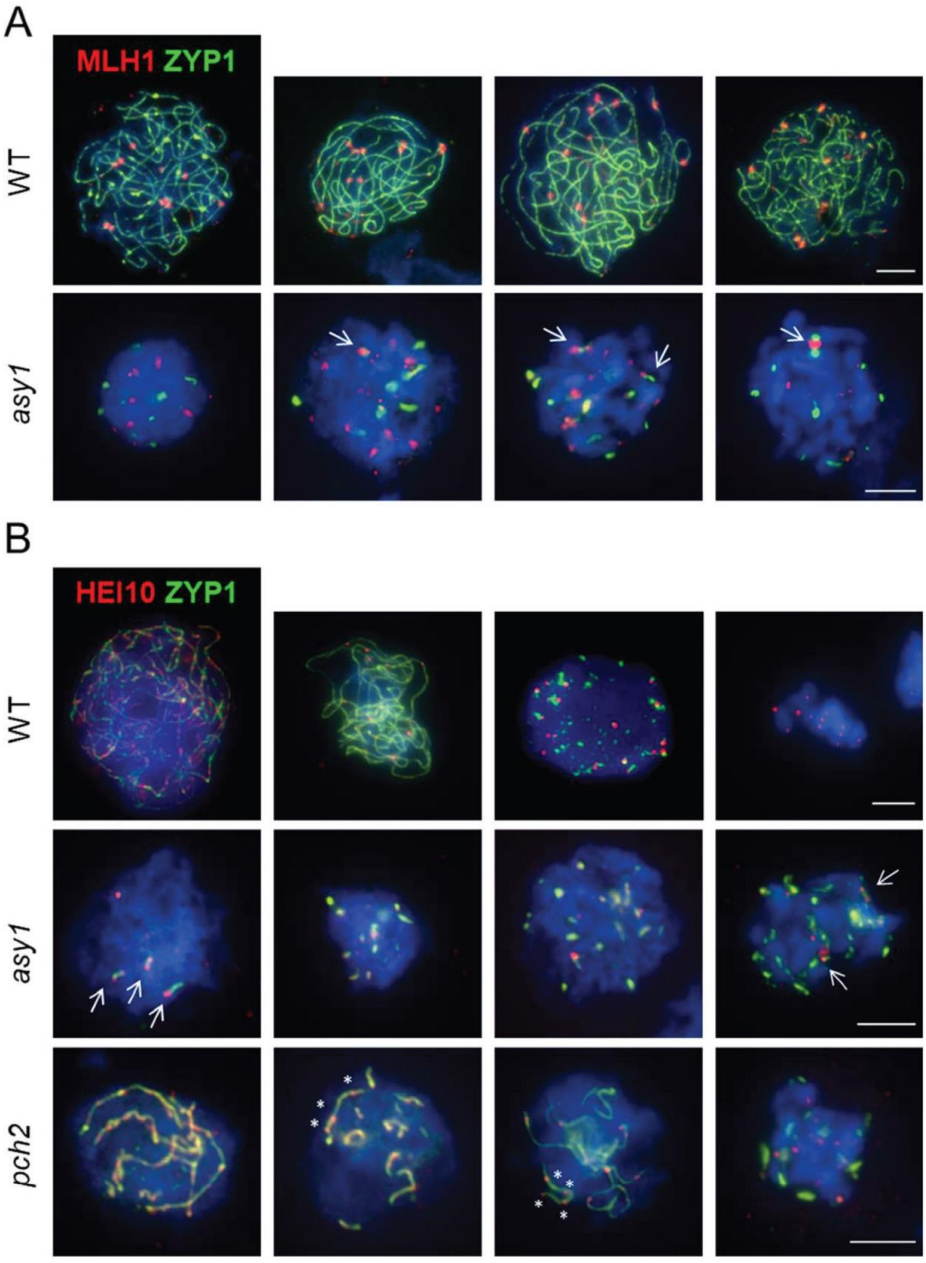


Fig. 6. Class I CO formation in *asy1* and *pch2*. Immunolocalization of MLH1 (A, red) and HEI10 (B, red) together with ZYP1 (green) in the WT, *asy1*, and *pch2*. In *asy1*, a subset of MLH1/HEI10 foci co-localize with ZYP1 foci/short stretches (arrows). In *pch2*, several HEI10 signals appear close to each other in a single ZYP1 stretch (asterisks). Note, to depict HEI10 dynamics in the WT, cells are shown ranging from zygotene (left) to diakinesis (right), whereas in all other cases representative examples of cells used for quantification are shown. DNA is counterstained with DAPI and shown in blue. Scale bars=5μm.

To corroborate our cytological finding on altered chiasma patterning in *pch2* with proportionally increased terminal and decreased interstitial chiasmata, we asked whether in Arabidopsis *pch2* a similar situation occurs. We re-analysed published recombination data from six genetic intervals (Lambing *et al.*, 2015) and extended this study by analysing

Table 1. ASY1-independent CO formation in *Arabidopsis thaliana*

	Average bivalent/cell	Range	Average chiasmata/cell	Range	Average ring/cell	Range	*n*
asy1	2.30±0.88	1–4	2.77±1.22	1–5	0.47±0.63	0–2	30
shoc1	2.38±1.04	0–5	2.79±1.41	0–7	0.41±0.61	0–2	34
mus81	5±0	5–5					30
asy1/shoc1	0.69±0.69	0–2	0.78±0.91	0–3	0.09±0.30	0–1	32
asy1/mus81	2.14±1.01	1–4	2.18±1.09	1–5	0.04±0.19	0–1	28

Average, SD, and range of bivalents, chiasmata, and ring bivalents per cell in Arabidopsis *asy1*, *shoc1*, *mus81* single mutants and *asy1/shoc1* and *asy1/mus81* double mutants. Note: the bivalent frequency between *asy1* and *asy1/mus81* was not significantly different, while the number of ring bivalents in *asy1/mus81* was reduced, causing the observed reduction in chiasma frequency. *n*=number of cells.

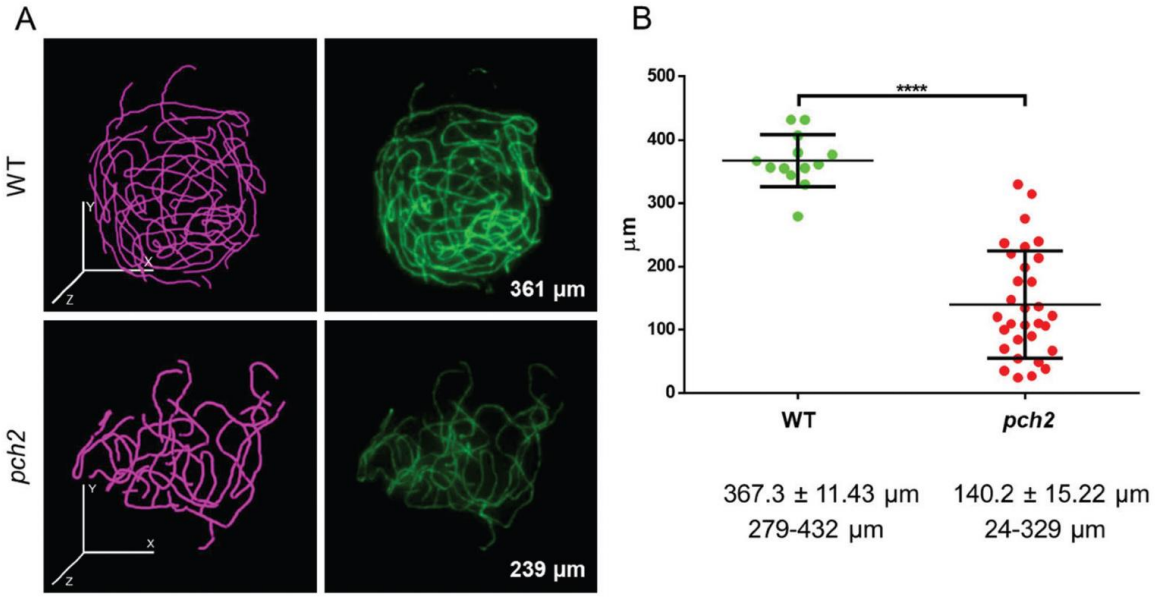


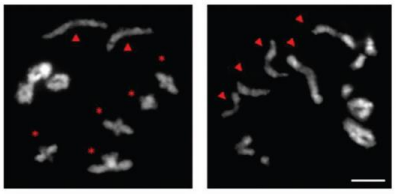
Fig. 7. Compromised SC formation in *pch2*. (A) 3D reconstruction of the SC with simple neurite tracer (ImageJ) (pink, left) of representative pachytene cells immunolabelled with ZYP1 (green, right) in the WT and *pch2*. SC length is indicated in the bottom right corner. (B) SC measurements in individual WT and *pch2* cells. Average, SD, and range are indicated.

recombination frequency in three more genetic intervals. We classed the genetic intervals based on their chromosomal locations as subtelomeric, interstitial, and centromeric. We found that subtelomeric intervals show increased recombination frequency, while interstitial intervals show few changes, and centromeric intervals show a drastic reduction in recombination frequency in *pch2* (Fig. 8C). These data suggest that COs are repressed in the heterochromatic centromeric regions and that they are distalized in the absence of PCH2. Immunostaining of MLH1 revealed that total MLH1 foci are reduced in *pch2* (10.4 versus 9.0, Mann–Whitney–Wilcoxon test, $P<0.01$, $n=41$ WT and $n=20$ *pch2*) and that the reduction is mostly seen on the DAPI-dense regions that are representative of the heterochromatic (peri-)centromeric regions (1.7 versus 0.8, Mann–Whitney–Wilcoxon test, $P<0.001$, $n=41$ WT and $n=20$ *pch2*) (Fig. 8D). Together, these data reveal that PCH2 is required for CO patterning control.

Discussion

In this work, we have characterized *asy1* and *pch2* in *B. rapa*. Both mutants display reduced chiasma formation and univalents at metaphase I that lead to unbalanced gametes and reduced fertility, highlighting the importance of the axis and SC morphogenesis for CO formation. Depletion of ASY1 or PCH2 strongly impacts SC formation, resulting in differential patterning of residual chiasmata being proportionally enriched towards chromosome ends.

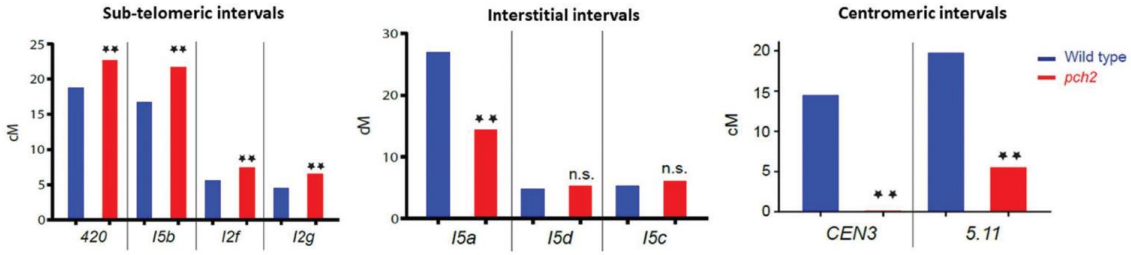
A



B

	Total chiasmata	Interstitial chiasmata	% Interstitial chiasmata
WT	1606	226	14.07
pch2	977	79	8.09
asy1	285	18	6.32

C



D

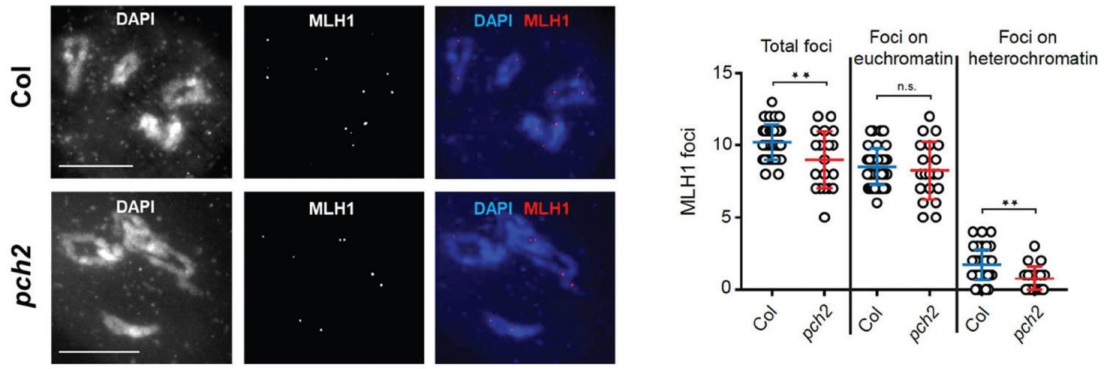


Fig. 8. Distalization of chiasmata in *pch2* and in *asy1*. (A) Representative example of *B. rapa* diakinesis with a majority of chiasmata being interstitial (asterisks) in the WT (left) and distal (arrowheads) in *pch2* (right). DNA is counterstained with DAPI and shown in grey. Scale bar=5 µm. (B) Quantification of interstitial versus total chiasmata in *B. rapa* WT, *pch2*, and *asy1* reveals reduced interstitial CO frequency in the mutants. (C) Recombination frequency in Arabidopsis at genetic intervals defined with genes coding for fluorescent proteins. Genetic intervals are classed based on their locations on the chromosomes. Asterisks represent statistically significant differences (generalized linear model) and 'n.s.' means non-significant. (D) Left: staining of MLH1 (red) and DAPI (blue) at diakinesis in Arabidopsis WT and *pch2*. Scale bars=10 µM. Right: plots showing total MLH1 foci count, MLH1 foci count on euchromatin, and foci count on heterochromatin per cell. Error bars represent the SD. Asterisks represent statistically significant differences (Mann–Whitney–Wilcoxon test) and 'n.s.' means non-significant.

ASY1-independent meiotic chromosome axes are insufficient for synaptonemal complex and crossover formation

Our analyses indicate that *asy1-13* and *asy1-14* are allelic and probably represent null mutations. Similar to *asy1* in other plant species (Armstrong *et al.*, 2002; Nonomura *et al.*, 2004), *B. rapa asy1* is largely, if not completely, asynaptic (Figs 1D, 3). ZYP1 forms foci and occasionally short stretches which are commonly distorted in appearance (Fig. 3), probably representing ZYP1 aggregates (Zickler and Kleckner, 1999) or polycomplexes forming at sites where ZYP1 polymerization/extension along lateral elements is impaired due to a defect in ASY1-dependent interhomologue bias and recombination progression (Higgins *et al.*, 2005).

Despite the absence of an SC, residual chiasmata form in *B. rapa asy1* (Fig. 1C, D). This is reminiscent of Arabidopsis and the corresponding *hop1* mutant in budding yeast (Hollingsworth

and Johnson, 1993; Ross *et al.*, 1997) but contrasts with rice *pair2* (Nonomura *et al.*, 2004). Axis mutants *asy3* or *asy4* in Arabidopsis also show reduced COs (but to a lesser extent than *asy1*), and *asy1* is epistatic to them in terms of chiasma frequency (Ferdous *et al.*, 2012; Chambon *et al.*, 2018), suggesting that ASY1 is needed upstream from ASY3/ASY4 to regulate DMC1 dynamics and thus interhomologue recombination (Sanchez-Moran *et al.*, 2007). Moreover, ASY4 is required for axial organization of ASY1 and ASY3 in Arabidopsis (Chambon *et al.*, 2018), and ASY3 for correct ASY1 localization in Arabidopsis, maize, and rice (Wang *et al.*, 2011; Ferdous *et al.*, 2012; Lee *et al.*, 2015), while cytologically ASY3 and the cohesin SMC3 localize correctly in *asy1* (Sanchez-Moran *et al.*, 2007; Ferdous *et al.*, 2012). Similarly, in *B. rapa*, SMC3 and ASY3 display WT-like axes localization in *asy1* (Fig. 4), suggesting WT-like dynamics of the core axis-associated proteins despite subsequent synaptic and CO defects.

In Arabidopsis axis mutants, the majority of the remaining COs are dependent on the class I CO (ZMM) pathway similar to the WT; for example, in *asy1*, MLH1 foci form on bivalents (Lambing *et al.*, 2020), in *asy3/msh4* double mutants chiasma formation is abolished (Ferdous *et al.*, 2012), or in *asy4/zip4* and *asy4/msh5* double mutants bivalent formation is reduced by ~95% compared with *asy4* (Chambon *et al.*, 2018). In *B. rapa asy1*, both HEI10 and MLH1 foci numbers scored around pachytene-/diplotene-like stages were highly variable compared with the WT, exceeding the number of cytologically scored chiasmata. This observation could be attributed to different causes. First, HEI10 foci numbers vary significantly through prophase I and therefore variation could stem from the difficulty in selecting late prophase cells due to complete absence of synapsis. Second, interestingly, in Arabidopsis *asy1*, *dmc1* or haploid meiosis MLH1 foci were reported on univalent chromosomes, possibly representing sites of intersister repair (Cifuentes *et al.*, 2013; Lambing *et al.*, 2020). Similarly, HEI10 has been indicated to mark intersister events (Voelkel-Meiman *et al.*, 2012) and it follows initial WT dynamics in mutants with severely impaired CO formation such as the ZMM mutant *mer3* (Wang *et al.*, 2012). Third, non-co-localizing HEI10 and MLH1 foci were found in *B. napus* allohaploids (Grandont *et al.* 2014). Finally, MLH1 in *Sordaria* is important for interlock resolution (Storlazzi *et al.*, 2010), and although the presence of MLH1 at interlocks has not been shown, this could arise in *asy1* due to defective SC polymerization. Assuming that only ZYP1-associated ZMM foci or a subset of these are CO competent (Ferdous *et al.*, 2012), then probably only a proportion of observed foci will mature into class I CO sites.

In *B. rapa asy1*, chiasmata were strongly reduced but not abolished, and cytologically foci corresponding to class I CO markers HEI10 and MLH1 formed, suggesting that residual chiasmata may arise via the class I CO pathway. In support of this, by using available Arabidopsis resources, we showed that a majority of ASY1-independent chiasmata are dependent on the ZMM pathway, while a subset is also MUS81 dependent, indicative of class II CO formation (Table 1). Interestingly, as in the WT, roughly similar proportions of class I and class II COs arise in the Arabidopsis *asy1* mutant, suggesting that both CO pathways are similarly dependent on ASY1. In future, to determine if the same applies in *B. rapa*, it will be interesting to evaluate CO formation in *asy1/msh4* (class I CO-defective mutant with ~4 residual chiasmata; Blary *et al.*, 2018).

Residual chiasmata in asy1 *are proportionally enriched in terminal chromosome regions and on the major 45S rDNA-carrying chromosome*

Residual chiasmata in *B. rapa asy1* are proportionally enriched towards chromosome ends and, except for the major 45S rDNA-carrying chromosome, all discernible chromosomes appear as univalents with similar frequencies, suggesting no positive correlation between chromosome size and chiasma formation.

Terminal dominance of residual chiasmata was also found in Arabidopsis *asy1* and further axis-associated mutants such as *asy3* and *asy4* (Sanchez-Moran *et al.*, 2007; Ferdous *et al.*, 2012; Chambon *et al.*, 2018). It has been proposed that this could be a consequence of recombination initiating by telomeric regions (Sanchez-Moran *et al.*, 2007) and that ASY1 could be antagonizing this telomere-led recombination (Lambing *et al.*, 2020). This highlights the key role of axis components in regulating CO frequency and distribution.

Notably, residual chiasmata showed a strong bias towards the 45S rDNA-carrying chromosome and, in particular, towards the 45S rDNA chromosome end (Fig. 2). Due to limited cytological resolution, we cannot distinguish whether chiasmata involved ribosomal repeats or rather formed in non-ribosomal repeat-free regions distal to the 45S rDNA or intermingled with it. We prefer that CO enrichment is found in non-ribosomal repeat-free chromosome ends, as bivalents were typically linked via what seems to be cytologically a very terminal chiasma, and also because we could not see any signs of repair/chromosome segregation problems which would be likely to arise if recombination would occur within highly repetitive regions due to the possibility of non-allelic exchanges (Sasaki *et al.*, 2010). This would agree with recent data from Arabidopsis indicating that exclusion of ASY1 from the NOR in chromosomes 2 and 4 early during prophase is implicated in restricting DSB formation and thus HR in the NOR (Sims *et al.*, 2019). Nonetheless, chiasma enrichment towards the 45S rDNA-carrying chromosome (arm) has also been observed in Arabidopsis *asy1* (Sanchez Moran *et al.*, 2001; Lambing *et al.*, 2020). Thus, in *asy1*, the rDNA probably promotes CO formation in the 45S rDNA-carrying chromosome (arm) (Sanchez Moran *et al.*, 2001; Lambing *et al.*, 2020).

pch2 *plants fail to remodel ASY1 and only achieve partial synapsis leading to reduced chiasma formation*

Both *pch2-9* and *pch2-12* appear allelic in terms of meiotic behaviour and probably represent null mutants. However, despite

three backcrosses, compared with the WT, a slight reduction in fertility was found in *pch2-12* segregating families independent of *PCH2*, suggesting secondary mutation load impacting overall plant fertility. Thus, data were acquired on *pch2-9*.

In *B. rapa pch2*, full synapsis was never observed (Figs 1D, 3) despite substantial variation in SC extension (based on ZYP1 immunolocalization) and, on average, SC length was ~62% reduced compared with the WT (Fig. 7). This reduction in SC length is similar to *pch2* in Arabidopsis (~68%; Lambing *et al.*, 2015) but differs from rice *pch2/crc1*, where SC formation is completely abolished (Miao *et al.*, 2013). Notably, in rice *pch2*, no chiasmata form, while in *B. rapa pch2* chiasmata are reduced by ~40% and in Arabidopsis *pch2* by ~30%. Moreover, observed chiasma numbers are variable across cells, and often univalents occurred in cells with at least 10 chiasmata, suggesting a defect in CO assurance. Overall, despite species-specific differences, PCH2 in plants is critical for WT levels of synapsis and CO formation.

Brassica rapa pch2 plants form a partial SC while axes are not remodelled; that is, ASY1 loading during leptotene is reduced and ASY1 is not depleted from synapsed regions. This dual function of PCH2 in *B. rapa* is consistent with data from Arabidopsis and budding yeast (Börner *et al.*, 2008; Lambing *et al.*, 2015; Yang *et al.*, 2020*a*, *b*), showing that PCH2 is critical for chromosomal localization of ASY1 as well as for depletion of ASY1 from synapsed regions. In Arabidopsis, in addition to PCH2, the axis proteins ASY3 and ASY4 are also critical for WT dynamics and correct localization of ASY1; for example, in *asy4*, ASY1 is not depleted from synapsed regions and ASY3 is involved in correct ASY1 recruitment to the chromosome axes (Ferdous *et al.*, 2012; Chambon *et al.*, 2018). Thus, a complex interplay between axis components and associated proteins exists, and not only axis formation but also axis morphogenesis is critical for HR, including DSB repair, template choice, SC formation and, ultimately, CO formation.

Redistribution of chiasmata in pch2

Residual COs in *B. rapa pch2*, contrary to Arabidopsis (Lambing *et al.*, 2015), do not significantly deviate from a Poisson-predicted distribution which could be interpreted as suggesting that they are interference insensitive, typical for class II COs. However, the fact that the chiasma frequency distribution does not differ from a Poisson distribution only means that chiasma formation in the mutant has a high random component. In fact, HEI10 foci marking putative class I CO sites appear in *pch2* with similar numbers as cytologically scored chiasmata (minimum CO number), with some nuclei having HEI10 foci closely spaced along ZYP1 stretches and at the same time ZYP1 stretches devoid of HEI10 foci (Fig. 6). Possibly maturation of designated COs might be compromised in *B. rapa pch2* due to the defect in chromosome axis remodelling, resulting in a CO deficit as in Arabidopsis *pch2* (Lambing *et al.*, 2015). Notably, the average reduction in SC length (62%) is larger than the average reduction in chiasmata (~40%), suggesting that similar to Arabidopsis (Lambing *et al.*, 2015), the mean reduction in CO frequency was not coordinated with that in SC length. A similar phenotype has been observed in Arabidopsis mutants for the kinesin PSS1 and the E1 enzyme of the neddylation complex AXR1 (Duroc *et al.*, 2014; Jahns *et al.*, 2014), both being strongly defective for synapsis, showing univalents at metaphase I, and with chiasma frequencies similar to the WT but COs being redistributed with closely spaced HEI10 foci along residual synapsed regions.

Furthermore, PCH2-independent chiasmata are cytologically skewed towards terminal chromosome regions in *B. rapa*. To support this cytological observation, in Arabidopsis *pch2*, CO rates were established in different genetic intervals, revealing increased CO rates in telomeric chromosome regions at the expense of decreased (peri-)centromeric CO rates compared with the WT (Fig. 8). Thus, considering terminal initiation of SC formation (Hurel *et al.*, 2018), recombination events on limited extended ZYP1 stretches in *pch2* might be proportionally enriched in distal regions, explaining the skewed chiasma distribution.

Altogether, in *B. rapa*, a majority of residual PCH2-independent COs are likely to be ZMM-dependent class I COs that are redistributed, being proportionally enriched towards chromosome ends.

Conclusions

Altering CO frequency and distribution is of special interest for plant breeding, since in many crop species CO numbers are limited and skewed towards chromosome ends, limiting recombination and access to naturally available genetic variation and creating linkage drag.

We have analysed mutants of axis-associated ASY1 and axis-remodelling PCH2. Both mutants show reduced CO formation due to defects in meiosis, but interestingly COs are redistributed and at least *pch2* plants produce some viable seeds. Considering this altered patterning of chiasmata that arise via the class I and class II CO pathways in *asy1* and *pch2*, it would be interesting to determine whether in combination with HEI10 overexpression (increasing class I CO) or *hyperrec* mutants (increasing class II COs) (Lambing *et al.*, 2017). ASY1-/PCH2-independent chiasmata could be increased, thus potentially increasing bivalent formation and seed setting while maintaining an altered recombination pattern. In any case, considering their general influence on DSB and CO formation including DNA repair template choice, axis-associated or remodelling proteins such as ASY1 or PCH2 are interesting targets to modify meiotic recombination landscapes in the context of plant breeding.

Supplementary data

The following supplementary data are available at *JXB* online.

Table S1. Primers used in this study.

Table S2. Plant fertility in the *B. rapa* WT, and *asy1* and *pch2* mutants.

Table S3. Relative occurrence (%) of 5S/45S-labelled chromosomes as either univalents or bivalents.

Table S4. ASY1 immunofluorescence relative signal intensity in WT and *pch2* cells.

Fig. S1. Alternative splicing of *PCH2* in *pch2-12*.

Fig. S2. Male meiotic chromosome behaviour in *B. rapa*.

Fig. S3. Localization defect of ASY1 in Arabidopsis *pch2*.

Acknowledgements

We would like to acknowledge Jana Lorenz, Franziska Hartmann, and Steve Price for excellent technical assistance, Karen Staples at UoB and the gardeners at IPK for horticultural support, and all lab members for fruitful discussions. CL and IRH would like to thank Mathilde Grelon for sharing the MLH1 antibody. We would also like to thank the Bundesministerium für Bildung und Forschung (grant FKZ-031B0188), the IPK Gatersleben, the Biotechnology and Biological Sciences Research Council UK (grants BB/M004902/1, BB/J007633/1, and BB/M014908/), the European Union's Seventh Framework Programme FP7/2007-2013 (grant KBBE-2009-222883), and the European Union's Marie Sklodowska-Curie Innovative Training Network MEICOM (grant 765212-H2020-MSCA-ITN-2017) for financial support.

Author contributions

MC, CL, and MP-P performed the experiments; MC, CL, MP-P, and KO analysed the data; SJA, IRH, ES-M, FCHF, and SH acquired funding; MC and SH drafted the manuscript; all authors edited and approved the final text.

Data availability

All data supporting the findings of this study are available within the paper and within its supplementary data published online.

References

Alonso JM, Stepanova AN, Leisse TJ, *et al.* 2003. Genome-wide insertional mutagenesis of *Arabidopsis thaliana*. Science **301**, 653–657.

Armstrong SJ, Caryl AP, Jones GH, Franklin FC. 2002. Asy1, a protein required for meiotic chromosome synapsis, localizes to axis-associated chromatin in *Arabidopsis* and *Brassica*. Journal of Cell Science **115**, 3645–3655.

Armstrong SJ, Sanchez-Moran E, Franklin FCH. 2009. Cytological analysis of arabidopsis thaliana meiotic chromosomes. In: Keeney S, ed. Meiosis: volume 2, cytological methods. Totowa, NJ: Humana Press, 131–145.

Berchowitz LE, Copenhaver GP. 2008. Fluorescent Arabidopsis tetrads: a visual assay for quickly developing large crossover and crossover interference data sets. Nature Protocols **3**, 41–50.

Berchowitz LE, Francis KE, Bey AL, Copenhaver GP. 2007. The role of AtMUS81 in interference-insensitive crossovers in *A. thaliana*. PLoS Genetics **3**, e132.

Bhalla N, Dernburg AF. 2005. A conserved checkpoint monitors meiotic chromosome synapsis in *Caenorhabditis elegans*. Science **310**, 1683–1686.

Blary A, Gonzalo A, Eber F, *et al.* 2018. FANCM limits meiotic crossovers in Brassica crops. Frontiers in Plant Science **9**, 368.

Börner GV, Barot A, Kleckner N. 2008. Yeast Pch2 promotes domainal axis organization, timely recombination progression, and arrest of defective recombinosomes during meiosis. Proceedings of the National Academy of Sciences, USA **105**, 3327–3332.

Boutte J, Maillet L, Chaussepied T, *et al.* 2020. Genome size variation and comparative genomics reveal intraspecific diversity in *Brassica rapa*. Frontiers in Plant Science **11**, 577536.

Cai X, Dong F, Edelmann RE, Makaroff CA. 2003. The *Arabidopsis* SYN1 cohesin protein is required for sister chromatid arm cohesion and homologous chromosome pairing. Journal of Cell Science **116**, 2999–3007.

Campell BR, Song Y, Posch TE, Cullis CA, Town CD. 1992. Sequence and organization of 5S ribosomal RNA-encoding genes of *Arabidopsis thaliana*. Gene **112**, 225–228.

Carballo JA, Johnson AL, Sedgwick SG, Cha RS. 2008. Phosphorylation of the axial element protein Hop1 by Mec1/Tel1 ensures meiotic interhomolog recombination. Cell **132**, 758–770.

Caryl AP, Armstrong SJ, Jones GH, Franklin FC. 2000. A homologue of the yeast *HOP1* gene is inactivated in the Arabidopsis meiotic mutant *asy1*. Chromosoma **109**, 62–71.

Chambon A, West A, Vezon D, *et al.* 2018. Identification of ASYNAPTIC4, a component of the meiotic chromosome axis. Plant Physiology **178**, 233–246.

Chelysheva L, Diallo S, Vezon D, *et al.* 2005. AtREC8 and AtSCC3 are essential to the monopolar orientation of the kinetochores during meiosis. Journal of Cell Science **118**, 4621–4632.

Chelysheva L, Gendrot G, Vezon D, Doutriaux MP, Mercier R, Grelon M. 2007. Zip4/Spo22 is required for class I CO formation but not for synapsis completion in *Arabidopsis thaliana*. PLoS Genetics **3**, e83.

Chelysheva L, Grandont L, Vrielynck N, le Guin S, Mercier R, Grelon M. 2010. An easy protocol for studying chromatin and recombination protein dynamics during *Arabidopsis thaliana* meiosis: immunodetection of cohesins, histones and MLH1. Cytogenetic and Genome Research **129**, 143–153.

Chelysheva L, Vezon D, Chambon A, Gendrot G, Pereira L, Lemhemdi A, Vrielynck N, Le Guin S, Novatchkova M, Grelon M. 2012. The Arabidopsis HEI10 is a new ZMM protein related to Zip3. PLoS Genetics **8**, e1002799.

Chen C, Jomaa A, Ortega J, Alani EE. 2014. Pch2 is a hexameric ring ATPase that remodels the chromosome axis protein Hop1. Proceedings of the National Academy of Sciences, USA **111**, E44–E53.

Chen C, Zhang W, Timofejeva L, Gerardin Y, Ma H. 2005. The *Arabidopsis* ROCK-N-ROLLERS gene encodes a homolog of the yeast ATP-dependent DNA helicase MER3 and is required for normal meiotic crossover formation. The Plant Journal **43**, 321–334.

Choulet F, Alberti A, Theil S, *et al.* 2014. Structural and functional partitioning of bread wheat chromosome 3B. Science **345**, 1249721.

Cifuentes M, Rivard M, Pereira L, Chelysheva L, Mercier R. 2013. Haploid meiosis in Arabidopsis: double-strand breaks are formed and repaired but without synapsis and crossovers. PLoS One **8**, e72431.

Demirci S, van Dijk AD, Sanchez Perez G, Aflitos SA, de Ridder D, Peters SA. 2017. Distribution, position and genomic characteristics of crossovers in tomato recombinant inbred lines derived from an interspecific cross between *Solanum lycopersicum* and *Solanum pimpinellifolium*. The Plant Journal **89**, 554–564.

Dreissig S, Mascher M, Heckmann S. 2019. Variation in recombination rate is shaped by domestication and environmental conditions in barley. Molecular Biology and Evolution **36**, 2029–2039.

Duroc Y, Lemhemdi A, Larchevêque C, Hurel A, Cuacos M, Cromer L, Horlow C, Armstrong SJ, Chelysheva L, Mercier R. 2014. The kinesin AtPSS1 promotes synapsis and is required for proper crossover distribution in meiosis. PLoS Genetics **10**, e1004674.

Farmer S, Hong EJ, Leung WK, Argunhan B, Terentyev Y, Humphryes N, Toyoizumi H, Tsubouchi H. 2012. Budding yeast Pch2,

a widely conserved meiotic protein, is involved in the initiation of meiotic recombination. PLoS One **7**, e39724.

Ferdous M, Higgins JD, Osman K, *et al.* 2012. Inter-homolog crossing-over and synapsis in Arabidopsis meiosis are dependent on the chromosome axis protein AtASY3. PLoS Genetics **8**, e1002507.

Fukuda T, Daniel K, Wojtasz L, Toth A, Höög C. 2010. A novel mammalian HORMA domain-containing protein, HORMAD1, preferentially associates with unsynapsed meiotic chromosomes. Experimental Cell Research **316**, 158–171.

Fukui K, Nakayama S, Ohmido N, Yoshiaki H, Yamabe M. 1998. Quantitative karyotyping of three diploid Brassica species by imaging methods and localization of 45s rDNA loci on the identified chromosomes. Theoretical and Applied Genetics **96**, 325–330.

Gerlach WL, Bedbrook JR. 1979. Cloning and characterization of ribosomal RNA genes from wheat and barley. Nucleic Acids Research **7**, 1869–1885.

Grandont L, Cuñado N, Coriton O, Huteau V, Eber F, Chèvre AM, Grelon M, Chelysheva L, Jenczewski E. 2014. Homoeologous chromosome sorting and progression of meiotic recombination in *Brassica napus*: ploidy does matter! The Plant Cell **26**, 1448–1463.

Grelon M, Vezon D, Gendrot G, Pelletier G. 2001. AtSPO11-1 is necessary for efficient meiotic recombination in plants. The EMBO Journal **20**, 589–600.

Hasterok R, Wolny E, Hosiawa M, Kowalczyk M, Kulak-Ksiazczyk S, Ksiazczyk T, Heneen WK, Maluszynska J. 2006. Comparative analysis of rDNA distribution in chromosomes of various species of Brassicaceae. Annals of Botany **97**, 205–216.

Higgins JD, Armstrong SJ, Franklin FC, Jones GH. 2004. The Arabidopsis MutS homolog AtMSH4 functions at an early step in recombination: evidence for two classes of recombination in Arabidopsis. Genes & Development **18**, 2557–2570.

Higgins JD, Buckling EF, Franklin FC, Jones GH. 2008*a*. Expression and functional analysis of AtMUS81 in Arabidopsis meiosis reveals a role in the second pathway of crossing-over. The Plant Journal **54**, 152–162.

Higgins JD, Sanchez-Moran E, Armstrong SJ, Jones GH, Franklin FC. 2005. The Arabidopsis synaptonemal complex protein ZYP1 is required for chromosome synapsis and normal fidelity of crossing over. Genes & Development **19**, 2488–2500.

Higgins JD, Vignard J, Mercier R, Pugh AG, Franklin FC, Jones GH. 2008*b*. AtMSH5 partners AtMSH4 in the class I meiotic crossover pathway in *Arabidopsis thaliana*, but is not required for synapsis. The Plant Journal **55**, 28–39.

Hollingsworth NM, Goetsch L, Byers B. 1990. The HOP1 gene encodes a meiosis-specific component of yeast chromosomes. Cell **61**, 73–84.

Hollingsworth NM, Johnson AD. 1993. A conditional allele of the *Saccharomyces cerevisiae* HOP1 gene is suppressed by overexpression of two other meiosis-specific genes: RED1 and REC104. Genetics **133**, 785–797.

Hurel A, Phillips D, Vrielynck N, Mézard C, Grelon M, Christophorou N. 2018. A cytological approach to studying meiotic recombination and chromosome dynamics in *Arabidopsis thaliana* male meiocytes in three dimensions. The Plant Journal **95**, 385–396.

Jackson N, Sanchez-Moran E, Buckling E, Armstrong SJ, Jones GH, Franklin FC. 2006. Reduced meiotic crossovers and delayed prophase I progression in AtMLH3-deficient Arabidopsis. The EMBO Journal **25**, 1315–1323.

Jahns MT, Vezon D, Chambon A, Pereira L, Falque M, Martin OC, Chelysheva L, Grelon M. 2014. Crossover localisation is regulated by the neddylation posttranslational regulatory pathway. PLoS Biology **12**, e1001930.

Joshi N, Barot A, Jamison C, Börner GV. 2009. Pch2 links chromosome axis remodeling at future crossover sites and crossover distribution during yeast meiosis. PLoS Genetics **5**, e1000557.

Joshi N, Brown MS, Bishop DK, Börner GV. 2015. Gradual implementation of the meiotic recombination program via checkpoint pathways controlled by global DSB levels. Molecular Cell **57**, 797–811.

Joyce EF, McKim KS. 2009. Drosophila PCH2 is required for a pachytene checkpoint that monitors double-strand-break-independent events leading to meiotic crossover formation. Genetics **181**, 39–51.

Keeney S, Giroux CN, Kleckner N. 1997. Meiosis-specific DNA double-strand breaks are catalyzed by Spo11, a member of a widely conserved protein family. Cell **88**, 375–384.

Keeney S, Kleckner N. 1995. Covalent protein–DNA complexes at the 5′ strand termini of meiosis-specific double-strand breaks in yeast. Proceedings of the National Academy of Sciences, USA **92**, 11274–11278.

Kim KP, Weiner BM, Zhang L, Jordan A, Dekker J, Kleckner N. 2010. Sister cohesion and structural axis components mediate homolog bias of meiotic recombination. Cell **143**, 924–937.

Kleckner N. 2006. Chiasma formation: chromatin/axis interplay and the role(s) of the synaptonemal complex. Chromosoma **115**, 175–194.

Koo DH, Plaha P, Lim YP, Hur Y, Bang JW. 2004. A high-resolution karyotype of *Brassica rapa* ssp. *pekinensis* revealed by pachytene analysis and multicolor fluorescence *in situ* hybridization. Theoretical and Applied Genetics **109**, 1346–1352.

Kurzbauer MT, Pradillo M, Kerzendorfer C, *et al.* 2018. *Arabidopsis thaliana* FANCD2 promotes meiotic crossover formation. The Plant Cell **30**, 415–428.

Lam WS, Yang X, Makaroff CA. 2005. Characterization of *Arabidopsis thaliana* SMC1 and SMC3: evidence that AtSMC3 may function beyond chromosome cohesion. Journal of Cell Science **118**, 3037–3048.

Lambing C, Franklin FC, Wang CR. 2017. Understanding and manipulating meiotic recombination in plants. Plant Physiology **173**, 1530–1542.

Lambing C, Heckmann S. 2018. Tackling plant meiosis: from model research to crop improvement. Frontiers in Plant Science **9**, 829.

Lambing C, Kuo PC, Tock AJ, Topp SD, Henderson IR. 2020. ASY1 acts as a dosage-dependent antagonist of telomere-led recombination and mediates crossover interference in *Arabidopsis*. Proceedings of the National Academy of Sciences, USA **117**, 13647–13658.

Lambing C, Osman K, Nuntasoontorn K, *et al.* 2015. Arabidopsis PCH2 mediates meiotic chromosome remodeling and maturation of crossovers. PLoS Genetics **11**, e1005372.

Lee DH, Kao YH, Ku JC, Lin CY, Meeley R, Jan YS, Wang CJ. 2015. The axial element protein DESYNAPTIC2 mediates meiotic double-strand break formation and synaptonemal complex assembly in maize. The Plant Cell **27**, 2516–2529.

Li X, Li L, Yan J. 2015. Dissecting meiotic recombination based on tetrad analysis by single-microspore sequencing in maize. Nature Communications **6**, 6648.

Lim KB, de Jong H, Yang TJ, *et al.* 2005. Characterization of rDNAs and tandem repeats in the heterochromatin of *Brassica rapa*. Molecules and Cells **19**, 436–444.

Macaisne N, Novatchkova M, Peirera L, Vezon D, Jolivet S, Froger N, Chelysheva L, Grelon M, Mercier R. 2008. SHOC1, an XPF endonuclease-related protein, is essential for the formation of class I meiotic crossovers. Current Biology **18**, 1432–1437.

Macaisne N, Vignard J, Mercier R. 2011. SHOC1 and PTD form an XPF–ERCC1-like complex that is required for formation of class I crossovers. Journal of Cell Science **124**, 2687–2691.

Martinez-Perez E, Schvarzstein M, Barroso C, Lightfoot J, Dernburg AF, Villeneuve AM. 2008. Crossovers trigger a remodeling of meiotic chromosome axis composition that is linked to two-step loss of sister chromatid cohesion. Genes & Development **22**, 2886–2901.

Martinez-Perez E, Villeneuve AM. 2005. HTP-1-dependent constraints coordinate homolog pairing and synapsis and promote chiasma formation during *C. elegans* meiosis. Genes & Development **19**, 2727–2743.

Melamed-Bessudo C, Yehuda E, Stuitje AR, Levy AA. 2005. A new seed-based assay for meiotic recombination in *Arabidopsis thaliana*. The Plant Journal **43**, 458–466.

Mercier R, Jolivet S, Vezon D, *et al.* 2005. Two meiotic crossover classes cohabit in arabidopsis: one is dependent on MER3, whereas the other one is not. Current Biology **15**, 692–701.

Mercier R, Mézard C, Jenczewski E, Macaisne N, Grelon M. 2015. The molecular biology of meiosis in plants. Annual Review of Plant Biology **66**, 297–327.

Miao C, Tang D, Zhang H, Wang M, Li Y, Tang S, Yu H, Gu M, Cheng Z. 2013. Central region component1, a novel synaptonemal complex component, is essential for meiotic recombination initiation in rice. The Plant Cell **25**, 2998–3009.

Mun JH, Kwon SJ, Seol YJ, *et al.* 2010. Sequence and structure of *Brassica rapa* chromosome A3. Genome Biology **11**, R94.

Muyt A, Mercier R, Mézard C, Grelon M. 2009. Meiotic recombination and crossovers in plants. Genome Dynamics **5**, 14–25.

Neale MJ, Pan J, Keeney S. 2005. Endonucleolytic processing of covalent protein-linked DNA double-strand breaks. Nature **436**, 1053–1057.

Neff MM, Neff JD, Chory J, Pepper AE. 1998. dCAPS, a simple technique for the genetic analysis of single nucleotide polymorphisms: experimental applications in *Arabidopsis thaliana* genetics. The Plant Journal **14**, 387–392.

Neff MM, Turk E, Kalishman M. 2002. Web-based primer design for single nucleotide polymorphism analysis. Trends in Genetics **18**, 613–615.

Niu H, Wan L, Baumgartner B, Schaefer D, Loidl J, Hollingsworth NM. 2005. Partner choice during meiosis is regulated by Hop1-promoted dimerization of Mek1. Molecular Biology of the Cell **16**, 5804–5818.

Nonomura KI, Nakano M, Murata K, Miyoshi K, Eiguchi M, Miyao A, Hirochika H, Kurata N. 2004. An insertional mutation in the rice PAIR2 gene, the ortholog of Arabidopsis ASY1, results in a defect in homologous chromosome pairing during meiosis. Molecular Genetics and Genomics **271**, 121–129.

Osman K, Higgins JD, Sanchez-Moran E, Armstrong SJ, Franklin FC. 2011. Pathways to meiotic recombination in *Arabidopsis thaliana*. New Phytologist **190**, 523–544.

Page SL, Hawley RS. 2004. The genetics and molecular biology of the synaptonemal complex. Annual Review of Cell and Developmental Biology **20**, 525–558.

Pan J, Sasaki M, Kniewel R, *et al.* 2011. A hierarchical combination of factors shapes the genome-wide topography of yeast meiotic recombination initiation. Cell **144**, 719–731.

Panizza S, Mendoza MA, Berlinger M, Huang L, Nicolas A, Shirahige K, Klein F. 2011. Spo11-accessory proteins link double-strand break sites to the chromosome axis in early meiotic recombination. Cell **146**, 372–383.

Perumal S, Waminal NE, Lee J, Lee J, Choi BS, Kim HH, Grandbastien MA, Yang TJ. 2017. Elucidating the major hidden genomic components of the A, C, and AC genomes and their influence on Brassica evolution. Scientific Reports **7**, 17986.

Phillips D, Wnetrzak J, Nibau C, Barakate A, Ramsay L, Wright F, Higgins JD, Perry RM, Jenkins G. 2013. Quantitative high resolution mapping of HvMLH3 foci in barley pachytene nuclei reveals a strong distal bias and weak interference. Journal of Experimental Botany **64**, 2139–2154.

Ross KJ, Fransz P, Armstrong SJ, Vizir I, Mulligan B, Franklin FC, Jones GH. 1997. Cytological characterization of four meiotic mutants of Arabidopsis isolated from T-DNA-transformed lines. Chromosome Research **5**, 551–559.

Sanchez Moran E, Armstrong SJ, Santos JL, Franklin FC, Jones GH. 2001. Chiasma formation in *Arabidopsis thaliana* accession Wassileskija and in two meiotic mutants. Chromosome Research **9**, 121–128.

Sanchez-Moran E, Santos JL, Jones GH, Franklin FC. 2007. ASY1 mediates AtDMC1-dependent interhomolog recombination during meiosis in Arabidopsis. Genes & Development **21**, 2220–2233.

San-Segundo PA, Roeder GS. 1999. Pch2 links chromatin silencing to meiotic checkpoint control. Cell **97**, 313–324.

Sasaki M, Lange J, Keeney S. 2010. Genome destabilization by homologous recombination in the germ line. Nature Reviews. Molecular Cell Biology **11**, 182–195.

Sims J, Copenhaver GP, Schlögelhofer P. 2019. Meiotic DNA repair in the nucleolus employs a nonhomologous end-joining mechanism. The Plant Cell **31**, 2259–2275.

Snowdon RJ, Friedrich T, Friedt W, Köhler W. 2002. Identifying the chromosomes of the A- and C-genome diploid *Brassica* species *B. rapa* (syn. *campestris*) and *B. oleracea* in their amphidiploid *B. napus*. Theoretical and Applied Genetics **104**, 533–538.

Stephenson P, Baker D, Girin T, Perez A, Amoah S, King GJ, Østergaard L. 2010. A rich TILLING resource for studying gene function in *Brassica rapa*. BMC Plant Biology **10**, 62.

Storlazzi A, Gargano S, Ruprich-Robert G, Falque M, David M, Kleckner N, Zickler D. 2010. Recombination proteins mediate meiotic spatial chromosome organization and pairing. Cell **141**, 94–106.

Subramanian VV, MacQueen AJ, Vader G, Shinohara M, Sanchez A, Borde V, Shinohara A, Hochwagen A. 2016. Chromosome synapsis alleviates mek1-dependent suppression of meiotic DNA repair. PLoS Biology **14**, e1002369.

Vader G, Blitzblau HG, Tame MA, Falk JE, Curtin L, Hochwagen A. 2011. Protection of repetitive DNA borders from self-induced meiotic instability. Nature **477**, 115–119.

Voelkel-Meiman K, Moustafa SS, Lefrançois P, Villeneuve AM, MacQueen AJ. 2012. Full-length synaptonemal complex grows continuously during meiotic prophase in budding yeast. PLoS Genetics **8**, e1002993.

Wang K, Wang M, Tang D, Shen Y, Miao C, Hu Q, Lu T, Cheng Z. 2012. The role of rice HEI10 in the formation of meiotic crossovers. PLoS Genetics **8**, e1002809.

Wang K, Wang M, Tang D, Shen Y, Qin B, Li M, Cheng Z. 2011. PAIR3, an axis-associated protein, is essential for the recruitment of recombination elements onto meiotic chromosomes in rice. Molecular Biology of the Cell **22**, 12–19.

Wang Y, Copenhaver GP. 2018. Meiotic recombination: mixing it up in plants. Annual Review of Plant Biology **69**, 577–609.

West AMV, Rosenberg SC, Ur SN, *et al.* 2019. A conserved filamentous assembly underlies the structure of the meiotic chromosome axis. eLife **8**, e40372.

Wijeratne AJ, Chen C, Zhang W, Timofejeva L, Ma H. 2006. The *Arabidopsis thaliana* PARTING DANCERS gene encoding a novel protein is required for normal meiotic homologous recombination. Molecular Biology of the Cell **17**, 1331–1343.

Wojtasz L, Daniel K, Roig I, *et al.* 2009. Mouse HORMAD1 and HORMAD2, two conserved meiotic chromosomal proteins, are depleted from synapsed chromosome axes with the help of TRIP13 AAA-ATPase. PLoS Genetics **5**, e1000702.

Wu G, Rossidivito G, Hu T, Berlyand Y, Poethig RS. 2015. Traffic lines: new tools for genetic analysis in *Arabidopsis thaliana*. Genetics **200**, 35–45.

Xiong Z, Pires JC. 2011. Karyotype and identification of all homoeologous chromosomes of allopolyploid *Brassica napus* and its diploid progenitors. Genetics **187**, 37–49.

Yang C, Hu B, Portheine SM, Chuenban P, Schnittger A. 2020*a*. State changes of the HORMA protein ASY1 are mediated by an interplay between its closure motif and PCH2. Nucleic Acids Research **48**, 11521–11535.

Yang C, Sofroni K, Wijnker E, *et al.* 2020*b*. The Arabidopsis Cdk1/Cdk2 homolog CDKA;1 controls chromosome axis assembly during plant meiosis. The EMBO Journal **39**, e101625.

Yelina NE, Choi K, Chelysheva L, *et al.* 2012. Epigenetic remodeling of meiotic crossover frequency in *Arabidopsis thaliana* DNA methyltransferase mutants. PLoS Genetics **8**, e1002844.

Zanders S, Alani E. 2009. The pch2Delta mutation in baker's yeast alters meiotic crossover levels and confers a defect in crossover interference. PLoS Genetics **5**, e1000571.

Zanders S, Sonntag Brown M, Chen C, Alani E. 2011. Pch2 modulates chromatid partner choice during meiotic double-strand break repair in *Saccharomyces cerevisiae*. Genetics **188**, 511–521.

Zickler D, Kleckner N. 1999. Meiotic chromosomes: integrating structure and function. Annual Review of Genetics **33**, 603–754.

Zickler D, Kleckner N. 2015. Recombination, pairing, and synapsis of homologs during meiosis. Cold Spring Harbor Perspectives in Biology **7**, a016626.

Ziolkowski PA, Berchowitz LE, Lambing C, *et al*. 2015. Juxtaposition of heterozygous and homozygous regions causes reciprocal crossover remodelling via interference during Arabidopsis meiosis. eLife **4**, e03708.

Ziolkowski PA, Underwood CJ, Lambing C, *et al.* 2017. Natural variation and dosage of the HEI10 meiotic E3 ligase control Arabidopsis crossover recombination. Genes & Development **31**, 306–317.